The role of MITF in regulating transcriptional cell states in melanoma

Remina Dilixiati

Thesis for the degree of Philosophiae Doctor

Supervisor/s:
Eiríkur Steingrímsson

Doctoral committee:
Arnar Pálsson, PhD

Erna Magnúsdóttir, PhD

Lionel Larue, PhD

Þórunn Rafnar, PhD

March, 2019

UNIVERSITY OF ICELAND
SCHOOL OF HEALTH SCIENCES
FACULTY OF MEDICINE

MITF og umritun í sortuæxlum

Remina Dilixiati

Ritgerð til doktorsgráðu

Leiðbeinandi/leiðbeinendur:
Eiríkur Steingrímsson

Doktorsnefnd:
Arnar Pálsson, PhD

Erna Magnúsdóttir, PhD

Lionel Larue, PhD

Þórunn Rafnar, PhD

Mars, 2019

UNIVERSITY OF ICELAND
SCHOOL OF HEALTH SCIENCES
FACULTY OF MEDICINE

ISBN 978-9935-9455-0-1

Printing by Háskolaprenta.

Reykjavik, Iceland 2019

Ágrip

Litfrumur (e. melanocytes) eiga uppruna sinn í taugakambi (e. neural crest) sem forverafrumur sem fjölga sér síðan og ferðast til áfangastaða sinna í húð, hári og öðrum líffærum þar sem þær sérhæfast og mynda litarefnið melanín. Litfrumur geta ummyndast í æxlisfrumur og myndað sortuæxli en eitt einkenna þeirra er fareiginleikar. Umritunarþátturinn MITF (Microphthalmia-associated transcription factor) er nauðsynlegur fyrir myndun og sérhæfingu litfruma og stjórnar tjáningu gena sem eru nauðsynleg fyrir lifun, fjölgun og sérhæfingu frumanna. Sortuæxlisfrumur nýta MITF til æxlismyndunar. Hlutverk MITF í stjórnun frumufars og íferðar hefur hins vegar ekki verið að fullu ljóst.

Í verkefni þessu var skoðað hvað gerist þegar MITF genið er slegið út í sortuæxlisfrumum með hjálp CRISPR tækninnar. Í ljós kom að frumur þessar skipta sér hægar en viðmiðunarfrumur og áhrif sáust á tjáningu gena sem eru mikilvæg fyrir frumuhringinn og eru þekkt markgen MITF. Þetta staðfestir fyrri niðurstöður um að MITF er mikilvægt fyrir stjórnun frumuskiptinga í sortuæxlisfrumum. Hins vegar höfðu sortuæxlisfrumurnar sem skortir MITF mun minni fareiginleika en viðmiðunarfrumurnar. Þegar MITF var tímabundið slegið niður með miRNA aðferð sáust hins vegar engin áhrif á frumufar. Með því að raðgreina RNA fruma sem skortir MITF og bera saman við viðmiðunarfrumur kom í ljós að tap á MITF leiddi til taps á genum sem hafa með myndun litarins að gera en aukningar í tjáningu gena sem tengjast utanfrumuefni (e. extracellular matrix), og taugamyndun. KO frumurnar líkjast helst taugakambs- og Schwann- frumum. Einnig kom í ljós að gen sem tjá fyrir mikilvægum proteinum sem mynda “focal adhesions” í frumum, svo sem paxillin (*PAX*) og Focal Adhesion Kinase (*FAK*) eru markgen MITF og tjáning þeirra var örvuð þegar MITF vantaði. Í frumum án MITF (bæði CRISPR og miRNA frumum) jókst fjöldi FAK og PAX-jákvæðra punkta. Tjáning N-cadherin jókst en E-cadherin minnkaði við tap á MITF en þetta eru merki um að frumurnar hafi breytt sér úr þekjuvefsfrumum í bandvefsfrumur en það ferli kallast bandvefsumbreyting þekjufruma (e. epithelial-mesenchymal transition eða EMT) og er mikilvægt í ummyndun fruma í krabbameinsfrumur. Greining á ChIP-seq gögnum sýna að bæði N- og E-cadherin genin eru með MITF bindiset í innröðum og stýrisvæði en það bendir til að MITF stjórni beint tjáningu þeirra.

Í frumum sem skortir MITF verða miklar breytingar í tjáningu gena, mun meiri en unnt er að skýra einungis með beinum áhrifum MITF. Til að athuga hvort hluta breytinganna mætti skýra með utangenaerfðum var skoðað hvort

breytingar hefðu orðið á histónaumbreytingunum H3K4me3 og H3K9me3 en umbreytingar þessar eru merki um virkt litni annars vegar og óvirkt litni hins vegar. Umbreytingar þessar fundust í stýriröðum gena sem voru mismunandi tjáð í frumum sem skortir MITF og viðmiðunarfrumum sem tjá MITF. Áhugavert er að gen sem tákna fyrir umbreytingarensímunum *PRDM7* og *SETDB2* voru mun minna tjáð í frumum sem skortir MITF en í viðmiðunarfrumum. Vinna þessi sýnir að tap á MITF leiðir til þess að frumurnar fá einkenni taugakambsfruma og að viðhald slíkar fruma er háð umbreytingarensímum sem setja utangenamerki á histón og að þau ensím eru háð MITF.

MITF getur unnið með öðrum umritunarþáttum svo sem IRF4 og TFEB í litfrumum og sortuæxlisfrumum en ekki er ljóst hversu margþætt þetta samstarf er í raun. Í seinni hluta ritgerðarinnar var skörun í bindingu umritunarþáttanna þriggja MITF, IRF4 og TFEB skoðuð í sortuæxlisfrumum með notkun ChIP-seq aðferðarinnar. Notast var við eGFP-merkt TFEB og IRF4 prótein of ChIP-seq aðferðin notuð til að greina bindiset próteinanna í erfðamengi 501mel sortuæxlisfruma. Greining á skörun bindiseta sýndi að MITF og TFEB bindast við gen sem taka þátt í myndun lýsósóma en MITF og IRF4 skarast þegar kemur að genum sem mynda lit og taka þátt í ónæmiskerfinu. MITF var frábrugðið hinum þáttunum í að bindast við gen sem taka þátt í myndun taugakerfisins, TFEB var einstakt í að bindast við gen sem taka þátt í efnaskiptum DNA en IRF4 binst við gen sem tengjast myndun og starfsemi blóðfruma. Við höfum því greint skörun þessara umritunarþátta en einnig einstakt hlutverk þeirra. Þetta leyfir okkur að greina hvernig þessir þættir vinna saman í litfrumum og hvaða hlutverki þeir gegna í þeim.

Lykilorð:

MITF, TFEB, IRF4, sortuæxli, umritun

Abstract

The pigment producing melanocytes are derived from the neural crest cells and form precursor cells called melanoblasts. These cells proliferate and migrate to their destination in skin, hair and other organs where they differentiate into melanocytes which produce the pigment melanin. The Microphthalmia-associated transcription factor (MITF) is indispensable for the establishment of fully differentiated melanocytes. MITF controls the expression of genes required for melanocyte survival, proliferation and differentiation. Melanoma cells thus exploit the transcriptional activity of MITF to foster cancer progression. However, the role of MITF in regulating the metastatic potential of melanoma cells is complex and often leads to inconsistent findings. The scope of this thesis was to further elucidate the functional role of MITF in melanoma development.

Our findings revealed that MITF knock out (KO) melanoma cells exhibit a reduced proliferation rate compared to the control cell line. Consistent with that, the expression of cell cycle regulators that are known targets of MITF was affected in the KO cells. Surprisingly, both the migration and invasion potential of MITF-KO cells were significantly reduced compared to empty vector cell lines. In contrast, transient depletion of MITF did not affect the invasion potential of melanoma cells. RNA-sequencing followed by differential gene expression analysis revealed a gain of extracellular matrix and neuronal related genes in MITF-KO cells, whereas pigmentation genes that are specific to melanocyte differentiation were lost. Accordingly, the gene expression profile of MITF-KO cells was negatively correlated with the gene signature of melanocytes, whereas a positive correlation was observed with neural crest and Schwann cell signature. Interestingly, the major components of focal adhesions, including paxillin (*PAX*) and focal adhesion kinase (*FAK*) are direct targets of MITF and their expression was induced upon MITF depletion. Well in line, the number of FAK and PAX positive focal points were increased in MITF-KO and transient knockdown cell lines. Additionally, expression of N-cadherin was increased in both models whereas E-cadherin was decreased, reflecting marks of mesenchymal transition. Published ChIP-seq data show that both E- and N-cadherins have MITF binding sites in their introns and promoter regions, suggesting that they are direct MITF targets. The level of histone modifications reflected major changes in gene expression observed in the MITF-KO cells. The H3K4me3 active mark and

the H3K9me3 repressive mark were both altered in the promoter of genes that showed differential expression in MITF-KO cells. Consistent with this, the expression of the histone modifiers *PRDM7* and *SETDB2* was reduced in the MITF-KO cells. Taken together, we conclude that the loss of MITF drives cells into a de-differentiated state that is governed by a neural crest-like transcriptional program. Furthermore, the maintenance of neural crest gene repertoire is facilitated by epigenetic modifiers that are under MITF regulation.

The second part of this thesis investigated the genome wide overlapping targets of the transcription factors MITF, IRF4 and TFEB. All three factors have been shown to collaborate in regulating gene expression in melanoma and melanocytes. Chromatin immunoprecipitation sequencing was performed using eGFP tagged TFEB and IRF4 proteins and genome wide binding sites were identified for each factor. Analysis of the overlapping target genes revealed that MITF and TFEB share binding to lysosomal genes whereas MITF and IRF4 share binding to pigmentation and immue-related genes. Statistically differentially bound sites were identified for each factor, in which MITF displayed unique binding to genes related to neuronal development. TFEB showed exclusive binding to genes related to DNA metabolic processes, whereas IRF4 revealed exlusive binding to genes involved in the hematopoietic system. Thus, the distinct and overlapping binding regions of each factor were identified, which enabled us to dissect the co-operative and independent transcriptional activity of each factor.

Keywords:

MITF, TFEB, IRF4, melanoma, transcription

Acknowledgements

First and foremost, I wish to thank my supervisor Prof. Eiríkur Steingrímsson for his immense patience and continuous support. He possesses a rare combination of being a nice person and a good scientist. His professional guidance, critical comments and motivation helped me throughout my research and during writing of this thesis. Above all, he created a friendly environment in the lab which helped me overcome difficult times during my research life.

I would also like to thank my PhD committee members Prof. Arnar Pálsson, Dr. Erna Magnúsdóttir, Prof. Lionel Larue, Dr. Þórunn Rafnar, for their assisstance and encouragment through my studies and stimulating discussions on my project. I am particularly grateful for the assistance given by Dr. Erna Magnúsdóttir, who not only taught me to perform ChIP-seq and other numerous lab techniques but also provided insightful comments, critical suggestion and shared valuable knowledge with me which helped me greatly during these years. I would also like to thank unofficial member of my PhD comittee Dr. Margrét H. Ögmundsdóttir, for her encouragment, kind support and suggestions during my studies.

I wish to acknowledge the department of Biochemistry and Molecular Biology (BMC) and other colleagues for providing me with the resources and lively research environment. I am grateful to the members of SCRU lab, EM lab and GV lab for generously providing me with the antibodies and protocols for my experiments. Withought the collaborative effort from everybody I would not be able to finish this thesis. Thank you to Icelandic Research Fund Rannís and Eimskip doctoral fellowship for financially supporting my PhD study.

I must thank my brilliant labmates Valerie Fock, Sara Sigurbjörnsdóttir, Josué Ballesteros, Hilmar Gunnlaugsson, Freyja Imsland, Lára Stefansson, Berglind Einarsdóttir, Diahann Atacho, Katrin Möller, Ásgeir Örn Arnþórsson for their moral, emotional, academic support and professional advices. Our interesting and sometimes inappropriate converstations during lunch time have always been a great pleasure. I thank Sara Sigurbjörnsdóttir, Katrin Möller, Ilse Gerritsen and Hilmar Gunnlaugsson their direct contribution to some of the work in this thesis.

Thank you to my friend Valerie Fock (FiFi) for being more than just a friend. You are like p53 (pi pitithree) guarded me from my problems, for instance student housing resulted homelessness and many others. Radiating “negativity” with you is just like tartufo on tagliatelle. And that “FiFi laugh” in the background while writing my thesis was an impressive experience. I would also like to thank my dear friend Kimberley Anderson, for the help with protocols and advices, importantly the amazing food sessions. I am also grateful for my lovely friends Yue Tuan Zhang and Han Xiao, cooking the spiciest food in Iceland with you two made me feel home.

Thank you Viktoría Birgisdóttir for your kindness, patience and tolerating my grumpiness. You have been my greatest support during these most difficult times.

With all my heart, I would like to thank my mother Risalet Yasen, for always believing in me and encouraging me to do what I want to do in life. You are the best mother.

Contents

List of abbreviations

Symbol	Name
3’ UTR	3 prime untranslated region
5’ UTR	5 prime untranslated region
bHLH-Zip	Basic helix-loop-helix leucine zipper
BrdU	Bromodeoxyuridine
CDH1	Cadherin 1/E-cadherin
CDH2	Caderin 2/N-cadherin
CDKN1C	cyclin dependent kinase inhibitor 1C
CDKN2A	cyclin dependent kinase inhibitor 2A
CDKN2B	cyclin dependent kinase inhibitor 2B
cDNA	Complementary deoxyribonucleic acid
ChIP	Chromatin immunoprecipitation
ChIP-seq	Chromatin immunoprecipitation sequencing
COL11A2	Collagen type XI Alpha 2 chain
COL4A2	Collagen type IV Alpha 2 chain
COL4A3	Collagen type IV Alpha 2 chain
COL5A2	Collagen type V Alpha 2 chain
DCT	Dopachrome Tautomerase
DEGs	Differentially expressed genes
DNA	Deoxyribonucleic acid
DUSP1	Dual specificity phosphatase
ECM	Extracellular matrix
eGFP	Enhanced green fluorescent protein
EMT	Epithelial to mesenchymal transition
FAK	Focal adhesion kinase
H3K4Me3	Histone 3 Lysine 4 trimethyl
H3K9Me3	Histone 3 Lysine 9 trimethyl
IRF4	Interferon regulatory factor 4
ITGA10	Integrin Subunit alpha 10
ITGA2	Integrin Subunit alpha 2

ITGA3	Integrin Subunit alpha 3
ITGA4	Integrin Subunit alpha 4
ITGA5	Integrin Subunit alpha 5
ITIH5	Inter-alpha-trypsin-inhibitor heavy chain member 5
LAMP1	Lysosomal associated membrane protein 1
M2	Activated macrophage
MAFB	MAF BZIP transcription factor B
MITF	Microphtalmia associated transcription factor
MLANA	Melanocyte antigen A
MMP15	Matrix metallopeptidase 15
NF-kB	Nuclear factor kappa B
NGFR	Nerve growth factor receptor
nM	Nanomolar
NR4A3	Nuclear receptor subfamily 4 group A member 3
PAX	Paxillin
PCR	Polymerase chain reaction
PRDM7	PR/SET domain 7
PRNP	Prion protein
RNA	Ribonucleic acid
RNA-seq	RNA sequencing
RT-qPCR	Quantitative reverse transcription PCR
SETDB2	SET domain bifurcated 2
SNAI2	Snail family transcriptionally repressor 2/Slug
SOX2	SRY-Box2
TFEB	Transcription factor EB
TGFβ	Transforming growth factor beta
TRE	Tetracycline response element
TYR	Tyrosinase
ZEB1	Zinc finger E-box binding homeobox 1
ZEB2	Zinc finger E-box binding homeobox 2
ZNF703	Zinc finger protein 703
µL	Microliter
µM	Micromolar

List of tables

List of figures

List of original papers

I. R. Dilshat, S. Sigurbjornsdottir, K. Möller, I. Gerritsen, E. Magnusdottir, M. H. Ogmundsdottir, E. Steingrimsson. **MITF regulates extracellular matrix-related genes in melanoma**. *Manuscript in preparation.*

II. R. Dilshat, E. Magnusdottir, E. Steingrimsson. **MITF transcriptional network with IRF4 in melanoma**. *Manuscript in preparation.*

III. R. Dilshat, K.Moller, S. Sigurbjornsdottir , V.Fock, E. Magnusdottir , E. Steingrimsson, **SETDB2 and PRDM7, new cell cycle regulators in melanoma** . *Manuscript in preparation.*

Papers to which I contributed:

M. H. Ogmundsdottir, V. Fock, L. Sooman, V. Pogenberg, R. Dilshat, C. Bindesbøll, H. M. Ogmundsdottir, A. Simonsen, M. Wilmanns & E. Steingrimsson. **A short isoform of ATG7 fails to lipidate LC3/GABARAP**. *2018,* Scientific Reports, DOI: 10.1038/s41598-018-32694-7

K. Möller, S. Sigurbjornsdottir, A. O. Arnthorsson, V. Pogenberg, R. Dilshat, V. Fock, S. H. Brynjolfsdottir, C. Bindesboll, M. Bessadottir, H. Ogmundsdottir, A. Simonsen, L. Larue, M. Wilmanns, V. Thorsson, E. Steingrimsson, & M. H. Ogmundsdottir. **MITF has a central role in regulating starvation-induced autophagy in melanoma**. *Accepted for publication, 2018,* Scientific Reports

S. Wojciechowska, J. Travnickova, A. Khamseh, P. Gautier, D. Brown, A. Ewing, A. Capper, M. Spitzer, R. Dilshat, C. Semple, M. Mathers, J. Lister, E. Steingrímsson, T. Voet, C. Ponting, & E. Patton. **MITF-low melanoma subtype models in zebrafish reveal transcriptional sub-clusters and a MITF-resistant cell subpopulation**. *Submitted, 2019,* Cancer Research.

Declaration of contribution

I designed the experiments with the assistance of my supervisor Prof. Eiríkur Steingrímsson and I carried out all the experiments involving functional characterization of MITF knock out cells. Generation of MITF knock out cell lines were carried out by Katrin Möller and Sara Sigurbjörnsdóttir. I performed transcriptomic profiling of MITF knock out cells and control cell lines using RNA-seq and carried out bioinformatics analysis. I generated inducible MITF knock down cell lines using piggy-bac constructs cloned by Sara Sigurbjörnsdóttir.

I designed the experiments described in the second part of thesis with the help of Prof. Eiríkur Steingrímsson. I conducted ChIP-seq for eGFP-IRF4 and eGFP-TFEB and carried out ChIP-seq analysis and downstream bioninformatics analysis.

1 Introduction

1.1 Melanocyte

Melanocytes are derived from multipotent neural crest cells, a temporary group of cells which arises from the neural tube during development and gives rise to a diverse array of cell types (Le Douarin, 1999). The specified premigratory neural crest cells will undergo epithelial to mesenchymal transition (EMT) and reorganize their cytoskeleton to migrate underneath the ectoderm, a region called migration staging area (Le Douarin, 1999). These early pre-migratory neural crest cells are multipotent and express neural crest cell markers including *Sox10*, *Sox9* and SNAI2 (Serbedzija et al., 1994). After this stage, the neural crest cells migrate either ventrally or dorso-laterally away from the neural tube. The ventrally migrating cells will give rise to the peripheral nervous system, whereas the dorso-lateral migrating cells that express *Mitf* and *Kit* give rise to melanocyte precursor cells called melanoblasts (Gudjohnsen et al., 2015). The melanoblasts then proliferate and migrate to their target sites throughout the body to become fully differentiated mature pigment producing melanocytes (Le Douarin, 1999). Melanocytes have been found not only in the epidermis, hair and iris where they give colour to these organs but they have also been found in the inner ear, nervous system (Tachibana, 1999), olfactory bulb and heart (Yajima & Larue, 2008). In the skin, each melanocyte resides in the basal layer of the epidermis where they are surrounded by 30-40 keratinocytes (Fitzpatrick & Breathnach, 1963). In response to UV radiation, the pigment melanin is synthesized inside specialized vesicular organs called melanosomes which are then transferred to adjacent keratinocytes where they protect cells from further UV-induced damage. Melanocyte stem cells are found in the hair follicle bulge-subbulge area, which serves as a reservoir for melanocyte skin and hair pigmentation (Nishimura et al., 2005; Nishimura et al., 2002).

1.2 The Microphthalmia associated transcription factor

Microphthalmia-associated transcription factor (MITF) plays a major role in biological pathways involved in skin pigmentation and pathology, as well as in hearing and eye development. MITF was initially discovered as a mutated gene underlying a mouse phenotype. In the offspring of irradiated mice, Paula Hertwig discovered mice with white coat color and small eyes; she called the mutation microphthalmia (abbreviated mi) due to the small eyes (Hertwig, 1942). Subsequently, many different mutant alleles were

discovered at the *mi* locus (reviewed in Steingrimsson et al., 2004). Later, the gene mutated in the *mi* mutants was cloned and characterized by Hodgkinson and colleauges (Hodgkinson et al., 1993; Hughes et al., 1993) and many of the mutations were characterized at the molecular level (Steingrimsson, 1994). These studies characterized MITF as a key transcription factor in melanocyte development since its inactivation led to microphthalmic and white mice.

MITF is a basic helix-loop-helix leucine zipper (bHLHZip) transcription factor that binds to the promoters of genes involved in pigment cell biology in melanocytes. It also participates in regulating the expression of genes in mast cells (Morii et al., 1996), retinal pigment epithelium (Yasumoto et al., 1997) and osteoclasts (Weilbaecher et al., 2001). The expression of MITF is activated during the transition from neural crest cells to melanoblasts and is required for survival and migration of melanoblasts (Nakayama et al., 1998; Opdecamp et al., 1997).

In humans, the *MITF* locus resides on chromosome 3p12-p14.1 and spans over 200 kbp. The MITF protein is most related to the TFEB, TFE3 and TFEC transcription factors and together they are sometimes called the MiT family of proteins. By alternative usage of promoters and the creation of unique 5' sequences, the *MITF* gene has been shown to produce at least nine different isoforms including *Mitf-A* (Amae et al., 1998), *Mitf-B* (Udono et al., 2000), *Mitf-C* (Fuse et al., 1999), *Mitf* (Takeda et al., 2002), *Mitf-E* (Oboki et al., 2002), *Mitf-H* (Steingrimsson et al., 1994), *Mitf-J* (Hershey & Fisher, 2005), *Mitf-Mc* (Takemoto et al., 2002) and *Mitf-M* (Hodgkinson et al., 1993; Tassabehji et al., 1994). These isoforms encode proteins which differ at their N-termini but they all share a common C-terminal portion. *MITF-M* is the shortest isoform (a 419 amino acid residue protein) and it is exclusively expressed in melanocytes and melanoma cells. There are also internal alternative splice events which result in the production of several different splice products. The best characterized is the alternative 18bp exon located just before the basic domain of MITF, which is found in most tissues where MITF is expressed (Steingrimsson et al., 1994).

The centrally located basic DNA binding domain and the helix-loop-helix and leucine zipper (HLH-Zip) dimerization domains are essential for normal MITF function. These domains form two helices connected by a loop, where the basic domain and helix 1 of the HLH domain form one continuous helix and helix 2 and the leucine zipper form another one (Pogenberg et al, 2012). The dimerization ability of MITF is restricted to the MiT family of transcription factors, namely TFEB, TFEC and TFE3. Hence, it fails to interact with other

bHLHZip factors such as MYC, MAX or USF (Hemesath et al., 1994). This is because MITF and the other TFE transcription factors have a three amino acid sequence in the zipper region that creates a structural kink in the dimerization domain, which restricts the dimerization ability to only the MiT family. Removing this three amino region eliminates the ability to dimerize with wild type MITF but introduces the ability to interact with MAX (Pogenberg et al., 2012). MITF binds to DNA as a homodimer or heterodimer with other MiT transcription factors such as TFEB, TFEC and TFE3. Furthermore, analysis of the promoter of *Tyrp-1,* an important pigmentation gene, led to the identification of a sequence motif termed the M-box motif (AGTCATGTG) which was specifically bound and activated by a melanocyte-specific transcription factor, later shown to be MITF. Analysis of the promoter elements of the genes encoding the pigmentation enzymes *Tyr*, *Tyrp1* and *Tyrp2* showed that the M-box motif (AGTCATGTGCT) was conserved in both mouse and human promoters (Budd & Jackson, 1995). MITF preferentially recognizes the Ephrussi (E)-box motif with CACGTG sequence flanked by A or T (Aksan & Goding, 1998), as well as the M-box motif CATGTG (Hemesath et al., 1994).

1.2.1 Transcriptional regulation of MITF

The transcription of MITF is controlled by an array of transcription factors and signalling events working in coordination to stimulate its expression. The transcription factors that have so far been shown to positively regulate MITF expression are PAX3, SOX10, CREB, LEF1 and ZEB2. Additionaly, MITF negatively regulated by GLI2 and BRN2, as well as signalling pathways such as TGFβ and WNT. The MITF promoter is recognized and regulated by PAX3 *in vitro* and *in vivo* (Galibert et al., 1999). PAX3 belongs to the paired-class of homeodomain transcription factors. It is expressed in the neural crest, melanoblasts, developing brain, neural tube and limb buds (Goulding et al., 1991). It not only controls MITF expression but also activates *TYRP1* expression (Galibert et al., 1999). Interestingly, PAX3 has been suggested to promote a poised state of melanocytic commitment (Lang et al., 2005). In melanoblasts, *PAX3* competes with MITF for binding to an enhancer region of the *DCT* gene, an enzyme required for melanin synthesis. The derepression *PAX3* by activated β-catenin triggers differentiation of melanocytes in response to environmental cues (Lang et al., 2005). SOX10 and PAX3 have been shown to synergistically regulate MITF expression (Bondurand et al., 2000). SOX10 belongs to the Sex Determining Region Y family of transcription factors containing a so-called high mobility group (HMG)-type DNA binding domain. It is widely expressed in various cell types throughout neural development, including melanoblasts and melanocytes

(Southard-Smith et al., 1998). SOX10 is not only essential for neural crest stem cell survival but is also required for maintaining growth of giant congenital naevi and melanoma (Mollaaghababa & Pavan, 2003; Shakhova et al., 2012). SOX10 transactivates the *MITF* promoter through evolutionarily conserved binding sites (Potterf et al., 2000). A mutation in *SOX10* results in Waardenburg syndrome type 4, which is a rare genetic disorder associated with sensorineural hearing loss and pigmentary abnormalities. Mutation in *SOX10* disrupts neural crest cell development in the *Dominant megacolon* mouse (Southard-Smith et al., 1998). Melanomagenesis can be regulated by UV exposure which activates MITF expression to induce expression of pigmentation genes. This cellular process is initiated by the release of melanocyte stimulating hormone (αMSH) in keratinocytes after UV exposure. Followed by this, binds to the MC1R G-protein coupled receptor on melanocytes and leads to the elevation of cAMP which then mediates *MITF* activation through binding of the CREB transcription factor to the CREB-responsive element in the *MITF* promoter (Bertolotto et al., 1998; Cui et al., 2007; Rees, 2000).

Wnt proteins play a pivotal role in the development of melanocytes from the neural crest precursors (Dorsky et al., 1998). Wnt binds the frizzled transmembrane receptor which initiates the formation of a receptor complex that prevents phosphorylation and degradation of β-catenin. Unphosphorylated β-catenin then translocates to the nucleus and binds to the N terminus of *LEF1* and enhances its expression (Hsu et al., 1998; Milatovich et al., 1991). WNT3A leads to the recruitment of LEF1 to the *MITF* promoter resulting in stimulation of its expression (Takeda, Yasumoto, et al., 2000). Moreover, MITF can autoregulate its own transcription via physical cooperation with LEF1 and binding to the *MITF* promoter (Saito et al., 2002).

ZEB1 and ZEB2 are part of the Zinc-Finger-E-box binding transcription factor family, which binds to the same sequence (CACGTG) as MITF (Postigo & Dean, 2000). The ZEB1 and ZEB2 factors have been shown to play a major role in epithelial to mesenchymal transition during development (Vandewalle et al., 2009). A link between ZEB2 and MITF has been established, where loss of ZEB2 to leads to decreased *MITF* expression (Denecker et al., 2014). However, ZEB1 has been shown to repress *MITF* in retinal pigment epithelium cells (Liu et al., 2009). MITF expression is negatively regulated by Glioma associated oncogene family member 2 (GLI2), and GLI2 is a direct target of TGFβ/SMAD signalling (Dennler et al., 2007). In melanoma, GLI2 and MITF expression levels are inversely correlated. In addition, high GLI2 expression is associated with increased invasion and metastatic potential (Javelaud et al., 2011). A GLI2 binding site was identified in the promoter

region of *MITF* at location -334/-226 (Pierrat et al., 2012). Similarly, BRN2 (N-Oct-3) directly binds to the *MITF* promoter. BRN2 is widely expressed in melanoma cell lines, is a target of ERK, which is downstream of $BRAF^{V600E}$ (Goodall et al., 2004). Depletion of BRN2 has been linked to a reduction of *MITF* expression (Thomson et al., 1995; Thurber et al., 2011; Wellbrock et al., 2008a). Furthermore, an opposing mechanism of BRN2-mediated repression of *MITF* expression has been reported (Goodall et al., 2008). This suppressor function of BRN2 is observed in $BRAF^{WT}$ B16 cells where BRN2 expression is not controlled by $BRAF^{V600E}$ (Goodall et al., 2008).

On the chromatin level, a chromatin remodelling complex, BRG1, has been shown to promote *MITF* expression. A ChIP study showed the direct binding of BRG1 to the *MITF* promoter (Vachtenheim et al., 2010).

1.2.2 Post-translational regulation of MITF

The transcriptional activity of MITF can be regulated through posttranslational modifications. This involves phosphorylation or sumoylation of MITF at different amino acid residues. Phosphorylation of MITF can be mediated by the MAPK signalling pathway, where ERK1/2 downstream of the receptor tyrosine kinase KIT phosphorylates MITF at two serine residues, S73 and S409 (Hemesath et al., 1998). S409 can also be phosphorylated by p90 ribosomal S6 kinase (Wu et al., 2000). Phosphorylation of S73 resulted in enhanced transcriptional activity upon continued activation of the RAF kinase (Hemesath et al., 1998). Consistent with that observation, the transcriptional activity of MITF was reduced when Ser73 was mutated to Ala (Price et al., 1998; Wu et al., 2000). This was shown to be due to the loss of interactions of MITF with the transcriptional cofactors p300 and CBP (Price et al., 1998). At the same time, phosphorylation at S73 promotes MITF interactions with the protein inhibitor of activated Stat 3 (PIAS3), resulting in inhibition of MITF transcriptional activity (Levy et al., 2003). The S409 phosphorylation inhibits PIAS3 interactions (Levy et al., 2003). Moreover, phosphorylation at S73 has been shown to be needed for proteasome-dependent turnover (Xu et al., 2000). It further acts as a priming site for Ser69 phosphorylation of MITF, thereby affecting nuclear export of the protein (Ngeow et al., 2018).

GSK3β-mediated phosphorylation of MITF at S298 has been shown to lead to increased MITF transcriptional activity (Takeda, Takemoto, et al., 2000; Terragni et al., 2011). Consistenly, GSK3β inhibition induced by cAMP, has been shown to reduce the trancriptional activity of MITF from the tyrosinase promoter (Khaled et al., 2002). This is further substantiated by findings from Ploper et al. (2015) who showed that MITF has three conserved putative GSK3β priming sites, and that stabilization of MITF through GSK3β-signaling

drives the biosynthesis of multivesicular bodies (Ploper et al., 2015).

SUMOylation can modulate MITF activity. The SUMOylation reaction usually occurs on a lysine residue of the canonical YKXE sequence, which is recognized by small ubiquitin related modifiers (Fuhs & Insel, 2011). MITF can be SUMOylated at residues Lys182 and Lys316 (Murakami & Arnheiter, 2005). Mutating K316R has been shown to hinder MITF SUMOylation and enhance MITF transcriptional activity (Miller et al., 2005). Importantly, the E318K germ line heterozygous missense substituition has been identified in melanoma and renal cell carcinoma (RCC) patients (Bertolotto et al., 2011). The 318-codon in MITF is located at the end of a sumoylation consensus site (YKXE). Consistent with that, a germline mutation of E318K in MITF severely perturbs sumoylation of MITF *in vitro* and in tumours (Bertolotto et al., 2011; Yokoyama et al., 2011). This mutation has been described as a medium penetrance gene in melanoma, and was also shown to predispose to renal cell carcinoma (Sturm et al., 2014). Carriers of this mutation have a 14-fold increased risk for developing melanoma and RCC (Bertolotto et al., 2011). Luciferase reporter assays showed that the MITF-E318K mutant protein activates expression from the TRPM1 luciferase reporter at 1.3-1.4 fold higher levels than wild type MITF, indicating that the transcriptional activity of MITF-E318K is modestly enhanced (Yokoyama et al., 2011).

Mice carrying homozygous and heterozygous $MITF^{E318K}$ mutation exihibit a hypopigmentation phenotype (Bonet et al., 2017). $MITF^{E318K}$ mutant cells can bypass $BRAF^{V600E}$-mediated senescence in melanocytes. In addition, in $BRAF^{V600E}$ and $Pten^{-/-}$ mice, the $MITF^{E318K}$ mutation accelerates melanoma progression (Bonet et al., 2017).

1.2.3 MITF mutations in humans

Germ line *MITF* mutations in humans lead to Waardenburg Syndrome Type 2A (WS2A) and Tietz syndrome. WS2 is characterized by abnormalities in the pigmentation of eyes, skin and hair and partial or bi-lateral loss of sensorineural hearing (Amiel et al., 1998; Tassabehji et al., 1994). Tietz syndrome is another hypopigmentation disorder which is characterized by partial albinism and congenital deafness (Tietz, 1963). Two mutations in MITF have been associated with Tietz syndrome; one is a deletion of arginine R217 and another is a substituition of lysine to asparagine (N210K) (Smith et al., 2000). Both of these mutations reside in the basic domain of MITF and make it transcriptionally inactive (Shigemura et al., 2010).

The latest research on the biochemical effects of the WS2 and TS mutations showed that mutations present in the DNA binding region of MITF (E213D, R214X, R216K, R217Del, R217G) abrogate its DNA binding ability and transcription activation potential. Additionally, mutations affecting the HLH

domain of MITF (I224S, S250P and R259X) as well as the leucine zipper region (N278D/L283P) also hindered DNA binding, possibly due to effects on dimerization (Grill et al., 2013).

A recent report described two unrelated patients that had obtained WS2A alleles from each of their parents. The compound heterozygous condition of the two MITF alleles resulted in a phenotype consisting of coloboma, osteopetrosis, microphthalmia, macrocephaly, albinism and deafness (COMMAD syndrome). Both of these patients had biallelic MITF mutations. One individual carried the Arg318del and Lys307Asn MITF mutations. The Lys307Asn allele exhibits a partial DNA binding ability, and therefore affects MITF target gene activation (George et al., 2016). The Arg318del mutation corresponds to the Arg217del mutation in MITF-M, which is a well-known mutation found in patients with Waardenburg and Tietz syndromes (Tassabehji et al., 1995) and is mutated in the first mouse Mitf mutation found by Paula Hertwig in 1942 (Steingrimsson, 1994). The other individual was compound heterozygous for the Arg318Gly mutation and a splice site mutation Leu312fs*, which results in a truncated MITF protein (George et al., 2016).

1.3 Melanoma

1.3.1 Melanoma epidemiology

Melanocytes arise from highly migratory and invasive neural crest cells that populate all parts of the body including skin, eyes, meninges and mucous membranes. Melanoma, the deadliest form of skin cancer, originates from melanocytes. Melanoma can be separated into three types: i) cutaneous melanoma, which originates from melanocytes in the epidermis, ii) mucosal melanoma, which is derived from melanocytes residing in the mucous membrane and iii) uveal melanoma, which arises from melanocytes in the ocular stroma. Cutaneous melanoma is, by far, the most common subtype, accounting for 90% of all cases of melanoma (Chang et al., 1998). Melanoma is reported as the 19th most common type of cancer worldwide with an incidence rate of 2.8-3.1 per 100,000 individuals. The highest incidence rate is found in Australia (37 per 100,000) and the lowest in Central-Asia (0.2 per 100,000) (Ferlay et al., 2010). Melanoma incidence decreases with the increasing distance from the equator, thus the highest incidence occurs in equatorial regions (Bulliard et al., 1994). Fair skinned individuals have an increased melanoma risk due to their sensitivity to UV radiation compared to people with dark skinned phenotype (Rees, 2003). This is directly related to UV radiation exposure, especially UVB (Pennello et al., 2000). While the incidence of other cancer types is decreasing, melanoma incidence continues to increase (Kohler et al., 2011). Early stage melanoma can be easily cured

with surgical resection. However, metastatic melanoma is highly invasive with poor prognosis and treatment often leads to drug resistance.

1.3.2 Mutations in melanoma

Like many cancers, melanoma develops through a multistep process governed by accumulated genetic aberrations that activate oncogenes which eventually leads to malignancy (Hanahan & Weinberg, 2011; Miller & Mihm, 2006). There are different genomic subtypes of melanomas with distinct somatic mutations: mutant BRAF, mutant RAS, mutant NF1 and triple-negative tumors (Cancer Genome Atlas, 2015).

Around 50-70% of melanomas harbour mutations in BRAF, a serine/threonine protein kinase (Davies et al., 2002). BRAF forms part of the MAPK/ERK signalling pathway which is important for the regulation of cell growth (Wan et al., 2004). Among BRAF mutations observed, approximately 90% of them are found at codon 600 and are a single nucleotide mutation resulting in the substitution of glutamic acid to valine, termed $BRAF^{V600E}$ (Davies et al., 2002; Forbes et al., 2008). The mutant $BRAF^{V600E}$ kinase is 500-fold more active than WT BRAF (Wan et al., 2004). Ectopic expression of $BRAF^{V600E}$ was shown to transform the melanocyte cell line, Melan-a (Wellbrock et al., 2004). Furthermore, inhibition of BRAF induces tumour shrinkage *in vivo* (Karasarides et al., 2004). Importantly, during melanoma progression, oncogenic activation of BRAF inhibits MITF expression via ERK (Wellbrock & Marais, 2005).

The Ras GTPase family is crucial for transducing extracellular signals (Ji et al., 2012). Activating mutations have been found in all three members of the RAS family (KRAS, HRAS and NRAS) in many tumours (Lowy & Willumsen, 1993). The activity of RAS is controlled by the ratio of bound GTP/GDP. It is activated upon binding to GTP, but is inactive when bound to GDP and fails to interact with downstream effectors (Shields et al., 2000). Activated GTP-bound RAS can activate downstream enzymes. The most studied RAS effectors are proteins of the RAF family, consisting of CRAF, BRAF and ARAF. After activated RAF proteins relocate to the plasma membrane, they phosphorylate mitogen-activated protein kinases 1 and 2 (MEK1 and MEK2) which in turn activates ERK1 and ERK2 (Downward, 2003). Activating RAS mutations occur in a smaller fraction of melanoma tumours (~10-15%); the majority of RAS mutations found in melanoma patients involve NRAS (Papp et al., 1999). The most common *NRAS* mutation is found in codon Q61 and less frequently mutations are present in codons G12 and G13 (Tsao et al., 2012). *NRAS* hotspot mutations including Q61R (n=35), Q61K (n=23) and Q61L (n=11) were found in TCGA melanoma samples (Cancer Genome Atlas, 2015).

NF1 is another frequently mutated gene which is part of the MAPK pathway, present in 14% of melanoma tumour samples in the TCGA database (Cancer Genome Atlas, 2015). It is a GTPase activating protein that activates GTPase hydrolysis in RAS protein (Bollag et al., 1996). The majority of mutations found in NF1 involve loss of function mutations which may contribute to an alternative mechanism of activating the MAPK pathway (Cancer Genome Atlas, 2015).

Mutations and deletions of *CDKN2A* locus have been found in families with inherited melanoma, and this locus encodes for two distinct proteins $p16^{INK4a}$ and $p14^{ARF}$ (Chin, 2003). $p16^{INK4a}$ targets CDK4/6 and thereby inhibits phosphorylation of RB. Therefore, loss of $p16^{INK4a}$ triggers G1-S transition in tumours (Koh et al., 1995). $p14^{ARF}$ targets HDM2, which in turn ubiquitinates p53 for degradation (Stott et al., 1998; Zhang et al., 1998). Thus, with the loss of $p14^{ARF}$, the degradation of p53 is deregulated. Carriers of *CDKN2A* mutations have an increased risk of developing melanoma. The $Cdkn2a^{-/-}$ mouse with oncogenic *NRAS* and *HRAS* mutations formed tumours frequently (Chin et al., 1997; VanBrocklin et al., 2010). The *CDKN2B* gene is adjacent to *CDKN2A*, and in 90% of tumours with a *CDKN2A* deletion, *CDKN2B* is also deleted (Gao et al., 2013). Benign nevi harbouring a BRAF mutation transform into melanoma upon depletion of CDKN2B (McNeal et al., 2015).

1.4 MITF in melanoma

MITF is vital for melanocyte survival, proliferation and differentiation. Dependency on MITF is retained and exploited during the journey of melanocyte transformation to melanoma. High-density single nucleotide polymorphism arrays were used to screen the chromosomal landscape in melanoma and revealed amplification of *MITF* in 20% of melanomas. Therefore, MITF has been described as a lineage survival oncogene. In metastatic melanoma, *MITF* amplification was associated with reduced five years survival (Garraway et al., 2005). However, in a recent study involving targeted-capture deep sequencing, no focal amplification of the *MITF* locus was found in a panel of melanoma tumours (Harbst et al., 2014). MITF directly binds to and activates the expression of genes involved in various biological processes including cell cycle regulation, differentiation, migration and senescence (Hoek, Schlegel, et al., 2008; Strub et al., 2011). Also, MITF sustains melanoma cell survival and proliferation through activation of genes such as *CDK2* (Du et al., 2004) and *Bcl2* (McGill et al., 2002). In the following sections, various roles of MITF in melanoma cell proliferation, differentiation and invasion will be introduced separately.

1.4.1 MITF affects melanoma proliferation and differentiation

During melanoma progression, MITF maintains both cell proliferation and survival. This might explain why MITF expression is sustained throughout melanoma progression. At the same time, MITF drives a pigment cell differentiation program by activating the expression of pigmentation genes.

It is well established that depletion of MITF in melanoma cell lines leads to cell cycle arrest with high proportion of cells stalled in G1 phase (Carreira et al., 2006; Giuliano et al., 2010; Wellbrock & Marais, 2005). In line with this, ChIP-seq studies have suggested that MITF transcriptionally targets genes involved in DNA replication, e.g. *BRCA1, AURKB* and *TERT* (Strub et al., 2011). Thus, depletion of MITF causes genomic instability, and consistently silencing of MITF increases the expression of the γH2AX and p53 proteins, indicating the presence of DNA damage which eventually may lead to cell cycle arrest and senescence (Giuliano et al., 2010; Strub et al., 2011). However, MITF depletion does not induce senescence in p53 mutant SkMel28 cells (Giuliano et al., 2010).

Loss of MITF leads to failure in activating *CDK2* which in turn results in a stalled cell cycle, since CDK2 is a key regulator for the transition from G1 to S phase (Du et al., 2004; Ekholm & Reed, 2000). Du et al (2004) showed that MITF binds to an enhancer region upstream from the *CDK2* transcription start site and enhances its expression. Accordingly, the regulation of CDK2 by MITF is specific for melanocytes and melanoma cells. Interestingly, *MITF* expression has been shown to be tightly correlated with *CDK2* only in primary melanoma tumours and melanoma cell lines but not in human lymphomas, suggesting a cell-type specific relationship between MITF and CDK2 (Du et al., 2004). Another direct target of MITF is *CDK4*, where MITF depletion through $BRAF^{V600E}$ signalling reduced *CDK4* expression in melanoma cells (Wellbrock et al., 2008b). Furthermore, MITF represses *CDKN2B* (*$p27^{kip1}$*) indirectly through two steps: Firstly, depletion of MITF reduces Dia1, a regulator of the actin cyctoskeleton. Secondly, reduction of Dia1 results in depletion of Skp2, an F-box protein which targets degradation of $p27^{kip1}$ (Carrano et al., 1999; Carreira et al., 2006). Accordingly, an inverse correlation of $p27^{kip1}$ and Skp2 has been reported in primary melanomas (Li et al., 2004). Thus, MITF and $p27^{kip1}$ inveresely correlate in melanoma cells (Carreira et al., 2006).

Exit from the cell cycle is the prerequisite for activation of the melanocyte differentiation program. Thus, high levels of MITF expression have been shown to halt cell proliferation and kick start differentiation in melanocytes. Consistent with that, it has been reported that MITF, together with hypophosphorylated Rb1, results in enhanced expression of *CDKN1A*

($p21^{CIP1}$) (Carreira et al., 2005). In addition, $p21^{CIP1}$ can also regulate *MITF* expression, thus forming an autoregulatory loop that maintains the balance between differentiation and proliferation (Carreira et al., 2005; Sestakova et al., 2010). In addition, MITF regulates the expression of $p16^{Ink4a}$ and leads to cell cycle arrest in melanocytes (Loercher et al., 2005).

Hence, MITF has an opposing function in regulating cell cycle progression. Published data so far suggest that these opposing mechanisms are due to MITF expression levels. Despite this contrasting effect of MITF on cell cycle regulation, the regulation of pigmentation by MITF is consistent. MITF binds to the regulatory regions of many pigmentation genes and positively regulates their expression. Examples include *TYR, DCT* and *MLANA* (Bentley et al., 1994; Du et al., 2003; Yasumoto et al., 1994). Indeed, highly pigmented regions are observed in melanoma samples, validating the idea that the role of MITF in regulating differentiation is retained in melanoma development.

1.4.2 MITF lost in invasion

The underlying mechanism of how MITF modulates cell invasion is complex. To date, the impact of MITF on invasion has been investigated through manipulating the expression levels of MITF in melanoma cells. Both induction and depletion of MITF have been associated with increased invasion. This is partly due to the complicated nature of MITF regulation and signalling events which result from continuous changes in the tumour microenvironment. It has been proposed that MITF promotes differentiation while acting as a supressor of invasion. This concept is based on several studies introduced below.

Gene expression profiling of melanoma cell lines clearly indentifed “invasive phenotype” melanoma cell lines characterized by extremely low levels of *MITF* (Hoek et al., 2006). In addition, these $MITF^{low}$ cell lines were linked to a gene signature of stemness and EMT (Hoek et al., 2006). Accordingly, in cell lines depletion of MITF has been linked to enhanced invasion *in vivo* and *in vitro* (Carreira et al., 2006; Cheli et al., 2011; Javelaud et al., 2011). Several factors have been shown to manipulate MITF levels to gain an invasive phenotype. For example, hypoxia and *WNT5A* both reduce *MITF* expression and increase invasion (Weeraratna et al., 2002; Widmer et al., 2012). In line with this, oncogenic BRAF supresses MITF during melanoma progression through ERK-mediated degradation (Wellbrock & Marais, 2005). However, three years later, the same group reported contradictory results showing that the long-term inhibition of MEK/ERK resulted in complete loss of MITF and thus concluded that ERK phosphorylation is needed for MITF expression in

BRAF mutant melanoma (Wellbrock et al., 2008b). The assumption made to support that MITF is a suppressor of invasion was further substantiated with findings that reported low levels of the MITF protein in invasive melanoma which is associated with poor prognosis (Hoek, Eichhoff, et al., 2008; Salti et al., 2000; Selzer et al., 2002). Highly invasive and drug resistant *BRAF* mutant melanoma cells have been characterized as being negative for *MITF* and positive for *AXL* and *WNT5A* (Dissanayake et al., 2008; Muller et al., 2014; Sensi et al., 2011).

Strikingly, opposing results were obtained where depletion of MITF resulted in a decrease in invasion. In 501Mel melanoma cells, ectopic expression of MITF enhances invasion in response to HGF, a ligand for the MITF target gene *c-MET* (McGill et al., 2006). Additionally, hypoxia-induced suppression of MITF has been shown to reduce tumour growth (Feige et al., 2011). The SUMOylation defective $MITF^{E318K}$ mutant has enhanced transcriptional activity and promotes 501Mel cell invasion (Bertolotto et al., 2011; Yokoyama et al., 2011). The $Mitf^{E318K}$ knock-in mouse model displayed increased onset of tumour progression in $Pten^{-/-}$ and $Braf^{V600E}$ background (Bonet et al., 2017). The $Mitf^{E318K}$ mutation rescued $Braf^{V600E}$ induced senescence in melanocytes, indicating that enhanced transcriptionally active $Mitf^{E318K}$ mutant can reactivate the oncogenic role of BRAF (Bonet et al., 2017).

However, the expression of *MITF* is essential for melanoma tumour cell survival, since it has been shown to control expression of the apoptosis regulator *Bcl2* in melanoma cells (McGill et al., 2002). In fact, the frequency of tumour formation or tumour onset is delayed by months in cell lines that lack *MITF* compared to cell lines that express *MITF* (Hoek, Eichhoff, et al., 2008). In zebrafish, melanomas can be induced by expressing the $BRAF^{V600E}$ mutation together with MITF (Lister et al., 2014). However, using the temperature-sensitive $mitfa^{VC7}$ mutation to turn off MITF activity leads to substantially fewer tumors; while turning MITF off in already formed tumors leads to rapid tumor regression (Lister et al., 2014).

While the role of MITF in melanoma invasion is unclear, it is well established that melanoma tumours and cell lines with extremely low MITF exhibit resistance to current RAF/MEK inhibitors used in the clinic. In BRAF and *NRAS* mutant melanoma cell lines, highly drug resistant cells were characterized as $MITF^{low}/AXL^{high}$ (Muller et al., 2014). Treating these cells with cocktails of AXL inhibitors enhanced melanoma cell elimination (Muller et al., 2014). In line with this, single-cell RNA sequencing data on 4645 single cells isolated from 19 melanoma patients identified distinct populations of tumour cells with $MITF^{low}$ signature that have high *AXL* expression and

another distinct population of cells harbouring high *MITF* expression associated transcriptome signature (Tirosh et al., 2016).

Several studies have identified a drug adaptive resistant state characterized as de-differentiated state with overexpression of the melanoma stem cell marker NGFR (Boiko et al., 2010) and low expression of *MITF* (Fallahi-Sichani et al., 2017; Su et al., 2017). More recently, Rambow et al (2018) applied single cell RNA-seq to malignant melanoma samples derived from patients that were exposed to RAF/MEK inhibition. A distinct neural crest like transcriptional state was identified within melanoma minimal residual disease (MRD), which is the main cause for relapse after drug therapy (Rambow et al., 2018). This drug tolerant neural crest like transcriptional state was driven by RXRG and exihibited loss of *MITF* expression and pigmentation genes (Rambow et al., 2018). Thus, the studies mentioned above establish the link between low levels of *MITF* and the development of adaptive drug resistance. However, the role of MITF in determining the metastatic propensity of melanoma still requires further investigation.

1.4.3 The MITF rheostat model

The plasticity of *MITF* regulation and effects is reconciled in the “MITF rheostat” model. This model links *MITF* expression or activity to cell phenotypes. According to this model, high levels of *MITF* activity promote differentiation whereas intermediate levels of *MITF* promote proliferation and low levels of MITF result in a stem cell like phenotype with enhanced invasion (Carreira et al., 2006; Goding, 2011). The basis of this model came from studies where the metastatic potential of melanoma cells was studied by tuning MITF levels. The rheostat model suggests that changing MITF level in cells will lead to either proliferation or invasion. It is important to note that most of the studies performed above interchangeably discuss expression levels and activity. At present, however, we have no assay for MITF activity so it is a stretch to go from expression to activity.

Hoek and his colleagues proposed a phenotype switch model for explaining the different phenotypes observed. In this model a switch in phenotype was linked to genes which varied greatly between the two types of melanoma cells they observed, namely non- invasive proliferative and invasive cells. Cell lines with high MITF expression exhibited the proliferative phenotype and cells with low MITF expression exhibited an invasive phenotype and gene signature (Hoek, Eichhoff, et al., 2008; Widmer et al., 2012). Increasing evidence shows that MITF can have opposing roles, where depletion of MITF in various melanoma cell lines did not lead to changes in the invasive

phenotype but rather induced a de-differentiated state (Vlckova et al., 2018). While the models above are indeed convenient to describe the switch in phenotype during melanoma progression, they do not tell us whether MITF is really needed for melanoma invasion. Thus, the complex role of MITF in modulating melanoma cell invasion requires further exploration.

1.4.4 EMT in melanoma

Epithelial-to-mesenchymal transition is a reversible biological process that has an essential role during early embryogenesis. This process consists of the transitioning of polarized epithelial cells into mobile mesenchymal cells (Hay, 1995). It is characterized by decreased adhesion to both neighboring epithelial cells and the basement membrane. EMT is triggered by reduced expression of epithelial markers such as E-cadherin and abundant expression of extracellular matrix-related proteins and N-cadherin, leading to the acquisition of a mesenchymal cell state (Eastham et al., 2007; Hay, 1995; Lamouille et al., 2014). This process requires the degradation of the basement membrane by extracellular matrix components secreted by transitioned mesenchymal cells. Eventually this allows mesenchymal cells to migrate away from their original epithelial layer to a new destination (Kalluri & Weinberg, 2009). In fact, melanocytes originate from embryonic neural crest cells through the process of EMT which allows the melanoblast precursors to migrate and invade into their destination site where they settle and differentiate into pigment-producing mature melanocytes (Theveneau & Mayor, 2012). Therefore, melanocytes retain the expression of some EMT markers such as Vimentin, *ZEB2*, and *SLUG* which predisposes melanocytes to gain a high metastatic potential, once they have transformed into melanoma (Gupta et al., 2005). This sinister EMT mechanism is highly exploited in malignant melanoma to gain a high degree of phenotypic plasticity. Consistently, gene expression analysis comparing metastatic and non-metastatic melanoma showed increased expression of N-cadherin and *SPARC* and loss of E-cadherin expression in the course of developing metastasis (Alonso et al., 2007). Indeed, loss of E-cadherin was frequently observed in late stages of development of malignant melanoma towards metastasis (Alexaki et al., 2010; Miller & Mihm, 2006). However, melanoma cells do not go through the classical EMT pathway when they become invasive like since they are not epithelial cells. Instead melanoma cells rather de-differentiate towards their neural crest origin to acquire high motility (Vandamme & Berx, 2014).

1.4.4.1 Transcriptional regulation of EMT in melanoma

The transcription factors SNAIL, SLUG, TWIST and ZEB create the molecular driving force behind the EMT process by repressing the expression of E-cadherin (Batlle et al., 2000; Peinado et al., 2007). Unfortunately, this important developmental process is recapitulated during tumour development where tumour cells gain aberrant expression of the EMT-inducing transcription factors thus allowing them to acquire an invasive phenotype (Thiery, 2002). In melanoma, several EMT-related transcription factors have been reported to drive the invasive de-differentiated state. For example, ZEB1/TWIST1 and ZEB2/SLUG create an opposing expression pattern in different phenotypic states and drive progression of malignant melanoma (Caramel et al., 2013). Caramel et al. (2013) reported that the EMT inducing transcription factors *ZEB2* and *SLUG* are expressed at elevated levels in superficial sites of naevi and primary melanoma. Conversely, ZEB1 and TWIST1 were strongly expressed in deep sites of melanoma and naevi (Caramel et al., 2013). Importantly, reduction of ZEB2 expression has been shown to be associated with poor prognosis in melanoma patients (Denecker et al., 2014). *ZEB2* and *SLUG* were shown to be expressed in melanocytes where they activate expression of MITF which, in turn, drive the cells to a more differentiated and less invasive state (Caramel et al., 2013). Conversely, the expression of *ZEB1* and *TWIST1* was favored in malignant melanoma and resulted in reduced expression of MITF, and poor metastasis-free survival (Caramel et al., 2013). Accordingly, *SLUG* was found to be significantly higher in melanocytes and naevi than in melanoma cells, but *SLUG* expression was not required for melanoma metastasis (Shirley et al., 2012).

1.4.4.2 Signalling pathways regulating EMT in melanoma

Modulation of epithelial to mesenchymal transition is mediated by signalling pathways such as TGFβ, Wnt, Notch and receptor tyrosine kinase pathways (Gonzalez & Medici, 2014). In melanoma, it is well established that MEK-ERK signalling triggered by the *BRAF-NRAS* mutation is the main driver of melanoma progression. A link between EMT and MAPK signalling was reported where MEK inhibition induced expression of *ZEB2* and *SLUG* but led to reduced expression of *ZEB1* and *TWIST1*. In addition, the expression of *ZEB1* and levels of phospho-ERK were positively correlated in malignant melanoma (Caramel et al., 2013). Therefore, the BRAF/NRAS signalling pathway can reprogram the EMT-TF network to drive epithelial-to-mesenchymal transition, ultimately leading to higher metastatic potential (Caramel et al., 2013).

TGFβ signalling is the best studied inducer of epithelial to mesenchymal transition. It consists of the TGFβ ligand and a family of heteromeric serine-threonine kinase receptor proteins which form a complex. The TGFβ ligand induces activation of the receptors leading to the phosphorylation of transcription factors of the Smad family. Activated SMAD complexes translocate into the nucleus and act as transcription factors to regulate expression of target genes (Derynck & Zhang, 2003). In the tumour microenvironment, TGFβ is secreted abundantly by tumour cells to promote metastasis and invasion (Massague, 2008). In melanoma, TGFβ signalling is associated with loss of E-cadherin and increased melanoma metastasis (Alexaki et al., 2010). One of the hallmarks of mobile mesenchymal cells is reorganized F-actin and stress fibres. The activated TGFβ signalling pathway induces GTPases that target the Rho family of proteins which in turn regulate the remodelling of cytoskeletal structures, including the reorganization of F-actin, and this leads to the acquisition of a migratory phenotype (Zavadil & Bottinger, 2005).

It has been reported that TGFβ can repress cell cycle progression through inducing expression of cell cycle inhibitors (*p15, $p21^{CIP1}$, $p27^{KIP1}$ and p57*) in early carcinogenesis (Perrot et al., 2013). It can affect melanocyte differentiation and proliferation by reducing the expression of MITF (Kim et al., 2004; Rodeck et al., 1994). As discussed above, gene expression studies in melanoma cell lines identified two distinct phenotypes: one with high *MITF* expression and a proliferative phenotype and another representing a TGFβ gene signature with low *MITF* expression and an invasive phenotype (Hoek et al., 2006). Therefore, it can be concluded that TGFβ signalling participates in EMT in melanoma by reducing *MITF* expression which in turn drives cells into less proliferative and more de-differentiated cell states.

1.4.5 Cell adhesion

Cell adhesion molecules are important social players in mediating cell-cell recognition and cell-extracellular matrix interactions. In mammals, intercellular (cell-cell) adhesion is mediated by three types of junctions: tight junctions, adherens junctions and desmosomes, whereas focal adhesions modulate cells' interactions with the extracellular matrix (Figure 1). Tumour metastasis is characterized by an alteration in the adhesion preference of cells resulting in attachment and detachment events during the metastatic journey towards distant sites. The initial steps of metastasis start with the breakdown of intercellular adhesion where invasive cells disintegrate from the primary tumour. Invasion of tumour cells requires metastatic cells to form focal adhesion with the extracellular matrix components of the basement membrane in order to migrate and extravagate into distant organs eventually

forming a metastatic niche (Behrens, 1993). Therefore, changes in expression of cell adhesion molecules confer invasive properties to tumour cells and represent a prerequisite for metastatic dissemination.

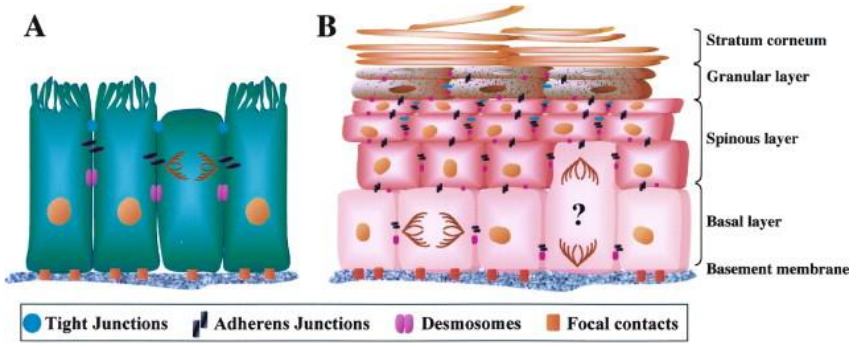

Figure 1. Organization of simple and stratified epithelia.
A. One layer of cells composed of simple epithelia makes contacts with the basement membrane via focal adhesions (orange square) and cell-cell contact via adherens junctions (black rectangles) and desmosomes (pink ovals). Apical-basolateral polarity is mediated by tight junctions (blue circles). **B.** Model of stratified squamous epithelia with four cell layers. Adherens junctions (black rectangles) and desmosomes (pink ovals) attach cells to each other, and integrins in focal contacts (orange squares) attach cells of the basal layer to the basement membrane. Tight junctions (blue circles) are located in the later spinous layers through the granular layer. Reproduced with permission from Elsevier Licence #4450300024676.

1.4.6 Intercellular adhesion

Approximately 90% of cancers arise in epithelial tissues (Weinberg, 2007), which are characterized by a tight association of individual cells through various junctions mediated by adhesion molecules. These cell-cell junctions are part of a large intercellular adhesion complex. Cadherins are the major component of intercellular adhesion, especially of adherence junctions. They are clustered at cell-cell contact sites in most solid tissues (Perez-Moreno et al., 2003; Yagi & Takeichi, 2000). The cadherin family consists of classical cadherins which are the mediators of calcium-dependent cell-cell adhesion (Gumbiner, 1996) and non-classical cadherins, which are desmosomal cadherin and protocadherins which are involved in neuronal plasticity.

E-Cadherins is the prototype of classical calcium dependent cadherins. These are 120 kDa transmembrane glycoproteins, specifically expressed in epithelial cells (Takeichi, 1991). The extracellular domain of classical cadherins contains five ectodomains which allow calcium binding and interact with E-cadherin on the surface of neighbouring cells. Through sequential binding of proteins, the intercellular domain of E-cadherin is linked to the

cytoskeleton and other signalling molecules resulting in the formation of mature adherence junctions (Adams & Nelson, 1998; Yonemura et al., 1995). Thus, E-caderin is the key player in cell-cell adhesion, cell polarity and epithelial cellular architecture. In many cancers, E-cadherin mediated cell-cell adhesion is lost towards malignant transformation. The same is true for melanoma where the loss of E-cadherin is observed in late stages and nodal metastasis (Miller & Mihm, 2006).

1.4.6.1 Focal adhesions

Cell-extracellular matrix adhesion is a key process that allows cells to interact and communicate with the environment (Figure 2). Focal adhesion is a large protein complex in which integrins physically link the extracellular matrix to the actin cytoskeleton of the cell. Adhesions between cell and extracellular matrix and neighbouring cells trigger various responses that have implications for cell fate and behaviour (Giancotti & Ruoslahti, 1999). The focal adhesion sites and their size, morphology and subcellular distribution can be quite heterogeneous. Focal adhesions have a flat elongated structure, several microns in area and are often located at the cell periphery (Izzard & Lochner, 1976; Sastry & Burridge, 2000). In many cells, centrally located adhesions are fibrillar adhesions which are elongated or dot-like structures that consist of extracellular fibronectin fibrils, α5β1 integrin (fibronectin receptor) and tensin (Zamir et al., 1999).

Another group of cell-ECM adhesions are focal complexes or small focal adhesions, which are located at the periphery of migrating or spreading cells. The spreading edge of the cell is known as a lamellipodium and forms in migrating cells. The lamellipodium consists of a branching network of actin filaments, which is extended from the cell periphery like a thin flat sheet; their formation is regulated by Rac and Cdc42, a small GTPases of the Rho family (Nobes & Hall, 1995). These small focal adhesion sites serve as a priming site for mature focal adhesions and their formation is mediated by the Rho GTPase family (Nobes & Hall, 1995; Rottner et al., 1999).

A complex molecular network of focal adhesion components has been identified primarily by immunofluorescence studies in different cell types. More than 50 focal adhesion molecules have been reported (Zamir et al., 1999). The outermost part of focal adhesions are the receptors of integrins which are heterodimeric transmembrane adhesion receptors consisting of α and β subunits. The integrins use their large extracellular domains to interact with extracellular matrix proteins which include fibronectin, collagen, laminins, vitronectin and fibrin (Hynes & Naba, 2012). The types of integrins can differ based on the binding specificity to ECM. For instance, integrins $\alpha_5\beta_1$ are the

classical fibronectin receptors and $\alpha_v\beta_3$ integrins form the vitronectin receptor. In the cytoplasmic region, integrins interact with plaque proteins and bridge them to the actin cytoskeleton. Plaque proteins include vinculin, paxillin, talin and tyrosine-phosphorylated proteins (Liu et al., 2000). Thus, integrins are mechanotransducers of cells that convey extracellular signals into the intercellular compartment, thereby regulating cell motility, cell polarity, cell growth and survival.

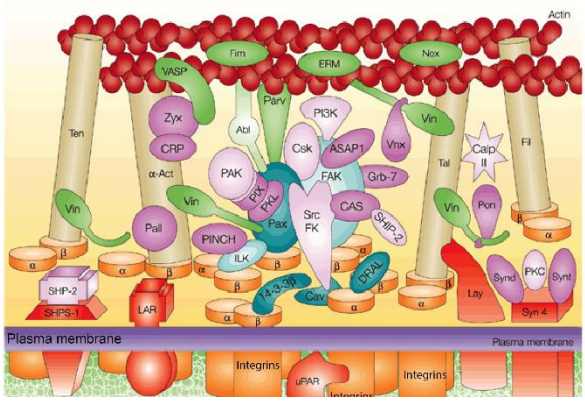

Figure 2. Focal adhesions

Schematic drawing depicting the components of cell-matrix adhesion complexes. Reproduced with permission from Springer nature Licence: 4451880150025.

1.4.6.2 Migration ahead with protrusion and adhesion

Cell migration is a necessary act in a wide variety of living cells. The initial step upon receiving migration inducing signals is to form blebs or protrusions in the direction of migration. These protrusions are broad and large like lamellipodia or spike-like filopodia and formation of these is driven by actin polymerization. The stabilization of protrusions is mediated by focal adhesions formed between the extracellular matrix or neighbouring cells through transmembrane receptors linked to the cytoskeleton. Therefore, cell migration requires signalling cues and reorganization of the cytoskeletal dynamics and cell adhesion (Ridley et al., 2003). A dynamic interplay between actin filaments and focal adhesion sites at the leading edge of cells creates the main traction force for cell migration (Brakebusch & Fassler, 2003). During migration, the adhesion sites need to disassemble rapidly at the rear end of the cells to allow cells to detach and move forward (Geiger et al., 2001). The traction force and signalling cues that are necessary for cell migration are brought by focal adhesions formed between the extracellular matrix and integrins (Miyamoto et al., 1995). One of the key signalling events at focal adhesion sites is tyrosine phosphorylation that requires a stepwise

accumulation of signalling molecules such as FAK, paxillin and tensin (Geiger et al., 2001). Once phosphorylated, signalling molecules activate the Rho family of proteins which will eventually dictate formation of membrane protrusions through conformational changes in the actin cytoskeleton that are essential for cell migration (Miyamoto et al., 1995; Nobes & Hall, 1995; Ren et al., 2000).

1.4.6.3 Focal adhesion kinase

Focal adhesion kinase (FAK) is highly tyrosine phosphorylated protein located at focal contact sites. It is a substrate for the viral Src oncogene that contains SH2 domains, through which it binds to tyrosine phosphorylated proteins and stabilizes protein-protein interactions (Guan et al., 1991; Hanks et al., 1992). FAK signalling promotes cell migration both in normal and tumour cells. However, *FAK* expression is elevated in malignant cancer cells (Cance et al., 2000). In many cancers, FAK signalling triggers changes in cell shape, promotes formation of invadopodia, eventually leading to an invasive phenotype (Hauck et al., 2002; Hsia et al., 2003). A major role of FAK is to mediate focal adhesion turnover and dynamics. However, it has been reported that FAK deficient cells have enlarged focal adhesions. Fibroblasts from FAK null mice show an overabundance of focal adhesions and exhibit defects in cell migration (Ilic et al., 1995).

FAK is a 125-kDa protein composed of an N-terminal FERM (protein 4.1, erzin, radixin and moesin homology) domain (Girault et al., 1999), a central catalytic domain and a C-terminal focal adhesion targeting (FAT) domain. The N-terminal domain interacts with β-integrin *in vitro* (Schaller et al., 1995). The N-terminal FERM domain is therefore important for the interaction of FAK with integrins and growth factors. The C-terminal FAT domain is an essential site for protein-protein interactions (Hildebrand et al., 1993).

Engagement of integrins with the ECM leads to rapid auto-phosphorylation of FAK at Tyr397. This leads to an increased catalytic activity of FAK (Calalb et al., 1995; Toutant et al., 2002). Phosphorylation of FAK at Tyr397 is essential for downstream signalling cascades, because it creates a docking site for the SH2 domain of Src family kinase, growth factor receptor-bound protein-7 (GRB7), p120RasGAP, and phosphatidylinositol 3-kinase (PI3K). FAK binding to Src leads to an activated FAK-SRC complex that procedes to phosphorylation of FAK at Tyr925, which creates a SH2-binding site for GRB2 adaptor protein. The interaction of FAK with GRB2 leads to activation of RAS and the MAPK/ERK2 cascade (Schlaepfer et al., 2004). ERK2 phosphorylation then mediates focal contact dynamics which mitigates the

propagation of survival and proliferative signals inside the cell (Hanks et al., 1992; Ridley et al., 2003).

1.4.6.4 Paxillin

Paxillin is another focal adhesion adaptor protein which serves as a scaffold for recruitment of structural and signalling molecules and is involved in cell migration (Turner et al., 1990). It contains protein-protein interaction motifs including LD (leucine-rich peptide region) motifs, SH2 and SH3 binding domains, and LIM binding domains (Brown et al., 1998). It does not have catalytic activity but coordinates various downstream signals by acting as a docking site for tyrosine/threonine kinase and GTPases activating proteins. In fact, FAK binds to the LD motif of Paxillin through its FAT domain and triggers tyrosine phosphorylation of paxillin (Schlaepfer et al., 1999). Phosphorylation of paxillin at Tyr31 and Tyr118 by the FAK-SRC complex has been shown to promote focal adhesion disassembly and is therefore important for focal adhesion turnover (Webb et al., 2004). High expression of phosphorylated paxillin has been implicated in several metastatic cancers and is correlated with EMT. In fact, phosphorylation of paxillin can indicate metastasis. Phosphorylation of paxillin at Tyr118 and Ser178 by FAK reorganizes focal adhesions and promotes cell motility in cancers (Devreotes & Horwitz, 2015).

1.4.6.5 Rho family – membrane protrusions

The Rho family of small GTPases is an important regulator of focal adhesions and formation of lamellipodia and filopodia (Nobes & Hall, 1994). The mammalian Rho GTPases comprise a family of 20 intercellular signalling molecules; the best studied members are Rho, RAC and CDC42. They all contribute to cell migration in living ogranisms. They are activated when they are bound to GTP and trigger downstream signalling necessary for cytoskeletal dynamics, morphogenesis, and migration. The switch from an inactive GDP bound state to an active GTP bound state is regulated by guanine nucleotide-exchange factors (GEFs), and inactivated by GTPase-activating protein (GAPs) (Heasman & Ridley, 2008). Actin polymerization in the lamellipodia is mediated by the Arp2/3 complex, which initiates the formation of new actin filaments through binding to pre-existing actin filaments (Goley & Welch, 2006). The activation of the Arp2/3 complex is mediated by related WASP/WAVE complex localized at the plasma membrane. RAC and CDC42 stimulate activation of the WASP/WAVE complex (Cory & Ridley, 2002; Welch & Mullins, 2002). Cell polarity is important in migrating cells, and CDC42 controls the directionality of

migration. Active Cdc42 is present at the leading edge of migrating cells (Smirnova et al., 1998) and loss of CDC42 has been reported to disrupt cell polarity (Etienne-Manneville & Hall, 2002)..

1.5 Epigenetic regulation

1.5.1 Histone modifications

Control of the transcription is maintained by a dynamic interplay between transcription factors and chromatin in the cell nucleus. Chromatin is a highly dynamic complex. Through its organization and modification it modulates gene expression in different cell states. The main component of the chromatin that is subjected to covalent modifications are the histones. The core histones are composed of Histone 2A (H2A), Histone 2B (H2B), Histone 3 (H3) and Histone 4 (H4), and are grouped into two H2.A-H2.B dimers and one H3-H4 tetramer. This histone octamer is wrapped by a stretch of 147-bp DNA segment to form nucleosomes. Histone H1 serves as a linker for the next nucleosome.The nucleosome is further packaged into 30-nm fibers with six nucleosomes per turn in a spiral arrangement (Kornberg & Lorch, 1999). All histones are subjected to post-translational modifications at their tails which dictate effects on gene expression, not only via shaping chromatin structure but also through recruiting factors to manipulate the DNA (Kouzarides, 2007). Chromatin can be broadly divided into two categories, namely eurochromatin which is an easily accessible active state, and a silent heterochromatin which is unaccessible to transcription factors. Each of these states are tightly associated with distinct sets of histone modifications.

Heterochromatin is characterized by low levels of acetylation and high levels of methylated sites such as H3K9, H3K27 and H4K20. Euchromatin is associated with high levels of acetylation and trimethylation at H3K4, H3K36 and H3K79. In addition, actively transcribed genes have H3K4me3, H3K27ac, H2BK5ac and H4K20me1 modified chromatin in their promoters (Li et al., 2007). Covalent modifications of histones are added or removed by enzymes often termed as “writers” and “erasers” which include methytransferases, histone demethylases and kinases, histone acetyltransferases (HATs) and histone deacetylases (HDACs) (Kouzarides, 2007).

1.5.2 SETDB2 – a histone 3 lysine 9 methyltransferase

The histone modifier SETDB2 (Suvar 3-9-enhancer-of-zeste-trithorax (SET) domain bifurcated 2) is a protein lysine methyltransferase (PKMT). *SETDB2* belongs to the SUV39 family that shares a SET domain with its family members. This SET domain transfers methyl residues from *S*-adenosyl-L-methionine to the amino group of a target lysine residues on histone and in

turn catalyses the reaction of histone H3 Lys9 (Dillon et al., 2005). SETDB1, implicated in viral gene silencing and onset of melanoma (Ceol et al., 2011; Matsui et al., 2010) is the family member closest to SETDB2.

Overexpression of *SETDB2* is found in primary gastric cancer compared to normal tissues, suggesting an oncogenic role (Nishikawaji et al., 2016). Depletion of *SETDB2* resulted in reduced cell proliferation, migration and invasion. The change in phenotype was explained by global reduction in H3K9 methylation, thereby affecting the gene expression profile of tumour suppressor genes which contribute to the progression of gastric cancers (Nishikawaji et al., 2016). However, Lin et al. (2018) showed that suppression of SETDB2 did not affect global H3K9me3 levels in lymphoblastic leukemia cells, suggesting that SETDB2 directed methylation is target specific (Lin et al., 2018). In lymphoblastic leukemia, SETDB2 is regulated by E2A-PBX1, a fusion protein which acts as a chimeric transcription factor involved in genomically distinct type of acute lymphoblastic leukemia (Nourse et al., 1990). Lin et al (2018) reported that SETDB2 directly mediates chromatin suppression of *CDKN2C*. Hence, the suppression of SETDB2 sentitized ALL to kinases and epigenetic inhibitors (Lin et al., 2018).

Furthermore, SETDB2 has been reported to play a role in regulating virus-induced susceptibility to superinfection, as its expression is regulated by type I interferon (Schliehe et al., 2015). Infection with pathogens induces the activation of type I interferon which is regulated by interferon regularoty factors (IRFs) or by the activation of nuclear factor kappa B (NF-κB) signalling (Taniguchi et al., 2001). Upon infection, NF-κB translocates to the nucleus and activates the expression of genes responsible for the pro-inflamatory response (Oeckinghaus & Ghosh, 2009). Gene expression profiling of bone marrow-derived macrophages (BMDMs) from mice with a hypomorphic gene-trap construct of Setdb2 revealed that Setdb2 negatively regulates NFκB target genes (Schliehe et al., 2015). In particular, Setdb2 occupied and repressed the *Cxcl1* promoter, a key chemoattractant for neutrophils (Navarini et al., 2006). Thus, SETDB2 plays a role in the innate immune response to virus infections and represses expression of NF-κB target genes (Schliehe et al., 2015).

1.5.3 PRDM7 – PR domain-containing protein 7

PRDM7 is a histone methyltransferase that catalyses the trimethylation of H3 lysine 4 (H3K4) both *in vitro* and *in vivo* (Blazer et al., 2016). It belongs to the PRDI-BF1 and RIZ homology domain (PRDM) family of proteins and is one of 17 proteins in this family. They all share a conserved N-terminal PR domain. The PR domain is closely related to another histone methyltransferase family

of Su(var)3-9, enhancer of zeste and trithorax (SET) domains of histone methyltransferases (Huang et al., 1998). The SET domain is responsible for the catalytic activity of the methyltransferase (Jenuwein, 2001). *PRDM7* originated from a tandem duplication of exon3 of *PRDM9*, which led to the acquisition of various new splicing sites that conferred primate-specific features to PRDM7 (Fumasoni et al., 2007). Interestingly, it has been reported that *PRDM7* expression is restricted to the melanocytic lineage (Fumasoni et al., 2007). In addition, enriched expression of *PRDM7* has been reported in the cochlea when compared to the utricle, indicating that PRDM7 might play a role in the inner ear (Hawkins et al., 2003).

1.6 Interferon regulatory factor 4 (IRF4)

IRF4, previously known as PIP (PU.1 interacting partner), was discovered by Eisenbeis and colleagues in myeloma cells (Eisenbeis et al., 1995). PIP and PU.1 synergistically activated transcription of composite elements from the immunoglobulin light chain enhancers (Eisenbeis et al., 1995). At the same time, IRF4 was cloned from mouse spleen by the Matsuyama group and was called lymphoid-specific interferon regulatory factor (LSIRF) (Matsuyama et al., 1995). They reported that the expression of LSIRF is induced by antigen recognition or IgM crosslinking but not by type I or type II interferons. DNA binding assays revealed that LSIRF binds to interferon stimulated response element (ISRE) containing the core motif (GAAAGTGAAAC) from the major histocompatibility complex (MHC) class I gene promoters (Matsuyama et al., 1995). Thus, LSIRF enhanced the expression of interferons (IFNs) through binding to response elements in the mouse genome. Later, the human homolog of PIP/LSIRF cDNA was cloned, encoding a 450 amino acid protein with a molecular weight of 51.6 kDa. It was mapped to chromosome location 6p23-p25 (Grossman et al., 1996; Yamagata et al., 1996). Interestingly, LSIRF was found to be expressed in the melanoma cell line G361 as well as in normal melanocytes (Grossman et al., 1996). Later, PIP/LSIRF was renamed interferon regulatory factor 4 (IRF4). The IRF family members, including IRF4, have highly similar DNA binding domains that contain five conserved tryptophan residues in the N-terminus. IRF4 has a couple of transcriptional activation domains including one that is rich in proline (amino acids 151-237), and another glutamine-rich domain (354-419) at the C-terminus. However, IRF4 binding to DNA is weak due to the presence of a putative alpha-helix inhibitory domain in the carboxy-terminal segment (residues 399-413), which causes auto-inhibition upon DNA binding (Brass et al., 1996). Nevertheless, this inhibition is overcome by an interaction between

the inhibitory domain of IRF4 and a phosphorylated (Tyr148) PEST region of PU.1. Together, IRF4/PU.1 cooperatively binds to composite elements found in promoters and enhancers of lymphoid and myeloid genes (Brass et al., 1996; Brass et al., 1999; Eisenbeis et al., 1995).

1.6.1 IRF4 in pigmentation

IRF4 expression is not only expressed in the immune cell lineage but is also expressed in skin melanocytes and melanoma cells (Grossman et al., 1996). A genome wide association study reported two SNPs (rs4959270, rs1540771) located between *IRF4* and *EXOC2* to be associated with freckling in Icelandic and Dutch samples. The A allele of rs1540771 showed an association to brown hair and sensitivity of skin to UV radiation. The frequency of this allele was shown to be highest in European populations (Sulem et al., 2007). Another independent GWAS study conducted on 10,000 individuals of European ancestry from the United States and Australia identified a SNP (rs12203592) in the intron 4 of IRF4 which showed the strongest association with hair colour (p=7.46x10^{-127}), skin colour (p=6.2x10^{-14}), eye colour (p=6.1x10^{-13}) and skin tanning response (p=3.9x10^{-89}) (Han et al., 2008). In fact, the rs12203592 SNP is located within 69.7 kb of the two other SNPs mapped in the Sulem study (rs4959270, rs140771), and shows 13 orders of magnitude smaller p-value with association to natural hair colour than the other SNPs. Consistent with the above-mentioned studies, a web-based approach study utilizing a database containing self-reported phenotypes, together with SNP genotypes, reported that the SNPs near IRF4 showed the strongest association to freckling, tanning response and blue/light eye colour (Eriksson et al., 2010). In addition, a follow-up study confirmed the association of this locus with skin colouration in Europeans (Liu et al., 2015).

A GWAS study on nevus count in Australian adolescent twins reported that the rs12203592 T allele was associated with high nevus counts and high freckling in adolescents but low nevus count and high freckling in adults (Duffy et al., 2010). Subsequently, the region where SNP rs12203592 is in the intron 4 of *IRF4* was described as a melanocyte-specific enhancer region. The presence of the T allele was shown to reduce the enhancer activity of this regulatory region (Praetorius et al., 2013). This elegant study showed the cooperative binding of the transcription factors TFAP2α and MITF to intron 4 of *IRF4*; the TFAP2α binding site overlapped with rs12203592. This mutual binding resulted in the enhanced expression of *IRF4*, indicating that this SNP acts as an intronic enhancer for *IRF4* expression. Followed by this, IRF4 and MITF collectively bind to the promoter region and increase the expression of tyrosinase, an enzyme required for production of the pigment melanin

(Praetorius et al., 2013). The rs12203592 SNP is also associated with rosacea, an immuno-inflammatory skin disease, (Aponte et al., 2018).

1.6.2 IRF4 in melanoma

IRF4 expression in melanoma was initially described by Grossman et al. in the G361 melanoma cell line (Grossman et al., 1996). Subsequently, a microarray study conducted on 1331 human malignancies and normal tissues showed *IRF4* expression uniquely present in malignant melanomas in addition to hematolymphoid neoplasms (Natkunam et al., 2001). IRF4 expression was interrogated in 61 melanocytic lesions which showed presence of IRF4 expression in 92% (33/36) of melanomas, of which 21/22 (95%) were primary melanomas and 12/14 (86%) were metastatic melanomas.

As discussed above several GWAS studies identified SNPs located near *IRF4* to be associated with fair skin, blue eye colour and poor tanning ability. Fair skin increases the risk for cutaneous melanoma and basal cell carcinoma. In fact, melanoma rates differ 50-fold between fair skinned and dark skinned individuals (Bliss et al., 1995). In addition, an increased number of nevi results in an increase in the risk for melanoma by 2% - 4% for every additional nevus counted (Chang et al., 2009). In a case control study from Australia, the *IRF4* rs12203592*C allele was associated with increased risk for melanoma (odds ratio=1.15, $p=4x10^{-3}$), most significantly on the trunk (odds ratio=1.33, $p=2.5x10^{-5}$). In addition, rs12203592*C was associated with increased nevus counts in adults, but the rs12203592*T allele was associated with increased flat nevi only in adolescents and decreased numbers of raised nevi (Duffy et al., 2010).

Later, rs12203592*T was associated with an increased risk of developing melanoma as well as non-melanoma skin cancers (Zhang et al., 2013). In addition, *IRF4* rs12203592*T increased the risk of dying from melanoma in two independent patient sets (Potrony et al., 2017). Furthermore, IRF4 rs12203592*T is associated with increased Breslow thickness in melanoma, the best prognostic feature for melanoma patients (Gibbs et al., 2017). Apart from melanoma, the rs12203592 SNP was associated with basal cell carcinoma and cutaneous carcinoma (Barrett et al., 2011; Chahal et al., 2016; Han et al., 2011).

1.6.3 IRF4 in immune cells

IRF4 is a key regulator of various biological processes in lymphoid, myeloid and dendritic cell maturation and differentiation. *IRF4* expression is required for lymphocyte activation and differentiation and is essential for both mature B and T cell homeostasis (Bollig et al., 2012; Man et al., 2017; Man et al.,

2013). IRF4 deficient mice display a lack of germinal centres in B cell follicles of spleen and lymph nodes, in addition to a lack of plasma cells and no antibody production (Mittrucker et al., 1997). In addition, IRF4 deficient T cells did not generate cytotoxic responses (Man et al., 2017; Mittrucker et al., 1997). No pigment phenotypes were reported in Irf4 homozygous mutant mice (Mittrucker et al., 1997). Interestingly, however, when the Irf4 homozygotes also carryed the $Mitf^{Mitf\text{-}white}$ allele, further dilution of the gray coat of $Mitf^{Mitf\text{-}white/+}$ was observed (Praetorius et al., 2013), suggesting that Irf4 is indeed important for pigmentation.

In B cell development, IRF4 is expressed in immature B cells, absent in the germinal centre, and then re-expressed in plasma cells. Interestingly, MITF has been shown to repress IRF4 expression in the germinal center (Lin et al., 2004). In response to antigen recognition, mature B cells interact with follicular helper T cells in the germinal centres, where B cells will differentiate into antibody secreting plasma cells and memory B cells (MacLennan, 1994). This process is called germinal centre reaction where antigen activated B cells undergo clonal expansion and modify their immunoglobulins through somatic hypermutation and class-switch recombination. The role of IRF4 in GC was studied in mice with conditional deletion of *Irf4* in germinal centre B cells. This showed that IRF4 is required for plasma cell formation and class switch recombination. IRF4 activates B lymphocyte-induced maturation protein 1 (Blimp1) and together they can activate Xbp1, all of which are essential for plasma cell development (Klein et al., 2006). In addition, Irf4 and Blimp1 have been shown to control the differentiation and function of regulatory T cells (Cretney et al., 2011). Expression of IRF4 is essential for the development of a subset of $CD4^+$ T helper cells (Staudt et al., 2010). In response to bacterial and viral infections, IRF4 deficient mice fail to mount a productive $CD8^+$ T cell response, and IRF4 is further required for clonal expansion of $CD8^+$ T cells. The expression of IRF4 has been linked to T cell receptor stimulation intensity via mTOR regulation, where inhibition of mTOR reduced IRF4 expression. In addition, IRF4 regulates the expression of genes involved in aerobic glycolysis and metabolic programming in $CD8^+$ T cells (Man et al., 2013).

1.6.4 IRF4 in hematolymphoid malignancies

1.6.4.1 IRF4 in multiple myeloma

Multiple myeloma is a malignancy of plasma cells, which arises from post germinal center B cells. It is characterized by an infiltration of malignant

plasma cells to the bone marrow, excess amount of monoclonal protein present in serum or urine, and osteolytic lesions. *IRF4* is highly expressed in B cells and plasma cells where it controls the differentiation of B cells to antibody producing plasma cells. The chromosomal translocation t(6;14)(p25;q32) which transcloates the IgH promoter to the IRF4 locus and in turn results in the overexpression of the *IRF4* gene and protein which leads to tumorigenesis in multiple myeloma (Iida et al., 1997). Furthermore, this IgH-mediated expression of *IRF4* is associated with a poor survival rate and prognosis (Heintel et al., 2008).

Shaffer et al. (2009) used shRNA against IRF4 in myeloma and lymphoma cell lines to investigate effects on proliferation and cell survival. They showed that depletion of IRF4 resulted in cell death within 3 days only in myeloma cell lines but not lymphoma cells. Gene expression profiling after induction of shIRF4 showed that IRF4 targets consist of a large set of genes that are more highly expressed in primary myeloma samples than in normal mature B cells. Moreover, chromatin immunopercipitation analysis uncovered direct IRF4 targets, namely genes involved in metabolic control, membrane biogenesis, cell cycle progression, cell death and transcriptional regulation and plasmatic differentiation (Shaffer et al., 2009). In addtion, IRF4 and MYC form a positive autoregulatory loop, where IRF4 can directly transactivate the MYC promoter and depletion of IRF4 leads to repression of *MYC* mRNA. MYC is another important factor implicated in the pathogenesis of multiple myeloma (Shou et al., 2000). Importantly, IRF4 targets have a high proportion of genes transactivated by MYC, suggesting that these transcription factors work co-operatively to target the same subset of genes (Shaffer et al., 2009).

1.6.4.2 B-cell lymphomas

The most common subtype of lymphoma is diffuse large B-cell lymphomas (DLBCL) and follicular lymphoma, both of which originate from germinal center derived B cells (Salaverria et al., 2011). Overexpression of the *IRF4* protein as a result of the t(6;14)(p25;q32) translocation is detected also in DLBCL (Tsuboi et al., 2000). One of the transcriptional targets of IRF4 was identified as a monokine induced by interferon gamma (MIG). Treating cells with neutralzing antibody against MIG slowed down the proliferation of two B-CLL cell lines tested (Uranishi et al., 2005). Microarray analysis reported that high expression of *IRF4* is clustered with a subset of DLBCL that is associated with worse prognosis (Alizadeh et al., 2000). Overexpression of *IRF4* is a hallmark of DLBCL, and *IRF4* is a direct target of NF-κB. Furthermore, the majority of DLBCL exhibits constitutive NF-κB activity (Davis et al., 2001; Rui et al., 2011). Overexpression of *IRF4* driven by the

IgH/IRF4 fusion has been identified in young adults and paediatric DLBCL as well as in follicular lymphoma (Salaverria et al., 2011). Similar to the multiple myeloma cells, the efficient knockdown of IRF4 in DLBCL resulted in cell death. This further confirmed the addiction of B cell malignancies to *IRF4* (Shaffer et al., 2009).

1.6.4.3 IRF4 and other haematological malignancies

Overexpression of *IRF4* is found in T cell lymphomas, chronic lymphocytic leukemia (CLL) and Hodgkin lymphoma cases. A SNP in the 3'-unstranslated region of *IRF4* is strongly associated with a risk of CLL (Di Bernardo et al., 2008). In addition, high expression of *IRF4* is found in CLL and associated with unfavourable disease outcome (Chang et al., 2002). In childhood acute lymphoblastic leukemia, expression of *IRF4* was observed in a subset of a more mature cell population from a patient (Do et al., 2010). Moreover, the intronic SNP rs12203590 in *IRF4* has been associated with ALL in males (Do et al., 2010).

A chromosome translocation between *IRF4* and the T-cell receptor-alpha (TCRA) locus t(6;14)(p25;q11.2) has been identified in peripheral T-cell lymphomas (PTCLs) and anaplastic large-cell lymphomas (ALCLs). PTCLs are malignant neoplasms of mature peripheral T lymphocytes, and make up 10% of non-Hodgkin lymphomas (Feldman et al., 2009).

1.7 Transcription factor EB - TFEB

TFEB is one of the MiT transcription factors and is the most related to MITF of all bHLH-Zip proteins. The MiT transcription factor family is comprised of four family members: MITF, TFE3, TFEC and TFEB. All MiT family members, including TFEB, can bind to the palindromic CACGTG E-box sequence as a homodimer or heterodimer (Hemesath et al., 1994). The human TFEB gene was isolated based on its ability to recognize E-box sequences in the heavy-chain immunoglobulin enhancer (Carr & Sharp, 1990). Mice carrying a *Tfeb* null mutation die at embroyonic day 9.5-10.5 because of placental defects (Steingrimsson et al., 1998). This is due to the absence of vasculature formation that was traced to the effects of *Tfeb* on *Vefg* expression, a potent mitogen implicated in normal vasculogenes. Recently, it has been shown that *Tfeb* regulates endodermal specification during embryogenesis (Young et al., 2016).

The transcriptional activity of TFEB is strictly regulated through posttranslational modifications, and cellular localization is controlled by its phosphorylation status. Phosphorylation of TFEB at Ser142 and Ser211 is crucial for nuclear localization and when these two sites are mutated, TFEB

is retained in the cytoplasm (Martina et al., 2012; Roczniak-Ferguson et al., 2012; Settembre et al., 2012). Under nutrient rich conditions, TFEB is cytoplasmic, but upon the induction of stress, such as starvation, TFEB translocates into the nucleus where it regulates the expression of its target genes (Sardiello et al., 2009; Settembre et al., 2012).

1.7.1 TFEB is at the center of autophagy and lysosome function

TFEB has been described as a master regulator of autophagy, an essential biological process needed for the maintenance of cellular homeostasis. The autophagy process involves the sequesteration of a double-membrane structure called the autophagasome to the cytoplasm (Ogata et al., 2006). The autophagosome then fuses with the lysosomal membrane to traffick the materials into the autolysosome (Huynh et al., 2007). The degradation process is facilitated by lysosomal digestive enzymes. After this, the different breakdown products, including amino acids, lipids and nucleosides are released into the cytosol for their re-use in metabolic pathways. Therefore, lysosomes are crucial organelles that take part in recycling processes, including endocytosis, autophagy and lysosomal exocytosis.

Interestingly, *in silico* analysis of the promoters of lysosomal genes identified a 10-basepair motif, highly similar to the E-box motif with an additional flanking T/A both at 3´ and 5´ end (5´-TCACGTGA-3´). The sequence was named coordinated lysosomal expression and regulation (CLEAR) motif. Genome-wide mapping of TFEB targets using ChIP-sequencing revealed that TFEB binds to CLEAR motifs in order to activate the expression of genes involved in the CLEAR network (Palmieri et al., 2011). Enhanced lysosomal catabolic activity was observed upon overexpression of *TFEB* as evidenced by an increased number of lysosomes and higher level of lysosomal enyzmes (Sardiello et al., 2009). TFEB is not limited to regulating only genes involved in lysosomal biogenesis. It also controls the regulation of genes involved in autophagy and lysosomal exocytosis, in which lysosomes fuse with the plasma membrane and empty their content to the extracellular space (Medina et al., 2011; Palmieri et al., 2011). Consistent with that, *TFEB* overexpression promotes degradation of long-lived proteins which indicates enhanced autophagic flux (Settembre et al., 2011). Interestingly, TFEB has been shown to regulate lipophagy, where the absence of TFEB impaired lipid catabolism and overexpression of TFEB rescued obesity and resulted in a metabolic syndrome (Settembre et al., 2013). Furthermore, TFEB regulates various genes involved in lipid catabolism, among which is *PGC1α*. During starvation, PGC1α regulates lipid metabolism in the liver via the downstream nuclear receptor peroxisome proliferator activated receptor alpha (PPARα) (Finck & Kelly, 2006).

In order to transcriptionally regulate genes responsible for the autophagy process, TFEB has to translocate into the nucleus. Several pathways, including MAPK, mTOR and lysosome calcium signalling, have been implicated in the de-phosphorylation of TFEB in response to cellular stress signals. Starvation induced autophagy is negatively regulated by mammalian target of rapamycin complex 1 (mTORC1), a serine/threonine protein kinase. mTORC1 responds to numerous cellular stresses such as nutrient, energy and oxygen levels, thereby maintaining the appropriate balance between anabolic and catabolic processes. The anabolic processes include macromolecule synthesis and nutrient storage, and catabolic processes are autophagy and energy consumption (Sengupta et al., 2010). The mTORC1 complex is localized at the cytoplasmic surface of the lysosome (Sancak et al., 2010). This enables mTORC1 to integrate signals which arise from cellular stress and nutrient status to control a wide variety of cellular pathways, including cell growth and repression of autophagy (Ma & Blenis, 2009).

Under nutrient rich conditions, mTORC1 phosphorylates TFEB at position Ser211 preventing it from translocating into the nucleus and activate autophagy response genes (Roczniak-Ferguson et al., 2012). The phosphorylation of TFEB at Ser211 has been shown to create a docking site for the chaperone 14-3-3, which promotes cytoplasmic retention of TFEB. In fact, the nuclear localization signal of TFEB is located between amino acids 241-252. Binding of the 14-3-3 chaperone to TFEB near S211 blocks the NLS, thereby preventing nuclear localization of TFEB (Roczniak-Ferguson et al., 2012). The MAPK pathway is involved in phosphorylating TFEB. It has been shown that the MAPK pathway phosphorylates TFEB at S142 and siRNA-mediated knockdown of ERK1/ERK2 inhibits phosphorylation at S142 and leads to nuclear accumulation of TFEB (Roczniak-Ferguson et al., 2012). In addition to this, TFEB can be dephosphorylated by the phosphatase calcineurin, which is activated via mucolipin 1 (MCOLN1) in response to lysosomal Ca^{2+} release (Medina et al., 2015). Therefore, in response to variouse stress stimuli, TFEB shuttles to the nucleus thereby enhancing the transcription of genes essential for the autophagy process.

1.7.2 TFEB function in different tissues

Several tissue-specific functions of TFEB have been reported, ranging from mediating osteoclast function in bone resorption to mitigating the immune response (Napolitano & Ballabio, 2016). Constant remodelling of bone is carried out by specialized cells called osteoblasts and osteoclasts. Osteoblasts are responsible for synthesizing and mineralizing the bone extracellular matrix, whereas osteoclasts resorb the mineralized ECM (Ducy

et al., 2000; Teitelbaum, 2000). To make this happen, osteoclasts attach to the bone surface and generate closed resorption lacunae which are characterized by an acidic pH around 4.5. The acidity of lacunae is determined by the presence of numerous proteases that are exported by lysosomes in the osteoclasts (Coxon & Taylor, 2008). TFE3 and MITF, close family members of TFEB, have been reported to be important for the differentiation of osteoclasts, where loss of these factors resulted in osteopetrosis in mice (Steingrimsson et al., 2002). Accordingly, TFEB function was also described to be important in osteoclasts, where TFEB activity is mediated by RANKL, a key regulator of osteoclast differentiation. RANKL treatment leads to the acculmuation of TFEB, which in turn activates the expression of lysosomal genes. The accumulation of TFEB is achieved through stabilization of TFEB through PKCβ phosphorylation at sites S461 and S462 or of S465 and S466 (Ferron et al., 2013).

Autophagy can be activated through pathogen-induced cell stress or nutrient deprivation caused by invading bacteria or virus (Deretic et al., 2013). The role of TFEB in the immune system came from studying the role of the TFEB ortholog HLH-30 in *C.elegans*, where HLH-30 KO worms are more susceptible to death following infection. Upon infection of worms, HLH-30 was translocated to the nucleus, and transcriptomic analysis revealed that HLH-30 is responsible for regulating the expression of 80% of genes involved in the immune response. In mammals, knockdown of *TFEB* in macrophages reduced the expression of several cytokines and chemokines after infection, suggesting that TFEB controls a subset of immune genes in these mammalian cells (Visvikis et al., 2014). LPS treatment of macrophages led to induced translocation of TFEB and TFE3 into the nucleus, and depletion of these factors resulted in decreased expression of several immune genes (*CSF2, IL-1β, IL-2, IL-27, CCL2*) (Pastore et al., 2016). Moreover, ChIP-seq analysis of TFE3 revealed that this protein binds to 85 immune genes that contain CLEAR sequences within 5 kb of the transcription start site. Most likely, TFEB also participates in activating these genes (Pastore et al., 2016). This suggests that these two factors have overlapping functions in regulating the innate immune response. In addition to this, TFEB is involved in antigen presentation in dendritic cells. In dendritic cells, lysosomal activity is crucial for antigen internalization and presentation to T cells (Honey & Rudensky, 2003; Lin et al., 2008). Overexpression of *TFEB* resulted in an increase in MHC class II presentation. In the absence of TFEB, phagosome acidification was impaired in dendritic cells (Samie & Cresswell, 2015). Thus, TFEB plays a role in mediating innate immunity through direct transcriptional regulation of genes and enhanced transcription of lysosomal and autophagy genes upon infection and phagocytosis (Nabar & Kehrl, 2017).

1.7.3 TFEB in tumourgensis

1.7.3.1 TFEB in renal cell carcinoma

Chromosomal rearrangements involving TFEB have been found in renal cell carcinoma (RCC). This cancer originates from the renal tubular epithelium and includes multiple heterogeneous cancer types. The most common types are clear cell, papillary and chromophobe types of renal cancer (Amin et al., 2002). The recurrent chromosomal translocation t(6;11)(p21;q13) results in a fusion of TFEB with MALAT1, and this TFEB-MALTA1 fusion can translocate to the nucleus (Kuiper et al., 2003). The rearrangement preserves the whole coding sequence of *TFEB*, in which MALAT1 is rearranged to just upstream of the *TFEB* initiation codon ATG in the first exon of the gene (Davis et al., 2003). Consequently, this fusion leads to a dramatic overexpression of *TFEB* in cells (Kuiper et al., 2003). Hence, enhanced expression of TFEB would affect the dynamic interaction between other MiT/TFE transcription factors, and potentially alter target selection of TFEB which ultimately gives rise to different disease outcomes, for better or worse. The *TFEB* and *MALAT1* fusion is not very common but predominantly occurs in younger patients (Inamura et al., 2012). However, the mechanistic function of this fusion protein in the course of RCC progression is not well studied.

1.7.3.2 TFEB in pancreatic cancer

Pancreatic cancer is highly lethal and is usually diagnosed in advanced stages, thus resulting in low survival (Hezel et al., 2006). High demand for autophagy is one of the characteristics of pancreatic cancers. Accordingly, inhibition of autophagy can drive growth suppression and tumour regression (Yang et al., 2011). As discussed above, TFEB plays a critical role in regulating autophagy. Hence, in pancreatic cancer, TFEB supplies the need for a high level of autophagy. In ductal pancreatic cancer, it has been reported that along with TFEB, TFE3 contributes to disease progression, where nuclear translocation of these factors is enhanced. This is followed by an increased expression of lysosomal genes that are essential for survival and growth of pancreatic ductal carcinoma (Perera et al., 2015). Reducing the level of MITF, TFEB and TFE3 utilizing siRNA significantly inhibits growth of pancreatic ductal carcinoma, indicating that the cooperative activity of TFEB with MITF and TFE3 is important for metabolic reprogramming in pancreatic ductal cancer (Perera et al., 2015)

2 Aims

2.1 Characterization of SkMel28 melanoma cell that lack MITF

i. Phenotypic and functional characterization of SkMel28 MITF knock out cells.

ii. Analyse transcriptome profile of MITF knock out cells to understand underlying mechanism for the resulting phenotypic changes.

2.2 Analysis of the transcription network involving MITF, TFEB and IRF4

i. To perform Chromatin immunopercipitation coupled sequencing to identify genome wide binding sites of TFEB and IRF4

ii. Identify the overlap in genome wide binding sites between MITF, IRF4 and TFEB.

3 Materials and methods

3.1 Cell cuture

Cell lines were cultured in 5% CO_2 at 37ºC in RPMI 1640 medium (#52400-25, Gibco) supplemented with 10% FBS (#10270-106, Gibco). The 501Mel cell line was a gift from Ruth Halaban, the LU1205 cell line was a kind gift from Lionel Larue/Meenhard Herlyn and the SkMel28 cell line was purchased from ATCC (HTB-72).

3.2 Generation of MITF knock out cell lines

In order to generate knock out mutations in the MITF gene, the CRISPR-Cas9 technology was used. The guide RNAs (gRNAs) used are listed in Table 1 and were designed to target exons 2 and 6 of MITF respectively. Then gRNAs were cloned into gRNA expression vector (Addgene plasmid #43860) using BsmBI restriction digestion. For this, we used SkMel28 human melanoma cell lines, transfected with gRNAs expression vectors and Cas9 vector a gift from Keith Joung. For transfection, the Fugene® HD transfection reagent (#E2312 from Promega) was used at a 1:2.8 ratio of DNA:Fugene. After transfection, the cells were treated 3 days with final contration of 3µg/ml Blasticidin S (stock 2.5mg/ml) for selection and then serially diluted to generate single cell clones. As a result, we obtained ΔMITF-X2 cell line from targeting exon 2 of MITF and ΔMITF-X6 cell line from targeting exon 6. The respective control cell line, termed EV-SKmel28, was generated by transfecting the cells with empty vector Cas9 plasmid.

Table 1: Guide RNAs used for targeting exons 2 and 6 of MITF

Target	Primer name	Sequence
Exon2	Exon2-gRNA	AGTACCACATACAGCAAGCC
Exon6	Exon6-gRNA	AGAGTCTGAAGCAAGAGCAC

3.3 Sanger sequencing preparation

Genomic DNA was isolated from the MITF knock out cell lines with following procedures: (i) first cells (~ 2 x 10^5) were trypsinized and spun down, supernatant was removed. Then cell pellete was resuspended in 25 µL of PBS. (ii) 250 µL Tail buffer (50mM Tris pH8, 100 mM NaCl, 100 mM EDTA, 1% SDS) with 2.5 µL of Protinase K (stock 20 mg/mL) was added to cell suspension in PBS then incubated at 56ºC overnight. (iii) After 50 µL of 5M

NaCI was added and mixed on shaker for 5 minutes and spun at full speed for 5 minutes at room temperature. (iv) Supernatent then transferred into new tube containing 300 µL isopropanol, mixed by inversion, then spun for 5 minutes at full speed. Resulting pellet washed with 70% Ethanol and pellets were air dried at room temperature. Finally, the dried pellet was dissolved in nuclease free water at least 2 hours at 37 ºC. After appropriate regions (exons 2 or 6) of MITF were amplified using region specific primers as listed in Table 2. The amplified DNA was run on a 1,5% agarose gel, at 70V for 60 minutes. The bands were cut out of the gel and extracted using Nucleospin ® Gel and PCR Cleanup Kit (#740609.50 from Macherey Nagel). The purified DNA fragments were cloned into the puc19 plasmid and 10 colonies were picked for each cell line, DNA isolated and sequenced using Sanger sequencing (Beckman Coulter Genomics).

Table 2: Primers used for amplifying genomic regions of exons 2 and 6 of MITF

Target	Primer name	Sequence	Tm(ºC)	Amplicon size
Exon2	MITF-2-Fw	CGTTAGCACAGTGCCTGGTA	60	505
	MITF-2-Rev	GGGACAAAGGCTGGTAAATG	56	
Exon6	MITFexon6-fw	GCTTTTGAAAACATGCAAGC	55	551
	MITFexon6-fw	GGGGATCAATTCTCCCTCTT	56	

3.4 Generation of piggy-bac vectors expressing eGFP tagged IRF4 and TFEB

To generate inducible stable cell lines, the IRF4 and TFEB cDNA cloned into a piggy-bac vector (pPBhCMV*1-cHA-pA) dowsntream of a tetracycline response element (TRE). The *IRF4* and *TFEB* cDNAs were amplified by Q5-High-Fidelity DNA polymerase (M0491, NEB) from expression plasmids IRF4-HA (provided by Brass et al. (1996) and EGFP-N1-TFEB purchased from Addgene (#38119), using the primers listed in Table 3. The primers contain restriction sites for the restriction enzymes Mlu1 and Not1 at the 5 ends to facilitated cloning. The piggy-bac vector used in our experiments was obtained from Dr.Kazuhiro Murakami (Hokkaido University) (Magnusdottir et al., 2013). The PCR products of IRF4 and TFEB and the backbone piggy-bac vector were digested with MluI and Not1 and the TFEB and IRF4 fragments ligated to the piggy-bac vector using a 3:1 molar ratio using instant sticky end ligation mix (M0370, NEB). A portion of the ligation mix (2 µL) was transformed into NEB5-alpha competent *E.coli* (NEB #C29871), spread on LB agar plates containing 200 µg/ml of ampicillin and incubated at 37ºC overnight. The following day, colonies were picked and cultured in 5 mL LB media and DNA isolated for further analysis by sequencing using primers that cover the entire cDNA of inserts.

Table 3: Primers used for cloning TFEB and IRF4 into *piggybac* vector

Target	Primer name	Sequence
IRF4	IRF4-MluI-FW	taattaacgcgtAGAGTCAGATCCGCTAGCG
	IRF4-Not1-REV	taattagcggccgcCACGGCATCACTCTTGGAT
	MluI-FW	taattaacgcgtTGAACCGTCAGATCCGCTAG
TFEB	Not1-REV	GGCTGATTATGATCTAGAGTCG

3.5 Generation of piggy-bac vectors expressing miR-MITF and cell lines

In order to generate inducible MITF knockdown stable cell lines, we cloned miR-RNA targeting MITF into piggy-bac vector dowsntream of a tetracycline response element (TRE). The piggy-bac transposable vector pPBhCMV-1-miR(BsgI)-pA-3 was obtained from Dr. Kazuhiro Murakami (Hokkaido Univeristy) (Magnusdottir et al., 2013). MicroRNA sequences targeting MITF were picked utilizing BLOCK-iT RNAi Designer, targeting both exons 2 (miR(MITF-X2) and 8 (miR(MITF-X8) of MITF. A non-targeting control (miR(NTC) was used as a negative control. The mature miRNA sequence, terminal loop and incomplete sense targeting sequences required for the formation of stem loop structures were designed utilizing the BLOCK-iT RNAi designer. Mature miRNAs and the primers used for generating the pre-miRNAs are listed in Table 4. To obtain short double stranded DNAs with matching BsgI overhangs, primers in Table 4 were first denatured at 95°C then allowed to slowly cool down in water bath for annealing. The piggy-bac vector pPBhCMV1-miR(BsgI)-pA-3 was digested with BsgI (#R05559S, NEB) and run on a DNA agarose gel and the digested vector excised from the gel and purified. Following this, the annealed primers and purified digested backbone were ligated at 15:1 insert to backbone molar ratio using Instant Sticky-end Ligase Master Mix (M0370S, NEB). The ligation products were then transformed to high-competent cells. Then purified plasmids were sequenced to verify the successful ligation.

Table 4: miR-RNA primers used for generating miR-MITF and miR-Ctrl cell lines

Name	mature miRNA sequence	pre-miRNA sequences
miR-NTC	AAATGTACTGCGCGTGGAGAC	F-5'-GAAATGTACTGCGCGTGGAGACGTTTTGGCCACTGACTGACGTCTCCACGCAGTACATTTCA-3' R-5'-AAATGTACTGCGTGGAGACGTCAGTCAGTGGCCAAAACGTCTCCACGCGCAGTACATTTCAG-3'
miR-MITF-X	AAAGGTACTGCTTTACCTGCT	F- 5'-GAAAGGTACTGCTTTACCTGCTGTTTTGGCCACTGACTGACAGCAGGTAGCAGTACCTTTCA-3' R-5'-AAAGGTACTGCTACCTGCTGTCAGTCAGTGGCCAAAACAGCAGGTAAAGCAGTACCTTTCAG-3'
miR-MITF-X	TAAGATGGTTCCCTTGTTCCA	F-5'-GTAAGATGGTTCCCTTGTTCCAGTTTTGGCCACTGACTGACTGGAACAAGAACCATCTTACA-3' R-5'-TAAGATGGTTCTTGTTCCAGTCAGTCAGTGGCCAAAACTGGAACAAGGGAACCATCTTACAG-3'

3.6 Generation of piggy-bac iducible cell lines

The PiggyBac transposon system was used to generate stable cell lines. The inducible promoter is a Tetracylin-On system which is called reverse-tetracyline-transactivator (rtTA). This system allows the regulation of expression by adding tetracyclin or doxycycline. For generation of stable cells carrying the inducible miR-MITF constructs, 501Mel and SkMel28 cell lines were seeded at 70%-80% confluency and then transfected with the following constructs: py-CAG-pBase a vector transiently expressing piggy-bac transposase, *MITF* targeting plasmids pBhCMV1-miR(MITF-X2)-pA and pPBhCMV1-miR(MITF-X8)-pA encoding miRNA equences targeting exons 2 and 8 of MITF, and pPB-CAG-rtTA-IRES-Neo, a plasmid which confers neomycin resistance and rtTA. The mixture was in the ratio of 10:5:5:1, respectively. To generate, miR-CTRL cell lines, 501Mel and SkMel28 cell lines were transfected at a ratio of 10:10:1 with pA-CAG-pBase, pPBhCMV_1-miR(NTC)-pA encoding a non-targeting miRNA and pPB-CAG-rtTA-IRES-Neo. After 48 hour transfection, miR-CTRL, miR-MITF and non-transfected cell lines were selected with 0.5mg/ml of G418 (#10131-035, GIBCO) for 2 weeks.

For generation of stable overexpression cell lines of TFEB and IRF4 using the piggy-bac vectors under inducible promoter as described above, the 501Mel cells were first seeded at 70%-80% confluency in 6 well plates. Then they were transfected using Fugene® HD reagent (#E2311) with the following plasmids: pPBhCMV1-TFEB-EGFP-cHA-Pa or pPBhCMV1-IRF4-EGFP-cHA-pA together with pPB-CAG-rtTA-IRES-Neo that confers neomycine resistance and rtTA. py-CAG-pBase that expresses piggy-bac transposase, at a ratio of 10:10:1 respectively. Drug selection with G418 (#10131-035, GIBCO) was carried out as described above. For induction of gene expression, 1ug/ml of doxycycline was used for 24/48 hours.

3.7 Protein extraction and immunoblotting

Cells were seeded on 12 or 6 well cell culture plates and lysed directly with 1X Laemmeli buffer and boiled at 95°C for 10 min and then chilled on ice for 5 minutes. Lysates were spun down for 1 min at 10,000 rpm then run on 8% SDS-polyacrylamide gel and transferred to 0,2µm PVDF membranes (#88520 from Thermo Scientific). The membranes were blocked with 5% BSA in TBS-T (Tris-bufferred saline, 0.1% Tween 20) for 1 hour at room temperature, and then incubated overnight (O/N) at 4°C with 5% BSA (Bovine Serum Albumin) in TBS-T (20mM Tris, 150mM NaCl, 0.05% Tween 20) and the appropriate primary antibodies (see Table 5). Membranes were washed with TBS-T and stained for 1 hour at RT with the appropriate secondary antibodies. The secondary antibodies used were the following:

Anti-mouse IgG(H+L) DyLight 800 conjugate (1:15000, #5257) and anti-rabbit IgG(H+L) DyLight 680 conjugate (1:15000, #5366) from Cell Signaling Technologies. The images were captured using Odyssey CLx Imager (LI-COR Biosciences).

Table 5: Antibodies used for western blot analysis

Target	#Nr	Manufacturer	Source	Dilution
β-Actin	4970	Cell signaling	Rabbit IgG	1:2000
β-Actin	MAB1501	Millipore	Mouse	1:20000
Cadherin, E	610182	BD	Mouse IgG2a	1:5000
Cadherin, N	610921	BD	Mouse IgG1	1:5000
MITF	MS771-PABX	Thermo Scientific	Mouse IgG1	1:2000

3.8 Gene expression analysis using quantitative real-time PCR

Cells were seeded on 6-well culture dishes and RNA isolated with TRIzol reagent (#15596-026, Ambion), DNase treated using the RNase free DNase kit (#79254, Qiagen) and re-purified with the RNeasy Mini kit (#74204, Qiagen). The cDNA was generated using High-Capacity cDNA Reverse Transcription Kit (#4368814, Applied Biosystems) with 1 µg of RNA. Primers were designed using NCBI primer blast (Table 6) and qRT-PCR was performed using SeniFAST™ SYBR® Lo-ROX Kit (#BIO-94020, Bioline) on the BIO-RAD CFX38 Real time PCR machine. Primer final concentration 0.1µM and 2 ng of cDNA used per reaction. Quantitative real-time PCR reactions were performed in triplicates and relative gene expression was calculated using the D-ΔΔCt method (Livak & Schmittgen, 2001). The geometric mean of β-actin and human ribosomal protein lateral stalk subunit P0 (RPLP0) was used to normalize gene expression of the target genes. Standard curves were made and the efficiency calculated using the formula $E=10^{[-1/slope]}$.

Table 6: List of primers used for RT-qPCR

Target	Primer name	Sequence (5'-3')	Primer efficiency
β-Actin	b-Actin publ fw	AGGCACCAGGGCGTGAT	
	b-Actin publ rev	GCCCACATAGGAATCCTTCTGAC	2,03
HumanRPLP0	hARP fw	CACCATTGAAATCCTGAGTGATGT	
	hARP rev	TGACCAGCCCAAAGGAGAAG	2
Mlana	Mlana-fw	TGGATACAGAGCCTTGATGGATAA	
	Mlana-rev	GAGACACTTTGCTGTCCCGA	1.93
MMP15	MMP15-fw	CCCCTATGACCGCATTGACA	
	MMP15-rev	CGCCAGTACCTGTCCTCTTG	1.92
ITIH5	ITIH5-fw	CATGCTCCTGCTGCTGGG	
	ITIH5-rev	AGTCCATCCTGCTCCGAAGA	2.15
PRDM7	PRDM7-fw	CCTGGCTAATCACCAAGGGG	
	PRDM7-rev	CGGGCACAGTTCACATACCT	1.95
SETDB2	SETDB2-fw	GGCAGGAAATGGACAGCAGTA	
	SETDB2-rev	ACAAATGGATGAAACATTCTGTGA	1.92
MAFB	MAFB-fw	CTCAGCACTCCGTGTAGCTC	
	MAFB-rev	GTAGTTGCTCGCCATCCAGT	1.90
MITF	cMITF-fw	ATGGAAACCAAGGTCTGCCC	
	cMITF-rev	GGGAAAAATACACGCTGTGAGC	1.94
CDH2	CDH2-fw	TGCAAGACTGGATTTCCTGAAGA	
	CDH2-rev	TGCAGTTGCTAAACTTCACATTG	1.91
CDH1	CDH1-fw	AGAAAATAACGTTCTCCAGTTGCT	
	CDH1-rev	TATGGGGGCGTTGTCATTCA	1.9
TGFB1	TGFB1-fw	GGAAATTGAGGGCTTTCGCC	
	TGFB1-rev	AGTGAACCCGTTGATGTCCA	1.89
ITGA2	ITGA2-fw	CTCGGGCAAATTATACCGGC	
	ITGA2-rev	GAGCCAATCTGGTCACCTCG	2
p15	p15-fw	CGTTGGCCGGAGGTCAT	
	p15-rev	GTGAGAGTGGCAGGGTCTG	2.01
p18	p18-fw	GAGACGGATGGAAACCGAGC	
	p18-rev	TAGGGTCCCTTGTTCACGGT	1.98
NGFR	NGFR-fw	TGTCTATTGCTCCATCCTGGC	
	NGFR-rev	CTGTTCCACCTCTTGAAGGC	2.09
IRF4	IRF4-fw	ATGTCCATGAGCCACCCCTA	
	IRF4-rev	TAGTTGTGAACCTGCTGGGC	1.81
NR4A3	NR4A3-fw	TCCAGGCCCTCATCACCTTTT	
	NR4A3-rev	GGACGCAGGGCATATCCACA	2.13
ZNF703	ZNF703-fw	CATTGAGCTGGACGCCAAGA	
	ZNF703-rev	AGTTGAGTTTGGAGGAGGGC	2.1
p57	p57-fw	GCGGTGAGCCAATTTAGAGC	
	p57-rev	TGCTACATGAACGGTCCCAG	2

3.9 siRNA mediate knockdown of genes

Cells were seeded at the density of $1x10^5$ per well in 12 well culture dishes before transfection with the appropriate siRNAs. Cells were transfected with 15μM siRNA and 1.5 μL Lipofectamine RNAiMAX Transfection Reagent (#13778030, ThermoFisher) per mL of culture medium. Cells were cultured for 2 days before extracting RNA or protein. The siRNAs used for the procedure were obtained from Ambion and are listed in Table 7.

Table 7: List of siRNAs used in the study

siRNA ID	#Nr	Gene Symbol
137035	AM16708	PRDM7
213811	AM16708	SETDB2
106815	AM16708	IRF4
107716	AM16708	MAFB
4390843	4390843	siCTRL

3.10 Immunostaining

Cells were seeded onto 8-well chamber slides (#354108 from Falcon) at 70% confluency. The cells were then fixed with 4% paraformaldehyde (PFA) in 1xPBS for 20 minutes and then washed 3 times with PBS and blocked with 150 µl blocking buffer (1x PBS + 5% Normal goat serum + 0.3% Triton-X100) for 1 hour at room temperature and stained O/N at 4°C with the appropriate primary antibodies (see Table 8) diluted in antibody buffer (1xPBS + 1% BSA + 0,3% Triton-X). The wells were washed 3 times with PBS and stained for 1 hour at room temperature with the appropriate secondary antibodies (see Table 8), diluted in antibody buffer. The wells were washed once with PBS, followed by DAPI staining final concentration 0.5 µg/ml in 1X PBS (1:5000, #D-1306, Life Technologies) and 2 additional washes with PBS. Subsequently, each well was mounted with Fluoromount-G™ (Ref 00-4958-02, ThermoFisher Scientific) and covered with cover slide. Slides were stored at 4°C in the dark.

Table 8: Primary and secondary antibodies used for immunostaining

Target	#Nr	Manufacturer	Source	Dilution
phospho-FAK (Tyr397)	3283	Cell signalling	Rabbit	1:100
Phospho-Paxillin (Tyr118)	2541	Cell signalling	Rabbit	1:100
Alexa Fluor 555 Phalloidin	8953	Cell signalling	Rabbit	1:20
Vimentin	3932	Cell signalling	Rabbit	1:250
MITF	MS771-PABX	Thermo Scientific	Mouse IgG1	1:500
Alexa Fluor 488	A-11070	Thermo Scientific	Goat IgG	1:1000
Alexa Fluor 546	1-11003	Thermo Scientific	Goat IgG	1:1000

3.11 BrdU assay and FACS analysis

Cells were seeded on 6-well plates and 10mM BrdU added to each well. The medium was removed after 4 hour of incubation and the cells trypsinized and washed with ice cold PBS. After fixation with 70% ethanol overnight, cells were centrifuged at 500*g* for 10 minutes, then permeabilised with 2N HCl/Triton X-100 for 30 minutes followed by neutralization with 0.1 M $Na_2B_4O_7.10\ H_2$.

3.12 Incucyte live cell imaging

Cell were seeded at a density of 2000 cells per well onto 96 well plates in triplicates. Images were recorded with the Incucyte system for every 2 hours for a 4-day period. Collected images were then analysed using the Incucyte software by measuring cell confluency. From that, doubling time was calculated with the following formula: Duration x log(2)/log(FinalConfluency) – log(InitialConfluency).

3.13 MTS (tetrazolium) cell viability assay

Cells were seeded at a density of 2,000 cells per well on 96-well plates, 24 hours before performing the MTS assay. For this assay CellTiter 96 Aqueous Reagent (G358C, Promega) was used following the protocol provided by the manufacturer. Measurements were taken with spectrophotometer at 490nm absorbance every 24 hour for four days.

3.14 Senescence assay

Senescence-associated beta-galactosidase (SA-βgal) acitivity, that is detectable at pH 6.0 is used to determine senescent cells. Senescence assay was perfomed using the protocol described by (Debacq-Chainiaux et al., 2009). Cells seeded on 6-well culture dishes were grown to 70% confluency. After cells were washed twice with PBS then fixed for 5 min at room temperature in fixation solution (2% formaldehyde, 0.2% glutaraldehyde (vol/vol) in PBS buffer). Then washed twice with PBS, after which staining was performed overnight at 37°C to detect SA-βgal activity. The staining solution contained chromogenic substrate 5-bromo-4-chloro-3-indoyl β-D-galactopyranoside (X-gal), which yields insoluble blue compound when cleaved by β-galactosidase. After the staining, the cells were washed twice with PBS and once with methanol, then air dried. Finally, images were taken for the respective cell lines. To obtain positive control, cells were transfected with LacZ gene containing expression plasmid wich encodes for β-galactosidase.

3.15 Transwell migration assay and matrigel Invasion assay

Tanswell chambers with 8μm pore size (Thermo Scientific Nunc™) were used for invasion and migration assays. For the Transwell migration assays, the cells were resuspended in cell culture medium RPMI 1640 supplemented with 0.1% FBS at a concentration of 100,000 cells in 300 ul and then added onto the upper chamber of the 24 well Transwell insert plate. Then 500μl of medium containing 10% FBS were added to the lower chamber as a chemoattractant. Cells were incubated for 8 hours after which the cells which migrated to the other side of the membrane were fixed with 4% PFA and stained with DAPI. Images were acquired using QImaging (Pecon, software Micro-Manager 1.4.22) with 10x magnification, and the cells were counted using Image J software. For Transwell invasion assay, the Transwell insert was pre-coated with 45 ul (1:100) matrigel matrix from corning (Thermo Scientific) and the same procedure used as decribed above.

3.16 Scratch assay

Each cell line (2 x10^4 cells /well) was cultured in triplicate in 96-well plates (Nunclon delta surface, Thermo Scientific, #167008). When they reached 100% confluency, scratches were made with Woundmaker 96 (Essen, Bioscience). Imaging was performed with IncuCyte Live Cell Imaging System (Essen, Bioscience). The recorded images of the scratches were analysed with IncuCyte software to quantify gap closure.

3.17 ChIP-seq and analysis

Chromatin immunoprecipitation was performed as described in (Palomero et al., 2006) following these steps: Twenty million cells were crosslinked with 0.4% formaldehyde for 10 minutes at room temperature, quenched by 0.125M glycine for 5 minute at RT. Chromatin was sheared by sonication for a 5-minute duration (25% amplitude, 30sec OFF and 30 sec ON) using a probe sonicator (Epishear, Active Motif). To collect twenty million cells, cells were grown on ten 10 cm^2 dishes and 1ug/ml of doxycycline used for induction of eGFP tagged TFEB or IRF4. For the TFEB-eGFP ChIP, cells were starved for 2 hours with HBSS prior to fixing the cells. Immunoprecipitation was performed with Protein G Dynabeads (Life technologies), with a total of 10 micrograms of anti-GFP (3E6) antibody (Molecular Probes, #A-11120). The bead bound immune complexes was washed 5 times with wash buffer (50M Hepes pH 7.6, 1mM EDTA, 0.7% Na-DOC, 1% NP-40, 0.5M LiCl) and once with TE. After this, the washed immuncomplex and sonicated lysate input were incubated in elution buffer (50mM Tris pH 8, 10mM EDTA, 1% SDS) overnight at 65 ºC. After reverse crosslinking, samples were treated with 0.2 µg/µL of RNase A for 1 hour at 37ºC and then with 0.2 µg/µL Proteinase K for 2 hours at 55ºC. For purification of DNA, RNase and Proteinase K treated samples were extracted once with Phenol: Chloroform: Isoamyl alcohol using phase lock tube and once with Chloroform subsequently precipitated by adding 20 µg of glycogen and 0.2M of NaCl with 2.5 volumes of ethanol. This mixture was incubated overnight at -80ºC, the DNA spun down at full speed and the precipitated DNA washed with 70% ethanol and resuspended in 100 µL volume of TE buffer. Purified ChIP DNA samples and corresponding input DNA were analyzed by real-time PCR using region-specific primers (see Table 9) and 2xSYBR green master mix (Sigma) on an ABI 7500 machine (annealing at 60°C). Input DNA was diluted 500 times and ChIP DNA was diluted 5 times. Primer final concentration of 0.2 µM used for qPCR. The resulting qPCR data were then analyzed using the relative quantification method taking primer amplification efficiencies into account, as assessed by standard curves of DNA dilutions series (Pfaffl, 2001). The percentage of input is calculated

using following formula: primer efficiency$^{CT\ Input-CT\ ChIP}$ /dilution factor respect to input.

Table 9: List of ChIP-qPCR primers

Target	Primer name	Sequence (5'-3')	Region	Primer efficiency
Mlana	mlana-F	TGGGTTCTTCCAATGTGTCA	Intron 2	1.9
Mlana	mlana-R	TTTATGCATGGTCACGTGGT		
ATP6V1C1	ATP6V1C1-F	CTTAGGTCGGGAAGGGATG	Promoter	1.85
ATP6V1C1	ATP6V1C1-R	AGGAAGGTGTCAAACGAGGA		
ATP6V0E1	ATP6V0E1-F	GCGGTCAGCTATTGACACTTC	Promoter	1.87
ATP6V0E1	ATP6V0E1-R	AGTGAGGCCGTGATACGC		
RRAGD	RRAGD-F	GCCACCTCCTCATGTCTCAT	Promoter	2.11
RRAGD	RRAGD-R	CACTCCCCTACTCCCACAAA		
TTYH2	TTYH2-F	GGCTGAGAGGTTCAGGAGTG	Intron 1	2.02
TTYH2	TTYH2-R	TTGTTCAGTCTCCCCCAATC		
QPCT	QPCT-F	TGTTCAGCAGACGTCGATTC	Promoter	2.2
QPCT	QPCT-R	CAGACCCTGGGGAGTTATGA		
LINC00520	LINC00520-F	TGTTGCCTGCTGGTCTAGTG	Intron 1	2.18
LINC00520	LINC00520-R	CCCTGTGCCATTGTCTACCT		
ZEB1	ZEB1-F	ACAAGCACCGTGTGGGTATT	Promoter	2.1
ZEB1	ZEB1-R	GAGGCTAGAAGTTCCGCTTG		
NGFR	NGFR-F	GTGGGGTGATGGACTGAGAT	Proximal Promoter	2.3
NGFR	NGFR-R	CTCCCTAACTGCCCCCTATC		
SERPINA3	SERPINA3-F	CTTTGCCCTATGCTGCCTAC	Intron 6	2.1
SERPINA3	SERPINA3-R	CCCCTTGTCCTGTCTGATGT		
TYR	dTYR-F	TAAGCCTCCTTGTGGAGATCATGTG	Distal promoter	1.97
TYR	dTYR-R	TGTGTGGGTGAAGAGGAAGAGAAGT		
SUB1	SUB1-F	CTTAGAGAACCGAAACCCAAACCTACA	Promoter	1.96
SUB1	SUB1-R	TGCAACCCTTCCTGCTTTAACAAGTTT		
Actin	actin-ag-F	AGTGTGGTCCTGCGACTTCTAAG	Promoter	1.89
Actin	actin-ag-R	CCTGGGCTTGAGAGGTAGAGTGT		
Negative control	NegativeCtrl-F	AATATGTACATCAGGCAATCGGCTCTTC	Gene desert-Chr7	1.96
Negative control	NegativeCtrl-R	CAACTGGAATCAGATCCACTTCATGGAAA		

3.18 ChIP-seq DNA library preparations

ChIP-seq DNA libraries were prepared with purified ChIP DNA and Input DNA using NEBNext ChIP-seq Library Prep Kit (E6200, NEB) with following parameters: 8 -15 ng of fragmented ChIP DNA and 10 ng of DNA for Input were used for library preparation. Adaptors were freshly diluted 10X just before use. Adaptor ligated DNA cleaned up with AMPure XP beads withought size selection due to small quantities of DNA. PCR cycle of 10 was used for library amplification. Then amplified library purified with Agentcourt AMPure XP beads (A63881, Beckman Coulter). Firstly, 45 µL of AMPure XP beads were added to PCR reaction (~50µL), well mixed by pipetting up and down 10 times then incubated at room temperature for 5 minutes. After, tubes were quickly spun down and magnetized for 5 minutes until the solution is clear. Then supernatant was carefully removed without disturbing the beads. Next, freshly prepared 70% Ethanol was added to the PCR tubes on the magnetic stand and incubated for 30 seconds then carefully removed. After this, the PCR tubes were removed from magnetic stand and washed twice with 70% ethanol by resuspending the beads and magnetized to remove the supernatant. Then beads were air dried for 5 minutes while standing on magnetic stand. (Close attention was made not to overdry the beads). Then beads were resuspended with 0.1X TE (1mM Tris, 0.1mM

EDTA) by pipetting up and down at least 10 times and incubated for 2 minutes at room temperature. Finally, beads were magnetized for 5 minutes, then 28 µL of supernatant was transferred to clean PCR tube and stored at –20 ºC. The libraries were then quantified in Qubit DNA fluorometer (Q33226, Thermo scientific) to obtain DNA concentration. Then libraries diluted in the range of 5-500pg/µL with 0.1X TE to to check size distribution on an Agilent Bioanalyzer high sensitivity DNA ChIP kit (5067- 4626) and subsequently sent for high throughput sequencing.

3.19 ChIP-seq data analysis

Sequenced 30 million paired end raw reads for each sample were mapped to the human hg19 reference genome using Bowtie 2 (Langmead et al., 2009). The prebuild index for hg19 was downloaded from Bowtie 2 website. Aligment is performed using following command line:

```
bowtie2 --very-sensitive -k 1 -p 4 -q -t -s --un-conc /filepathforoutput –x /index.path -1 file1.fastq.gz -2 file2.fastq.gz –S aligned.sam
```

Parameters used in bowtie2 are: -- very-sentitive which is a preset parameter reports the most accurate alignment with less mismatch; -k1 reports only unique best alignment; -p specifies the number of core to use; -q indicates the reads are fastq file format; -t prints out the time required to load the index and alignment; -s writes out the summary of the alignment; –un-conc writes out reads failed to align concordantly; -S writes out file in Sequence alignment/Map (SAM) format, which is tab limited text format. Once alignment was done, the output SAM files were converted to Binary version of SAM format (BAM) using samtools (Li et al., 2009) and sorted based on chromosome number using following comman line:

```
samtools view -bS aligned.sam > alinged.bam
```

```
samtools sort alinged.bam alinged.bam.sorted
```

The sorted aligned reads were then used as an input for calling peaks using MACS (Zhang et al., 2008), a peak calling software for identifying sites bound by transcription factors. Following command line used for calling the peak with MACs:

```
macs14 -t ChIP.sorted.bam -c input.sorted.bam -f bam -g h -n IRF4CHIP_1 -w -S -p 1e-5
```

The input parameters repectively indicates as follows: -t ChIPseq aligned read in bam format; -c input aligned read; -f specifies the format; -g specifiying the genome; --wig write wiggle file format; -S write the wig file into single output; -p p-value

Peaks were called with various p-values ranging from 1e-5 to 1e-30. From these, peaksets were screened for regions that our transcription factor does not show binding. Then peakset that did not contain peaks for negative bound regions was chosen for downstram analysis.

MEME-ChIP tool (Machanick & Bailey, 2011) was used to discover motifs enriched by transcription factor binding. 1500 peaks with lowest p-value were selected for the motif analysis. The DNA sequences corresponding to the peak location were isolated from UCSC genome browser in following order: (i) go to Tools and select table browser; (ii) check the define region and paste in genomic coordinates of peaks; (iii) Finally obtain the sequences by selecting sequences for output format. Then these transcription factor bound sequences were used for de-novo motif enrichment analysis.

3.20 ChIP-seq differential binding analysis and GO term analysis

Resulting peak sets were annotated to genes with the Biocondoctor package Chipseeker (Yu et al., 2012), and peak distribution respect to transcription start sites were plotted using the same package. To do this, peaks were supplied as a Browser Extensible Data (BED) format. GO analysis was performed utilizing Cluster profiler package from R Bioconductor (Yu et al., 2012). This package requires gene names as an input for the analysis, therefore, genes were extracted from associated peaks based on distance to their transcription start site (TSS) 20 kilo base pairs upstreams or downstream. Detailed R scripts are included in the Appendix 1.

DiffBind package from R Bioconductor was used to perform differential binding analysis which identifies differentially bound sites of transcription factors between two sample groups. First, peak files called for each transcription factors with their biological replicates and alignment file of the peaks in bam format is submitted to the DiffBind package. Then consensus peaks were derived from each biological replicate for each transcription factor by merging common peaks present in both replicates. After this, a count file data was generated by counting the reads from the alignment (bam file) provided for each factor at every potential binding locus. Finally, differential binding analysis was performed using the DESeq2 method utilizing the count data file from the two groups of MITF and IRF4 samples. R script is included in Appendix 2.

3.21 RNA-seq sample preparation and analysis

RNA was isolated as described in method section 3.7. RNA with RNA

integrity (RIN) score above 8 were used for making RNA libraries. The RIN socore is indicative of RNA degradation calculated using the ratio of 18S to 28S ribosomal RNA which is decreased when RNA is degraded, 1 indicates most degraded RNA and 10 is most intact. The mRNA was isolated from total 800 ng RNA using NEBNext Poly(A) mRNA isolation module (E7490, NEB). RNA was fragmented at 94 ºC for 16 minutes in thermal cycler. Purified fragmented mRNA then used to generate cDNA libraries for sequencing using NEBNext Ultra Directional RNA library Kit (E7420S, NEB) following the protocol provided by the manufacturer with these parameters: Adaptors were freshly diluted 10X before use. PCR cycle of 15 was used to amplify the library. Total of 8 RNA libraries prepared with 4 biological replicates for each cell line including EV-SkMel28 and ∆MITF-X6 cells.

Then purified RNA sequencing libraries were then paried-end sequenced with 30 million reads per sample. Mapping of reads to GRCh38 human reference genome was performed by Kallisto (Bray et al., 2016). To do this, human transcriptome version GRCh38 was downloaded from Ensemble website using this command: `ftp://ftp.ensembl.org/pub/release-94/fasta/homo_sapiens/cdna/`

After, index was built for downloaded human transccriptome with command below:

```
kallisto index -i Homo_sapiens.GRCh38.cdna.all.release-94_k31.idx Homo_sapiens.GRCh38.cdna.all.fa.gz
```

Then alignment was performed with following options: 100 bootstraps, --pseudobam alignment file written in BAM format, --fr-stranded option was included for RNA libraries those were prepared strand specific manner. Aligned bam files then directly piped into samtools for sorting using this command:

```
kallisto quant - i /index.path - o filename  - b 100  --pseudobam --fr-stranded file1.fastq.gz  file2.fastq.gz | samtools view - Sb > filename.bam
```

Quantified transcripts from kallisto parsed to Sleuth (Pimentel et al., 2017) in R Bionconductor to perform differential expression analysis. For the analysis, quantified transcriptome profilies of ∆MITF-X6 and EV-SkMel28 were used in 4 biological replicates per cell line. Both likelihood ratio test (LRT) and wald test were used to model differential expression between MITF knock out cells (∆MITF-X6) and wild type EV-SkMel28 cells. LRT test is more stringent when estimating differentially expressed genes (DEGs), whereas wald test gives an estimate for log fold change. Therefore, results from LRT test was intersected with wald test to get significant DEGs with fold change included. Gene set

enrichment analysis was performed using GSEA software from the Broad Institute (Subramanian et al., 2005). GESA software was employed with pre-ranked options and gene lists were provided manually to assess enrichment. Differentially expressed genes were ranked combining p-value with log fold change for use gene set enrichment analysis. GO terms and KEGG pathway analysis were performed using the Biconductor package Cluster profiler (Yu et al., 2012) using the gene names of DEGs. R scripts used to perform the analysis are included in Appendix 3.

3.22 Differential gene expression analysis melanoma tumour samples in cancer genome atlas data base

The RNA-seq quantified data for 473 melanoma samples were extracted from cancer genome atlas data base using the TCGAbiolinks package in R Bionconductor (Colaprico et al., 2016). The lists of $MITF^{low}$ and $MITF^{high}$ samples were generated by sorting the samples from low to high based on MITF expression. The 40 tumour samples with highest MITF expression and 40 tumour samples with lowest MITF expression were selected for the downstream differential expression analysis built in in TCGAbiolinks package. The R script is included in Appendix 4.

4 Results

4.1 Characterization of MITF knock out cells

4.1.1 Generation of melanoma cells lacking MITF

MITF is crucial for melanocyte existence, and it has a pivotal role in melanoma progression. Importantly, tumour heterogeneity has been well characterized in melanoma tumour cell lines, where the different cell lines represent a distinct phenotype associated with certain cell state of tumour progression. Briefly, the melanoma cell lines have been divided into two major classes based on their behavior, namely proliferative MITF high cells and quiescent MITF low cells (Hoek, Eichhoff, et al., 2008). The different results observed upon MITF knockdown may therefore be due to the different cell lines used or the status of MITF expression in the cells at the time of study. Here the aim was to study the impact of long term effective depletion of MITF in melanoma cell lines. Thus, we sought to permanently knock out MITF from melanoma cell lines which would provide an efficient cell line model to study the MITF-low cell state in melanoma progression. To this end, we generated melanoma cell lines carrying mutations in the *MITF* gene using the clustered regularly interspaced short palindromic repeats (CRISPR/Cas9) technique. To this end, we generated melanoma cell lines carrying different mutations in the *MITF* gene using the clustered regularly interspaced short palindromic repeats (CRISPR/Cas9) technique. We used SkMel28 cells for this work. Due to partial tetraploid, SkMel28 cells have 4 copies of MITF (Lionel Larue, personal communication, information from ATCC) (Figure 3A) and might therefore be useful to generate a series of cells with different levels of wild type/mutant MITF proteins. They harbor the $BRAF^{V600E}$ and $p53^{L145R}$ mutations (Leroy et al., 2014) and wild type N-RAS (ATCC), and able to produce tumour in nude mice (Fogh et al., 1977; Leroy et al., 2014) (Appendix 5). Therefore, SkMel28 cells can provide a model to study the effect of MITF in tumour progression in the background of $BRAF^{V600E}$ and $p53^{L145R}$ mutations. We targeted exons 2 and 6 of the MITF isoforms separately. Exon 2 is the first exon shared between all isoforms and exon 6 encodes the DNA binding domain of MITF. We generated gRNAs targeting these exons (Table 1) and used them to target the exons of MITF in the SKmel28 melanoma cell line (Figure 3B). The gRNA targeted cells were treated with blasticidin for 3 days to select positive clones after which the cells were serialy diluted to obtain single cell clones. The resulting clones from targeting exons 2 and 6 of MITF were screened for loss of MITF by first

amplifying the regions with primers designed for exons 2 and 6 and then cloning the amplified DNA into puc19 plasmid. The plasmids containing amplified fragments covering exons 2 and 6 of MITF were used for Sanger sequencing. The resulting cell lines are hereafter referred to as ΔMITF-X2 and ΔMITF-X6. SKmel28 cells treated with empty vector gRNA were used as a control cell line and are termed EV-SKmel28.

The sequence analysis of the ΔMITF-X2 cells suggests that mutations were introduced into all four genomicof MITF. Two mutations were discovered by sequencing: (i) Insertion of a single base pair (A) resulting in a premature stop codon at amino acid position Y22 of M-MITF (ii) deletion of 5 bp resulting in deletion of amino acids Y22-H23 and a frameshift resulted in premature stop codon at position K43 of M-MITF (Figure 3B). Sequence analysis of the ΔMITF-X6 line showed three mutations: (i) a deletion of 17 bp leading to the deletion of the ALAKER amino acids from postion 198-203 and resulting in a frameshift which introduced stop codon at position amino acid position 212 of M-MITF; (ii) 6bp deletion, resulting in a two amino acids deletion at position R197-A198 of M-MITF, upstream of the DNA binding domain; (iii) 1 bp deletion at position encoding A198 resulting in a frameshift mutation which gave rise to stop codon at amino acid position 211 of M-MITF (Figure 3C). Additionally, RNA-sequencing of the ΔMITF-X6 line confirmed a 1 bp deletion in the codon for A198 and a 2 bp subsititution (c.589G>T, c.591G>T) which resulted in amino acid subsitituition at R197I and A198I (Appendix 6). All three mutations are likely to severely alter the function of the MITF protein. The two frameshift mutations might result in nonsense mediated decay and severe reduction in the mRNA levels, whereas the 6 bp deletion leads to an in-frame deletion of two residues in the basic domain. Since this is the beginning of the first of two helices, which form the DNA-binding and dimerization domain of the protein, lack of two amino acids will result in a protein where the residues of the helix will be out of register with respect to the rest of the protein (Pogenberg et al., 2012).

Western blotting showed that the ΔMITF-X6 cells express very little if any MITF protein whereas the ΔMITF-X2 cells express truncated forms of MITF (Figure 3D). Interestingly, these truncated forms of MITF are also detected in the wild type cells, albeit at lower levels suggesting that these are alternative isoforms of the protein. The C5 MITF antibody recognizes an epitope located between residues 120 and 170 which corresponds to exons 4 and exon 5 of MITF (Fock et al., 2018). Therefore, these truncated isoforms present in the ΔMITF-X2 cells must contain that domain. Immunostaining for MITF performed on cells in culture showed a mostly nuclear staining in both the EV-SKmel28 and ΔMITF-X2 cells. However, in the ΔMITF-X6 cells, no signal

was present in the nucleus and the only staining observed was low-level staining predominantly in the cytoplasm (Figure 3E). We conclude that both MITF KO cell lines lack fully functional MITF. The ΔMITF-X6 cells entirely lack functional MITF whereas the ΔMITF-X2 cells express a truncated protein of unknown significance which may be non-functional or exert dominant negative functions.

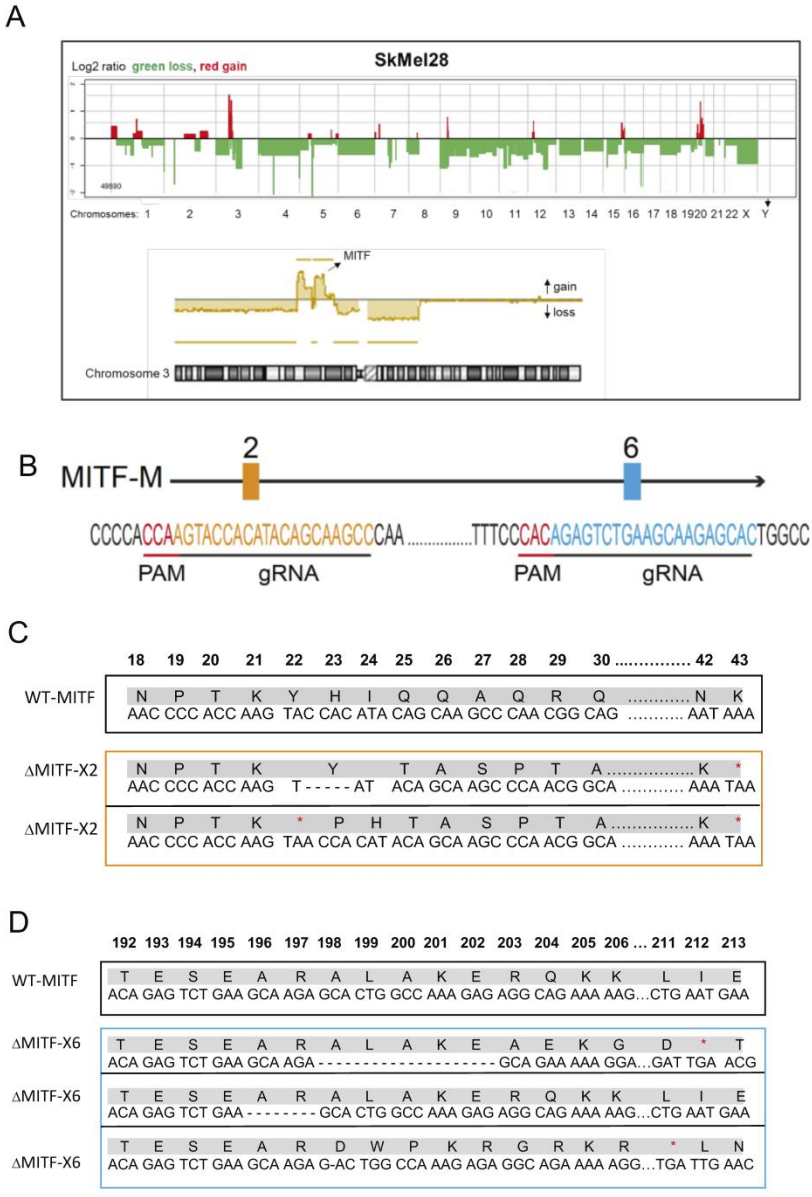

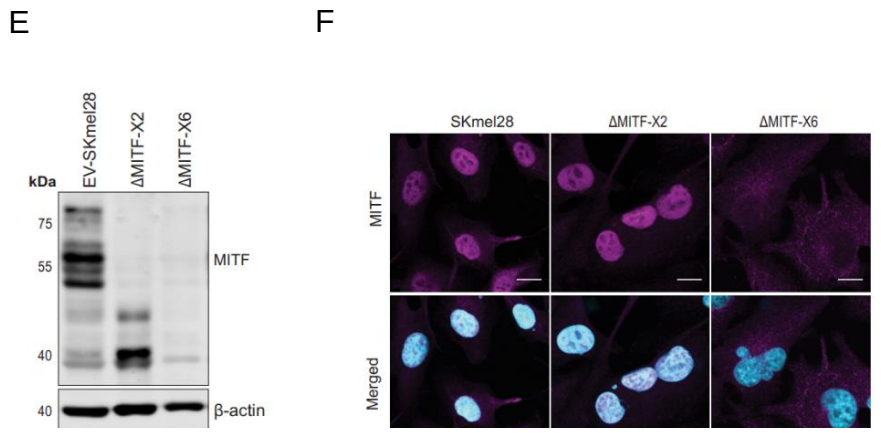

Figure 3. Generation of melanoma cells lacking MITF

A. CGH analysis shows chromosome duplication and deletion in SkMel28 cell line. Lower panel is chromosome 3, where MITF resides and is duplicated **B**. Schematic illustration of the targeted exons 2 and 6 of MITF. **C, D**. Mutations detected in the ΔMITF-X2 and ΔMITF-X6 cell lines. **E**. Western blot showing MITF bands in SkMel28, ΔMITF-X2 and ΔMITF-X6 cell lines. **F**. Immunostainining of MITF in SkMel28, ΔMITF-X2 and ΔMITF-X6 cells. Purple shows MITF staining whereas blue shows DAPI staining.

4.1.2 MITF knock out cells are larger in size

Phase contrast images of the ΔMITF-X2 and ΔMITF-X6 cells revealed an enlarged cell size when compared to the control cell line SKmel28. In addition, the ΔMITF-X6 cells showed dendritic structures (Figure 4A, top). Vimentin immunostaining of the cells showed altered cytoskeletal structure where the cytoplasm of cells was extended (Figure 4A). Flow cytometry confirmed these changes in cell size and showed that 38% of the ΔMITF-X2 and 55% of the ΔMITF-X6 cells were located in the upper right quadrant of the forward and side scatter plots as compared to 30% of wild type, indicating that the cells are larger and more granular than the EV-SkMel28 cells (Figure 4B).

To determine the growth pattern of the MITF KO cells on a 3D surface, we seeded the cells on top of Matrigel-coated slides supplemented with growth medium containing 2% Matrigel. After four days of growth on top of Matrigel, the EV-SkMel28 cell lines showed a flat, sheet-like morphology on top of the matrix whereas both MITF knock out cells formed spheres with cells tightly attached to each other (Figure 4C). Collectively, these results demonstrated that the absence of functional MITF causes morphological changes in cell shape, perhaps due to an increase in cell-cell adhesion, as observed when the cells were seeded on Matrigel-reconstituted basement membrane.

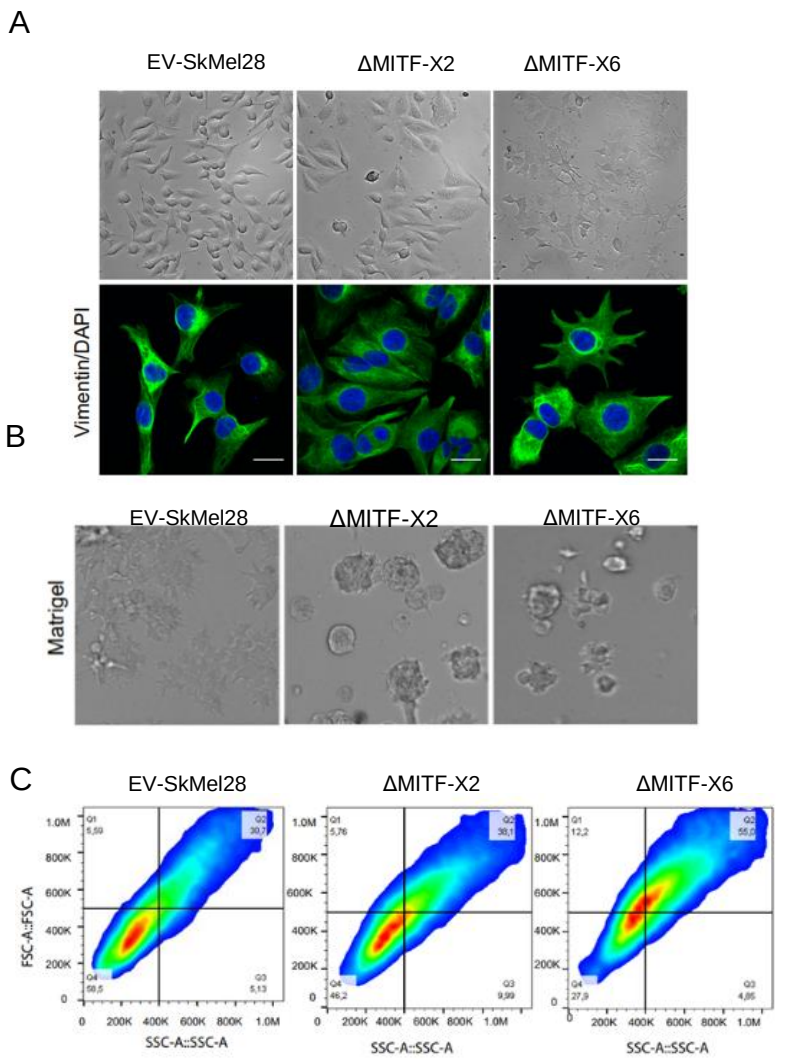

Figure 4. MITF KO affects cell size and morphology

A. Upper panel phase contrast images of EV-SkMel28, ΔMITF-X2 and ΔMITF-X6 cells displaying different morphology in cell culture. Lower panel Vimentin staining showed the cytoskeleton in MITF knock out cells and EV-SkMel28. **B**. Phase contrast images of EV-SkMel28, ΔMITF-X2 and ΔMITF-X6 cell lines grown on matrigel coated chamber slides. **C**. Flow cytometry images showing forward scatter and side scatter, representing size and granularity

4.1.3 MITF knockout cells proliferate slowly but are not senescent

Silencing MITF has been shown to induce G1 cell cycle arrest via Dia1 by elevating levels of $p27^{Kip1}$ (*CDKN1B*), a cyclin-dependent kinase inhibitor (Carreira et al., 2006). In addition, knockdown of MITF in p53 wild type melanoma cell lines led to senescence after cell cycle arrest (Giuliano et al., 2010). In contrast, increased levels of MITF can lead to cell cycle arrest by activating the expression of $p21^{CIP1}$ (*CDKN1A*) and $p16^{INK4A}$ (*CDKN2A*) in cells (Carreira et al., 2005; Loercher et al., 2005). In order to better assess the effects of complete MITF loss on cell proliferation, we performed a number of different experiments using the MITF knockout cells. First, we performed BrdU incorporation assays where cells were pulsed with BrdU for four hours, then stained with anti-BrdU antibody followed by flow cytometry. This showed a significant 25% and 40% decrease of BrdU positive cells in the ΔMITF-X2 and ΔMITF-X6 cell lines, respectively, as compared to the control EV-SkMel28 cell line (Figure 5A). We also performed live cell imaging using the IncuCyte system to follow differences in proliferation. This showed a 40% increase in the doubling time of ΔMITF-X2 and 50% increase for the ΔMITF-X6 cells compared to the control cell line (Figure 5B). Furthermore, we used the MTS cell viability assay which measures oxidoreductase acitivity of cells which reflects the number of viable cells. This showed that the MITF knock out cells exhibited a 50% reduction in cell number as compared to EV-SkMel28 cells (Figure 5C).

According to the published literature, depletion of MITF leads to senescence due to DNA damage through activation of the p53 pathway. The induction of $p16^{INK4a}$ has been linked with senescence in melanocyte and its expression is regulated by MITF (Sviderskaya et al., 2002). In order to determine if the lack of MITF leads to senescence, we performed SA-β-Gal staining on the knockout cells. Interestingly, we did not observe increased senescence in the MITF knockout cells; there was limited SA-β-Gal staining in both knockout cells as well as in the EV-SkMel28 control cells when compared to a positive control cell line transfected with the *LacZ* gene (Figure 5D). This is in agreement with previous work (Giuliano et al., 2010) where silencing of MITF in SKmel28 cells did not lead to senescence, possibly due to the presence of a p53 mutation in this cell line. It is worth noting that there was a faint staining for SA-β-Gal in all stained cell lines. This might be explained by the high lysosomal activity of melanoma cells (Debacq-Chainiaux et al., 2009). Together, these data indicate that the lack of MITF contributes to a significant delay in cell cycle progression, whereas senescence is not dependent on MITF in these cells.

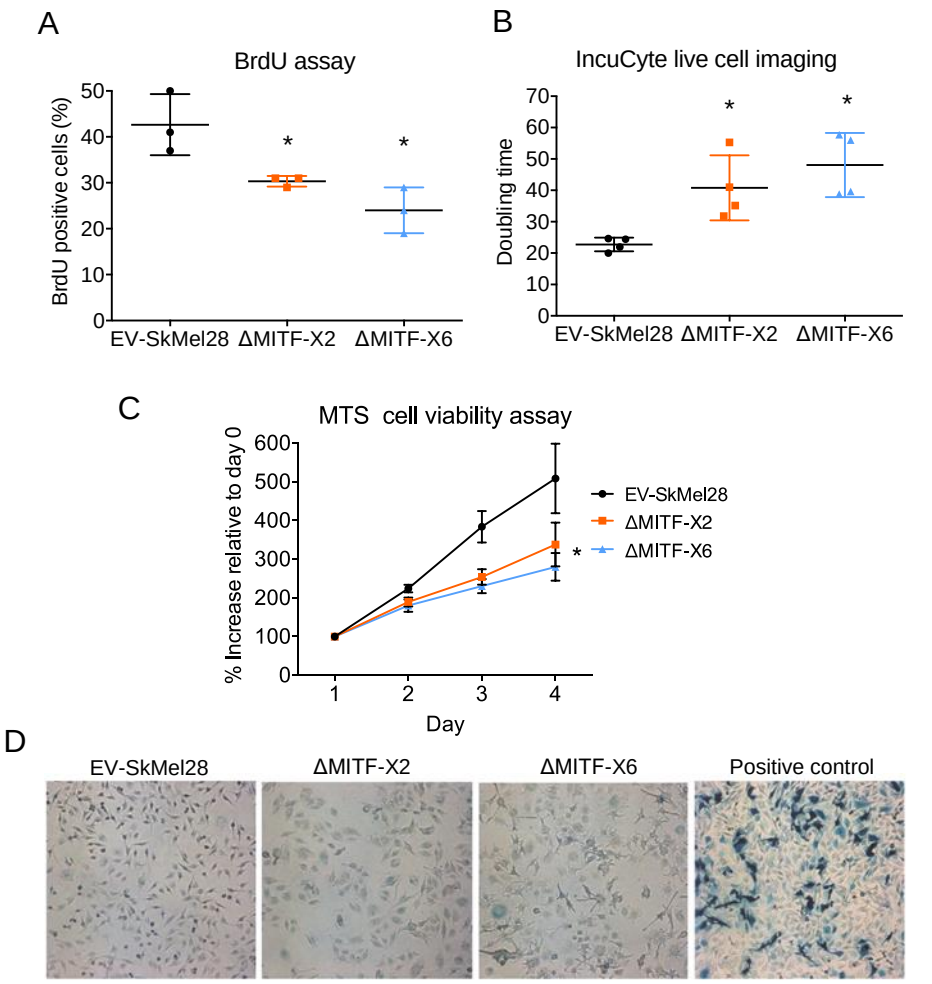

Figure 5. MITF KO cells proliferate slowly but do not induce senescence

A. Percentage of BrdU postive cells as assessed by flow cytometry for EV-SkMel28, ΔMITF-X2 and ΔMITF-X6 cell lines. Error bars represent standard deviation. *p-value<0.05, One way Anova. **B**. Doubling time in hours calculated from quantification of cell confluency over 4 days for the EV-SkMel28, ΔMITF-X2 and ΔMITF-X6 cell lines. *p-value<0.05, one way Anova. **C.** Percent increase of number of viable cells from day 1 measured with MTS assay. Error bars represent standard deviation. *p-value<0.05, one way Anova. **D**. X-gal staining for beta gal expression. From left to right: EV-SkMel28, ΔMITF-X2, ΔMITF-X6, and positive control (cells transfected with *LacZ* gene).

4.1.4 Generation of miR inducible MITF Knockdown cell lines

To further characterize the phenotype of melanoma cells expressing low levels of MITF and in order to validate the phenotype observed in the MITF-KO cells, we utilized piggy-bac transposon vector system to generate doxycycline inducible stable cell lines where MITF could be knocked down

using microRNA. To do this, we cloned miR-RNAs against MITF (Table 4) into the piggyBac vector (pPBhCMV_1-miR(BsgI)-pA-3) which expresses the microRNA under the reverse tetracycline transactivator promoter (Magnusdottir et al., 2013). The piggyBac vector was transfected into 501Mel and SkMel28 cell lines and treated with the neomycin antibiotic for two weeks for selection of positive cells. The inducible knockdown cell lines are termed miR-MITF. A control cell line was generated using miR(NTC) piggy-bac plasmid and was termed miR-CTRL. Similar to the SkMel28 cells, the 501Mel melanoma cell lines are easy to work with, they express high levels of MITF and harbour $BRAF^{V600E}$ mutation.

The knockdown efficiency was determined by western blotting. As expected, induction of miR-MITF expression by treating the cells with increasing concentrations of doxycycline 1µg/ml to 2 µg/ml to induce expression of the miRNAs, resulted in a significant reduction of MITF protein levels in 501Mel cells and practically eliminated MITF protein expression from the SKMel28 cells (Figure 6A). To further demonstrate the efficiency of the miR-MITF knockdown cell lines, we induced knockdown with doxycline for 24 hours and then performed qPCR for MITF and two MITF target genes; *MLANA* which is know to be activated by MITF and *MMP15* which we know to be suppressed by MITF (Du et al., 2003). We observed a 2-4 fold decrease of MITF as well as 2-fold decrease of *MLANA* and 2-5-fold increase of *MMP15* in each of the miR-MITF cell lines compared to their miR-CTRL cells (Figure 6B,C). Collectively our data showed that the piggy-bac inducible MITF knockdown cell lines can be used as a tool to validate and compare the observations made in the CRISPR-Cas9 mediated MITF knockout cells.

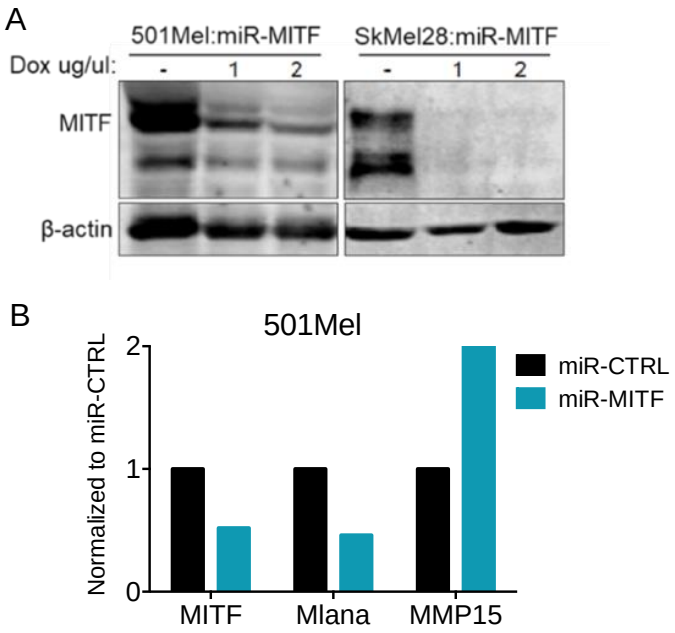

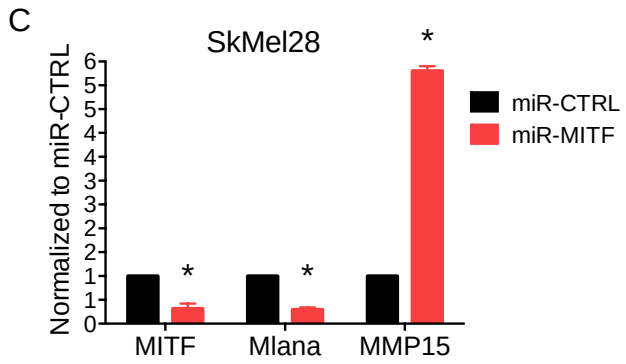

Figure 6. Generation of miR inducible MITF knockdown cell lines

A. Protein expression of MITF after inducing knockdown of MITF with 1 µg/ml and 2 µg/ml of doxycycline in the miR-MITF 501Mel and SKmel28 cell lines for 24 hours. Samples were analysed using western blotting. Actin was used as loading control. **B, C**. RNA-expression of MITF target genes as assessed by qPCR after miR-MITF induction with 1 µg/ml doxycycline for 24 hours in the SKmel28 and 501Mel cell lines. Error bars represent standard deviation. *p-value<0.05, one way Anova.

4.1.5 miR-MITF cell lines show reduced proliferation

To confirm whether the proliferation defect observed in MITF-KO cells is actually due to the lack of MITF, proliferation assays were carried out in stable miR-MITF cells lines. After inducing expression of the anti-MITF miRNAs in the cells, we analysed cell proliferation by live cell imaging at two-hour intervals for four days using the IncuCyte imaging system. The doubling time was calculated from quantification of live cell images. This showed a minor increase in doubling time upon miR-MITF induction in the SkMel28 cells whereas a stronger effect was seen in 501Mel cells. These cells had a doubling time of 26 hours upon miR-MITF induction as compared to 20 hours when miR-CTRL was induced in 501Mel cell, whereas in SkMel28 miR-MITF cells showed minor increase in doubling time compared to miR-CTRL lines (Figure 7A,B). Collectively, our data show that reduced levels of MITF in 501Mel cells lead to a reduced proliferation rate. However, in the SkMel28 cell line, transient depletion of MITF caused a minor delay in cell proliferation, possibly due to differences in cell lines or duration of knockdown, which could mask the effect of MITF in regulating the cell cycle. In addition, the defect in proliferation possibly contributed by cell death, which needs further investigation.

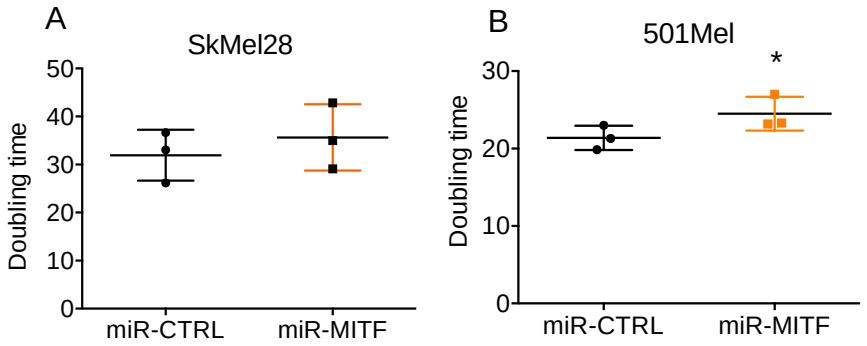

Figure 7. miR-MITF cell have reduced proliferation rates

A, B. Doubling time in hours calculated from quantification of cell confluency over 4 days for miR-MITF and miR-CTRL cell lines in 501Mel and SkMel28 cells. Error bars represent standard deviation. *p-value<0.05, t-test.

4.1.6 MITF-KO affects invasion

It has been shown that reduced MITF expression is associated with increased invasion in melanoma cell lines and melanoma tumours. It has been reported that silencing of MITF increases melanoma tumorigenicity, where MITF depeleted cells injected into mice formed more tumours compared to mice injected with scrambled sequence control (siScr) (Cheli et al., 2011). In addition, silencing of MITF has been shown to increase invasion assessed by matrigel coated Transwell assays, and consistenly increased MITF expression led to repressed invasion (Carreira et al., 2006). Hence, it has been proposed that MITF acts as suppressor of invasion. In contrast to this, low levels of MITF led to a reduction in tumour growth in mice (Feige et al., 2011). Thus, we asked whether permanent depletion of functional MITF in melanoma cells would increase the invasive potential of the MITF-KO cells as suggested by the studies mentioned above. To address the invasive potential of the MITF knockout cells, we performed Matrigel Transwell invasion assays. For this assay, the same number of cells were seeded on top of Matrigel-coated filters on the upper chamber of Transwell inserts in a 24-well plate. Of note, Matrigel mimics the basement membrane and is enriched with collagen and laminins. Cells that migrated through the Matrigel-coated filters were stained with DAPI and representative images of migrated cells were taken for analysis. Image quantification showed that both ΔMITF-X2 and ΔMITF-X6 cell lines had 50% fewer invaded cells when compared to the EV-SkMel28 cells (Figure 8A).

As reported in section in above 4.1.12, MITF-KO cells have increased cell-cell adhesion and have limited ECM interaction. Therefore, the migration capability of MITF-KO cells maybe compromised due to altered cell-ECM

interaction which lead to a redcution in invasion potential. In the future, the migration/invasion ability of MITF-KO cells can be challenged with different ECM components such as collagen, laminin or fibronectin coated matrix surfaces.

We wanted to investigate whether depletion of MITF would lead to increased migration. To do this, a wound-scratch assay was performed in which a scratch wound was made on a confluent layer of cells. The wound closure was then monitored by live cell imaging. Quantification of the scratch images showed that 22 hours after the scratch, the two MITF knock out cell lines were only able to close 50% of the gap compared to their parental counterpart which showed a full wound closure after this time (Figure 8B). We cannot fully exclude of the possibility that the differences in proliferation observed between the cells lead to differences in migration. The doubling time of EV-SkMel28 cell is around 24 hours. However, at 14 hours we already observe significant differences in the scratch assay between MITF-KO and EV-SkMel28 cells.

To further challenge the migration potential of MITF-KO cells with a different method, we performed a Transwell migration assay. For this assay, cells were seeded on the upper chambers of Transwell inserts and allowed to migrate through the 8 µm pores of the insert. After 8 hours of migration, only cells that had migrated to the other side of the filter were fixed and stained. Representative images of migrated cells were taken and the number of cells quantified. Quantification of the cells showed a minor decrease in the number of migrated cells for the ΔMITF-X2 knock out cells whereas no significant change was observed for the ΔMITF-X6 cells (Figure 8C). Together, our data indicate that the lack of MITF leads to a decrease in invasion potential of SkMel28 melanoma cells as evidenced by the Matrigel Transwell invasion assay. Furthermore, the migration potential of MITF-KO cells was significantly reduced when assayed on one dimensional surface with wound scratch assay. However, the Transwell migration assay only showed a minor decrease in the migration potential of the MITF-KO cells. This discrepancy might be explained by the different surfaces used in the migration assays.

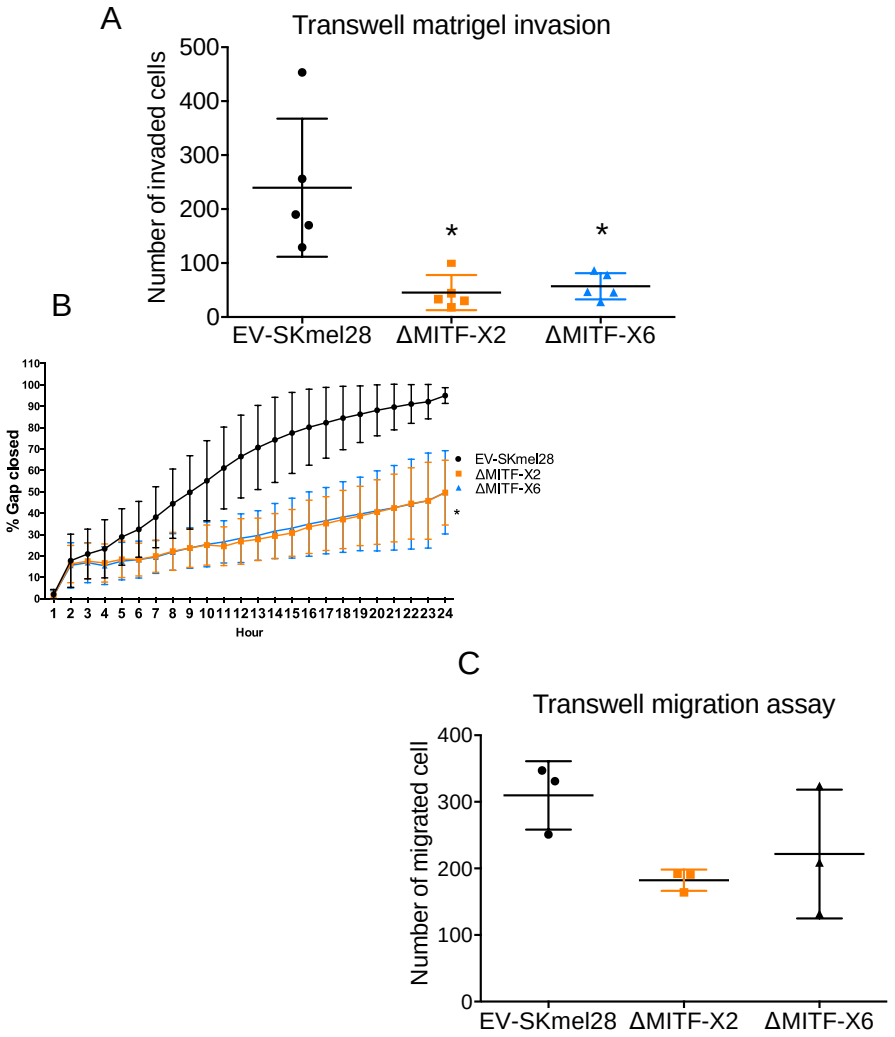

Figure 8. MITF KO cells are less invasive

A. The number of cells that have invaded through matrigel coated chambers. Error bars represent standard deviation. *p-value<0.05, one-way ANOVA. **B**. Quantified gap closure over 22 hours. Error bars represent standard deviation. *p-value<0.05, one-way ANOVA. **C**. Quantification of number of cells migrated through transwell chambers. Error bars represent standard deviation. Transwell inserts were stained with DAPI, representative images were taken and quantified with Fiji.

4.1.7 MITF knockdown cells are less motile

We asked whether short term depletion of MITF would lead to increased invasion and migration of the cells as reported previously (Carreira et al.,

2006). In addition, we wanted to compare the effects of short term knockdown of MITF with MITF-KO cells. Therefore, the invasion assay using Matrigel coated transwell chambers was repeated using the miR-MITF inducible SKmel28 cell line. First, MITF knockdown was induced for 24 hours before seeding the cells on Matrigel-coated transwell inserts. Then the cells were allowed to migrate through the Matrigel-matrix coated inserts for 45 hours. After that the Transwell inserts were stained with DAPI and representative images taken for quantification. Analysis of the images showed a minor increase in the number of invaded cells upon induction of miR-MITF as compared to the miR-Ctrl cell line (Figure 9A). Additionally, wound scratch assays were performed after a 24 hours induction of MITF knockdown. Quantification of scratch images showed that after 13 hours, the wound closure was 70% completed in the miR-MITF cell line when compared to 100% in miR-CTRL (Figure 9B,C). Our results indicate that short term reduction of MITF neither increased nor decreased the invasion ability of SkMel28 cells, whereas MITF-KO cells were significantly reduced in their invasion potential. Nevertheless, both transient depletion of MITF in miR-MITF cell lines and MITF-KO cells led to a decrease in migration ability, but the effect on migration was more pronounced in MITF-KO cells. Together our results suggest that there are functional differences in short- and long-term depletion of MITF in SkMel28 cell lines.

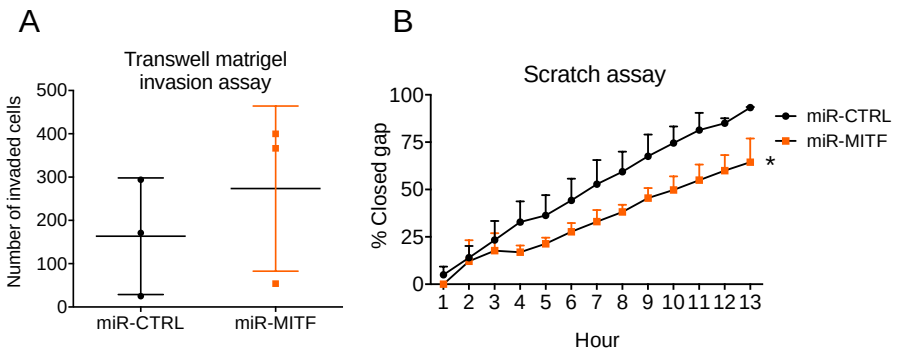

Figure 9. MITF knockdown cells are less motile

A. The number of cells that invaded through Matrigel upon the induction of miR-MITF or miR-CTRL in SkMel28 cell lines. Error bars represent standard deviation. **B.** Percent of closed gap over 13 hours for miR-CTRL and miR-MITF cell lines in SkMel28. Error bars represent standard deviation. *p-pvalue <0.0001, t-test.

4.1.8 Gene expression profile of Δ MITF-X6 cell

To study the underlying molecular mechanism for the dramatic changes observed in the phenotype of the MITF knockout cells, we performed mRNA sequencing of EV-SkMel28 and ΔMITF-X6 cells. We chose ΔMITF-X6 cells

for RNA-sequencing because they lack wild type MITF protein and therefore better represent melanoma cells lacking MITF. To do this, total RNA was isolated from both cell lines and mRNA purified. Subsequently, cDNA synthesis was performed and cDNA sequencing libraries were prepared for high throughput sequencing. Sequencing was performed on Illumina Hiseq at deCODE genetics. The raw sequence reads were aligned back to the human transcriptome using the Kallisto alignment tool (Bray et al., 2016). The alignment file was parsed into Sleuth (Pimentel et al., 2017) in order to perform differential gene expression analysis (see Appendix 3 for the details of the analysis). We identified 1516 differentially expressed genes (DEGs) between the ΔMITF-X6 and EV-SkMel28 cells with a cut-off FDR of <0.05 and 2-fold change in expression (Figure 10A). Of those, 937 were increased in expression in the ΔMITF-X6 cells compared to EV-SkMel28 and 580 were reduced in expression (Figure 10B). Several known targets of MITF were found among the DEGs, including *IRF4*, *MLANA*, *DCT, SEMA3C, PMEL, TRPM1*, *GRP143* and *MITF* itself. However, we did not see a change in the expression of *Tyr*, a known MITF target gene (Yasumoto et al., 1994).

In order to assess whether these genes are directly regulated by MITF, we analysed published MITF ChIP-seq data (Laurette et al., 2015) and assigned peaks to genes based on the distance from the TSS (10kb+/-) ($p < 1.113e-06$), and found that MITF is bound to 2068 genes. Among the 1516 DEGS, 200 genes were directly bound by MITF, 98 of which were induced in expression, whereas 102 of the bound genes were reduced in expression (Figure 10B). This indicates that a small subset of the differentially regulated genes are directly regulated by MITF. This suggests that only a fraction of genes directly bound by MITF were affected by its loss.

To further validate these results, we performed RT-qPCR on genes which showed differential expression in the RNA-seq data. Consistent with the RNA-seq results we found decreased expression of *MLANA, IRF4, ZNF703* and *NR4A3* and increased expression of *PRNP, DUSP1, ITIH5, MMP15* and *NGFR* (Figure 10C,D).

To classify the differentially expressed genes into functional groups, gene ontology analysis was carried out. This revealed that genes showing reduced expression in the ΔMITF-X6 cells were enriched for participation in cellular components such as melanosomes, pigment granules, melanosome membrane and chitosome. However, genes showing increased expression in the ΔMITF-X6 cells were enriched for terms such as endoplasmic reticulum lumen, proteinaceus extracellular matrix, basement membrane, extracellular matrix component and focal adhesion (Figure 10E). Similarly, KEGG pathway analysis demonstrated that genes showing reduced expression in the ΔMITF-X6 cells were associated with pathways involved in Fc gamma Receptor

mediated phagocytosis, mTOR signalling pathway, B cell receptor signalling and axon guidance. However, genes showing increased expression were involved in ECM receptor interaction, focal adhesion, proteoglycans in cancer, cell adhesion molecules and P13-Akt signalling pathway (Figure 10F). Together, the gene expression profile of ΔMITF-X6 revealed that MITF-KO cells exhibit a distinct expression profile when compared to EV-SkMel28 cells. The lack of MITF reprograms expression of genes involved in differentiation, extracellular matrix and cell adhesion pathways. In addition, the indirect effects of knocking out MITF resulted in major changes in the gene expression profile of MITF-KO cells suggesting a multilevel regulation of gene expression triggered by the loss of MITF.

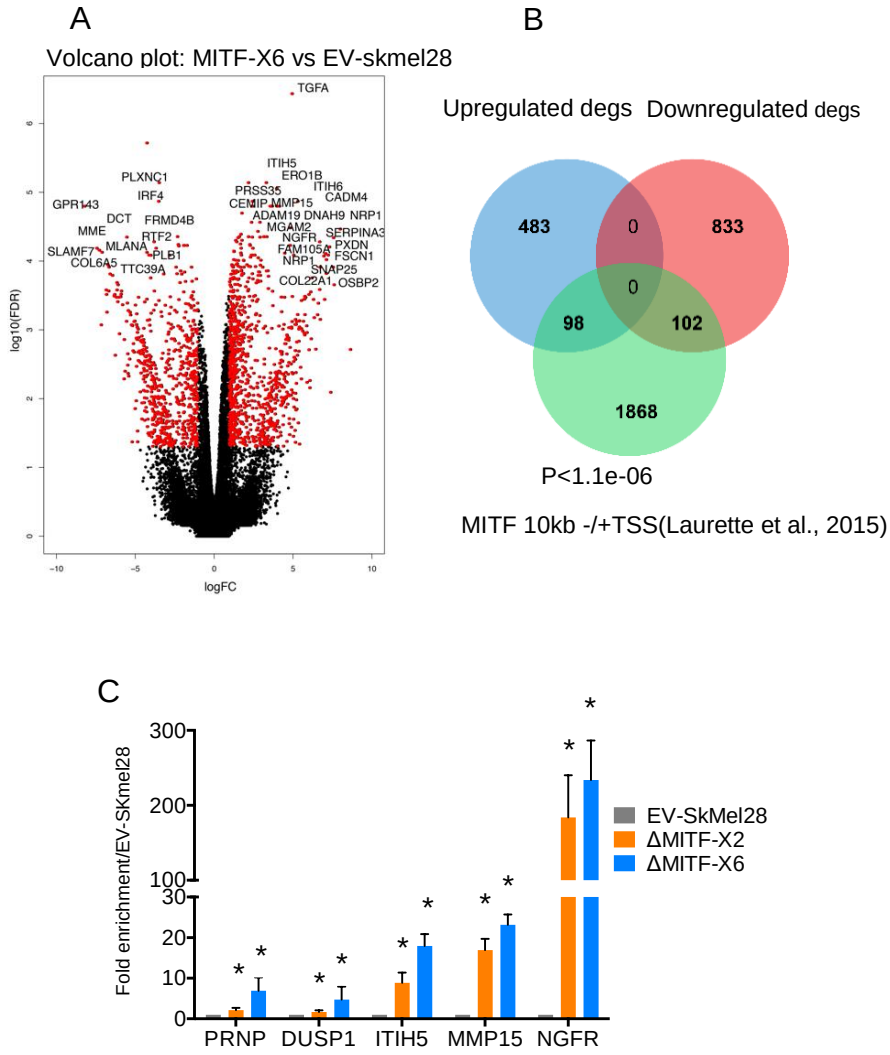

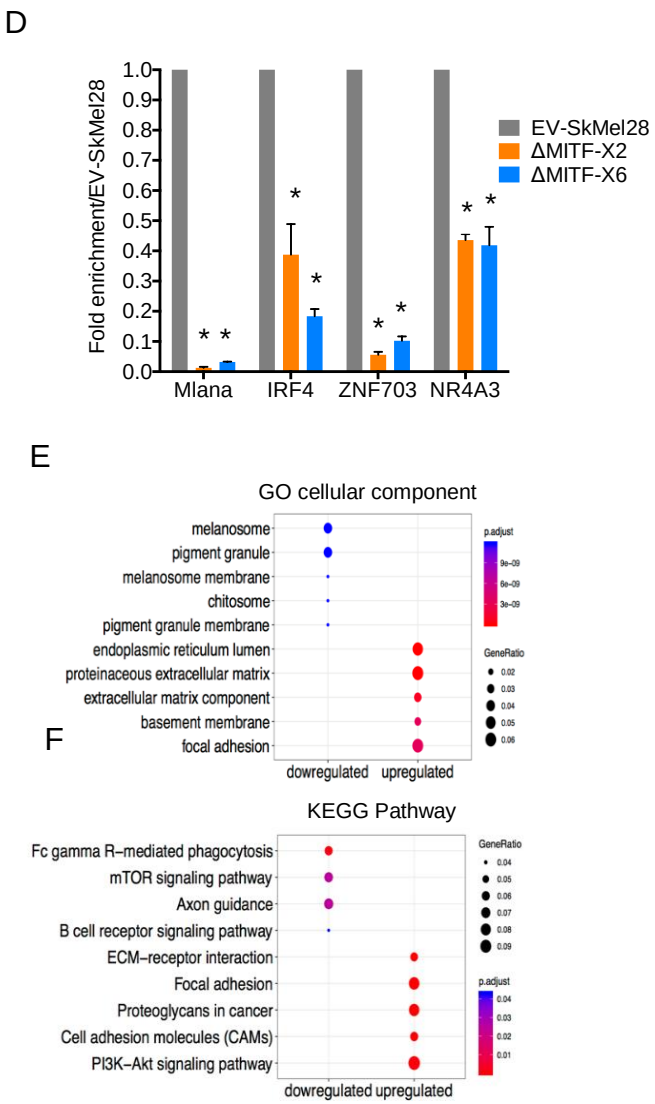

Figure 10. Gene expression profile of ΔMITF-X6 cell lines

A. Volcano plot showing differentially expressed genes (DEGs) (1516) with $\log_2$ 2-fold change and and FDR<0.05 represented in red dots. **B**. VennDiagram showing the number of overlapping genes between DEGs and MITF bound targets from 10kb up and down stream of TSS. **C, D.** RT-qPCR showing increased and decreased genes in MITF-KO cells, fold enrichment normalized to EV-SkMel28 cells. Error bars represent standard deviation. *p-value<0.05, Two way Anova **E, F.** GO and KEGG pathway analysis on increased and decreased genes in ΔMITF-X6 cells. Colour indicates the (qvalue<0.05) and size of circle indicates the gene ratio.

4.1.8.1 Gene expression profile of ΔMITF-X6 associates with Hoek proliferative, Tirosh MITF and Rambow neural crest signatures

Hoek et al (2006) performed gene expression analysis in melanoma samples and cells and devised a set of 96 genes which they termed melanocyte phenotype specific expression (*MPSE*). This gene set was further divided into two groups based on whether the cells/tumors exhibitied a proliferative or invasive phenotype (Hoek et al., 2006; Widmer et al., 2012). By utilizing this set of genes, we performed gene set enrichment analysis (Subramanian et al., 2005) in order to determine if there was a correlation between our data set and the Hoek proliferative and invasive signatures. Our analysis showed that ΔMITF-X6 cells were negatively enriched for the Hoek proliferative signature (Normalized enrichment score (NES): - 2.94) and positively enriched for the Hoek invasive signature (NES: 1.33) (Figure 11A,B). However, only 50% of the Hoek invasive signature genes were significantly increased in the ΔMITF-X6 cells (Figure 11C). This includes increased expression of *WNT5A, ZEB1* and *ITGA2*, but we did not see increased expression of *AXL* and *TWIST.* However, over 70% of the proliferative signature genes were reduced in expression in the ΔMITF-X6 cells (Figure 11C), including genes like *IRF4, PMEL, MLANA, DCT and CDH1*, all of which are well known differentiation/proliferative markers during melanoma development (Behrens, 1993; Budd & Jackson, 1995; Du et al., 2003; Praetorius et al., 2013). A transcriptomic signature driven by $MITF^{high}$ tumour cells was derived from single cell RNA-sequcing carried out on malignant melanoma tumours (Tirosh et al., 2016). Consistently, ΔMITF-X6 cells showed negative enrichment (NES: - 2.66) for the signature of $MITF^{high}$ melanoma tumours cells (Figure 11D). In line with this, the $MITF^{low}$ tumours in melanoma samples from TCGA database positively correlated (NES: 1.69) with transcriptome profile of ΔMITF-X6 cells (Figure 11E).

We also compared the transcriptome profile of ΔMITF-X6 cells to two gene signatures obtained from applying single cell RNA-sequcing to RAF inhibitor treated melanoma tumours (Rambow et al., 2018). These are: (i) Invasive Signature and (ii) Neural crest signature which was characterized to represent a population of cells of minimal residual disease. We found a poor positive correlation with ΔMITF-X6 and the Rambow invasive signature (NES:1), whereas the neural crest cell signature was significantly increased (NES: 1.56) in the ΔMITF-X6 cells (Figure 11F,G).

Thus, the delay in cell cycle progression observed in MITF knockout cells might be explained by a major decrease in the expression of the proliferative gene set in the ΔMITF-X6 cells, whereas reduced migratory and invasion

potential can be partly explained by the incomplete expression of invasive signature genes in these cells. Importantly, ΔMITF-X6 cells signature showed loss of MITF^{high} gene signature and gained neural crest transcriptome signature.

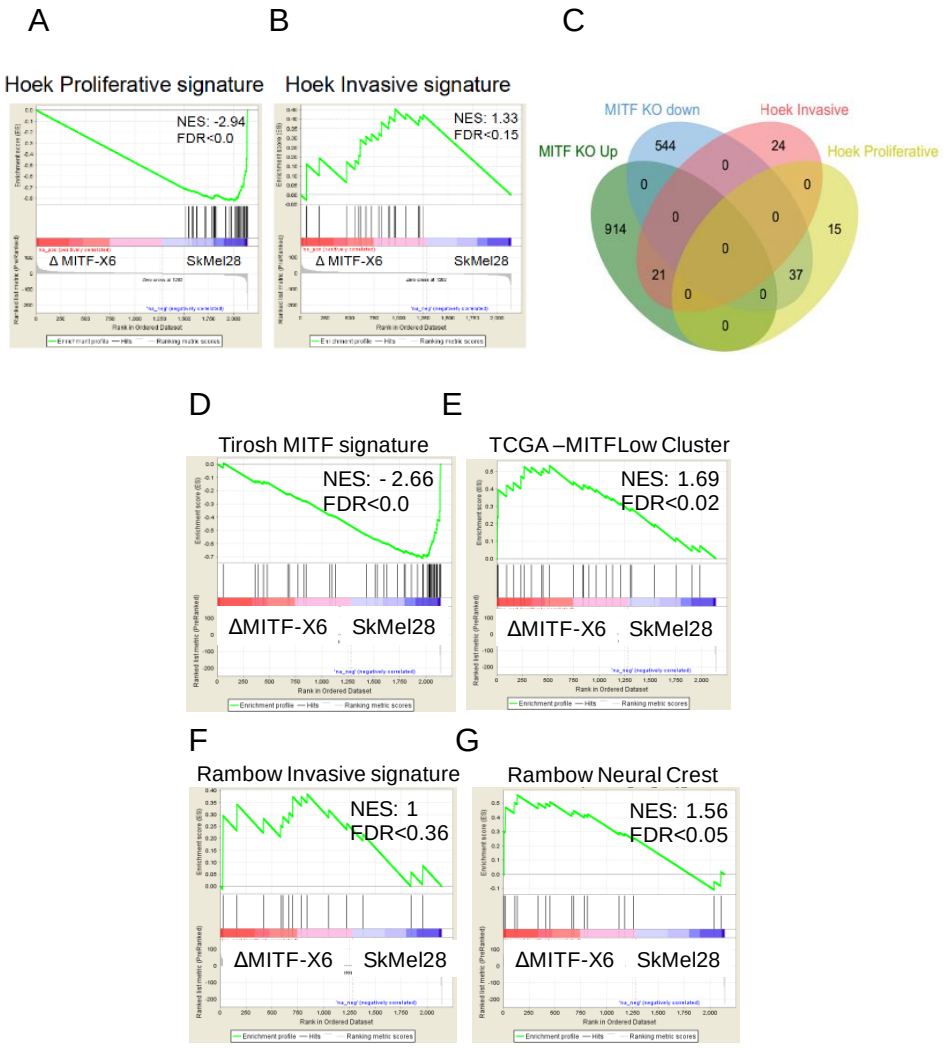

Figure 11. Gene expression profile of ΔMITF-X6 cell positively correlates with Heok proliferative gene signature

A, B. GSEA analysis on ΔMITF-X6 vs SkMel28 degs for Hoek proliferative/invasive gene signature. **C**. Venn diagram showing number overlapping genes between Heok proliferative/invasive signature and differentially expressed genes in ΔMITF-X6 vs SkMel28 cells. **E-G**. GSEA analysis on ΔMITF-X6 vs SkMel28 degs for Tirosh MITF, TCGA MITF-low, Rambow invasive, Rambow Neural Crest signature.

4.1.8.2 Gene expression profile of ⊿MITF-X6 cells resembles MITF low tumours

Melanoma tumours fall into distinct transcriptional profiles based on the level of MITF expression. Hence, melanoma tumours can be classified as $MITF^{high}$ and $MITF^{low}$ tumours where $MITF^{high}$ tumours are characterized as proliferative and $MITF^{low}$ tumours favour invasion and are susceptible to drug resistance by inducing oncogenic factors such as AXL, ZEB1 and SOX2 (Caramel et al., 2013; Hoek & Goding, 2010; Santini et al., 2014; Sensi et al., 2011; Strub et al., 2011). Thus, we asked whether the gene expression profile of the MITF knockout cells reflect the transcription profile of $MITF^{low}$ tumours *in vivo*?

To answer this, we performed differential gene expression analysis on $MITF^{high}$ versus $MITF^{low}$ tumours using RNA-seq data of cutaneous melanoma samples from the Cancer Genome Atlas (TCGA) (Cancer Genome Atlas, 2015). To do this, we separated the tumour samples based on MITF expression and then picked the 40 tumour samples with the highest MITF expression and the 40 tumours with the lowest expression and then performed differential gene expression analysis comparing $MITF^{low}$ versus $MITF^{high}$ groups. Our analysis revealed 2655 differentially expressed genes between $MITF^{low}$ and $MITF^{high}$ tumours (FDR<0.05 and LogFC (log2 fold change) >1). Among those, 1835 were induced in expression in $MITF^{low}$ tumours and 820 were repressed in $MITF^{low}$ skin cutaneous tumour samples (Figure 12A,B).

The differentially expressed genes were functionally classified by assigning them to gene ontology classes and pathways. Therefore, we performed GO term analysis for cellular component and KEGG pathway analysis for the genes differentially expressed in the $MITF^{low}$ vs $MITF^{high}$ tumours. GO term analysis for cellular component location showed that decreased genes in $MITF^{low}$ tumours enriched for melanosome, pigment granule, melanosome membrane, chitosome, pigment granule membrane, lysosomal membrane, lytic vacuole membrane, dendrite and vascular membrane, whereas induced genes in $MITF^{low}$ tumours were enriched for proteinasceuous extracellular matrix, extracellular matrix component, collagen trimer, basement membrane, endoplasmic reticulum lumen, synaptic membrane and external side of plasma membrane (Figure 12C).

The KEGG pathway analysis for genes showing increased expression revealed enrichment of the same pathways as MITF-KO cells, with additional pathways like hematopoietic cell lineage, protein digestion and absorption, cytokine-cytokine receptor interaction and complement and coagulation cascades. For genes showing reduced expression, the enriched pathways

were melanogenesis, platinum drug resistance and estrogen signalling pathway (Figure 12D). Collectively, we observed that MITF^{low} tumours and ΔMITF-X6 cells are enriched for the same functional class of genes and pathways indicating that ΔMITF-X6 cells have similar altered cellular pathways as melanoma tumours *in vivo.*

This led us to assess the extent of overlap of genes differentially expressed in melanoma tumours on the one hand and ΔMITF-X6 cells on the other. Overlapping analysis identified a total of 556 shared genes between melanoma tumours (TCGA) and ΔMITF-X6 data sets. From this, 211 genes were induced in expression and 302 genes were decreased in expression in both data sets. However, 15 genes that were repressed in ΔMITF-X6 cells were induced in MITF^{low} tumours, and 26 genes that were induced in epxression in ΔMITF-X6 cells were repressed in tumours (Figure 12E). Together, our analysis strongly suggests that MITF^{low} tumours in the TCGA data sets share an extensive list of gene expression programme with ΔMITF-X6 cells. Therefore, the ΔMITF-X6 cells mimick the melanoma tumours and serve as a model to study melanomagenesis.

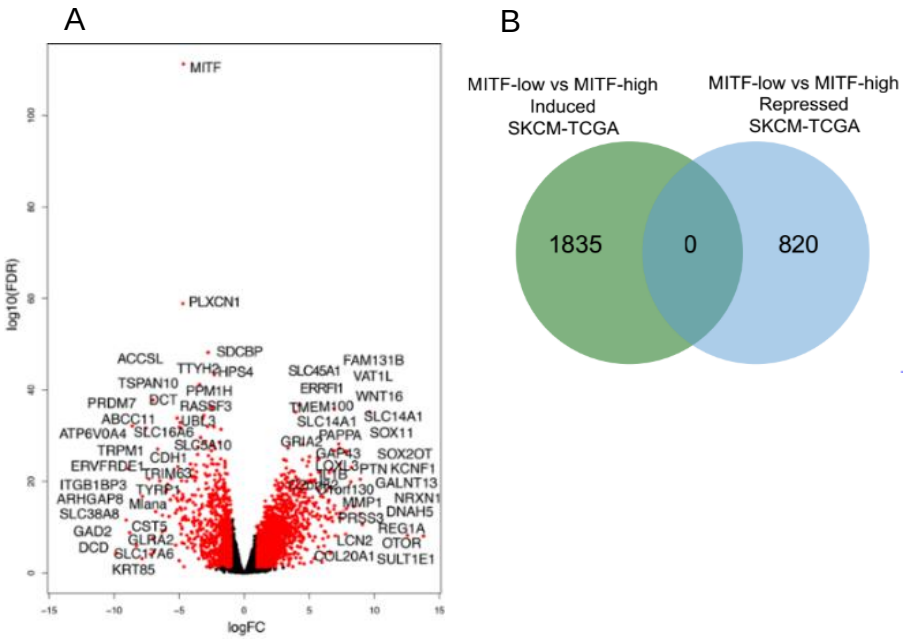

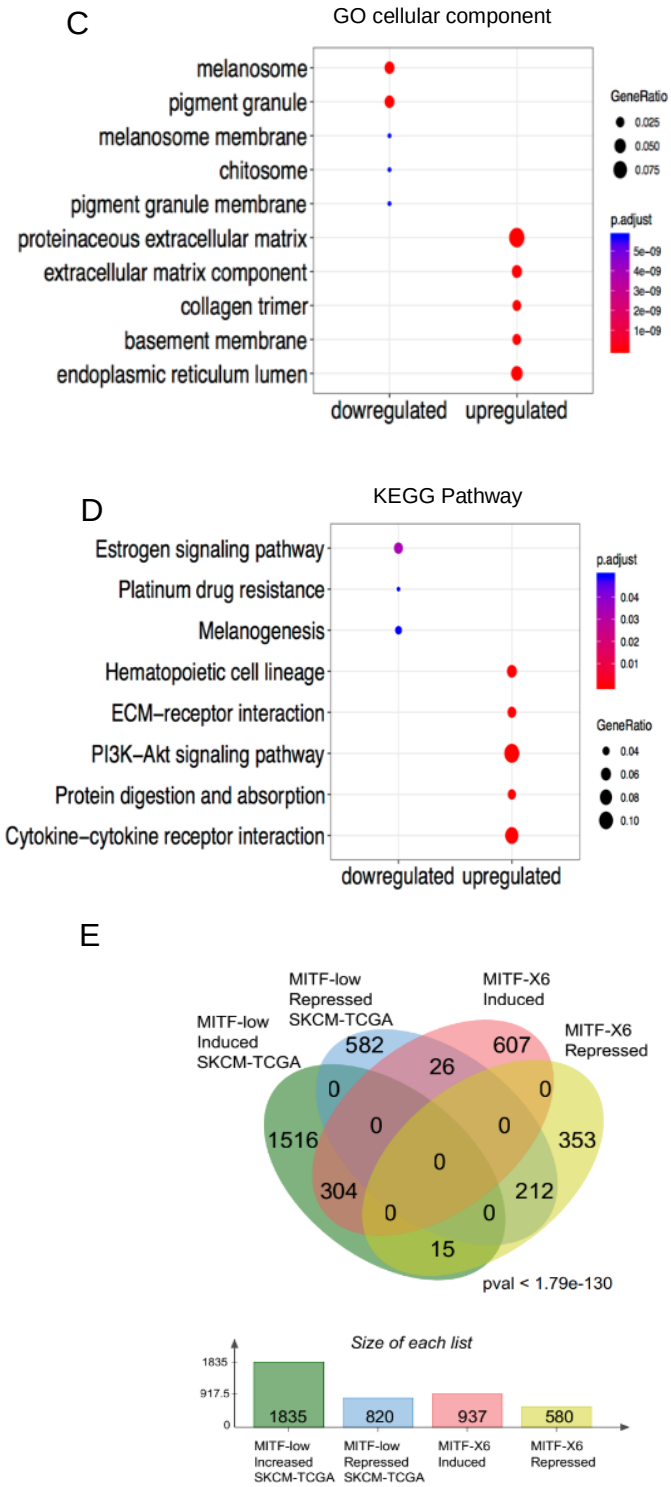

Figure 12. Gene expression profile of ΔMITF-X6 cells is similar to MITF^{low} tumours

A. Volcano plot showing differentially expressed genes (2655) with $\log_2$ 2-fold change and FDR<0.05 represented in red dots. **B**. Venn diagram showing the number of differentially expressed genes (DEGs) that are increased and reduced in TCGA-SKCM $MITF^{low}$ vs $MITF^{high}$ tumours and degs of ΔMITF-X6 vs SkMel28 cells. **C,D**. Gene ontology and KEGG pathway analysis on increased and decreased genes in $MITF^{low}$ and $MITF^{high}$ tumours. Color indicates the p-value and size of circles indicates the gene ratio. **E.** Venn diagram shows the number of shared genes between degs of TCGA-SKCM $MITF^{low}$ vs $MITF^{high}$ tumours and degs of ΔMITF-X6 vs SkMel28 cells.

4.1.8.3 Loss of MITF leads to de-differentiation of SKmel28 cells

The gene expression profile of ΔMITF-X6 cells showed that the cells lacked the expression of many melanocyte-specific differentiation genes such as *MLANA, DCT* and *PMEL* but not *TYR*. Expression of MITF has been positively correlated to E-Cadherin and inversely corelated to N-Cadherin, both of which are key players in epithelial to mesenchymal transition (Kim et al., 2013). In agreement with this, *GSEA* analysis on differentially expressed genes in ΔMITF-X6 and $MITF^{low}$ tumours showed positive enrichment for EMT hallmark genes and negative enrichment for pigmentation genes (Figure 13A), indicating the loss of a melanocyte-specific differentiation signature and a gain of expression of an EMT hallmark signature. Furthermore, Sennette et al. (2015) published their transcriptomic atlas of embryonic hair progenitor cells and embryonic skin. This atlas revealed gene signatures for each cell type including the hair follicle stem cell, melanocytes, Schwann cells, epidermal keratinocytes and fibroblasts (Rezza et al., 2016; Sennett et al., 2015). Therefore, we interrogated the genes expressed in the ΔMITF-X6 cells and EV-SkMel28 against these cell type specific gene signatures. Interestingly, the ΔMITF-X6 cells showed negative enrichment for the gene signature of melanocytes but, positive enrichment for Schwann cell and hair follicle stem cell signatures (Figure 13B). No enrichment was observed for genes of the Epidermis (Figure 13B).

Interestingly, there are MITF ChIP-seq peaks in intron 2 of both the E-Cadherin (*CDH1*) and N-cadherin (*CDH2*) genes (Figure 13C). In addition, RNA-seq data from ΔMITF-X6 identified a 4-fold increased expression of N-Cadherin (*CDH2*) and a 16-fold decrease in expression of E-Cadherin (*CDH1*). Moreover, we observed changes in the expression of other classical EMT-related genes with *TGFβ1, ZEB1* and *SOX2* showing increased expression in the ΔMITF-X6 cells and $MITF^{low}$ tumours. However, *SLUG* (or *SNAI2*) expression was decreased (Figure 13D). We used RT-qPCR to validate the expression of *TGFβ1*, *ITGA2*, *CDH1* and *CDH2* by RT-qPCR in MITF knock out and miR-MITF cell lines. Consistent with previous results, we saw decreased expression of *CDH1* and increased expression of *CDH2*, *ITGA2* TGFβ1 in all the cell lines tested (Figure 14A,B).

In a next step, E-Cadherin, N-Cadherin and SNAI2 (Slug) protein levels were assessed by Western blotting in both the inducible miR-MITF cell lines and the MITF KO cell lines. Both showed reduced levels of E-Cadherin, Slug and increased N-Cadherin expression (Figure 14C). However, the E-Cadherin protein resolved as a double band only in SkMel28 cells where the lower band corresponds to the correct size of the E-Cadherin. We do not know what the upper band represents. Collectively, our data showed that the lack of MITF directly leads to a loss of E-Cadherin and gain of N-Cadherin. Moreover, the lack of MITF promotes the expression of EMT hallmark genes in MITF-KO cell lines and MITF ^{low} tumours including *SOX2*, *TGFβ1* and *ZEB1* except *SLUG* expression is repressed. Finally, MITF-KO cells and MITF^{low} tumours are driven to a more de-differentiated state by the loss of expression of melanocyte and pigmentation genes and gain of not only EMT hallmark genes but also neural crest cell specific genes, suggesting that the loss of MITF promotes EMT. This process directs the melanoma cells towards neural crest origins.

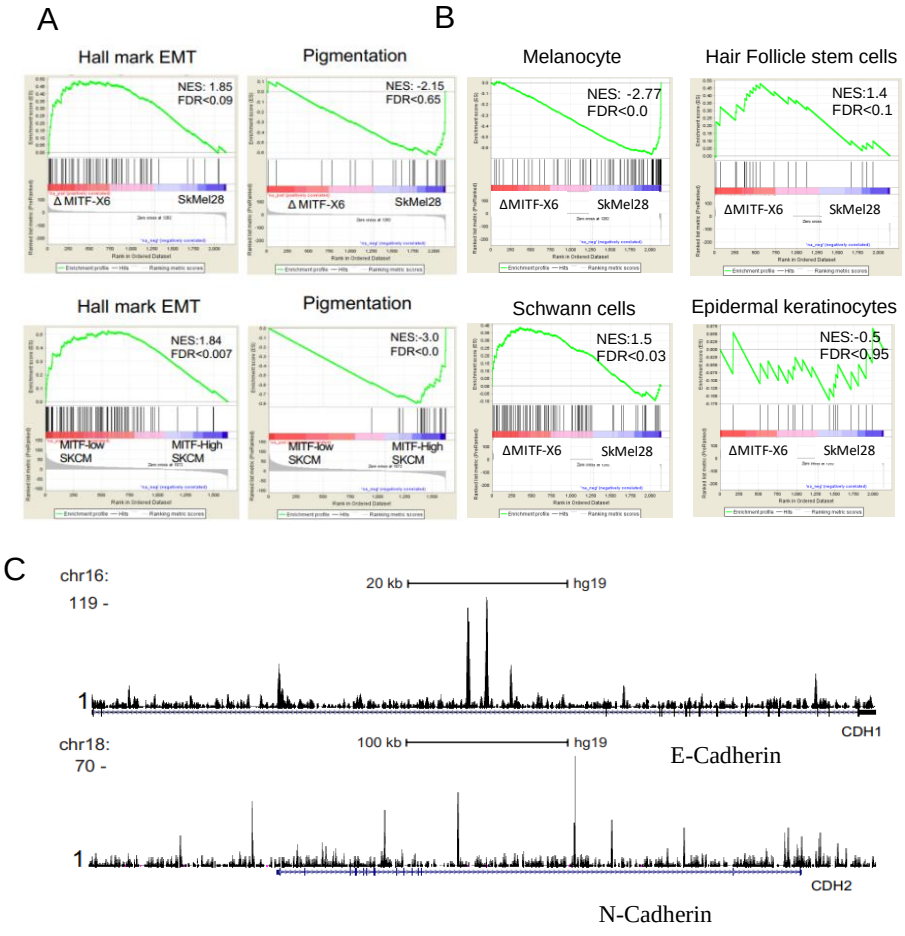

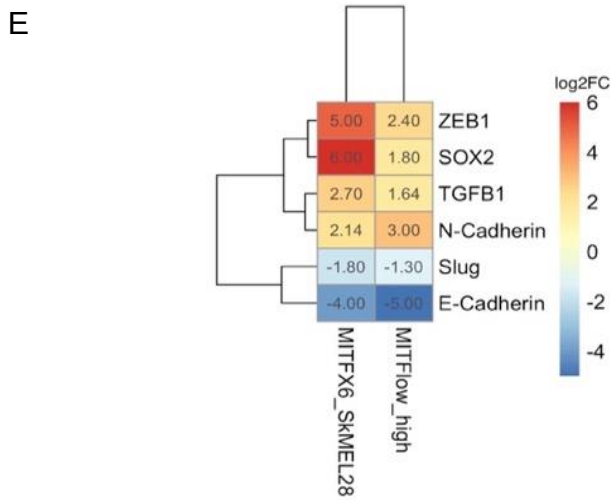

Figure 13. Loss of MITF drives de-differentiation of SkMel28 melanoma cells

A. *GSEA* analysis on MITF^{low} tumours and ΔMITF-X6 showed enrichment for EMT hallmark genes and negative enrichment for pigmentation genes. **B**. Mitf ChIP-seq peaks on intron2 of *CDH1* and *CDH2* .**C**. Heatmap of EMT marker genes, log2Fold change value plotted for MITF ^{low} vs MITF ^{high} tumours and ΔMITF-X6 vs SkMel28.

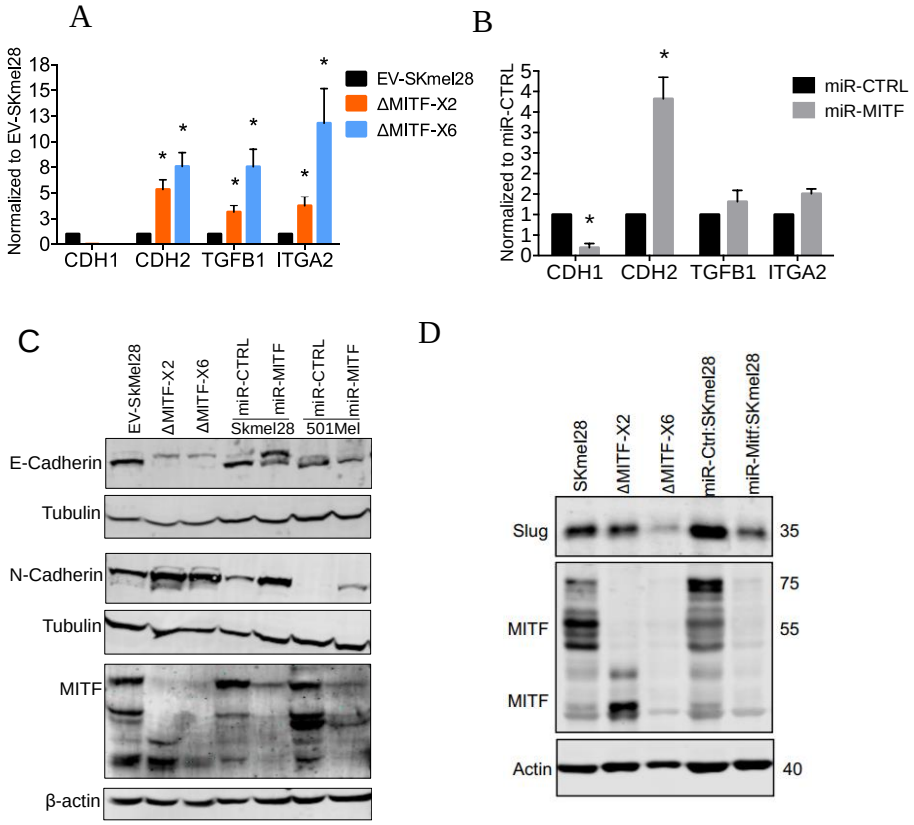

Figure 14. MITF regultes expression of E and N cadherins

A, B. Expression of EMT markers assessed by RT-qPCR in MITF KO cells and miR-MITF cell lines. Error bars represent standard deviation. *p-value<0.05, two-way Anova. **C**. Expression of MITF, E-Cadherin and N-Cadherin proteins was measured in MITF KO and miR-MITF (501Mel and SkMel28) cell lines by western blot analysis. Tubulin and β-actin were used as loading controls. **D.** Expression of Slug and MITF proteins in EV-SkMeL28 and MITF-KO cells and miRCTRL and miRMITF SkMel28 cells.

4.1.8.4 Differential expression of extracellular matrix and adhesion related signature in ΔMITF-X6 cells

From Gene ontology and KEGG pathway analysis of the genes differentially expressed between ΔMITF-X6 and EV-SkMel28 and MITF^{low} and MITF^{high} tumours, we observed an enrichment for genes involved in focal adhesion and extracellular matrix (Figure 15). It showed reduced expression of many integrins (including *ITGA2, ITGA3, ITGA4, ITGA5, ITGA*10), collagens (including *COL4A2, COL4A3, COL11A2, COL5A2*) and laminins (*LAMA4*, *LAMB3*). In the ChIP-seq data of Laurette et al (2015), a majority of these genes showed binding of MITF close to the genes. Particularily strong binding was found for MITF in *COL5A2, COL11A2* and *COL4A2*. Collectively, our data indicate that MITF binds and affects the expression of extracellular matrix-related adhesion genes in melanoma cells.

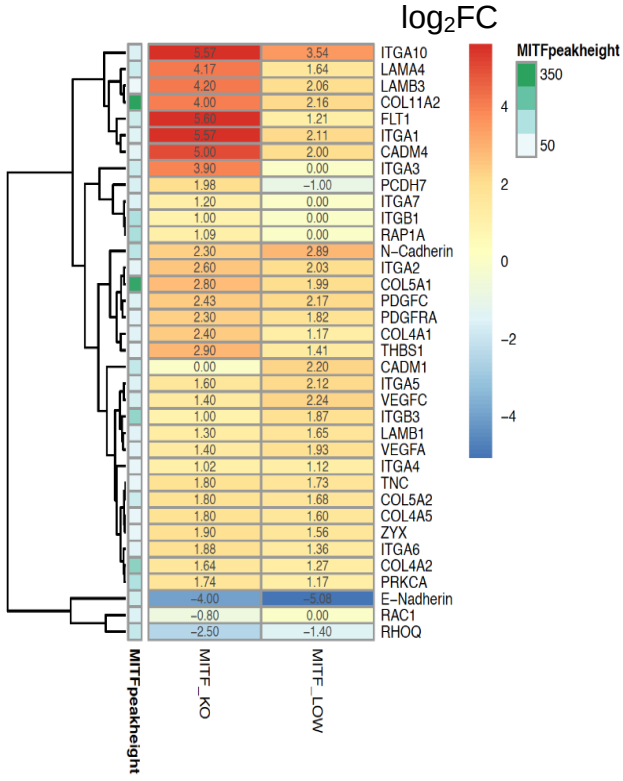

Figure 15. Increased adhesion signature in MITF-KO cells and MITF^{low} tumours

Expression of a subset of adhesion-associated genes plotted in a heatmap. Log fold enrichment of ΔMITF-X6 vs EV-SkMel28 and MITF^{low} vs MITF^{high} were used for plotting. MITF peak height was plotted next to each corresponding gene.

4.1.9 MITF regulates paxillin directly

We also characterized the expression of the focal adhesion regulators focal adhesion kinase (FAK) and Paxillin. They localize at focal adhesion points and regulate the dynamics between integrin and the F actin cytoskeleton in order to regulate cell migration (Deakin & Turner, 2008; Lim et al., 2008). Interestingly, both genes were directly bound by MITF in the ChIP-seq data- we observed valid binding as measured by peak height compared to negative control actin (30) with pvalue<1e-10 (Figure 16A). MITF binding sites in intron 6 of Paxillin has 4 E-box CANNTG/A and 1 CATGTG M-box sites suggesting direct binding. The FAK gene contains only one MITF peak with an M-box located in intron 1. RNA-seq data showed increased expression of Paxillin in the ΔMITF-X6 cells, whereas the expression of FAK was unchanged (Figure 16B). This suggests that MITF has direct effects on regulating the cell adhesion network in melanoma through repressing Paxillin expression. This needs to be verified further in additional cell models and using assays for gene repression.

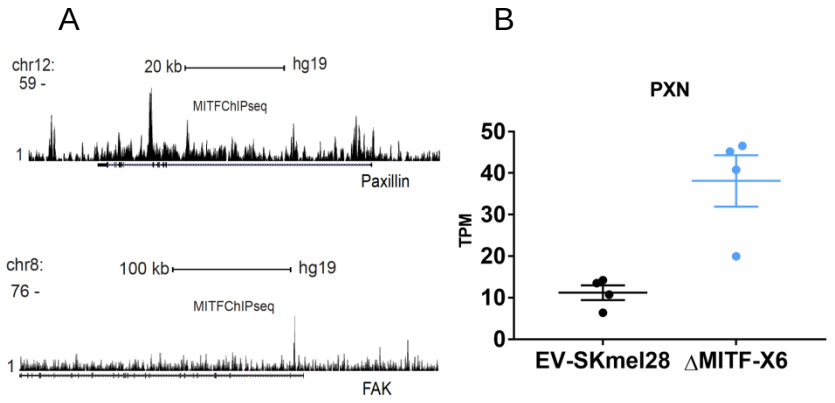

Figure 16. MITF regulates paxillin directly

A. Schematic of ChIP-seq tracks generated from UCSC genome browser. MITF ChIP-seq peaks at intron 4 of Paxillin and at the promoter of FAK. Chromosome number and ChIP-seq peak height indicated on right corner. **B**. RNA-expression of Paxillin in tpm (transcript per million) in ΔMITF-X6 and SkMel28.

4.1.10 Increased Paxillin and FAK focal points in MITF knock out and MITF knockdown cell lines

In order to investigate the expression of Paxillin and FAK in the ΔMITF-X6 cells, we performed immunostaining for phosphorylated forms of Paxillin (Tyr 111) and FAK (Tyr397) as phosphorylation is needed to potentiate the localization of Paxillin and FAK to focal points (Panetti, 2002). The results from our immunostainings showed that ΔMITF-X6 cells had increased numbers of focal points with a stronger staining of Paxillin (Tyr111) and FAK (Tyr397) at the cell periphery (Figure 17A,B). In agreement with this, the miR-MITF cell lines (both 501Mel and SkMEL28) also showed stronger Paxillin (Tyr111) and FAK (Tyr397) staining; noticeably the focal points were clustered near the cell edges in the knockout cells when compared to the wild type (Figure 18A,B). Our results suggest that MITF positively regulates the expression of FAK and Paxillin which in turn increases the adhesion of MITF-KO cells.

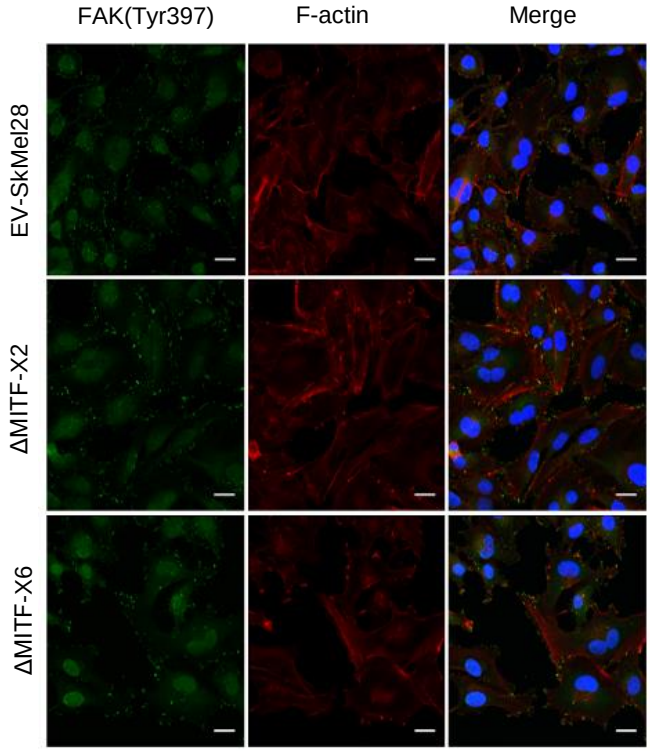

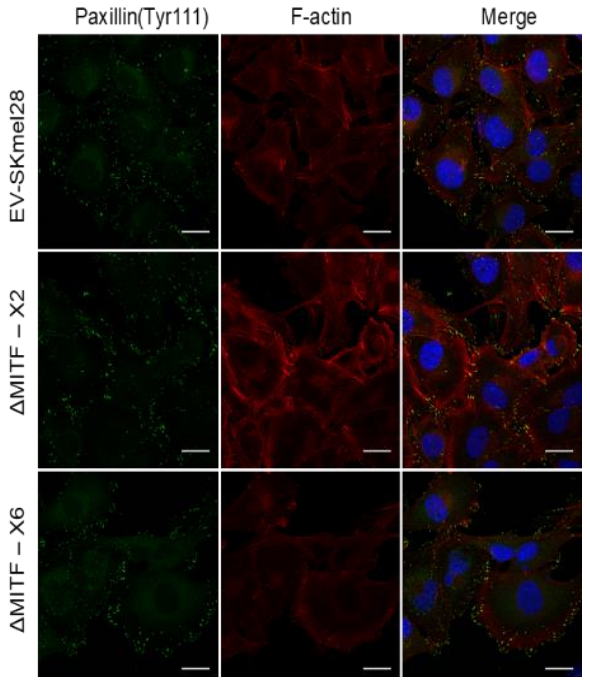

Figure 17. Paxillin and FAK focal points are increased in the MITF-KO cell lines

Immunostaining for FAK (Tyr 397), Paxillin(Tyr111) and F actin in MITF-KO and EV-SkMel28 cell lines. Scale bars: 21µM

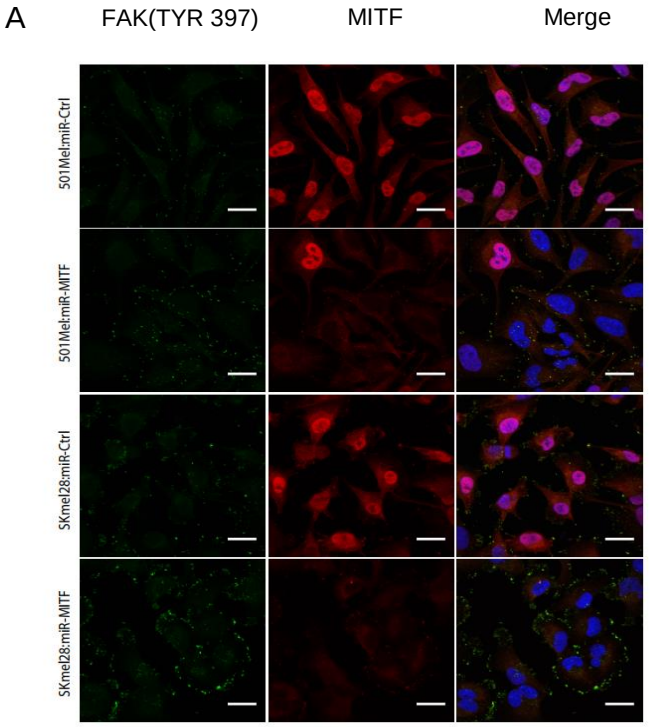

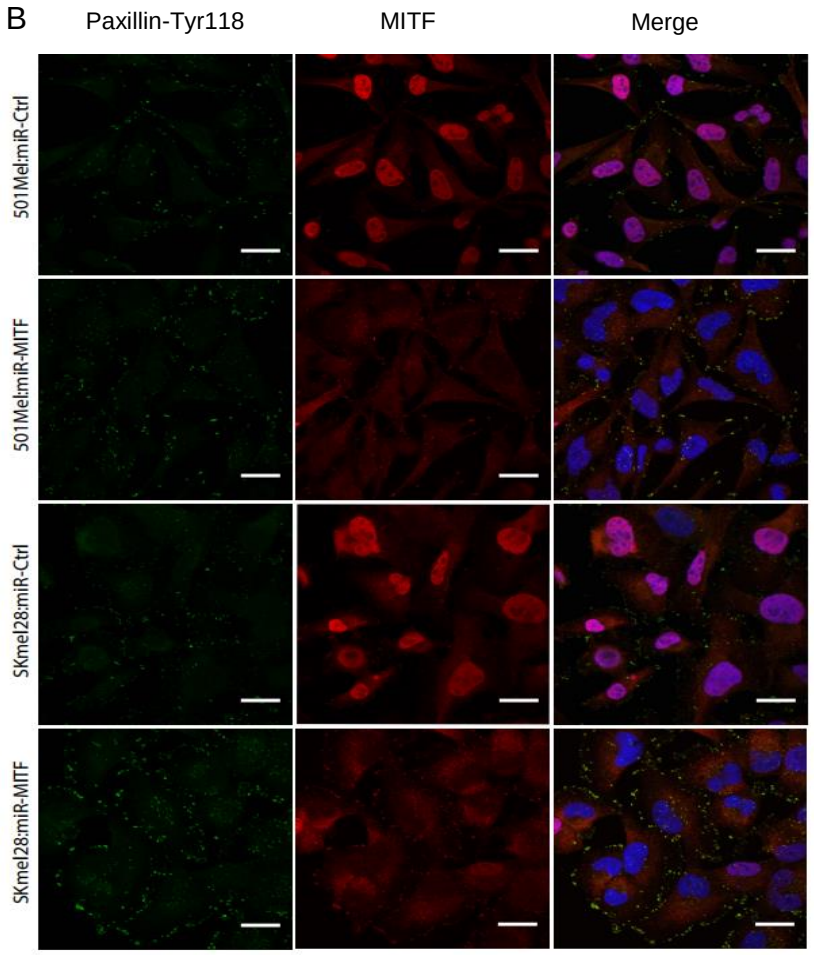

Figure 18. Paxillin and FAK focal points incresased in miR-MITF cells

Immunostaining for FAK (Tyr 397), Paxillin(Tyr111) and F actin in MITF-KO and EV-SkMel28 cell lines. Scale bars: 21µM

4.1.11 Loss of MITF induced epigenetic change

In spite of the fact that we saw major changes in the gene expression profile of MITF-KO cells compared to wild type cells, around 15% of those differentially expressed genes are directly bound by MITF based on MITF ChIP-seq data. So, what might be affecting the changes not caused directly by MITF? One possible explanation is epigenetic modifcation, including histone modifications. In order to test this, we performed ChIP against the active mark H3K4Me3 and the repressive mark H3K9me3 for selected genes that show differences in expression in the knockout cells and quantified the

enrichment by RT-qPCR. The H3K4Me3 mark is present at the promoters of actively transcribed genes. For this, we checked the level of H3K4me3 mark on promoters of genes that are implicated in melanoma differentiation and invasion. We observed decreased tri-methylation of H3K4 in the *MLANA*, *RRAGD* and *QPCT* promoters, these genes are reduced in expression in MITF-KO cells which is in line with the reduction of active mark H3K4me3. Interestingly, increased tri-methylation of H3K4 was observed in the promoters of *TGFB1*, *ZEB1*, *NGFR*, *AMOTL1* and *TLR2*, and these genes are induced in expression in MITF-KO cells (Figure 19A-H). In the next step, we performed ChIP-qPCR for the repressive mark H3K9me3 and checked the promoters of two genes; one is *SERPINA3* which showed a 5791-fold increase in expression in ΔMITF-X6 cells compared to EV-SkMel28 and is the most significantly induced gene in ΔMITF-X6 cells. The second gene we analysed was *TGFB1*, which has been shown to dominate the transcription program of MITF^{low} cells (Hoek et al., 2006). Conversely, ChIP-qPCR for H3K9Me3 showed decreased enrichment for *SERPINA3* and *TGFB1* (Figure 19I,J). Consistently, expression of both of these genes was increased in the ΔMITF-X6 cells. Together, our data show that long term loss of MITF may reshape the chromatin landscape. This could be partly through covalent modification of histones, which in turn allows cells to reprogram their gene expression profile to cope with the insult caused by the loss of MITF. Whether these are immediate changes that later get reversed, or permanent changes to chromatin in cells lacking MITF awaits further analysis.

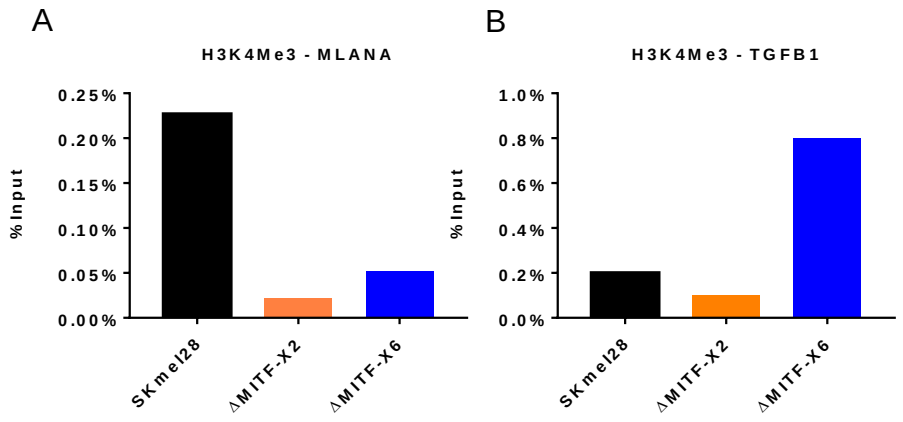

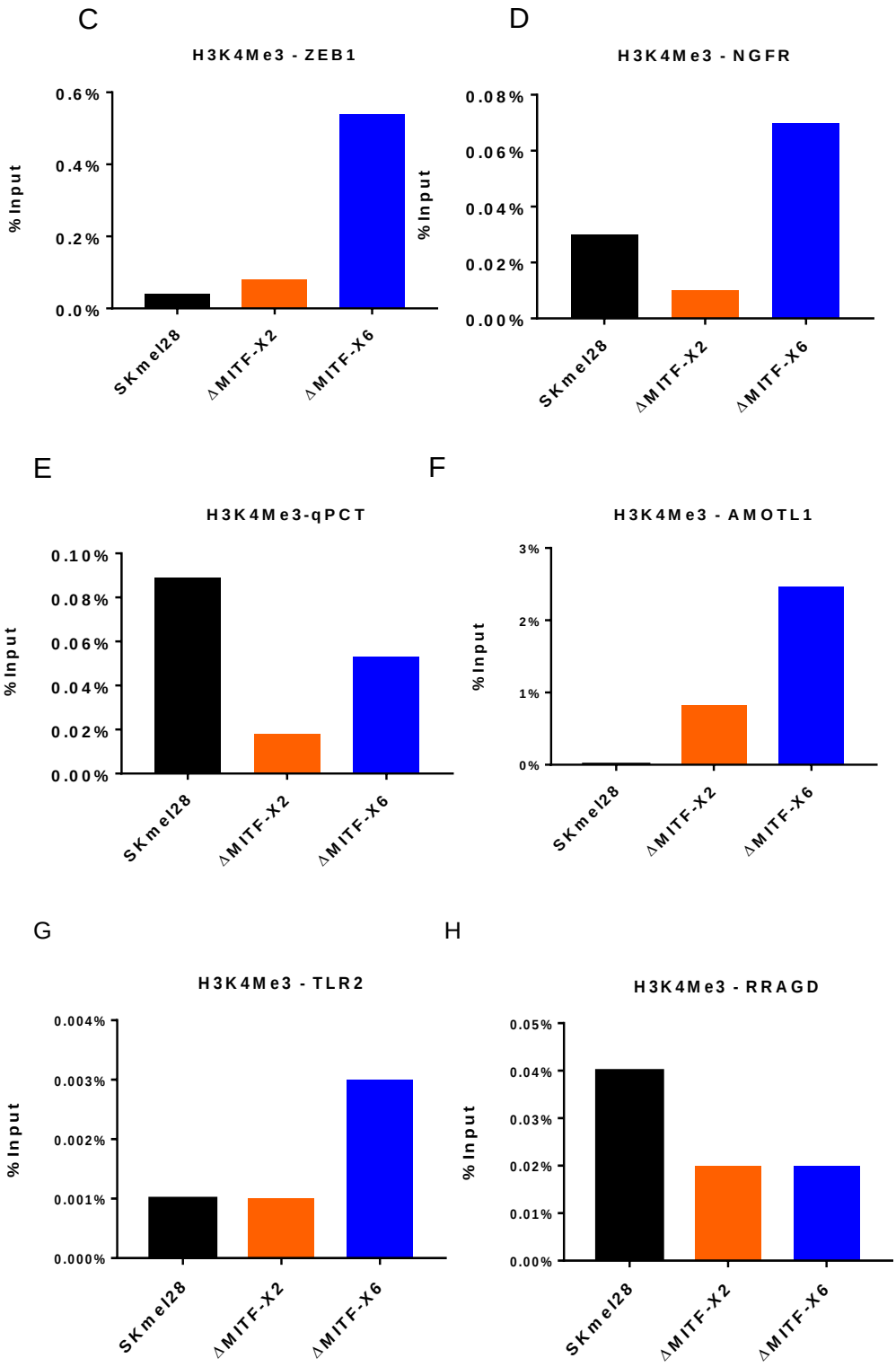
C
H3K4Me3 - ZEB1
% Input
0.6%
0.4%
0.2%
0.0%
SKmel28
ΔMITF-X2
ΔMITF-X6
D
H3K4Me3 - NGFR
% Input
0.08%
0.06%
0.04%
0.02%
0.00%
SKmel28
ΔMITF-X2
ΔMITF-X6
E
H3K4Me3-qPCT
% Input
0.10%
0.08%
0.06%
0.04%
0.02%
0.00%
SKmel28
ΔMITF-X2
ΔMITF-X6
F
H3K4Me3 - AMOTL1
% Input
3%
2%
1%
0%
SKmel28
ΔMITF-X2
ΔMITF-X6
G
H3K4Me3 - TLR2
% Input
0.004%
0.003%
0.002%
0.001%
0.000%
SKmel28
ΔMITF-X2
ΔMITF-X6
H
H3K4Me3 - RRAGD
% Input
0.05%
0.04%
0.03%
0.02%
0.01%
0.00%
SKmel28
ΔMITF-X2
ΔMITF-X6

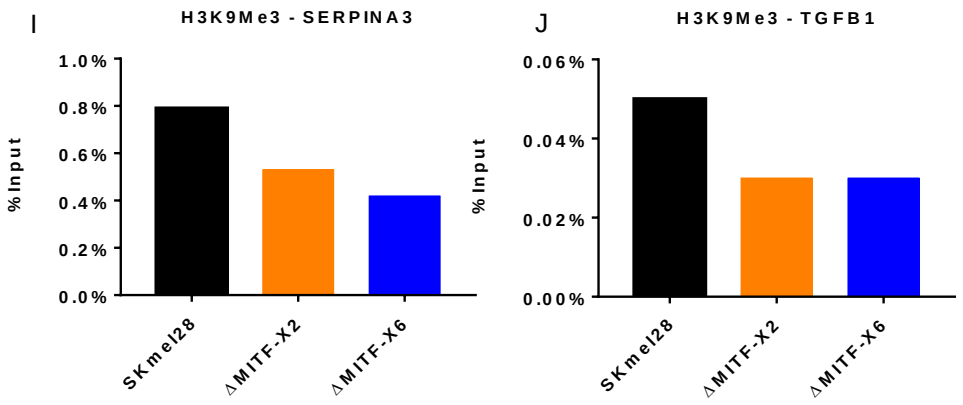

Figure 19. Changes in the epigenetic landscape in MITF-KO cells

A-J. ChIP-qPCR for H3K4Me3 and H3K9Me3. Primers used were designed to target the gene promoter; the enrichment was calculated using input.

4.1.12 SETDB2 is highly expressed in melanoma tumours and positively correlates with MITF expression

RNA-seq data showed that *SETDB2* expression was reduced 3-fold in the ΔMITF-X6 cells as compared to wild type cells (Figure 20A). This effect on SETDB2 was further validated by RT-qPCR, which showed a 2-3-fold decrease in *SETDB2* expression in the ΔMITF-X2 and ΔMITF-X6 cells as compared to EV-SKmel28 cells (Figure 20B). To determine the expression of *SETDB2* across different cancers, we interrogated the transcriptome data from the Cancer Genome Atlas. It showed that *SETDB2* had the highest expression in acute myeloid leukemia (AML), immediately followed by uveal melanoma and cutaneous melanoma (Figure 20C). In cutaneous melanoma tumour samples, *SETDB2* mRNA expression was positively correlated with the expression of MITF mRNA (Pearson correlation 0.6); the expression of *SETDB2* was significantly higher in $MITF^{high}$ tumours compared to $MITF^{low}$ tumours (Figure 20D,E). Together, our data show that *SETDB2* is highly expressed in melanoma tumours and that its expression is significantly correlated with MITF expression in melanoma tumours.

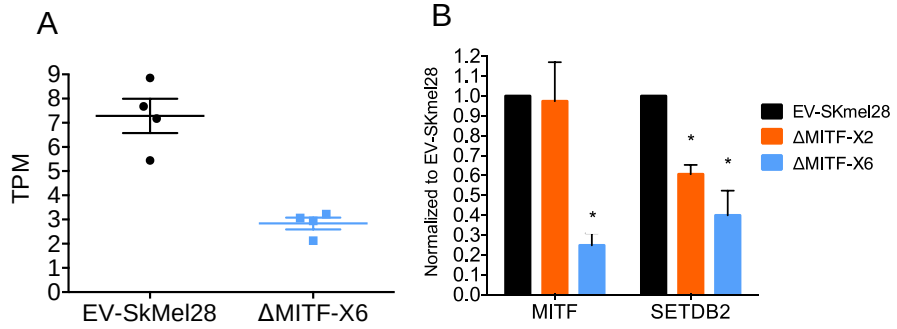

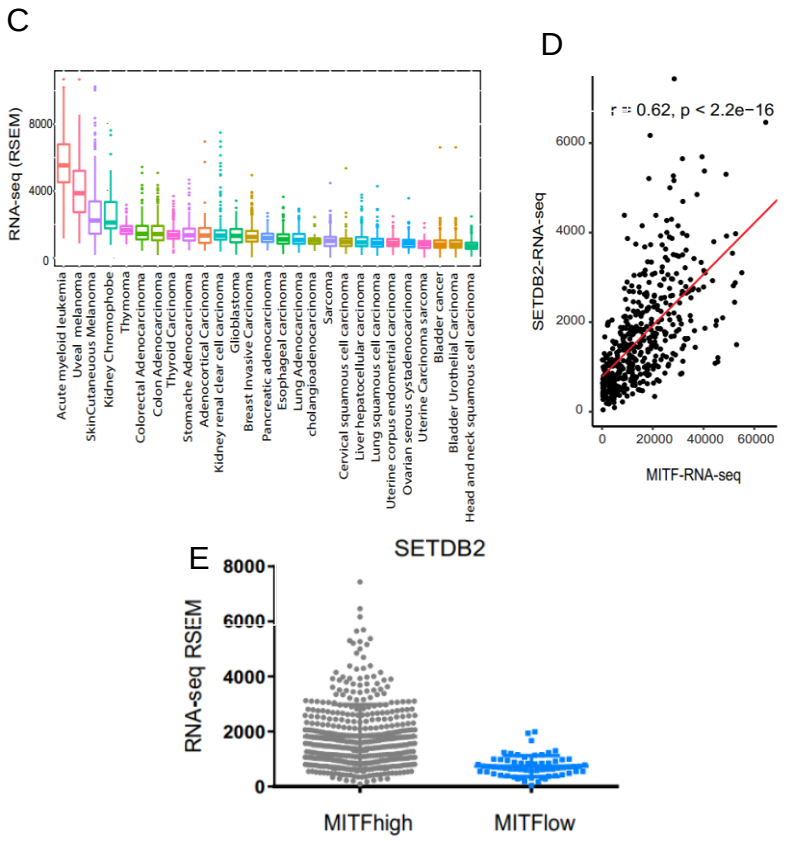

Figure 20. SETDB2 is highly expressed in melanoma tumours

A. RNA-seq expression of SETDB2 in ΔMITF-X6 and SkMel28 cell lines. Error bars represent standard deviation. **B**. RNA expression of SETDB2 assessed by RT-qPCR in MITF knock out cells. Error bars represent standard deviation. *p-value<0.05, One way Anova. **C**. SETDB2 transcript expression across 30 cancer types in TCGA data base. **D**. Scatter plot showing SETDB2 and MITF expression in 482 melanoma tumour samples with Pearson correlation of 0.62 and p-value <2.2E-16. **E**. RNA-expression of SETDB2 in $MITF^{low}$ and $MITF^{high}$ tumour samples.

4.1.12.1 SETDB2 is a direct target of MITF

The MITF ChIP-seq (Laurette et al., 2015) data showed two MITF binding sites in the *SETDB2* promoter and second last intron. One site is located in the *SETDB2* promoter and contains an E-box sequence (CACGTG). A second peak is located in intron 11 and contains a CACATG motif (Figure

21A). In order to determine if MITF directly affects SETDB2 expression, we performed RT-qPCR after inducing MITF knockdown in the miR-MITF cell lines. Inducing miR-MITF led to a 60% decrease in *SETDB2* expression in miR-MITF cells as compared to miR-CTRL cells (Figure 21B). Furthermore, ectopic expression of MITF in LU1205 cells, a cell line expressing low levels of endogenous MITF, *SETDB2* expression was increased 2-fold as compared to an empty vector control (Figure 21C). Our data suggest a direct link between MITF and SETDB2 in melanoma cells as well as in melanoma tumours.

A

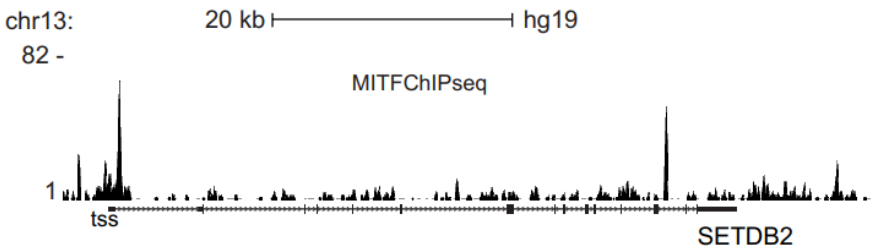

B

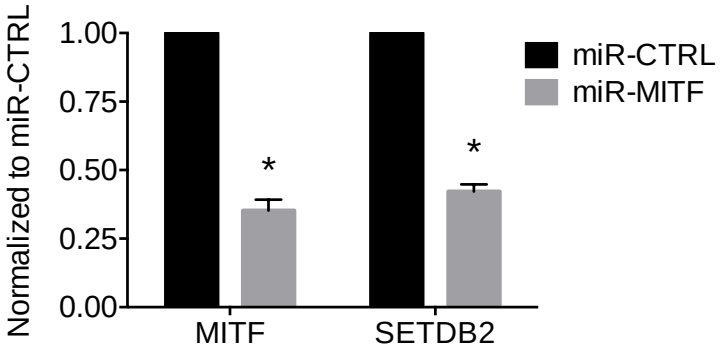

C

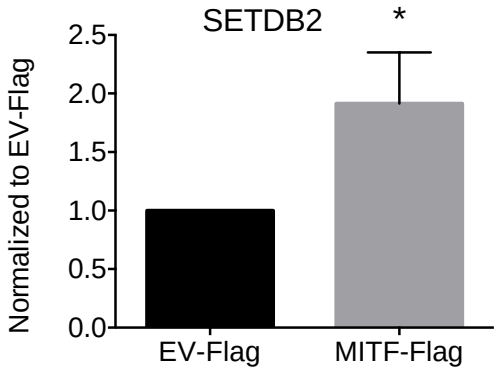

Figure 21. SETDB2 is a direct target of MITF

A. ChIP-seq track for MITF taken from UCSC genome browser illustrating MITF binding sites on *SETDB2* promoter and second last intron. **B.** RT-qPCR expression of *SETDB2* and *MITF* in miR-MITF cell lines. The expression was normalized to the miR-CTRL SkMel28 cell line. Error bars represent standard deviation. *p-value<0.05, One way Anova **C.** mRNA expression of *SETDB2* measured by RT-qPCR by ectopically expressing MITF-Flag in Lu1205 cells. Expression was normalized to EV-Flag. *p-value< 0.05, t - test

4.1.12.2 SETDB2 affects proliferation by modulating cell cycle inhibitors

As reported above (See section 4.5), MITF knock out and knockdown cell lines exhibit a decreased proliferation rate. Therefore, we characterized the expression of cell cycle regulators in the ΔMITF-X6 knock out cells. This showed increased expression of the cell cycle inhibitors *p57, p21^{CIP1}, p15* and *p18* and decreased expression of *CDK2* and *CDK5R1* (Figure 22A). Interestingly none of the cell cycle inhibitors have ChIP-seq peaks for MITF in their promoters or in 10 kb distance upstream or downstream from the transcription start site. Interestingly, a recent publication (Lin et al., 2018) showed that in acute lymphoblastic leukemia, *SETDB2* suppresses *p18* (*CDK2NC*) expression through H3K9 trimethylation of the promoter. Furthermore, induced expression of *TGFB1* was observed in MITF-X6 cells, which is a known potent inhibitor of the cell cycle (Pietenpol et al., 1990; Shipley et al., 1986).

Thus, we asked whether *SETDB2* might play a similar role in regulating the expression of the cell cycle inhibitors in melanoma cells. We used siRNA to knockdown *SETDB2* in 501Mel and SKmel28 cell lines and then characterized the expression of cell cycle regulators using real time qPCR. We observed increased expression of *p57*, *p15,* and *TGFB1* upon siRNA-mediated *SETDB2* knockdown (Figure 22B,C). We also checked the protein expression of additional cell cycle inhibitors such as p21^{CIP1} and p27^{KIP1}, both of which were previously reported to be affected by depletion of MITF. Western blotting performed after siSETDB2 showed increased expression of p21^{CIP1} in the SKmel28 cells whereas p27^{KIP1} was unchanged in SkMel28 cells (Figure 22D). Expression of *p21^{CIP1}* was not affected in 501Mel cells because *p21^{CIP1}* promoter has been reported to be highly methylated in this cell line and its protein is not detectable (Halaban et al., 2009). Instead, p27^{KIP1} was increased upon loss of MITF in 501Mel cells (Figure 22D). The effects of *SETDB2* on cell proliferation were studied using Incucyte live cell imaging over four days after siSETDB2 treatment. Quantification of the doubling time showed that the siSETDB2 cells had a significantly increased doubling time in 501Mel cells, going from 25 hours in siCTRL cells to 32

hours in siSETDB2 cells; a minor increase was observed in the doubling time of SKmel28 cells. This might be due to inefficient knockdown of SETDB2 or by masking of the effect by the p53 mutation in SkMel28 (Figure 22E,F). Together, our data indicate that *SETDB2* regulates cell cycle progression through repression of cell cycle inhibitors in melanoma cells. In addition, *TGFB1* expression was induced upon knockdown of *SETDB2*, indicating that it might participate in maintaining cell cycle progression through repression of *TGFB1* expression.

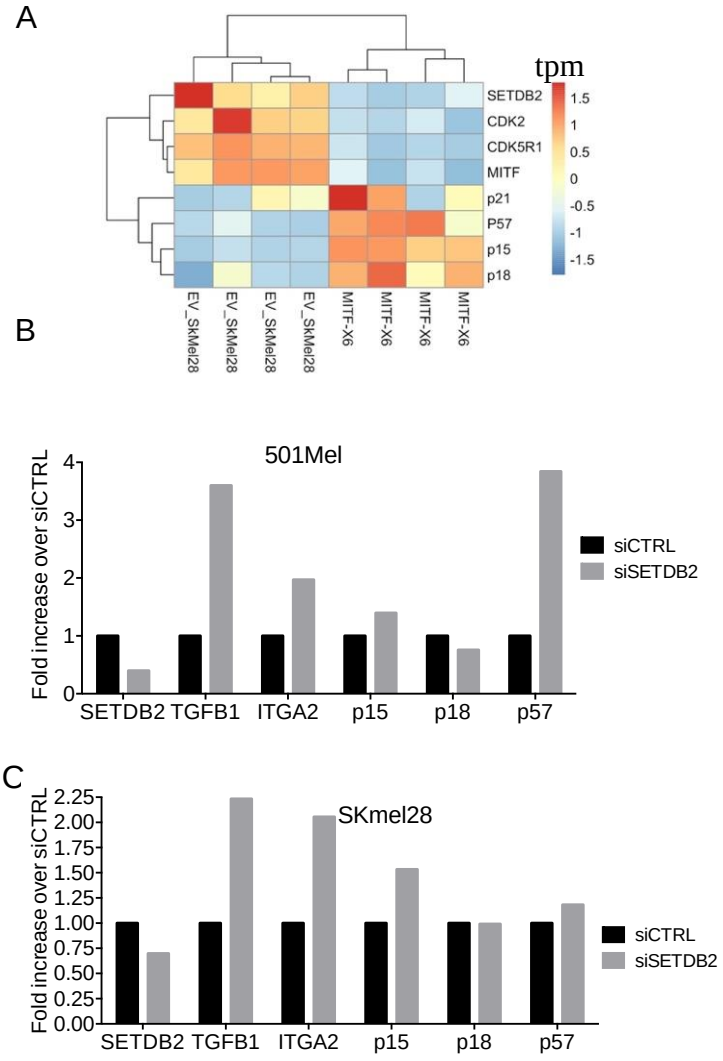

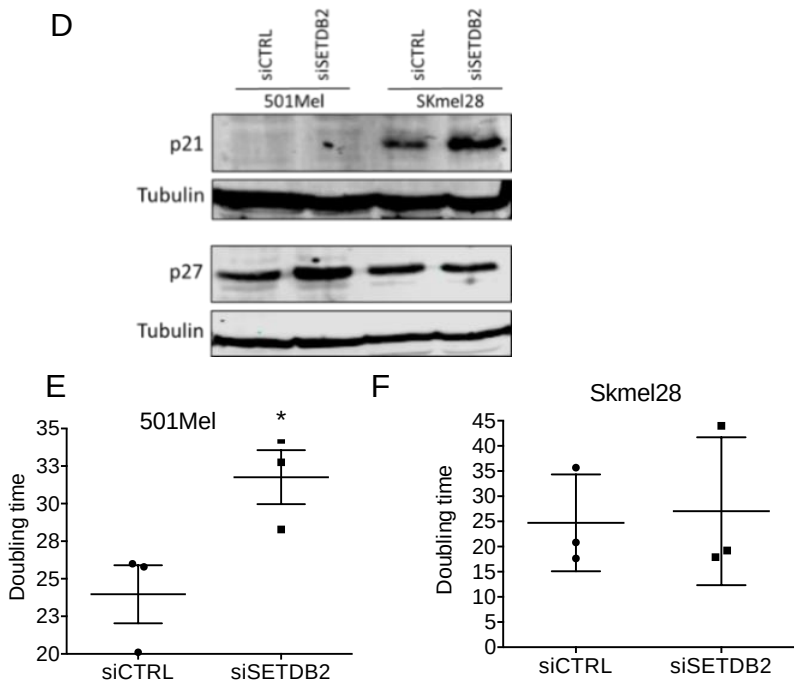

Figure 22. SETDB2 affects cell proliferation by modulating cell cycle inhibitors

A. Heatmap plotted using scaled expression *SETDB2*, *CDK2*, *CDK5R1*, *MITF*, *p21*^{CIP1}, *p57*, *p15*, *p18* from RNA-seq data in ΔMITF-X6 and EV-SkMel28 cells. **B, C**. RNA-expression of *TGFB1*, *CDH2*, *ITGA2*, *p15*, *p18* measured by RT-qPCR with *SETDB2* knockdown in 501Mel and SkMel28 cell lines. **D**. Expression of the p21^{CIP1} and p27^{kip1} proteins were assessed by Western blot analysis upon SETDB2 knockdown in 501Mel and SkMel28 cell lines. Tubulin was used as loading control. **E, F**. 501Mel and SkMel28 cell lines were seeded in monolayer in 96well plates and transfected with siRNA against *SETDB2*, proliferation assay carried out in Incucyte live cell imaging system over a 4 day period. The doubling time for siCTRL and siSETDB2 cells is plotted. Error bars represent standard deviation. *p-value<0.05, t-test.

4.1.13 Expression of the histone modifier PRDM7 is restricted to melanoma tumour samples

We noticed a sharp decrease in *PRDM7* expression in our ΔMITF-X6 RNA-seq data (Figure 23A). Furthermore, RT-qPCR showed an 80% decrease in *PRDM7* expression in the ΔMITF-X2 and ΔMITF-X6 cell lines (Figure 23B). We characterized the expression of the *PRDM7* transcript in 27 different types of cancer in the TCGA database. To our surprise, *PRDM7* expression was restricted to melanoma samples among all cancers (Figure 23C). In 479 cutaneous melanoma tumour samples, *PRDM7* mRNA expression was

positively correlated with *MITF* mRNA expression (Figure 23D). Consistenly, *PRDM7* expression was elevated in MITF^{high} tumours when compared with MITF^{low} tumour samples (Figure 23E). Together, we showed that *PRDM7* expression is restricted to melanoma tumours and loss of MITF led to a major reduction of *PRDM7* levels in MITF-KO cells.

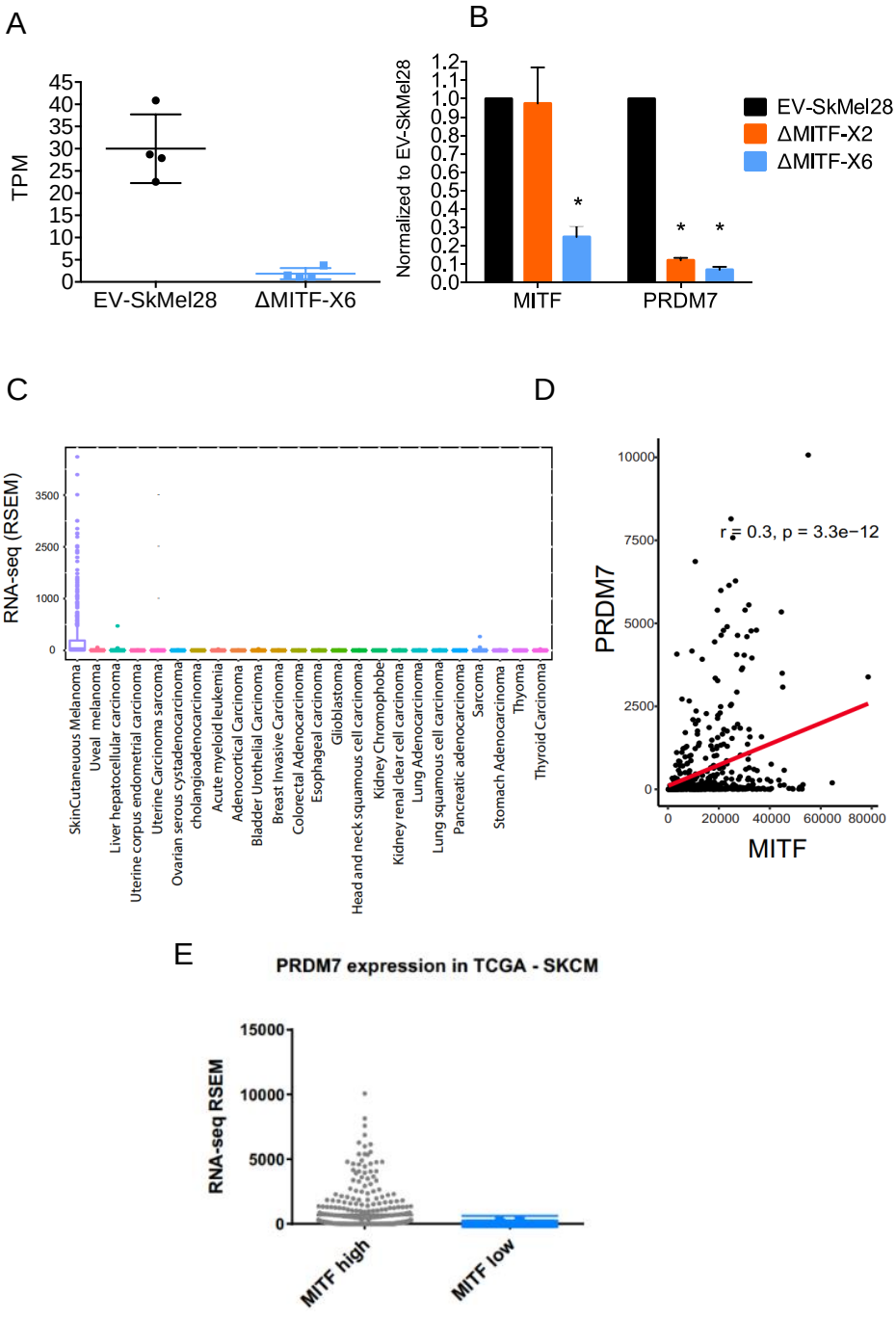

Figure 23. PRDM7 is higly expressed in melanoma tumour samples

A. RNA-expression of *PRDM7* in ΔMITF-X6 and EV-SkMel28 measured by RNA-seq method. Error bars represent standard deviation**. B**. mRNA expression of *PRDM7* and *MITF* validated in *MITF* knock out cells unsing RT-qPCR. Espression was normalized to EV-SkMel28. Error bars represent standard deviation. *p-value<0.05, One way Anova. **C**. *PRDM7* mRNA expression across 30 cancer types in the TCGA data base. **D**. Expression of *PRDM7* and *MITF* transcripts in cutaneous melanoma tumour samples (479) displayed as scatter plot (Pearson=0.3, p <3.3e-12). **E**. *PRDM7* expression in MITF ^{high} and MITF ^{low} TCGA cutaneous melanoma tumour samples.

4.1.13.1 Stepwise regulation of PRDM7 by MITF and MAFB

To further study the link between *PRDM7* and *MITF*, we used the MITF^{low} melanoma cell line LU1205 and ectopically expressed MITF and an empty vector construct using the piggy-bac system and then carried out RT-qPCR. The results showed a 20-fold induction of *PRDM7* expression upon MITF induction, as compared to the empty vector control (Figure 24A). Knocking down *MITF* using the inducible miR-MITF SKmel28 cell line resulted in a 70% decrease in *PRDM7* expression (Figure 24B). Together, this suggests that MITF is involved in regulating *PRDM7* expression.

Surprisingly, we did not see any evidence for direct binding of MITF, neither at the *PRDM7* promoter nor 10 kb up- or downstream from the transcription start site. To find possible direct regulators of PRDM7, we performed in silico motif analysis of the *PRDM7* promoter utilizing the online Transfac motif tool. One of the strongest hits was the transcription factor *MAFB*, which contains a binding site (AAGGTGCTGAGA motif) located 89 bp upstream of the PRDM7 transcription start site (P< 1.21e-4) (Figure 24C). In line with this, RNA-seq data showed that *MAFB* expression was decreased in the ΔMITF-X6 out cells. Interestingly, the ChIP-seq data showed that MITF binds to an E-box sequence with flanking T/A (TCAGCTGA) 500-bps upstream from the *MAFB* promoter (Figure 24D,E).

To further establish the direct link between *PRDM7* and *MAFB*, we performed siRNA-mediated *MAFB* knockdown in the 501Mel cell line. This resulted in 80% knockdown of *MAFB* as compared to siCTRL. We observed 70% reduction of *PRDM7* expression upon *MAFB* knockdown (Figure 24F). This suggests a regulatory loop consisting of *PRDM7*, *MITF* and *MAFB*, where *MITF* directly regulates *MAFB* expression, and MAFB in turn binds and positively regulates *PRDM7* expression.

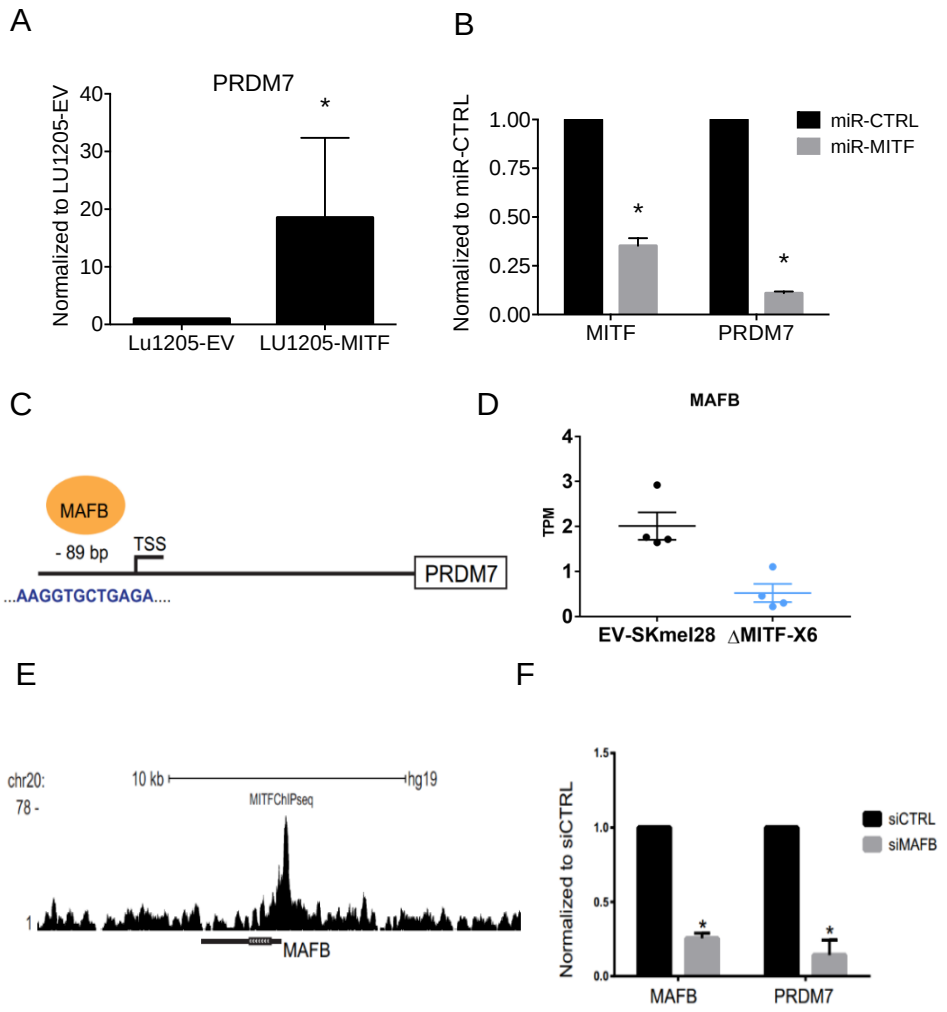

Figure 24. Stepwise regulation of PRDM7 by MITF and MAFB

A. Expression of *PRDM7* quantified by RT-qPCR in inducible MITF KD miR-MITF SkMel28 cell line. Error bars represent standard deviation. *p-value<0.05, One way Anova. **B.** Flag-tagged MITF ectopically expressed in the $MITF^{low}$ LU1205 cell line. mRNA expression of *PRDM7* measured by RT-qPCR. Expression was normalized to empty vector cell line. Error bars represent standard deviation. *p-value<0.05 t-test. **C**. Schematic representation of *PRDM7* gene promoter with MAFB binding motif, located 89bp upstream from TSS (P<1.21e-4). **D**. Box-plot showing expression (TPM) of *MAFB* transcript in ΔMITF-X6 and EV-SkMel28 cell lines. Error bars represent standard deviation**. E**. ChIP-seq peak of MITF extracted from UCSC genome browser showed MITF binding on *MAFB* promoter. **F**. RT-qPCR of *PRDM7* and *MAFB* in siCTRL and in siMAFB- 501Mel cell lines. Error bars represent standard deviation *p-value<0.05, One way Anova.

4.1.13.2 PRDM7 and MAFB affect cell proliferation

To test the functional effects of *PRDM7*, we used siRNA to knockdown *PRDM7* in 501Mel and SkMel28 cell lines and monitored cell proliferation using the IncuCyte live cell imaging system. Live images were taken every two hours over a four day period. The doubling time was calculated from quantification of images of cells treated with siCTRL and siPRDM7. Interestingly, siPRDM7-treated 50Mel cells showed a significant increase in their doubling time whereas a minor increase was observed in the SKmel28 cells (Figure 25A,B). As reported in the previous section, *MAFB* negatively regulates *PRDM7* expression. Therefore, we knocked down *MAFB* in 501Mel and SKmel28 cell lines utilizing siRNA and monitored proliferation using live cell imaging as described above. We observed a severe reduction in proliferation upon *MAFB* knockdown in 501Mel cells, with a 2-fold increase in doubling time, whereas siMAFB treatment of SKmel28 cells resulted in a minor increase in doubling time (Figure 25C,D). To test the effects of *PRDM7* on the migratory potential of cells, we knocked down *PRDM7* utilizing siRNA, performed a wound scratch assay on a confluent cell layer and followed the gap closure using the IncuCyte live imaging system. Quantification of wound scratch images showed that PRDM7 knockdown had no effect on the migration rate in neither 501Mel nor SkMel28 cell lines (Figure 25E,F). Collectively, our data show that *PRDM7* and *MAFB* affect cell proliferation in melanoma cells but do not influence their migration rate. Interestingly, the MAFB knock down affected proliferation more severely than the PRDM7 knockdown, suggesting that MAFB has broader role in regulating proliferation possibly through regulating other factors in addition to PRDM7.

To summarize the results in the sections above, we proposed a model (Figure 25G), which depicts the possible role of PRDM7 and SETDB2 in regulating genes responsible for proliferation and differentiation during melanoma development. This model assumes that MITF is involved in regulating expression of the histone modifiers SETDB2 and PRDM7, directly or indirectly, respectively and this in turn leads to chromatin changes and effects on proliferation (Figure 25G). The model is based on our observations in the 501mel cells but the same assays performed in the SkMel28 cell lines did not show statistical significance after depletion of PRDM7 or SETDB2. To verify if this model applies to other melanoma cells, we will need more effective systems for performing the knockdowns in SkMel28 cells. Additionally, the functional assays need to be carried out in other cell melanoma cell with various genetic backgrounds especially with respect to p53 and $BRAF^{V600E}$ mutations.

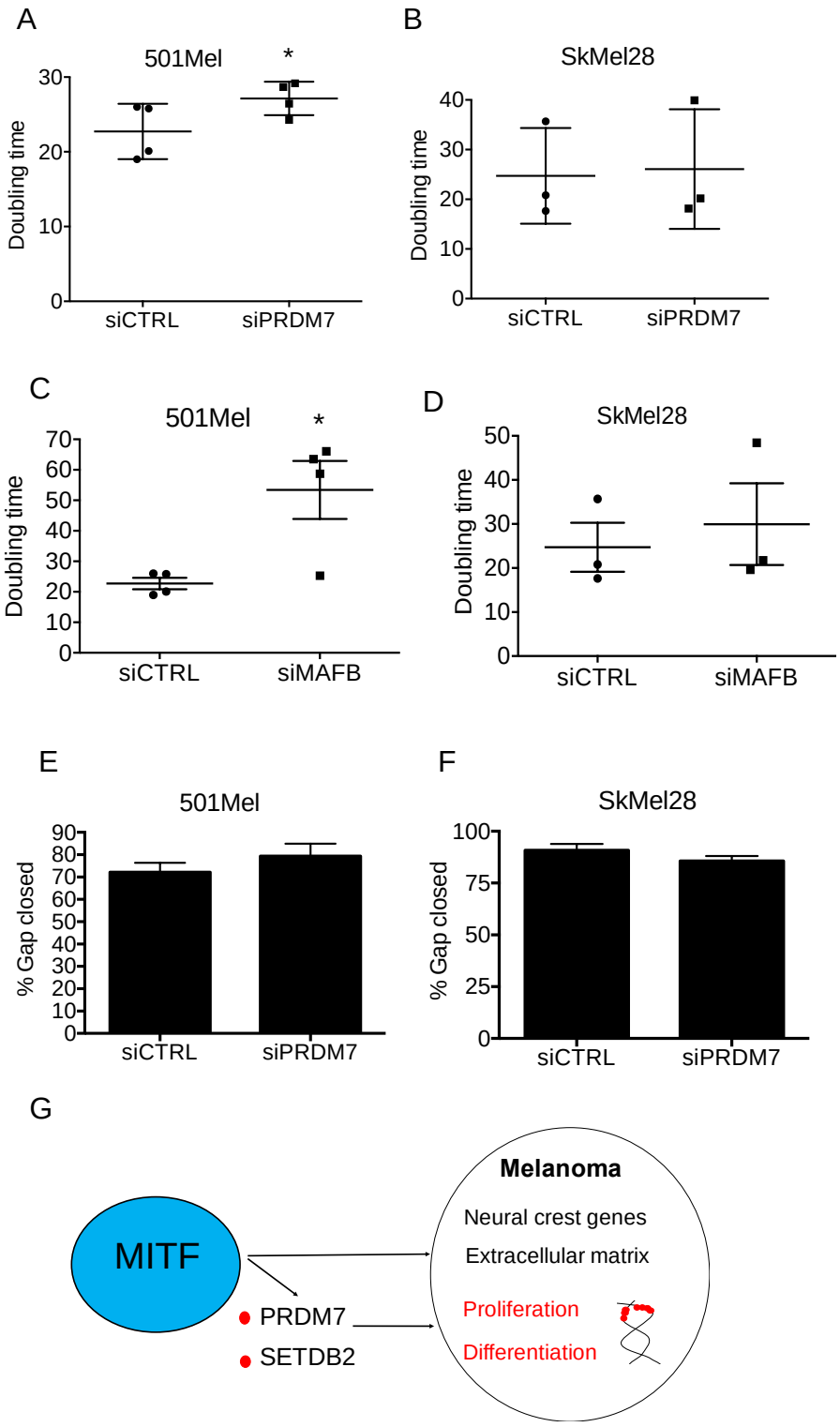
A
501Mel
*
Doubling time
30
20
10
0
siCTRL
siPRDM7
B
SkMel28
Doubling time
40
30
20
10
0
siCTRL
siPRDM7
C
501Mel
*
Doubling time
70
60
50
40
30
20
10
0
siCTRL
siMAFB
D
SkMel28
Doubling time
50
40
30
20
10
0
siCTRL
siMAFB
E
501Mel
% Gap closed
90
80
70
60
50
40
30
20
10
0
siCTRL
siPRDM7
F
SkMel28
% Gap closed
100
75
50
25
0
siCTRL
siPRDM7
G
MITF
PRDM7
SETDB2
Melanoma
Neural crest genes
Extracellular matrix
Proliferation
Differentiation

Figure 25. PRDM7 and MAFB reduce cell proliferation

A-D. Box plot of doubling time of siPRDM7, siMAFB and siCTRL cells in 501Mel and SkMel28 are derived from quantification from Incucyte live cell imaging. Error bars represent standard deviation. *p-value<0.05, t-test. **E, F**. Quantification of area of wound scratch over 24 hours in SkMel28 and 501Mel cells, treated with siCTRL and siPRDM7. Error bars represent standard deviation. **G.** A model summarizing the possible roles of PRDM7 and SETDB2 in melanoma development.

4.1.14 Partial rescue of MITF-KO cells upon MITF overexpression

To link functional and molecular changes observed in the MITF-KO cells to loss of MITF, several rescue attempts were made by introducing MITF back into MITF-KO cells.

The pPBhCMV-mMITF-3XFlag construct which contains the melanocyte specific form of mMITF tagged with 3XFlag downstream of the TRE element was ectopically expressed in ΔMITF-X2 and ΔMITF-X6 cells. Empty vector plasmid containing 3XFlag was transfected as control. After 48 hours of transfection, we isolated RNA and generated cDNA for RT-qPCR experiments to assess whether expression of MITF target genes can be rescued by re-introduction of MITF.

The expression of *IRF4 and MLANA* was reduced 3-30 fold in ΔMITF-X2 cells as compared to EV-SkMel28 cells when transfected with empty vector control. We observed 1.5-fold increase in IRF4 and MLANA expression in ΔMITF-X2 cells compared to EV-Flag transfected cells when transfected with wild type MITF. The expression of *NR4A3* was rescued as its level reached to the same level as in the parental EV-SkMel28 cells, but ZNF703 expression did not show any change in the ΔMITF-X2 cells as compared to control cells (Figure 26A). The expression of *MMP15*, *ITIH5*, and *NGFR* was induced 10-200 fold in the ΔMITF-X2 cells compared to the EV-SkMel28 cells. Upon MITF overexpression, *MMP15* and *NGFR* expression level were reduced 1.3-1.4-fold compared to EV-SkMel28; ITIH5 did not show any change compared to control (Figure 26B).

In ΔMITF-X6 transfected with empty vector control, the expression of *IRF4, ZNF703, NR4A3* and *MLANA* were reduced 2-20-fold compared to EV-SkMel28. When MITF was overexpressed, a 1.3-fold expression of *IRF4* and *MLANA* were observed, and *NR4A3* expression was identical to the expression observed in the EV-SkMel28 cells; ZNF703 did not show change in expression (Figure 26C). The expression of ITIH5, MMP15, and NGFR were induced 20-200 fold in ΔMITF-X6 cells compared to parental EV-SkMel28 cells. While overexpression of MITF in ΔMITF-X6 cells led to 1.4-fold reduction of NGFR and MMP15 compared to empy vector transfected ΔMITF-X6, the ITIH5 level remained unchanged (Figure 26D).

To rescue the proliferation defect observed in the MITF-KO cells, MTS assay measuring oxidoreductase acitivity of live cells was perfomed by ectopically overexpressing MITF as described above. We observed a 2-3-fold reduction in empty vector transfected MITF-KO cells when compared to EV-SkMel28 cells. Overexpression of MITF did not lead to any increase in proliferation in both ΔMITF-X2 and ΔMITF-X6 cells (Figure 26E,F). All together, we showed that MITF was only able to fully restore *NR4A3* expression, whereas *MLANA*, *IRF4*, *MMP15*, and *NGFR* showed partial rescue compared empty vector transfected cells. Finally, the proliferation defects observed in MITF-KO cells could not be rescued by overexpressing MITF.

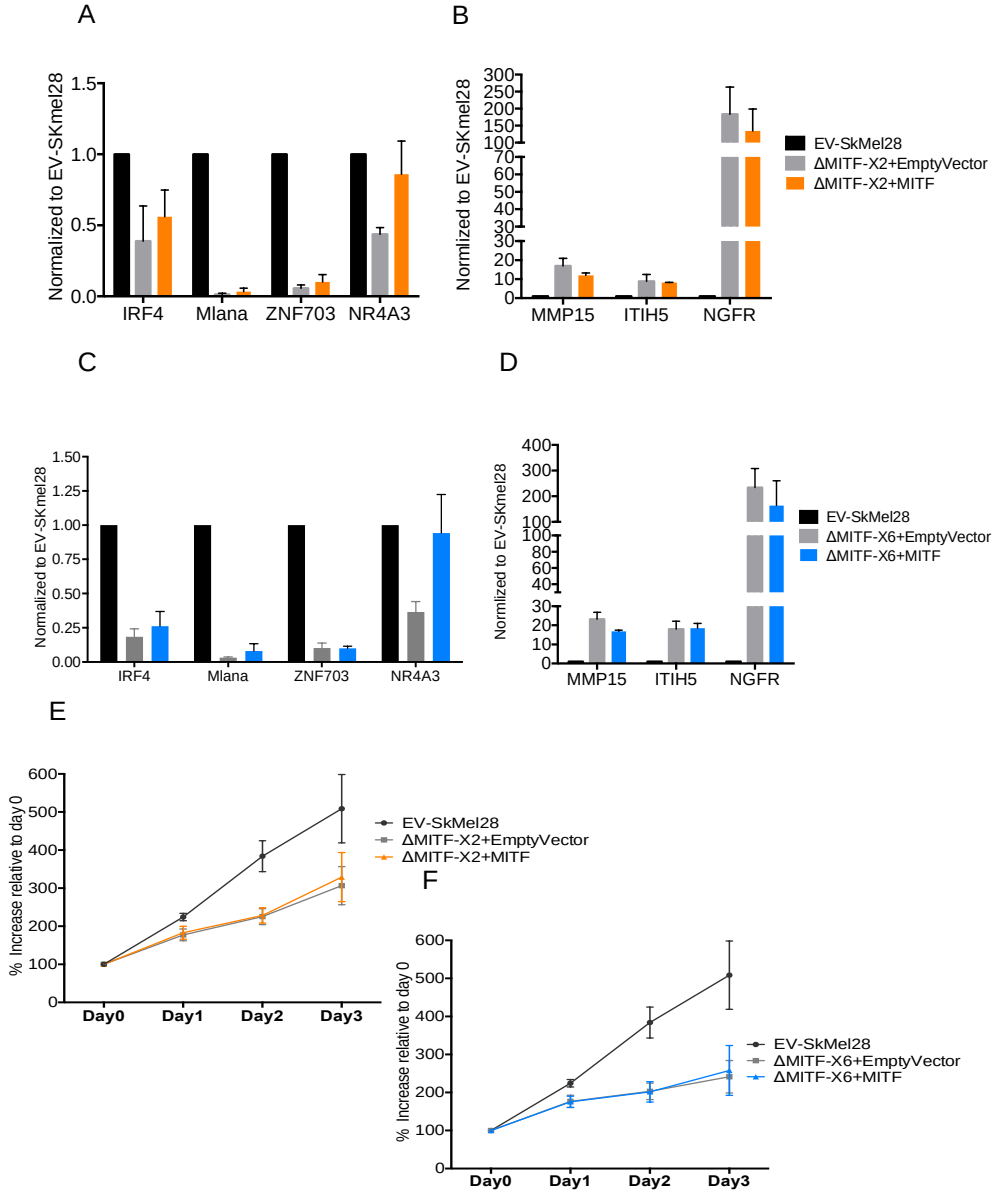

Figure 26. Partial rescue of MITF-KO cells upon MITF overexpression

A-D. RT-qPCR showing expression of genes after overexpression of MITF and empty vector control. Expression normalized to EV-SkMel28. Error bars represent standard deviation. **E,F.** Percent increase of viable cells from day 0 measured with MTS cell viability assay. Error bars represent standard deviation.

4.2 MITF transcription network with TFEB and IRF4

4.2.1 MITF and IRF4 positively correlate in expression whereas TFEB is negatively correlated with MITF

To characterize the gene expression network involving *MITF*, *IRF4* and *TFEB* in melanoma cells, we first investigated the expression of these three factors across various tumour samples in the TCGA database. To do this, we extracted normalized RNA-seq expression values of the TCGA pancancer data set from the UCSC-Xena browser. The plotted expression values of each factor showed that: (i) MITF had the highest expression in uveal melanoma samples followed by cutaneous melanoma. (ii) IRF4 expression was highest in uveal melanoma followed by diffused large B-cell lymphoma (DLBC) and cutaneous melanoma. (iii) *TFEB* had the strongest expression in diffuse large B-cell lymphoma (DLBC) but rather low in cutaneous melanoma and uveal melanoma tumour samples (Figure 27A).

To determine if co-expressed gene sets are shared between *MITF*, *TFEB* and *IRF4* in TCGA data sets, we collected negatively and positively correlated genes for each factor, limiting our analysis to genes which have a Pearson correlation > 0.3 and < -0.3. We then determined the extent of the overlap in the co-expressed gene sets. This analysis showed that MITF had an overlap of 235 genes with *TFEB* and 204 genes with *IRF4*. However, there were only 9 genes shared between TFEB and IRF4 and only 7 shared between all three factors (Figure 27B).

Moreover, we separated the overlapping correlated genes based on whether they showed positive or negative correlation with each factor. For the 235 genes shared between *TFEB* and *MITF*, 65 were positively correlated with *MITF* but anti-correlated with *TFEB*, whereas the remaining 175 genes negatively correlated with *MITF* but positively correlated with *TFEB* (Figure 27C). Interestingly, *MITF* and *IRF4* positively correlate with the same subset of 115 genes and anti-correlate with the same 113 genes (Figure 27D).

Furthermore, we investigated if *MITF* mRNA expression correlates with *TFEB* and *IRF4* expression in melanoma tumour samples. In agreement with their co-expression profile discussed above, the mRNA expression of *MITF* and *TFEB* across 479 melanoma tumour samples showed negative correlation with a Pearson coefficient of - 0.1 and p value of 0.02 (Figure 27E), whereas mRNA expression of *MITF* and *IRF4* was strongly positively correlated with a

Pearson coefficient of 0.58 and P<2.2e-16. Collectively, our analysis showed that *MITF* and *IRF4* positively correlate in expression and share a co-expression gene profile in melanoma tumours, whereas *TFEB* and *MITF* expression is negatively correlated.

A

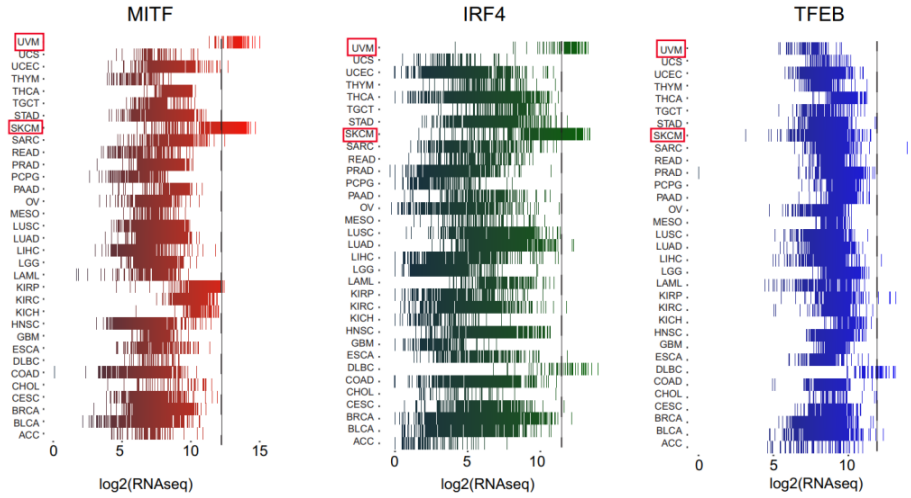

B

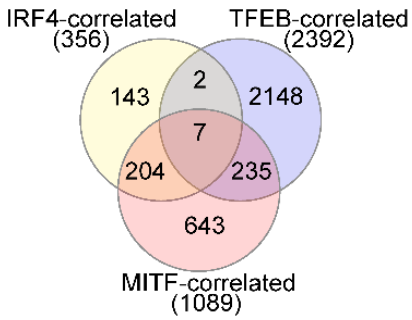

C

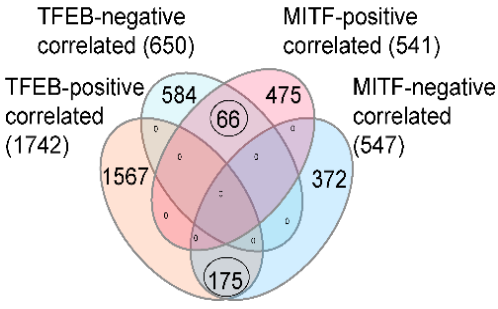

D

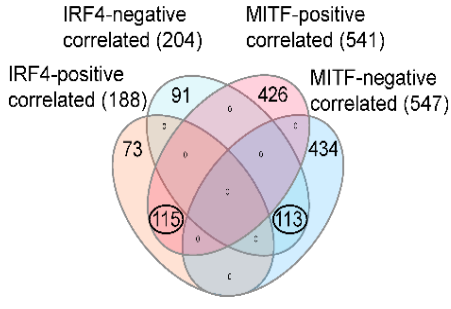

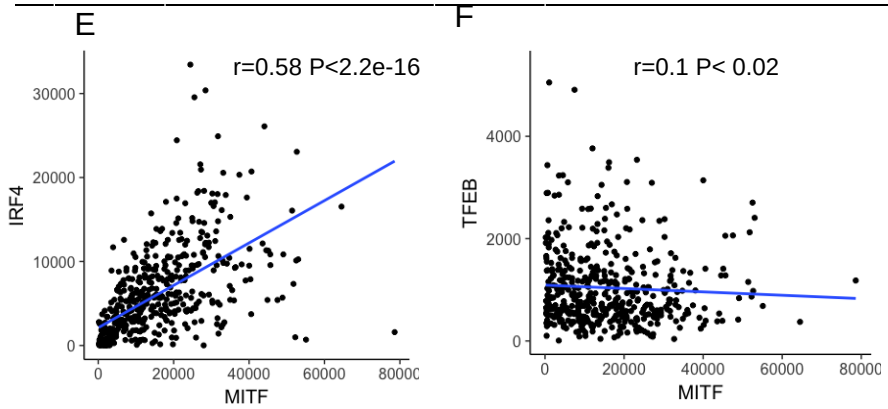

Figure 27. Expression of MITF and IRF4 is positively correlated and TFEB expression is negatively correlated with MITF expression

A. RNA-expression of *MITF*, *IRF4* and *TFEB* in 34 tumour samples. **B**. Venn diagram showing overlap of MITF, IRF4 and TFEB correlated genes in SKCM-TCGA data. **C,D**. Venn Diagram illustrating the number of overlapping genes that are positively and negatively correlated in expression with each factor. **E**. RNA-expression of MITF and IRF4 over 472 samples is plotted in scatterplot (Pearson=0.58). **F**. Scatter plot of MITF and TFEB RNA-expression (Pearson=-0.1)

4.2.2 Targeted ChIP-qPCR showed enrichment for *IRF4* and *TFEB* targets

To identify common genome-wide binding sites of MITF, IRF4 and TFEB, we used the ChIP-sequencing method, which enables us to map binding sites of transcription factors in the genome. First, the proteins are crosslinked to the DNA and then the bound DNA complexes are pulled down with antibodies against the transcription factor of interest. This is then followed by high throughput sequencing of the immunoprecipitated DNA, followed by bioinformatics analysis in order to identify the binding sites of transcription factors across the genome (Farnham, 2009; Park, 2009). We performed ChIP against eGFP tagged IRF4 and TFEB proteins in 501Mel human melanoma cell lines to overcome the limitation of ChIP grade antibodies against IRF4 and TFEB. To do this, we first generated inducible eGFP-tagged IRF4 and TFEB inducible stable cell lines using the PiggyBac transposon system as described in more detail in section 3.5. Subsequently, we performed targeted ChIP-qPCR to validate the efficiency of ChIP before proceeding to high-throughput sequencing. ChIP-qPCR was performed on targets that have known binding sites for TFEB or IRF4. Results from the ChIP-qPCR for TFEB-eGFP showed a 3-6-fold enrichment for *ATP6V0E1* (Ludwig et al., 1998), *ATP6V1C1* (Vanhille et al., 1993) and *LAMP1* (Carlsson et al., 1988) when compared to promoter region of Actin used as a negative control (Figure 28A). For the IRF4 ChIP-qPCR, enrichment of 2-5-fold was observed for *SUB1*, *TYR* and *TFEB* over the negative control actin and a genomic region both TFEB and IRF4 show no binding (Figure 28B). Collectively, ChIP-

qPCR showed sufficient enrichment to follow the next step with high-thoughput sequencing.

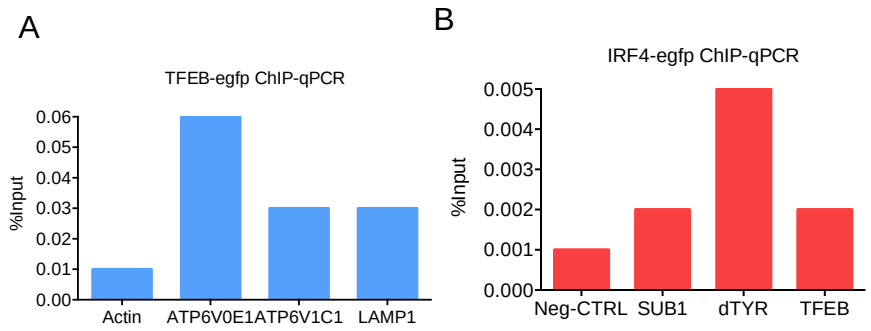

Figure 28. Targeted ChIP-qPCR shows an enrichment for IRF4 and TFEB targets

A. ChIP-qPCR showing MITF binding to *ATP6V0E1, ATP6V1C1* and *LAMP1*, Actin promoter used as a negative control for binding. **B**. ChIP-qPCR showing IRF4 binding to its targets *SUB1*, *TYR* and *TFEB*.

4.2.3 ChIP-seq identified 3694 IRF4 binding sites in 501Mel melanoma cells

ChIP-seq analysis of IRF4-eGFP binding sites in 501Mel melanoma cells identified different numbers of binding events for each of biological replicates. For replicate 1, 4901 peaks (P<1e-15) were called whereas 12831 peaks were called for replicate 2 (P<1e-15). For each peak calling experiments, the p-values were chosen based on genes where they have been shown no binding. We then checked whether the IRF4 binding motif was enriched within the region of IRF4 bound sites in two of the experimental replicates. For this we took 1500 peaks with the lowest p-values for each replicate and performed de-novo motif enrichment analysis using the MEME-ChIP online software (Machanick & Bailey, 2011). For both replicates, IRF4 binding motifs were reported with significant expected value (E-value) which indicates the number of motifs expected to be found by chance if the input sequences were shuffled (Figure 29 A,B).

Common peak sets were generated by intersecting peaks from the two biological replicates using DiffBind package in R bioconductor, which resulted in a core set of 3694 IRF4 binding sites (Figure 29C). The distribution of peak sets showed majority of the peaks are located less than 1kb away from gene promoters whereas the rest of the peaks are at distal intergenic region, introns and exonic regions (Figure 29D). The peaks were then assigned to

their bound genes based on peak distance of 20 kb +/-from transcription start sites, resulting in 3143 genes containing IRF4 binding sites.

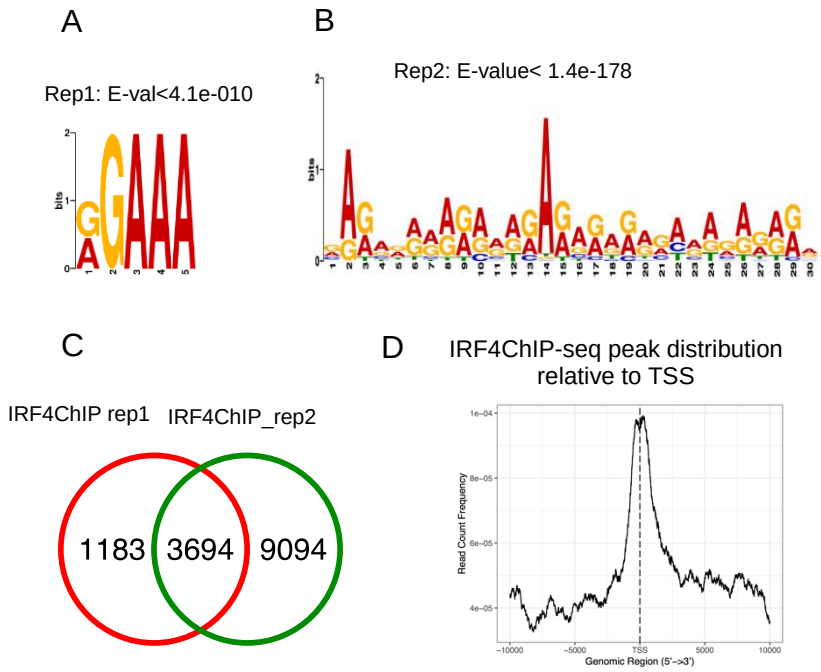

Figure 29. IRF4 ChIP-seq identifies 3694 binding sites in 501Mel melanoma cell

A, B. MEMEChIP analysis of highly represented motif in peaks (1500) with the lowest p-value; *E* values represent their statistical significance. **C**. Venn Diagram demonstrating the number of binding sites shared between two individual ChIP-seq experiments. **D**. IRF4 peaks (3694) density distribution relative to transcritption start site 10kb +/-.

4.2.3.1 IRF4 and MITF share 452 binding sites

To investigate the extent of overlap between MITF and IRF4 binding sites, we downloaded the publicly available MITF ChIP-seq performed in 501Mel cells (Laurette et al., 2015) from the GEO archive. We then analysed the data following the same procedure as for the IRF4 and TFEB ChIP-seq data sets (chapters 4.2.3 and 4.2.4). After peak calling with MACs (Zhang et al., 2008), 11173 of MITF peaks with p-value lower than (1e-10) and 8747 peaks with p-value lower than (1e-12) were identified. These two peak sets called with different p-values were treated as individual replicates for MITF ChIP-seq separately due to the lack of a second replicate performed by Laurette et al (2015). A consensus peak set, containing 8710 MITF binding peaks was obtained from the two replicates. We then performed overlapping analysis

using 8710 core peak sets for MITF and 3694 for IRF4. A total of 452 common peaks were identified (P<1.176e-146, hypergeometric test) (Figure 30A). By plotting the IRF4 individual peaks located within 10 kb +/- relative to MITF peaks as a tagHeatmap showed that the IRF4 peaks are more distantly located from TSS relative to the MITF peaks (Figure 30B).

We also analysed the overlap of genes that are directly bound by MITF and IRF4 within 20 kb +/- from the transcription start site. This analysis showed that MITF and IRF4 both bind to 652 genes (P<1.359e-11, hyper geometric test) (Figure 30C). Among these commonly bound genes, 26 were pigmentation related genes (P<3.9-07, hypergeometric test) (Figure 30D).

In order to characterize further the nature of the overlapping genes, functional gene annotation analysis was conducted. This showed enrichment for pathways involved with processing of capped intron-containing pre-mRNA, mRNA splicing, interferon signalling, clatherin derived vesicle budding, trans-Golgi vesicle budding, circadian clock and Golgi associated vesicle biogenesis (Figure 30E). We also performed GO analysis for biological pathways, showing common enrichment for pathways associated with autophagy and pigmentation, whereas IRF4 showed preferential enrichment for pathways associated with mRNA processing and histone modification (Figure 30F).

Taken together our analysis shows that MITF and IRF4 share extensive overlap in their binding genes and those commonly bound genes are associated with pigmentation and autophagy pathways.

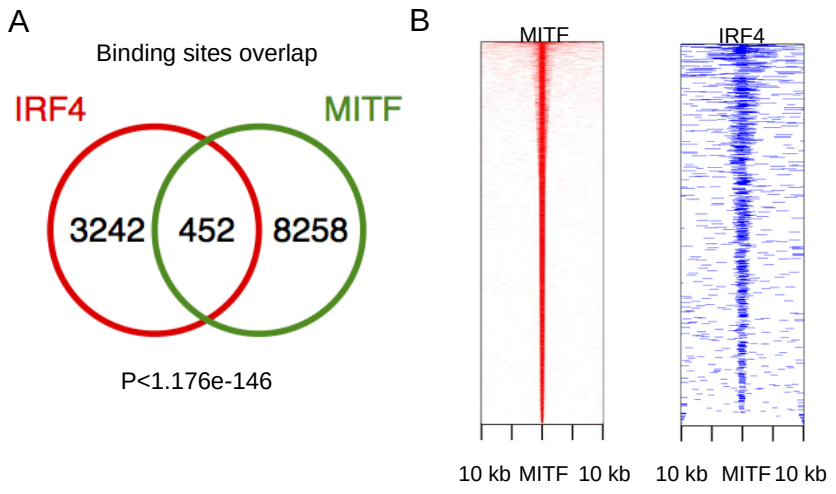

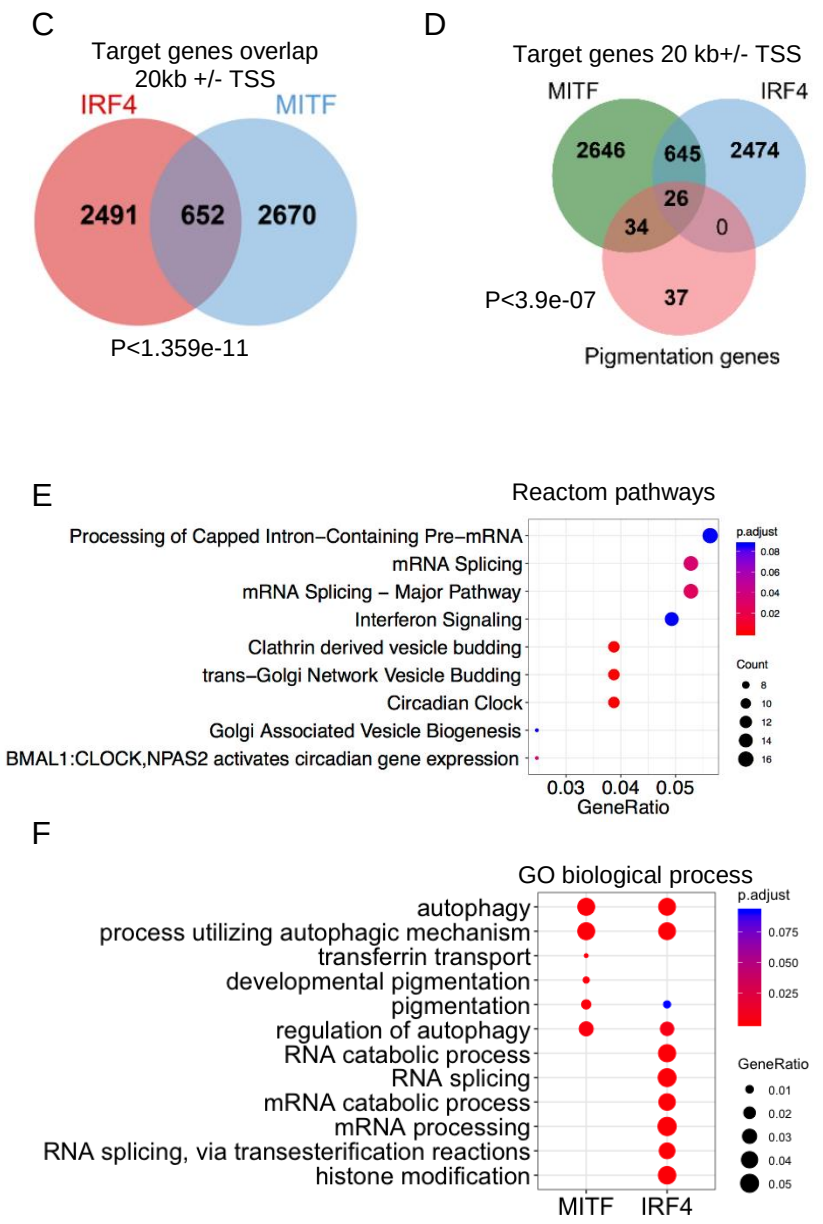

Figure 30. MITF and IRF4 share 452 binding sites and 515 overlapping genes

A. Venn diagram showing the number of overlapping MITF and IRF4 binding sites. **B**. Heatmap showing IRF4 and MITF peak distribution around 10kb +/- TSS. **C**, **D** Venn Diagram showing the number of shared bound genes between IRF4 and MITF target genes. **E, F**. Gene ontology analysis of common bound genes (652) of MITF and IRF4.

4.2.3.2 IRF4 and MITF differentially bound to 8167 sites

About 12% of the IRF4 peaks overlapped with MITF ChIP-seq peaks (P<1.176e-146). Thus, we asked which are the genes uniquely bound by each of the two factors MITF and IRF4. To discover sites which are statistically differentially bound by IRF4 and MITF, we utilized DiffBind package in R. This package is designed to identify differentially bound loci of transcription factors between two sample groups. The differential binding analysis takes the count number of sequences corresponding to each binding sites of transcription factor then uses it for differential binding analysis. The count number of sequence tags with respect to each binding sites was used as a proxy for binding affinity. The analysis resulted in two separate binding profiles which can be separated using principal component analysis (Figure 31A). This differential binding analysis identified 8167 differentially bound sites with 2-fold difference in terms of number of aligned tags corresponding to each binding event (FDR<0.05) between the IRF4 and MITF ChIP-seq experiments (Figure 31B). Among the 8167 differentially bound sites, 905 sites are bound 2-fold more in IRF4 binding events whereas 7262 sites were increased for MITF binding.

Next, each of these sites was assigned to genes and GO term analysis was carried out to check if they clustered into distinct functional groups. This showed that IRF4 preferentially binds to sites associated with biological processes involved in epigenetics, regulation of hemopoiesis, homeostasis of a number of cells, myeloid cell homeostasis, histone H3-K4 trimethylation, megakaryocyte differentiation, histone modification, chromatin remodelling and regulation of hematopoietic progenitor cell differentiation. However, MITF showed distinct binding to sites associated with axon development, axogenesis, positive regulation of nervous system development, neuron projection guidance, axon guidance, positive regulation of neurogenesis, potassium ion transport, forebrain development, cellular potassium ion transport and potassium ion transmembrane transport (Figure 31C).

Our data indicates that although MITF and IRF4 overlap significantly in target genes in melanoma cells, they have a distinct regulatory network, where MITF binds and regulates genes involved in neuron development whereas IRF4 uniquely regulates gene involved in immune cell differentiation and histone modification.

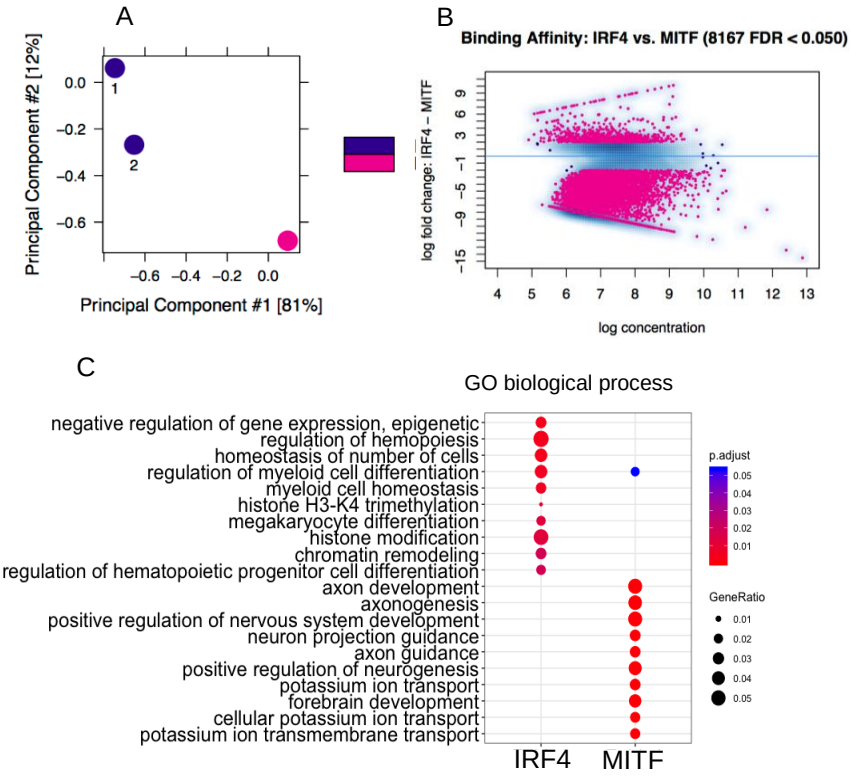

Figure 31. Differentially bound sites of MITF and IRF4

A. PCA plot of IRF4 and MITF ChIP-seq. Each replicate numbered 1, 2. **B**. Differetially bound sites between IRF4 versus MITF represented in MA plot (FDR<0.05, logFold change >2). **C**. GO term analysis for biological processes. Differentially bound associated genes were utilized for the analysis (P<0.05).

4.2.4 TFEB ChIP-seq identified 4307 sites in 501Mel cell lines

In order to identify TFEB binding sites in melanoma cells using genome-wide analysis, ChIP-sequencing was conducted in 501Mel cell line with inducible EGFP tagged TFEB in a piggybac expression vector. The experiment was performed in two biological replicates and the peaks were called using MACS (Zhang et al., 2008). The total number of peaks identified for the two replicates differed, which resulted in 49319 peaks (p-value <1e-05) for replicate 1 and 9889 peaks (p-valuel< 1e-15) for replicate 2.

Motif enrichment analysis was performed using the MEME-ChIP software (Machanick & Bailey, 2011). For the 1500 peaks with the lowest p-value for each of the two replicates, an E-box motif (CACGTG) with a flanking T was

identified within the regions bound by TFEB for both replicate experiments (Figure 32A,B). The intersecting peaks from the two replicates resulted in a core peak set consisting of 4307 TFEB binding sites (Figure 32C). The majority of the TFEB peaks were distributed around promoters and the rest were located at distal intergenic region and intronic regions (Figure 32D). Subsequently, the core peak sets from the anti-gfp-TFEBChIP-seq were assigned to genes based on 20kb +/- distance from transcription start site. A total of 3432 genes were annotated to TFEB binding sites.

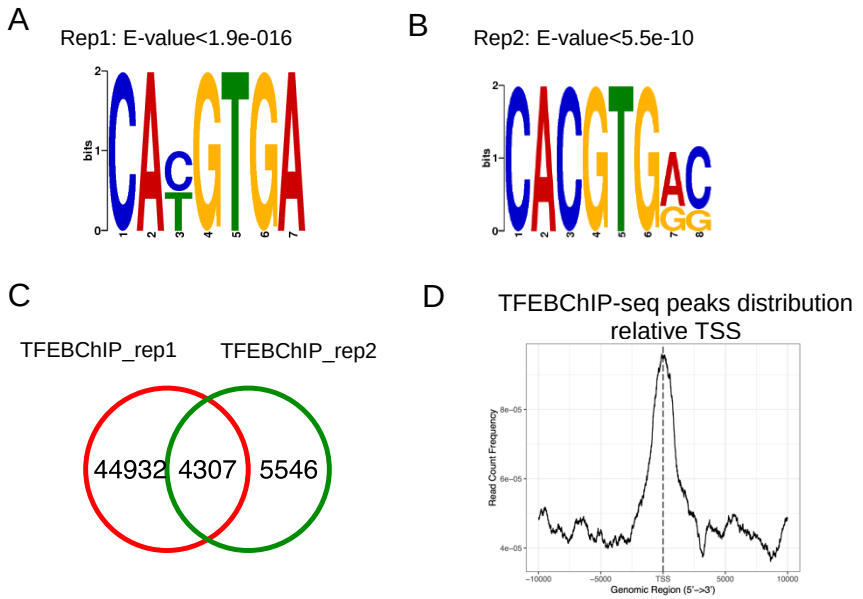

Figure 32. TFEB ChIPseq identifies 4307 binding site in 501Mel cell lines

A,B. MEME analysis of highly represented motifs in TFEBChIP-seq peaks (1500) with lowest p-value; *E* value represent their statistical significance. **C**. Venn Diagram demostrating number of binding sites shared between two biological replicate of ChIP-seq experiments. **D**. Distribution of TFEB peaks relative to transcription start site within 10 kb upstream and downstream.

4.2.5 MITF and TFEB bind to 1266 common genes

To explore the number of genome wide shared binding sites between MITF and TFEB, we analysed the overlap between MITF and TFEB ChIP-seq peaks. We utilized publicly available MITF ChIP-seq data (Laurette et al., 2015) where ChIP was performed against 3xflag tagged MITF in 501Mel melanoma cells. Intersecting peaks (8710) obtained from the MITF ChIP-seq data and core peaks (4305) from the TFEB ChIP-seq data identified a set of 1207 common peaks (P<1.210e-122, hypergeometric test) (Figure 33A). Individual binding sites of TFEB and MITF were aligned to 10kb+/- from

transcription start site and plotted in a Heatmap showing that TFEB peaks were closely located to the promoter region compared to MITF binding events (Figure 33B). Using a distance of 20kb+/- from the transcription start site we saw that MITF and TFEB commonly bound to 1266 genes (P<3.322e-172, hypergeometric test), of which 64 were lysosomal genes (P<4.288e-70, hypergeometric test) (Figure 33C,D).

Gene ontology analysis was carried out to classify the gene sets based on their function and assign them to respective GO terms. Analysis showed MITF and TFEB peaks were commonly enriched with pathways such as cellular response to stress, chromatin organization, chromatin modifying enzyme, cellular senescence, PTEN regulation, Rab regulation and trafficking, circadian clock and RAF-independent MAPK1/3 activation (Figure 33E). In addition, both MITF and TFEB showed enrichment for biological processes involved in autophagy, process utilizing autophagy mechanism, transferrin transport, developmental pigmentation, pigmentation, regulation of autophagy, ferric ion transport, trivalent inorganic cation transport, vesicle organization, endosome transport, cytosolic transport. Whereas uniquely enriched processes for TFEB were histone modification, peptidyl-lysine modification, proteasomal protein catabolic process and *in utero* embryonic development (Figure 33F).

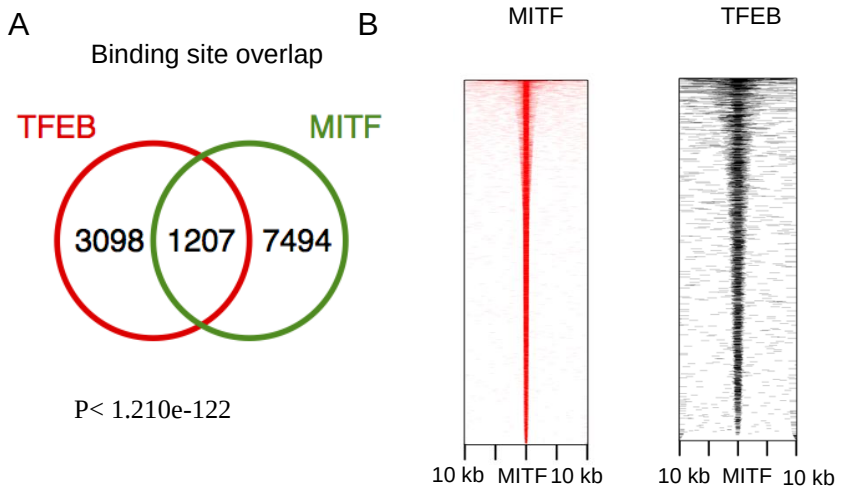

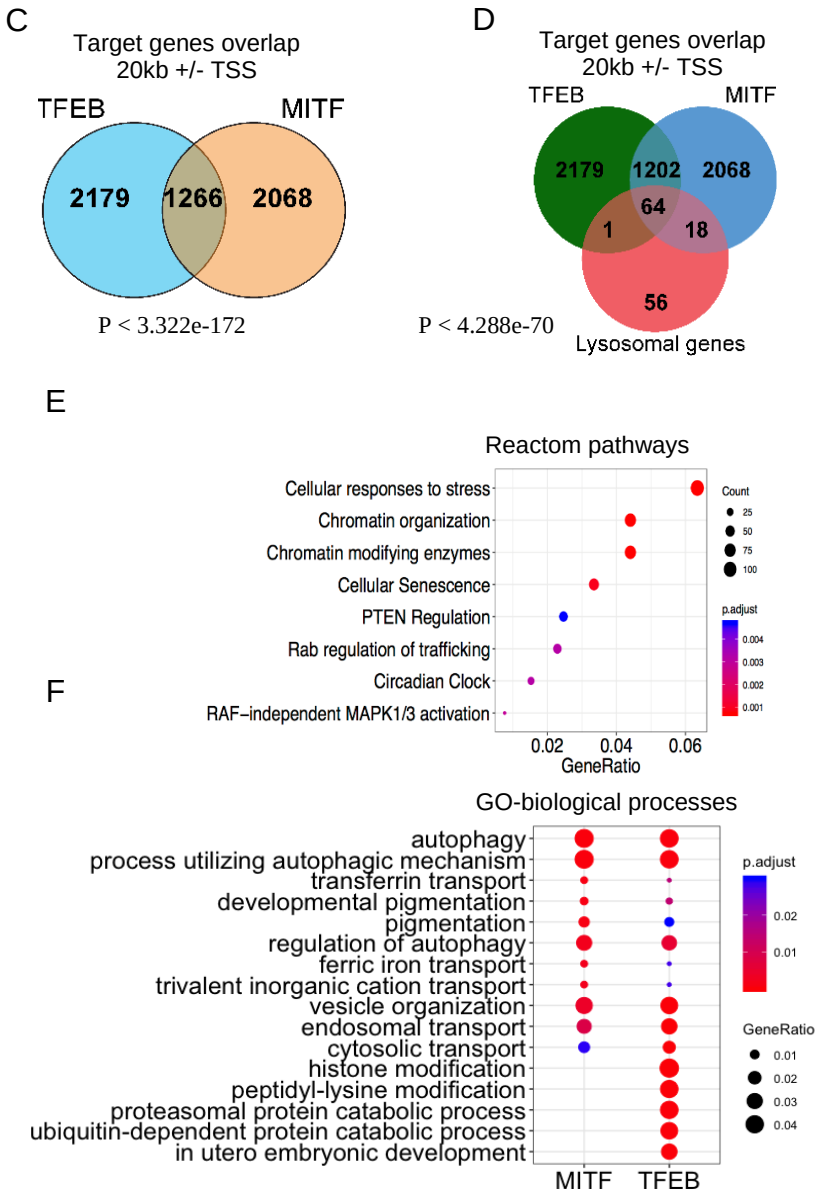

Figure 33. MITF and TFEB co-bind to 1266 genes

A. Venn diagram showing the number of overlapping MITF and TFEB binding sites. **B**. Heatmap showing IRF4 and MITF peak distribution within 10kb +/- of TSS. **C**. Venn Diagram showing the number of shared bound genes between TFEB and MITF target genes (P<1.873e-172). **D**. Venn Diagram showing the number of lysosomal genes shared between TFEB and MITF target genes **E**. Reactom pathway analysis of genes commonly bound (1266) by MITF and TFEB. **F**. GO bioplogical process analysis for MITF and TFEB co-bound genes, TSS (20 kb+/-).

4.2.6 Differential binding analysis revealed 6493 differential sites bound by MITF and TFEB

As reported above, overlap analysis revealed that 32.54% of TFEB peaks were shared with MITF. This raised our interest in identifying unique MITF and TFEB binding events. To retrieve statistically significant and differentially bound sites between TFEB and MITF, we utilized the DiffBind package in R. This package is designed to identify differentially bound sites of transcription factors between two sample groups. Principal component analysis revealed a separation of MITF and TFEB binding events (Figure 34A) and identified 6493 differential bound sites among TFEB and MITF peaks; sites with 2-fold change in binding intensity and FDR<0.05 were displayed in an MA plot (Figure 34B).

Among the 6493 differentially bound sites, 575 sites were bound 2-fold stronger in TFEB binding events, whereas 5918 sites were increased in binding events for MITF (Figure 34B). Each of these sites were assigned to genes and GO term analysis performed. GO biological process analysis showed that TFEB preferentially bound sites were enriched with terms such as negative regulation of transcription elongation, from RNA polymerase II promoter, negative regulation of DNA-template transcription elongation, glutamine metabolic process and regulation of DNA metabolic process. On the other hand MITF preferentially bound sites were enriched for processes including axon development, axogenesis, positive regulation of nervous system development, neuron projection guidance and axon guidance (Figure 34C). Together, this data shows that MITF and TFEB have both common and unique target genes and can uniquely bind and regulate distinct cellular processes.

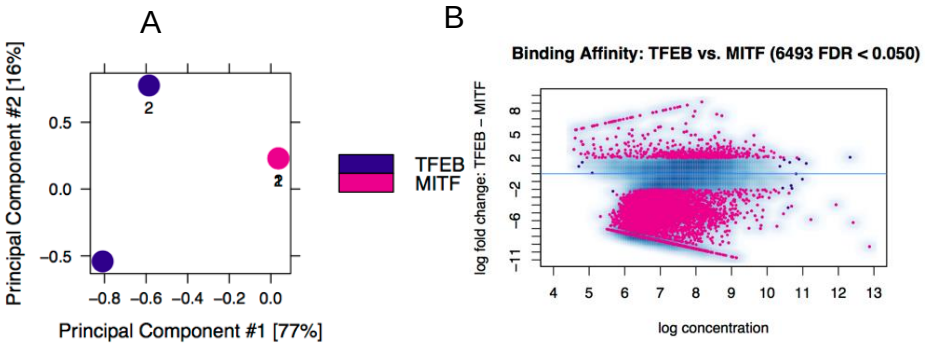

C

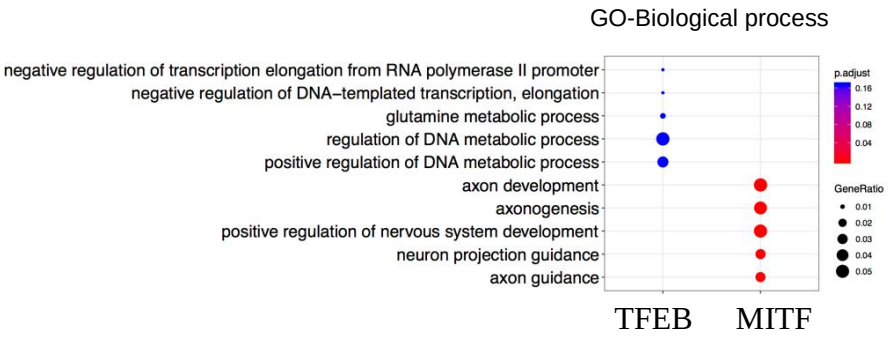

Figure 34. Differentially binding analysis revealed 6493 differential bound sites for MITF and TFEB

A. PCA plot of MITF and TFEB ChIP-seq peaks replicates. **B**. Differentially bound sites shown in MA plot (FDR<0.05, logFC>2). **C**. GO analyss of biological process on differentially bound sites between TFEB and MITF.

5 Discussion and Conclusion

This thesis has two major components. The first part focuses on characterizing the phenotype of melanoma cells lacking MITF and the molecular mechanisms behind the phenotypic differences observed. The cell lines generated and used for this analysis were (i) CRISPR-Cas9 mediated MITF knock out in SkMel28 melanoma cells; (ii) Stable MITF inducible knockdown in 501Mel and SkMel28 cell lines using the *piggybac* transposon system.

Using the CRISPR-Cas9 technique, we generated mutations in MITF targeting exons 2 and 6 separately. This resulted in two cell lines devoid of functional MITF, termed ΔMITF-X2 and ΔMITF-X6. Also, an empty control cell line was generated named EV-SkMel28. Phenotypic characterization of these cell lines revealed that lack of MITF led to an increase in cell size and granularity as measured by FACS analysis and phase contrast microscopy (Figure 4A,C). These cells displayed a more spherical growth pattern when seeded on matrigel matrix compared to EV-SkMel28 cells (Figure 4B).

BrdU proliferation assay revealed a 25-40% decrease in BrdU positive cells in ΔMITF-X2 and ΔMITF-X6 cells respectively as compared to the control EV-SkMel28 cells (Figure 5A). Live cell imaging with the IncuCyte system showed that MITF knock out cells had 30-40% increase in doubling time, confirming that knocking out MITF results in a negative influence on proliferation of melanoma cells (Figure 5B). The effect of MITF on proliferation was tested further using cells stably transfected with an miR-MITF construct. Live cell imaging using the IncuCyte system showed a delay in proliferation rate for miR-MITF cell lines which is in accordance with the published literature (Figure 7A,B). This further validated the role of MITF in regulating cell cycle progression in melanoma cells.

Using a wound scratch assay showed that the migration ability of MITF knock out cells was reduced significantly compared to EV-SkMel28 cells (Figure 8B). However, with the same assay miR-MITF SkMel28 cells showed a minor decrease in migration rate (Figure 9B). Furthermore, the Transwell invasion assay showed that MITF knock out cells had significantly reduced invasion ability (Figure 8A). In contrast, the miR-MITF SkMel28 knockdown cell lines displayed a minor increase in number of invaded cells (Figure 9A), suggesting that there are functional differences between the effects of transient and long term depletion of MITF on melanoma cell behaviour.

RNA-sequencing analysis of ΔMITF-X6 and EV-SkMel28 cells identified 1516 differentially expressed genes. Among the genes lacking upon *MITF* loss are melanocyte specific differentiation marker genes (Figure 10E, F). However, the cells expressed high levels of genes involved in generating the extracellular matrix (Figure 10E,F). Consistent with the observations of Hoek et al (2006), gene set enrichment analysis revealed that the gene expression profile of ΔMITF-X6 cells showed a reduction in the expression of genes involved in proliferation and increase in the expression of genes involved in invasion (Figure 11A,B) . Interestingly, ΔMITF-X6 cells had a similar gene expression profile as the melanoma samples in the TCGA which show low MITF expression ($MITF^{low}$ samples) (Figure 12B). These samples expressed genes related to the EMT hallmark and markers of neuronal cells while at the same time they lost the expression of melanocyte specific genes (Figure 13A,B). This indicates that the lack of *MITF* results in reprogramming of the gene expression program of melanoma cells to a de-differentiated state.

Gene ontology of the genes differentially expressed in the ΔMITF-X6 cells showed that genes involved in adhesion were increased upon the absence of MITF (Figure 10E,F). Consistent with that, immunostaining of the focal adhesion proteins FAK and Paxillin in the MITF knock out cells and in miR-MITF cell lines showed increased number of FAK and Paxillin focal points at the cell periphery (Figure 17&18).

Chromatin immunoprecipitation coupled by RT-qPCR against the histone modifications H3K9Me3 and H3K4Me3 indicated that the histone modification profile of *MITF* target genes was altered leading to effects on melanocyte differentiation and “stemness” state (Figure 19A-J).

Interestingly, differential gene expression analysis in ΔMITF-X6 cells showed severe reduction in expression of two epigenetic modifiers *SETDB2* (Figure 20A) and *PRDM7* (Figure 23A), which place H3K9Me3 or H3K4Me3 histone marks, respectively. Both factors are highly expressed in melanoma tumours, especially *PRDM7* which is highly expressed in the TCGA melanoma tumours. Notably, both PRDM7 and SETDB2 are regulated by *MITF* and both show a positive correlation in expression with MITF in melanoma tumours. Especially, there are two MITF binding sites in the SETDB2 gene, one at the promoter, another one at intron 11 (Figure 21A).

Motif analysis of the *PRDM7* promoter did not reveal any E- or M- box sequences, suggesting that MITF is not directly involved in regulating expression of PRDM7. However, we identified a binding motif for the *MAFB* transcription factor 89 base paris upstream of the TSS (Figure 24C). Interestingly, the expression of *MAFB* was decreased in the ΔMITF-X6 cells, and an MITF peak located 500 base pairs upstream of *MAFB* was identified

(Figure 24D), suggesting that *MAFB* might be regulated by MITF and that, in turn, MAFB may be directly involved in regulating expression of *PRDM7*. Proliferation assay after siRNA mediated knockdown of *PRDM7* and *MAFB* showed reduction in proliferation rate (Figure 25A-D), indicating that MITF, MAFB and PRDM7 form a regulatory cascade which severely affects cell proliferation in melanoma cells.

The second part of the thesis was designed to understand the transcriptional network involving *MITF*, *IRF4* and *TFEB*. Among the various tumours in the TCGA data set, *MITF* and *IRF4* displayed elevated expression in melanoma tumours compared to other cancers. Interestingly *TFEB* was expressed at a relatively low level in the TCGA melanoma tumours (Figure 27A). Importantly, we found that the mRNA expression of *MITF* and *TFEB* are negatively correlated in the melanoma samples whereas the expression of *MITF* and *IRF4* are highly correlated in 479 melanoma tumour samples (Figure 27E,F).

ChIP-sequencing analysis of *IRF4* identified 3694 binding sites in 501Mel cells (Figure 29C). The peaks observed were associated with GO terms related to RNA metabolic processes (Figure 30F). Analysis of the overlap in genes bound by *MITF* and IRF4 revealed 652 genes (Figure 30C). The overlapping genes are enriched with GO terms associated with Autophagy and Pigmentation. Genes uniquely bound by *IRF4* showed enrichment for the myeloid cell differentiation pathway whereas genes uniquely bound by MITF were enriched for genes involved in axogenesis and neuronal pathway.

Analysis of the *TFEB* ChIP-sequencing data identified 4307 binding sites in 501Mel cells (Figure 32C). GO analysis of binding sites showed enrichment for genes associated with lysosome, lytic vacuole and autophagy (Figure 33F). Analysis of the overlap between MITF and TFEB identified 1266 common target genes, enriched in pathways associated with the autophagy and pigmentation pathways (Figure 33C). GO analysis of MITF uniquely bound sites showed enrichment for axogenesis whereas *TFEB* unique sites were associated with DNA metabolic process and in utero development (Figure 34C).

5.1 Characterization of MITF knock out cells

5.1.1 Depletion of MITF leads to larger cell size in SkMel28 melanoma cells

Depletion of MITF has been associated with increased cell size and disorganized cytoskeletal structure in melanoma through regulation of Dia1 which promotes formation of actin filaments and stabilizes microtubules network at the cell periphery (Carreira et al., 2006; Nezami et al., 2006). The FACS analysis showed that the percentage of large and granular cells were increased to 38%-55% in MITF-X2 and MITF-X6 cells compared to 30% in EV-SkMel28 cell lines (Figure 4C). However, we did not observe any change in Dia1 expression in neither the knockout cell line nor in the knockdown cells. This might indicate that the changes observed in cell morphology in the MITF-KO cells are caused by other factors. However, we noticed a decrease in expression of *RhoQ* (Figure 15) , a RhO-GTPase that mediates signalling for actin cytoskeleton formation (Ridley & Hall, 1992). Lack of functional MITF also led to changes in cell shape from rounded to dendritic morphology as shown in bright field images (Figure 4A). In addition to this, immunostaining for the vimentin protein displayed enlarged cytoplasm in the MITF KO cells (Figure 4A).

Increase in cell size might also be due to a delay in cell cycle progression. Indeed, we found decreased expression of cell cycle regulators, consistent with effect on cell size. For instance, mutation in *CDC25*, an inducer of mitosis, caused a delay to entry into mitosis and produced abnormally large yeast cells (Russell & Nurse, 1986). Similarly, the *WEE1* kinase that controls timing of entry into mitosis was decreased in expression in ΔMITF-X6 cells (Nurse, 1975). Both *WEE1* and *CDC25* have MITF binding peaks at their promoter in melanoma cells indicating that MITF is an upstream regulator of genes that are responsible for controlling cell size.

Interestingly, MITF-KO cells seeded on reconstituted basement membrane such as matrigel matrix displayed spherical cell morphology compared to EV-SkMel28 cells which formed flatter cell shapes (Figure 4D). The ECM serves as a molecular scaffold which provides cells with physical and biochemical microenvironment for cell-cell and cell-matrix interaction, cell polarity and invasion (P. Lu et al., 2012). Thus, the lack of MITF might trigger expression of genes which are alter cell-cell and cell-ECM intereaction which allows cells to acquire cell shape or growth pattern.

Together we observed that the loss of MITF led to changes in cell morphology, possibly due to several factors from a stall in cell cycle progression to deregulation of signalling events that control actin cytoskeleton formation which ultimately leads to change in cell morphology.

5.1.2 MITF is important for proliferation of melanoma cells

In this thesis, we reported that lack of MITF delays proliferation rate in melanoma cells. It has been shown that MITF regulates cell cycle progression through cooperation with Rb1 and induction of *p21^{CipI}* (*CDKN1A*) expression (Carreira et al., 2005). Depletion of MITF caused a GO/G1 cell cycle arrest (Carreira et al., 2006). In addition, MITF directly binds and regulates the expression of *CDK2* and *CDK4*, in turn stimulating melanoma cell proliferation (Du et al., 2004; Wellbrock et al., 2008b). Consistent with the findings above, using a BrdU assay, we showed a 40-50% decrease in BrdU positive cells in MITF-KO cells compared to the EV-SkMel28 cells (Figure 5A). Analysis of live cell images using the IncuCyte system showed that MITF-KO cells had 40-50% increased doubling time (Figure 5B). The same results were obtained using the MTS cell viability assay where we observed a 50% decrease in viable cells in MITF-KO cells (Figure 5D).

An inverse relation of MITF with the cell cycle inhibitor p27^{kip1} has been reported, in which depletion of MITF led to cell cycle arrest with induction of p27^{kip1} (Carreira et al., 2006). However, we did not see induction of p27^{kip1} in the MITF-KO cells. This could be due to the fact that Dia1, which is an actin cytoskeleton organizer regulated by MITF, that controls p27^{kip1} expression was also unchaged in MITF-KO cells. However, gene expression analysis of ΔMITF-X6 cells revealed increased expression of other cell cycle inhibitors such as *p18* (CDKN2C), *p21^{CIP1}* (CDKN2A) and *p15^{INK4B}* (*CDKN2B*) as well as decreased expression of *CDK2* and *CDK5R1* (Figure 22A).

The p16^{Ink4a} protein has been implicated in senescence of melanocytes in nevi. This protein is a potent cell cycle inhibitor that targets CDK4/6 and induces senescence via activating p53 and inhibiting MDM2 (Bennett, 2003; Sviderskaya et al., 2002). In many cancers including melanoma, the *CDKN2A* locus which encodes for both p16^{Ink4a} and p14^{ARF}, is deleted or silenced (Ruas & Peters, 1998; Sharpless & DePinho, 1999).

The *CDKN2B* gene is another cell cycle inhibitor, which encodes for *p15^{INK4B}* and has been shown to be deleted in 90% of cancer that also carry a *CDKN2A* deletion (Gao et al., 2013). Induction of *p15^{INK4B}* has been implicated in the maintenance of growth arrest in nevus melanocytes (McNeal et al., 2015). Notably, most nevi harbour a high frequency of BRAFV600E mutation (Ichii-Nakato et al., 2006). It is well known that mutation of BRAFV600E causes transient proliferation of melanocytes to benign moles (Pollock et al., 2003). Once nevi reach 2-3 mm in diameter, the melanocytes stop dividing and enter senescence, despite constitutive activation of the BRAF mutation. Interestingly, McNeal et al. (2015) have reported that the molecular mechanism underlying BRAFV600E mediated

growth arrest in nevi, involves the BRAFV600E mutation which leads to increased activation of TGFβ, which in turn induces expression of *p15*^{INK4B}, which ultimately results in growth arrest of the nevi (McNeal et al., 2015). Furthermore, inhibition of TGFβ or BRAFV600E restored proliferation of the nevi. Consistent with the observation reported above, we found increased expression of both *TGFβ* and *p15*^{INK4B} in ΔMITF-X6 cells and this likely explains the growth arrest in MITF-KO cells.

While the BRAFV600E mutation was sufficient to activate TGFβ expression in nevi, the SkMel28 melanoma cells harbouring BRAFV600E mutation only showed increased expression of *TGFβ* and *p15*^{INK4B} upon lack of MITF. This indicates that the loss of MITF is critical for TGFβ mediated growth arrest in SkMel28 cells. Furthermore, neither TGFβ nor its target *p15*^{INK4B} are bound by MITF, suggesting that there are factors downstream of MITF that regulate their expression. Since, *p15*^{INK4B} expression could antagonize the oncogenic role of BRAFV600E in melanoma and melanocyte, it would be interesting to recapitulate the proliferation defect in MITF-KO cells with BRAFV600E or TGFβ inhibition.

While MITF-KO cells showed a delay in proliferation rate, we did not observe increased cell senescence as has been reported in other publications where depletion of MITF led to cell cycle arrest followed by senescence in 501Mel cells. However, this is most likely due to the fact that SkMel28 cells harbour a *p53* mutation, because p53 is essential for inducing senescence in cells (Giuliano et al., 2010).

Reduction in cell cycle progression could also be due to DNA damage since it has been shown that MITF regulates genes involved in DNA replication and mitosis including *CCNB1, AURKB* and *TERT* (Strub et al., 2011). It would be interesting to stain MITF-KO cells with DNA damage markers to determine if genome integrity is affected.

The role of MITF in cell proliferation was validated in the inducible miR-MITF piggy-bac cell lines. In contrast to MITF-KO cells, the miR-MITF SkMel28 cell lines displayed only minimal changes in cell proliferation rate (Figure 7A). As mentioned above, SkMel28 cells harbor the p53 mutation, thus explaining the ineffectiveness of cell cycle inhibition in these cells. Nevertheless, long term absence of MITF possibly causes accumulative long lasting genetic alterations in cells that result in irreversible changes in cellular phenotype that are independent of p53 mutation status. However, when miR-MITF was induced in 501Mel cells which are p53 wild type, doubling time increased to 26 hours compared to 20 hours in miR-CTRL cells (Figure 7B). Another explanation for the different effects of MITF observed in the two cell lines is both protein and mRNA level of MITF are higher in 501Mel cells than in

SKmel28 cells. Therefore, reducing MITF levels in MITF high cells may lead to a more pronounced effect on proliferation. In addition, this can be explained by intrinsic genetic differences present in each cell line.

5.1.3 Reduced expression of MITF did not affect invasion or migration

A dynamic molecular "Rheostat" model has been proposed, where $MITF^{high}$ cells attribute to the proliferative phenotype, whereas $MITF^{low}$ cells resulted in an invasive or "stem cell" like phenotype (Carreira et al., 2006). The role of MITF in regulating cell proliferation is well established. However, the effect of MITF in melanoma cell invasion is complicated and some of the observations are inconsistent. The reduced level of MITF is not only linked to enhanced invasiveness but also to an elimination of melanoma invasion.

Some studies have suggested that MITF is a suppressor of invasion. Indeed, transient MITF silencing in B16 melanoma cells resulted in increased tumour formation in mice (Cheli et al., 2011). Additionally, MITF depletion in 501Mel cells enhanced invasion ability of cells through modulation of β-catenin (Arozarena et al., 2011). The same findings were reported in SkMel28 and 501Mel cell lines where MITF knockdown led to an increased in invasion. The MITF depletion caused F-actin disorganization via Dia1 and invasion induced by Rock signalling. In the same paper, they showed that ectopic expression of MITF in the invasive SkMel28 melanoma cell lines led to a decreased tumour formation in mice as compared to empty vector transfected cell lines (Carreira et al., 2006).

Conversely, the proinvasive role of MITF is also supported by the fact that inhibition of MITF expression via HIF1α in UACC-62 human melanoma cell lines reduced xenograft growth in mice (Feige et al., 2011). Strikingly, other studies have found that ectopically expressing MITF in 501Mel cells enhanced invasion of melanoma cells in an HGF dependent manner (McGill et al., 2006).

In contrast to some of these findings above, here we reported that MITF-KO cells had reduced invasion potential as determined using a matrigel transwell invasion assay. The number of invaded cells was reduced by half in MITF-KO cells compared to EV-SkMel28 cells (Figure 8A). However, expression of Dia1, an important modulator of actin polymerization and invasion was not changed in the ΔMITF-X6 cells (Carreira et al., 2006; Fernandez-Borja et al., 2005). In addition to this, wound scratch analysis showed that MITF-KO cells had 50% reduced migration rate as compared to EV-SkMel28 cells (Figure 8B). Inconsistent with the literature above, other studies have shown that Dia1 is essential for cell migration where loss of Dia1 led to a decrease in cell movement (Brandt et al., 2007; Goulimari et al., 2005).

Nevertheless, it has been shown that RAC1 and small Rho-GTPases regulate signalling pathways which mediate the formation of lamellipodia and stress fibres (Ridley & Hall, 1992). These are essential for directional cell migration and indeed, decreased expression of *RAC1* and *RHOQ* were observed in ΔMITF-X6 cells (Figure 22A) (Katoh et al., 2006). Interestingly, both genes are directly bound by MITF at their promoter, suggesting that reduced migration ability of MITF-KO cells might partly be due to disorganized cytoskeletal structure induced by the loss of MITF.

To further study the effects of short term MITF depletion, we used the miR-MITF inducible knockdown cell lines to test invasion potential of melanoma cells. Wound scratch assay performed using the miR-MITF SkMel28 cells showed reduction in migration rate by 30% compared to miR-CTRL cell line (Figure 9B). Furthermore, matrigel invasion assay conducted in miR-MITF cells showed a minor increase in the number of invaded cells compared with miR-CTRL cells (Figure 9A). In accordance with the data presented in this thesis, a recent publication shows that the depletion of MITF did not enhance melanoma cell invasion nor migration (Vlckova et al., 2018).

Notably, there are several factors that induce invasion that also cause depletion of MITF. For example, WNT5 or TGFβ lead to reduced MITF expression and increased invasion (Cheli et al., 2012; Weeraratna et al., 2002; Widmer et al., 2013). Consistent with this, the gene expression profile of the ΔMITF-X6 cells showed increased expression of *WNT5A*. The *AXL*$^{+}$/*WNT5*$^{+}$ cells are characterized as MITF low and highly invasive and resistant to a range of inhibitors (Muller et al., 2014; Sensi et al., 2011). We did not observe increased expression of *AXL* in the ΔMITF-X6 cells, suggesting that the gene expression program governing invasion ability of melanoma cells is not fully expressed in our MITF-KO cells. Furthermore, this suggests that the mechanisms of how *MITF* regulates invasion are not entirely understood.

In all the published papers characterizing the effects of MITF on invasion, the functional assays were carried out by transiently depleting MITF cells where MITF knockdown duration and timing varied greatly between each study. In this thesis, we used two cell models for the lack of MITF; (i) cells devoid of functional MITF permanently, that are adapted to lack of MITF.; (ii) cells where depletion of MITF was induced using miRNA against MITF using an inducible piggy-bac system. This miRNA system allows effective stable knockdown for the desired duration of the experiment, where constant depletion of MITF was maintained throughout the experimental condition. Moreover, the choice of assays used in this study may affect the behaviour of the cells. For properly determining effects on invasion, *in vivo* assays in mice

should be performed for better assessing the metastatic potential of MITF-KO cells.

The relationship between MITF and the “invasive” gene signature might not be as simple as previously proposed and cannot fully explain the complex molecular mechanisms governing melanoma cell invasion. However, we might be able to use our models to further study the difference in cell behavior between the MITF-KO cells and transiently depleted MITF cells to find the underlying molecular mechanism involved in mediating these differences.

It is possible that the invasive state of melanoma cells occurs in a narrow time window and is a reversible event which coincides with changes in MITF expression. However, switching off MITF may impose an irreversible change in the epigenetic profile and behaviour of the cells. In our study, the reintroduction of MITF back into MITF-KO cells did not rescue the cell phenotype completely. At this point we do not know if this is due to permanent, irreversible changes to the cells upon MITF loss, e.g. through permanent changes in the chromatin landscape. Alternatively, there might be permanent mutations in the knockout cells that we have yet to find that change their fate and allow them to survive without MITF. This needs to be sorted out.

Due to the high plasticity of melanoma cells, they are likely to adapt and survive in the absence of MITF. This could be similar to *in vivo* condition of melanoma cells that lose MITF during drug inhibition and yet survive and later adopt drug resistance (Muller et al., 2014; Sensi et al., 2011; Titz et al., 2016). However, it has been reported that drug resistant state is reversible upon drug removal. And during this reversible process MITF levels are most likely be modulated. Therefore, it would be interesting to see how MITF-KO cells would react to drug inhibition and if drug resistance state emerges and is reversible. By studying this question, we could decipher whether MITF is a key to the reversible phenotype in drug resistance and phenotype switching in melanoma.

Like the role of MITF in cell invasion, drug resistance is also complex. Low MITF can lead to drug resistance but high levels have also been associated with drug resistance (Ji et al., 2015; Johannessen et al., 2013). Therefore, low and high levels of MITF can give rise to invasive and drug resistant melanoma cells. This requires cell line model such as miR-MITF cells where we can freely tune MITF level from high to intermediate to low and study melanoma cell invasion and drug resistance.

5.1.4 Transcriptional profile of MITF-X6 cells show distinct functional gene program

To understand phenotypic and genomic differences between MITF-KO and EV-SkMel28 cell lines, we carried out mRNA-sequencing of ΔMITF-X6 and EV-SkMel28 cells. Differential expression analysis led to the identification of 1516 differentially expressed transcripts between these two cell lines (Figure 8A). We observed decreased expression of previously identified MITF targets such as *MLANA*, *PMEL*, *DCT*, *IRF4*, *CDK2 and TYRP1.* This is consistent with previous results (Bertolotto et al., 1998; Du et al., 2003; Du et al., 2004; Praetorius et al., 2013). We also observed increased expression of genes including *SEMA3C*, *SERPINE1* and *CDKN1A* in the ΔMITF-X6 cells. This is consistent with the findings from Strub et al (2011), where all these genes have been shown to be bound by MITF and induced in expression with MITF delpletion (Strub et al., 2011). Comparison of MITF-ChIPseq and RNA-seq datasets revealed that among the 935 genes that showed increased expression in the knockout cells, 102 were bound by MITF and that among the 581 genes that showed reduced expression in the knockout cells, 98 are directs target of MITF (Figure 10B). Thus, only a subset of the deregulated genes are directly bound by MITF. This suggests that the remaining genes are regulated indirectly by MITF or that the regulatory elements involved are located further away from the TSS than 20 kb+/-, the distance might have limited our analysis to in this study.

Gene ontology and KEGG pathway analysis of the 935 genes showing increased expression in the knockout cells were primarily associated with terms such as extracellular matrix, cell adhesion and focal adhesion, which is in line with same analysis performed in Strub el (2011) (Figure 10E,F) where increased gene sets due to siMITF in 501Mel were also enriched with terms such as signalling, cytoskeleton and focal adhesion (Strub et al., 2011). These findings reflect the changes in cell morphology and growth pattern of MITF-KO cells on matrigel matrix. In contrast, the 581 genes that are reduced in expression are associated with terms like melanosome, pigmentation and axon guidance (Figure 10E). We suggest that loss of MITF can bring changes to transcriptional cell states of that orchestrate the phenotypic changes observed in the MITF-KO cells.

5.1.5 Subset of Hoek gene signatures are deregulated in MITF-KO cells

Previous work has assigned melanoma cells to two distinct transcription signatures, one representing a proliferative cells and the other invasive cells (Hoek, Eichhoff, et al., 2008; Hoek et al., 2006; Widmer et al., 2012), The 96 genes used to form the signature were termed melanoma phenotype specific expression genes (*MPSE*). Expression of *MPSE* genes in proliferative and invasive melanoma cells is distinct and undergoes significant changes between these two phenotypes. Gene set enrichment analysis on the genes differentially expressed in the ΔMITF-X6 cells in relation to the *MPSE* genes revealed a significant negative enrichment of the proliferative signature in ΔMITF-X6 cells (Figure 11A). This is consistent with the phenotype observed in the MITF-KO cells, where cell cycle progression was significantly delayed. In contrast, the gene expression profile of the ΔMITF-X6 cells showed positive correlation with the invasive gene signature (Figure 11B). However, only 50% of the invasive genes were induced in ΔMITF-X6, whereas 70% of the proliferative genes were decreased in expression (Figure 11C).

Collectively in the MITF-KO cells, we observed consistent changes in the proliferative phenotype and deregulation of its corresponding gene expression signature. This is in accordance with the *in vivo* tests of the proliferative cell lines that showed enhanced proliferation in mice, and that the invasive cells required a longer period to initiate tumour growth in mice (Hoek, Eichhoff, et al., 2008).

Despite positive correlation in expression with the invasive gene signature, MITF-KO cells did not exhibit an invasive phenotype in our assays. In contrast, the invasive potential of the MITF-KO cells was reduced compared to EV-SkMel28 cells. This could be explained by incomplete expression of Hoek invasive gene signature in MITF-KO cells. For instance, the expression of important modulators of melanoma invasion such as *AXL* (Caramel et al., 2013; Sensi et al., 2011) were not changed in the ΔMITF-X6 cells, indicating that full activation of the invasive gene signature program is required to acquire invasive cell state.

Therefore, we could conclude that MITF-KO cells lost significant number of genes that are characteristic of proliferative cells. However, the progression to invasive path is hampered by the lack of expression of some invasive genes which possibly placed the MITF-KO cells into a “premalignant” quiescent state. Additionallly, It would be interesting to ectopically introduce the remaining 24 Hoek invasive genes that were not induced in expression in

the MITF-KO cells. This will allow us to identify which are the crucial dirvers to acquire invasive state.

However, it is difficult to define whether the MITF-KO cells are premalignant or still malignant like its paternal cell, without placing these cells into the appropriate microenvironment. In fact, our collaborator Lionel Larue subcutaneously injected MITF-KO and EV-SkMel28 cells into mice in order to determine their potential for tumor formation. Preliminary results from this experiment showed that ΔMITF-X6 cells are faster at tumour growth compared to EV-SkMel28 lines. Surprisingly, ΔMITF-X2 cells showed a slight decrease in tumour growth compared to EV-SkMel28 and ΔMITF-X6 cells. This suggests that the MITF-KO cells still retain the ability to form tumours. The difference in tumour growth between ΔMITF-X6 and ΔMITF-X2 cells can partly be explained by the level of MITF. The ΔMITF-X6 cells do not have functional MITF whereas ΔMITF-X2 cells have increased protein expression of a truncated MITF protein. The truncated form of MITF in ΔMITF-X2 cells may participate in inhibition of tumour growth. This requires staining tumour samples with differentiation marker such as MLANA to check if MITF transcriptional activity is active in these tumours. Furthermore, this raises the need to investigate the difference in transcriptomic profile of ΔMITF-X2 and ΔMITF-X6 cells. Furthermore, we need to identify and characterize the truncated form of MITF to investigate if it is transcriptionally active.

All in all the melanoma phenotype switch model argues that the proliferative/invasive states are a repeated cycle of events triggered by tumour microenvironment to allow tumour cell to proliferate and invade. Due to the dynamic nature of these cycle of events, MITF activity is also changed to bring the transcriptional changes that are required for estabilishing distinct phenotypes. We can imagine that by permenantly depleting MITF we introduced a break into this continouse cycle, which perhaps halts the cell into in irreversible cell state of somewhere between proliferation and invasion.

5.1.6 $MITF^{low}$ tumours and ΔMITF-X6 cells are similar and de-differentiated

Tumours harbour multiple cell types which give rise to multiple level of complexity and tumour heterogeneity. Using single cell RNA sequencing to transcriptionally profile 4645 single cells isolated from melanoma tumours of 19 patients, led to the identification of transcriptionally distinct populations of cells within the same tumour. These include a population of cells with high MITF expression ($MITF^{high}$) as well as high expression of *TYR*, *PMEL* and

MLANA. Another distinct population of cells expressing little MITF ($MITF^{low}$) showed high levels of *NGFR* expression*,* a melanoma cancer stem cell marker and *AXL* (Boiko et al., 2010; Tirosh et al., 2016). Consistenly, the ΔMITF-X6 cells exihibited loss of the Tirosh $MITF^{high}$ gene signature (Figure 11D). In addition, of the 329 melanoma samples studied in TCGA, 18% were clustered as "MITF-low"; these samples had low expression of pigmentation genes and of genes related to epithelia but were preferentially enriched with genes expressed in the nervous system or neuronal development (Cancer Genome Atlas, 2015). In line with this, gene expression profile of the ΔMITF-X6 cells was positively enriched for the gene signature of $MITF^{low}$ tumours (Figure 11E). Thus, we asked if MITF-KO cells are like the $MITF^{low}$ tumours?

To answer this question, differential expression analysis was carried out, using $MITF^{low}$ and $MITF^{high}$ tumours in the TCGA data set which identified 2655 genes at least 2-fold differentially expressed between two groups (Figure 12A). This indicates that tumours samples with low and high MITF levels can be separated based on their gene expression profiles which likely reflects different phenotypes.

Overlapping analysis of differentially expressed genes obtained from $MITF^{low}$ tumours and ΔMITF-X6 cells revealed 557 overlapping genes, of which 227 of genes were increased in expression in both data sets and 329 genes were decreased (Figure 12B). In $MITF^{low}$ tumours, genes that were reduced in expression were associated with pigmentation and melanosome related genes, whereas highly expressed genes were primarily involved in extracellular matrix and focal adhesion (Figure 12C, D). This shows that the ΔMITF-X6 cells reflect the transcriptome profile of $MITF^{low}$ tumours and can therefore be used as a tool to investigate molecular changes happening in $MITF^{low}$ tumours.

Interestingly, gene set enrichment analysis of differentially expressed genes in $MITF^{low}$ tumours and ΔMITF-X6 cells revealed positive enrichment for EMT hallmark genes, and showed negative enrichment for pigmentation genes (Figure 13A). The process of EMT involves loss of E-Cadherin and gain of N-Cadherin which drives the process of epithelial to mesenchymal phenotype. This is the characteristic of epithelia tumour cells invade into the surrounding tissue (Brabletz et al., 2001).

Interestingly MITF ChIP-seq data identified binding sites containing an E-box motif with a flanking T in the intron 2 region of E-cadherin as well as in introns 2 and 5 of N-cadherin (Figure 13C). In addition, an MITF peak containing two E-box motifs was detected in intron 11 of *ZEB1*. Reduction of E-cadherin is the first step in the loss of differentiation and its expression is repressed by *ZEB1*/*BRG1*, *TWIST* and *SLUG* (Batlle et al., 2000; Sanchez-Tillo et al.,

2010). In line with this, expression analysis of ΔMITF-KO cells and MITF^{low} tumours showed increased expression of subset of EMT regulators such as N-cadherin, *ZEB1*, *TGFB1*, *SOX2* whereas the expression of E-Cadherin and Slug was reduced (Figure 13D).

It is worth noting that expression of the SLUG protein and RNA was reduced in the MITF-KO cells (Figure 14D). SLUG has been suggested to regulate cell motility in melanoma cells (Shirley et al., 2012), consistent with our report that MITF knockdown and knock out cells were reduced in migration rate by 50-70% compared to their respective control cell lines (Figure 8B&9B). Furthermore, expression of the E-Cadherin and N-Cadherin proteins were affected upon MITF depletion as determined using western blotting; N-cadherin was increased whereas E-cadherin was lost. This was further verified using RT-qPCR (Figures 14A,B,C). Our results indicate that MITF is directly involved in regulating the expression of *SLUG* as well as N- and E-cadherin.

As we know, melanoma cells are not from epithelial origin, but are from highly motile neural crest cells which have already undergone epithelial to mesenchymal transition during commitment to become melanocytes. As a consequence, melanocytes still retain expression of EMT marker genes such as *SLUG*, *ZEB2*, and *N-cadherin* (Gupta et al., 2005). It has been suggested that when melanoma become invasive, the classical EMT is different from what has been observed in epithelial cells. In this case, melanoma undergoes de-differentiation towards their neural crest origins (Vandamme & Berx, 2014). Consistent with this observation, we reported the transcriptomic profile of ΔMITF-X6 cells are negatively enriched with melanocyte cell specific gene signature whereas positively enriched with Schwann cell and hair follicle stem cell signature (Figure 13B). The Schwann cells or neurolemmocytes are cells of peripheral nervous system that produce myelin sheath around the axon. The hair follicle stem cell provides a niche for melanocyte stem cells (Nishimura et al., 2002). This indicates that the transcriptome profile of MITF-KO cells is deviated from melanocyte to neuronal cells and melanocyte stem cells. We can also suggest that MITF is not only essential for melanocyte differentiation, but also important for maintainenance of melanocyte stem cell state. In fact, TGFβ activation is required to maintaining melanocyte immaturity by supressing MITF expression during hair cycle, where melanocyte stem cells are quiescent (Nishimura et al., 2010). Melanoma cell lines have been shown to express higher levels of various TGFβ isoforms than melanocytes (Albino et al., 1991; Krasagakis et al., 1994; Rodeck et al., 1991). Additionaly, Hoek et al (2006) identified melanoma cell lines governed by TGFβ^{high} and MITF^{low} transcriptional state (Hoek et al., 2006). Interestingly, TGFβ has been shown to repress MITF by supressing cAMP response

through inhibition of PKCA which leads to a decreased activation of CREB dependent transcription of *MITF* (Pierrat et al., 2012). In line with this, we observed induction of TGFβ in MITF^{low} and MITF knock out cells (Figure13D). This indicates that the loss of MITF can directly/indirectly lead to induction of the TGFβ^{high} cell state. In turn, induction of TGFβ may rewire a transcriptional programme that helps maintaining melanoma stem cell state.

Recently, melanoma adaptive drug resistance state has been reported to be driven by a population of cells that have low MITF and high NGFR expression (Fallahi-Sichani et al., 2017; Su et al., 2017) . More recently, single cell RNA-seq applied to RAF inhibitor treated melanoma tumours identified a drug tolerant cell population that has the neural crest-like transcriptional programme (Rambow et al., 2018). This neural crest-like state lacked expression of pigmentation and invasion genes and was reported as a main driver of minimal residual disease (MRD) in melanoma, which is the main cause of relapse in cancers (Rambow 2018). Interestingly, ΔMITF-X6 cells displayed positive enrichment for neural crest signature, whereas it was poorly associated with the invasive gene signature (Figure 11F,G). Furthermore, the melanoma stem cell marker *NGFR* showed a 180-220-fold increase in the MITF-KO cells and 14-fold in MITF^{low} cells (Figure 10C). This further substantiates our proposition that lack of MITF results in de-differentiation towards neural crest state.

The drug tolerant MITF^{low} tumours are slow cycling and have lost melanocyte specific differentiation genes. This is similar to our MITF-KO cells. Therefore, the MITF-KO cells reflect the cell state of MITF^{low} melanoma tumours and cells that have acquired resistance to RAF inhibition. Melanoma drug resistance and adaptation to lack of MITF may exploit the same molecular mechanism to survive. By targeting the pathways specific to adaptation/survival of the MITF-KO cells will be important to tackle the question of acquired drug resistance. This is highly clinically relevant, because the co-existence of MITF^{high}/MITF^{low} populations within same tumour suggests a high degree of tumour heterogeneity. Better understanding of co-emergence of drug resistance state within heterogenous tumours will make targeted therapy feasible through different phases of treatment. Therefore, the MITF-KO cells can be used as a tool to identify molecular drivers behind this drug tolerant state. To do this, it would be best to treat the MITF-KO cells with RAF inhibitors and assess the ability to develop drug tolerance. Then perform RNA-seq and metabolomics screen on drug tolerant cells to understand the underlying reasons behind drug tolerance and the neural crest-like de-differentiated state.

Despite the lack of invasion potential of MITF-KO cells, we showed a direct participation of MITF in inducing a de-differentiation gene programme. We

also reported that the MITF-KO cells lost the melanocyte specific gene expression signature. Therefore, in theory we can question whether we can still call MITF-KO cells melanoma cells? Perhaps it is worth investigating the similarity between our MITF-KO cells with cancers of neuronal origins. This might help us to understand better the molecular mechanism underlying the nature of our cell line model.

5.1.7 MITF regulates adhesion through FAK and Paxillin

The interaction of cancer cells between each other and with the extracellular matrix is mediated by integrins and focal adhesions dynamics. Cell adhesion network formed between cells and the extracelluar matrix can bring together signals necessary to confer resistance to drug treatment and apoptosis (Tredan et al., 2007). The gene expression analysis identified increased expression of genes involved in extracellular matrix formation and focal adhesion in both the ΔMITF-X6 cells and the $MITF^{low}$ tumours from the TCGA (Figure 15). Various adhesion genes including integrins such as *ITGA2, ITGA3, ITGA4, ITGA5* and *ITGA10* showed 2-20-fold increase in expression in the ΔMITF-X6 cells and the $MITF^{low}$ tumors. Integrins are heterodimeric receptors which attach the cells to the extracellular matrix which in turn elicits phosphorylation of the Focal adhesion kinase (*FAK*) and Paxillin (*PXN*). Together FAK and PXN act as scaffold proteins and recruit other signalling factors important for cell migration (Petit et al., 2000; Slack, 1998). Importantly, we observed that MITF binds directly to the *PXN* and *FAK* promoters (Figure 16A). However, we only observed increased expression of Paxillin in the RNA-seq data of ΔMITF-X6 cells but not of FAK (Figure 16B), indicating that MITF can directly suppress the expression of *PXN*.

Immunostaining analysis for phosphorylated PXN (Tyr111) and FAK (Tyr397) displayed increased number of focal points at the cell periphery in both the ΔMITF-X2 and ΔMITF-X6 cells (Figure 17) and the miR-MITF cell lines (Figure 18). However, immunostaining for PXN (Tyr111) in MITF-KO cells did not show a major increase. The preliminary results from westernblot analysis showed an increased of PXN (Tyr111) protein in MITF-KO cells. This suggests that MITF plays a direct role in regulating *FAK* and *PXN* mediated focal adhesion proteins. To further validate the link between MITF, PXN and FAK, we are in the process of performing PXN and FAK staining on melanoma tumours from patient samples to investigate the clinical significance of their relationship with MITF.

Interestingly, cells from FAK (-/-) deficient mouse embryos show decreased migration ability (Ilic et al., 1995). We did not observe increased migration ability of the MITF-KO and miR-MITF cell lines despite an increased number of focal points. However, increased integrin mediated adhesions results in

large focal adhesion points, which could make cells more adherent and less migratory (Ridley et al., 2003). In addition, once activated, the affinity of integrins towards extracellular matrix is stabilized through activation of the GTPases *RAP1* or *PKC* (Ridley et al., 2003). Both kinases are increased 2-8 fold in the ΔMITF-X6 cells (Figure 15). The expression of *RAF1* kinase, a known suppressor of integrin activation, was decreased 30-fold in ΔMITF-X6 cells when compared to EV-SKmel8 cells. Therefore, the increased number of focal points in the MITF-KO cells might be explained by the increased expression of integrins, *PXN* and *FAK,* followed by their strong affinity to the ECM through *RAP1* and *PKC* activation.

The expression of the well know cell adhesion molecule *CEACAM1*, a driver of tumour cell invasion and a direct target MITF (Ullrich et al., 2015), was not changed in the MITF-KO cells, whereas a 5-fold reduction of *CEACAM1* expression was found in $MITF^{low}$ melanoma tumours from the TCGA data set.

Increased expression of several cell adhesion molecule genes (CADMs) was observed in the MITF-KO cells (Figure 15). The CADMs encode immunoglobulin superfamily molecules that are important for cell-cell adhesion maintenance, thus, they protect agains malignant conversion (Murakami, 2002). These proteins have been described as tumour suppressors in non-small cell lung cancer and have been shown to be inactivated in many cancers including liver, pancreatic and prostate cancers (Murakami, 2005). For instance, mast cells derived from MITF null mice failed to adhere efficiently to co-cultured NIH/3T3 fibroblast due to decreased expression of *CADM1* gene, a direct target of MITF (Ito et al., 2003). In contrast to this, in $MITF^{low}$ tumours, *CADM1* expression was increased 2-fold compared to the $MITF^{high}$ tumours, suggesting that MITF differentially regulates the expression of the same genes in a cell type specific manner. Interestingly, increased expression of *CADM4* was observed in both $MITF^{low}$ tumors and in the ΔMITF-X6 cells (Figure 15). The loss of *CADM1* and *CADM4* expression has been associated with advanced stage breast cancer (Saito et al., 2018).

Thus, we can suggest that increased expression of *CADM1/4* might enhance cell-cell adhesion in MITF-KO cells. Consistently, in this thesis we observed that MITF-KO cells exihibited globular growth pattern when seeded on matrigel, which mimics the basement membrane. Instead, EV-SkMel28 cells, displayed spread out growth pattern on matrigel (Figure 4C). This indicates that the adhesion dynamics between MITF-KO cells with each other and extracellular matrix altered is considerably which is most likely driven by induced expression of cell adhesion and extracellular matrix related genes.

Together, our observations suggest that MITF binds directly to the regulatory

regions of a set of genes responsible for the cellular adhesion programme and represses their expression. This eventually activates the expression of an extracellular matrix related adhesion profile in MITF^{low} melanoma cells and tumours. However, in this thesis the functional effect of extracellular matrix related changes has not been studied in detail but will be the focus of future research. It is worth investigating whether there is a link between adhesion signature and the drug tolerant de-differentiation state. In that case, it would be clinically important to modulate adhesion dynamics of cells to overcome the drug resistance state.

5.2 Chromatin modifications in MITF-KO cells

We argued the possibility of epigenetic modification in MITF-KO cells to accomodate major changes in gene expression. We carried out ChIP-qPCR against the H3K4me3 active mark and a repressive mark H3K9me3 in MITF-KO and EV-SkMel28 cells.

Notably, ChIP-qPCR against the H3K4Me3 active mark revealed that the *MLANA*, *QPCT* and *RRAGD* genes, which are melanocyte differentiation genes, had reduced level of H3K4Me3 at their promoters compared to the EV-SkMel28 cells, whereas this same histone mark was increased at the promoters of the *ZEB1, TGFB1, NGFR, AMOTL1* and *TLR2* genes (Figure 19 A-H). ChIP-qPCR for H3K9Me3, a repressive mark, showed a decreased presence of this mark at the *TGFB1* and *SERPINE3* promoters, consistent with the induced expression of these genes in MITF-KO cells (Figure 19 I-J).

This indicates that the loss of MITF could enforce cells to reshape their chromatin state to acquire a new phenotype supporting cell survival during tumour progression. It would be interesting to perform high throughput sequencing in order to follow the H3K4me3 and H3K9me3 marks to unbiasedly check for genome wide methylation of gene promoters and enhancer regions. This would add a new prespective in understanding the molecular mechanism underlying gene expression changes in MITF-KO cells. Moreover, it is worth investigating whether the histone modifications are restricted to long term depletion of MITF. Therefore, it would be interesting to assay miR-MITF cell lines for histone modifications and compare the chromatin states between cells where MITF has been transiently knocked down to those where MITF has been terminally depleted. Studying these differences could help us understand the reversible/irreversible nature of these two states, and might lead to therapeutical options by targeting specific chromatin states associated with disease.

5.2.1 MITF regulates SETDB2 directly

SETDB2 belongs to the member of *SUV39* gene family, which catalyses the methylation of lysine 9 of H3, a repressive chromatin mark (Dillon et al., 2005). *SETDB2* expression has been shown to be regulated by type 1 interferon signalling (Schliehe et al., 2015). In this thesis, we showed that MITF directly regulates *SETDB2* expression. This is supported by several pieces of evidence. First, differential gene expression analysis revealed that *SETDB2* expression was reduced 3-fold in the ΔMITF-X6 cells. This was confirmed using RT-qPCR which showed a 40-60% reduction of *SETDB2* expression in the MITF-KO cells compared to EV-SkMel28 cells (Figure 20A, B). Second, MITF ChIP-seq analysis revealed MITF peaks in the promoter and intron 11 of *SETDB2* (Figure 21A). Third, ectopic expression of *MITF* in LU1205 cells led to a 2-fold increase in *SETDB2* expression. Fourth, inducible knockdown of MITF in miR-MITF cell line resulted in a 50% reduction of *SETDB2* expression compared to miR-CTRL cell lines (Figure 21B,C) thus further validating the direct effects of *MITF* on *SETDB2* expression.

Further evidence for the link between MITF and SETDB2 was gained from interrogating the TCGA RNA-seq data of various tumour samples. This revealed that *SETDB2* was most highly expressed in acute myeloid leukemia followed by uveal melanoma and skin cutaneous melanoma (Figure 20C). More importantly, across 482 melanoma tumour samples, the expression of *SETDB2* and *MITF* showed a positive correlation (Pearson 0.6, P<2.2E-16) (Figure 20D); *SETDB2* is expressed at a low level in $MITF^{low}$ tumours (Figure 20E). This suggests that SETDB2 may mediate some of the effects of MITF in melanoma cells.

It is worth mentioning that *SETDB1,* the closest gene family member of *SETDB2*, has been shown to be amplified in melanomas and contributes to rapid onset of melanoma (Ceol et al., 2011). Similarly, the oncogenic role of *SETDB2* was described in gastric cancer, where overexpression of *SETDB2* was associated with shorter disease free survival and enhanced migration, invasion and proliferation of gastric cancer cells (Nishikawaji et al., 2016). Consistent with that, we reported that *SETDB2* knockdown led to a significant decrease in proliferation in 501Mel cells (Figure 22E,F). Additionally, a recent publication showed that *SETDB2* affects cell cycle progression through suppression of *p18* (*CDK2NC)* in acute leukemia (Lin et al., 2018). Consistent with that, ΔMITF-X6 cells had increased expression of *p18* among other cell cycle inhibitors such as *p15* (*CDKN2B)* and *p57* (*CDKN1C)* (Figure 22A).

In order to start probing the role of *SETDB2* in melanoma cells, we used siRNA to deplete the gene and then performed RT-qPCR. This showed increased expression of *p15* and *p57* in 501Mel and SkMel28 cell lines (Figure 22B,C). Interestingly, overexpression of *p15* has been observed in melanocytic nevi (McNeal et al., 2015). The activation of BRAF(V600E) mutation in melanocytes led to the induction of *CDKN2B* in a *TGFB1*-dependent manner, and halted proliferation rate of the melanocytes (McNeal et al., 2015). Notably, expression of *SETDB2* was negatively correlated with *TGFB1* in melanoma tumour samples from the TCGA data. In addition, *SETDB2* knockdown also led to increased level of *TGFB1* (Figure 22B, C) and chromatin immunoprecipitation coupled to qPCR in MITF-KO cells showed a loss of the repressive mark H3K9Me3 and gain of the active mark H3K4me3 at the promoter of *TGFB1*. This shows gene expression change observed in MITF-KO cells are reflected in histone modifications. A histone modifier such as *SETDB2* most likely plays a role in shaping the epigenetic landscape of the cells. Our data presented above therefore suggest that *SETDB2* supresses the expression of *TGFB1*, *p15* and *p18* in melanoma cells.

Preliminary results from western blotting analysis after *STEDB2* knockdown showed increased levels of $p21^{CIP1}$ in the SkMEL28 cell line (Figure 22C) However, the $p21^{CIP1}$ protein was not detected in 501Mel cells. It has been shown that there is an inverse relation between $p21^{CIP1}$ and *MITF* (Carreira et al., 2006). Consistent with this finding, $p27^{KIP1}$ levels were increased upon *SETDB2* knockdown in 501Mel cells, indicating SETDB2 might contribute to direct induction of $p27^{KIP1}$ through MITF (Figure 22C).

Another interesting finding reported that SETDB2 suppresses the expression of a subset of NF-κB target genes (Dillon et al., 2005; Schliehe et al., 2015). In human melanoma, NF-κB expression is elevated (Duffey et al., 1999). NF-κB activation has been reported to promote tumour cell survival, proliferation and metastasis. For instance, the chemokine CXCL8 which is regulated by NF-κB is associated with high level of aggressiveness in melanoma (Kunz et al., 1999). In addition, NF-κB activates anti-apoptotic pathways through induction of tumour necrosis factor receptor-associated factor 1 (TRAF-1) and TRAF-2 (Ueda & Richmond, 2006). Consistenly, we observed induced expression of *CXCL8, TRAF1* and *NFKB1* in ΔMITF-X6 cells. This suggests that, SETDB2 and NF-κB might cooperatively regulate expression NF-κB target genes.

Taken together, we have shown that MITF positively regulates *SETDB2* expression. Our data demonstrates the role of *SETDB2* as an effector of cell

cycle progression through the repression of various cell cycle inhibitors including $p21^{CIP1}$, $p27^{KIP1}$, *p15* and *p57*. Moreover, *SETDB2* is likely to de-repress *TGFB1,* thereby activating signalling cascades important for melanoma progression. Interestingly, SETDB2 could participate in regulating NF-κB target genes which are implicated in melanoma progression. For future experiments, it would be interesting to recapitulate the anti-proliferative effects of *MITF* by overexpressing *SETDB2* or by treating the cells with *TGFB1* inhibitors. Furthermore, depletion of MITF results in reduction of *SETDB2*, which can result in derepression of an array of genes which could ultimately affect gene repertoire of MITF-KO cells. Therefore, it is important to dissect the targets of SETDB2 in melanoma cells to better understand the epigenetic event during melanoma progression.

5.2.2 PRDM7 lineage specific expression in melanocyte

The role of PRDM7 as a histone lysine methyltransferase was recently described (Blazer et al., 2016). We observed a 30-fold decrease in expression of *PRDM7* in MITF-KO cells vs EV-SkMel28 cells (Figure 23A) and RT-qPCR analysis revealed a 70-80% decrease in *PRDM7* expression in the MITF-KO cells (Figure 23B). Interestingly, the expression of *PRDM7* showed a lineage-specific expression pattern in melanocytes (Fumasoni et al., 2007). Furthermore, TCGA data analysis across various tumour samples revealed that *PRDM7* has the highest expression in melanoma tumour samples (Figure 23C). Notably, in melanoma tumour samples *PRDM7* expression positively correlated with *MITF*, with a Pearson correlation of 0.3 (P=3.3e-12) suggesting that *PRDM7* expression is dependent on MITF (Figure 23D). *PRDM7* was expressed at a high level in $MITF^{high}$ tumours (Figure 23E). The effect of *MITF* on *PRDM7* expression was further tested in MITF-low LU1205 cells, where ectopic expression of *MITF* led to a 20-fold induction of *PRDM7*. Moreover, upon MITF knockdown in miR-MITF cell lines, we observed an 80% decrease in *PRDM7* expression (Figure 24A,B). Together, our findings indicate that *PRDM7* is exclusively expressed in melanoma tumours and its expression is modulated by MITF in different melanoma cell lines. The lineage restricted expression of *PRDM7* in melanoma makes this factor interesting. It might be participating in melanocyte/melanoma specific gene expression programme. If so, this could explain the loss of melanocyte gene signature in MITF-KO cells. We could speculate that MITF and PRDM7 maintain melanocyte indentity, in which MITF directly activates melanocyte differentiation genes while on the other hand PRDM7 reinforces this process by shaping the chromatin landscape.

5.2.2.1 PRDM7 expression regulated through MAFB

Despite the effects of *MITF* on *PRDM7* expression, we did not observe MITF binding sites in PRDM7 regulatory regions, neither at the *PRDM7* promoter nor 10kb+/- upstream from the transcription start site. This indicates that *PRDM7* expression is regulated indirectly by *MITF* through other factors. *In silico* motif analysis of the *PRDM7* promoter identified MAFB as a possible direct transcriptional regulator with a binding site located – 89 bp from the TSS (Figure 24C). Interestingly, the expression of *MAFB* was decreased in the ΔMITF-X6 cells (Figure 24D), and ChIP-seq analysis identified an MITF binding site in the MAFB promoter (Figure 24E). This may suggest that *MITF* directly regulates *MAFB* expression in melanoyctes which in turn regulates the expression of *PRDM7*.

In order to test if there is a direct link between *MAFB* and *PRDM7*, siRNA was used to knockdown *MAFB* in 501Mel cells and then the expression of PRDM7 was determined using RT-qPCR. This showed 80% reduction in *PRDM7* expression upon siMAFB as compared to siCTRL cells (Figure 24F). Together, this suggests that *MAFB* is activated by *MITF* which then binds and regulates expression of *PRDM7*. However, at present, we do not know the downstream targets of *PRDM7*.

5.2.2.2 PRDM7 and MAFB affect cell proliferation

In this thesis, we demonstrate the functional role of *PRDM7* as an effector of cell proliferation. Proliferation assays after siRNA-mediated knockdown of *PRDM7* in 501mel cells resulted in a 26 hour doubling time as compared to 23 hours upon siCTRL (Figure 25A). However, the effect of *PRDM7* knockdown on proliferation rate was not significant in SkMel28 cells (Figure 25B).

We also performed a wound scratch assay upon siPRDM7 knockdown. No significant differences were observed in migration ability of cells when compared to siCTRL in either 501Mel or SkMel28 cells (Figure 25E,F). This may suggest that *PRDM7* specifically regulates pathways involved in cell proliferation.

As reported above, *MAFB* directly regulated the expression of *PRDM7*. This led us to study whether *MAFB* has the same effects on cell proliferation. Thus, proliferation assays were performed in siMAFB and siCTRL treated 501Mel and SkMel28 cell lines. siMAFB knockdown resulted in a two-fold increase in cell doubling time of 501mel cells (Figure 25C). Again, knocking down *MAFB* in SKmel28 cells showed only a minor delay in proliferation (Figure 25D). In accordance with our report in this thesis, it has been shown that in mouse β-

cells, *MAFB* enhanced proliferation through inducing the expression of Cyclin D2 (J. Lu et al., 2012).

Notably, the effects of *MAFB* on proliferation were more severe than upon *PRDM7* knockdown, (doubling time of 50 hours with *MAFB* knockdown vs. 26 hours upon *PRDM7* knockdown) in 501Mel cells (Figure 25C). This might indicate that *MAFB* modulates cell cycle through several factors, including *PRDM7*. It would be interesting to try to rescue the defects seen in proliferation through re-introducing *PRDM7* or *MAFB* into MITF-KO and miR-*MITF* knockdown cells. Moreover, to find downstream targets of *PRMD7* and *MAFB*, unbiased method such as RNA-sequencing should be carried out to understand the mechanism behind regulation of cell cycle progression in melanoma.

In the first part of thesis we reported various functional and molecular changes due to permenant loss or transient MITF depletion. Permanent absence of MITF resulted in enlarged cell size. The MITF-KO cells seeded on matrigel matrix displayed spherical growth pattern compared to control EV-SkMel28 cell lines. This indicated increased cell-cell and cell-ECM adhesion. Permanent or transient depletion of MITF resulted in reduced a proliferation rate. However, migration and invasion ability of MITF-KO cells were also significantly reduced. Phenotypic changes observed in MITF-KO cells were further investigated by gene expression profiling of ΔMITF-X6 and EV-SkMel28 cells. It revealed a loss of pigmentation and melanocyte specific genes in ΔMITF-X6 cells whereas ΔMITF-X6 cells gained a gene expression signature of extracellular matrix, adhesion molecule and neuronal crest like cells. To summarize we propose a model (Figure 37) that argues that lack of MITF does not contribute to invasiveness but rather to a de-differentiated neural crest like cell state. This state is characterized by increased expression of genes related to extracellular matrix and neuronal cells. Importantly, MITF directly represses the expression of ECM related genes. The establishment of this state is further reinforced by changes in histone modifications due to loss of expression of histone modifiers such as PRDM7 and SETDB2. The histone modification of MITF-KO cells might put them into an irreversible state that makes the cells insensitive to MITF reintroduction. Unraveling how these histone modifications can be therapeutically exploited may lead to more treatment options for melanoma. Furthermore, our work focuses on the role of MITF in regulating the expression of genes involved in the establishement of the extracellular matrix. Understanding the alteration of ECM components has major implications in melanoma treatment. Increasing evidence suggests that increased expression of ECM related genes is associated with tolerance to drug inhibition. We believe that there is an association between ECM reprogramming and neural crest like state. Our

results point to the loss of MITF as being both directly and indirectly responsible for the estabilishment of these cell states in melanoma. Finding targetable pathways specific to either ECM or neural crest like transcriptional state might lead to therapeutical option to overcome drug tolerance in melanoma treatment.

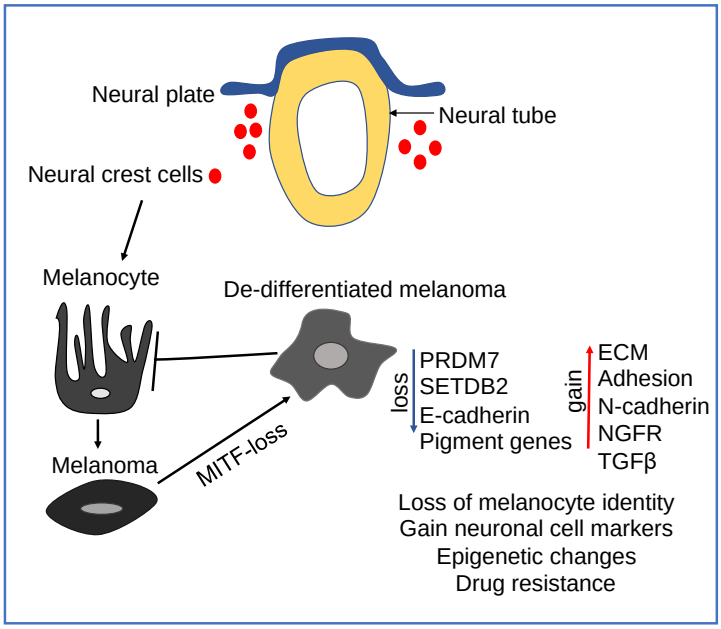

Figure 35. A model illustrating the path to de-differentiation driven by MITF loss.

5.3 MITF transcription network with TFEB and IRF4 in melanoma

5.3.1 Identification of IRF4 binding sites in melanoma

A genetic variant in IRF4 was associated with freckling hair, skin and eye colour in humans (Han et al., 2008; Sulem et al., 2007). The same SNP (rs12203592) was associated with increased risk of melanoma (Han et al., 2011). This was the first time that IRF4, a gene well known for its key role in the development of the haematopoietic system, was suggested to play a role in pigment cells. In order to characterize the role of IRF4 in pigment cells, we used the ChIP-sequencing method. A recombinant IRF4 protein was tagged with GFP and a ChIP-seq experiment performed using anti-GFP antibodies.

Two individual ChIP-seq experiments identified 3694 IRF4 binding sites in 501mel melanoma cells (Figure 29C).

Using the MEMEChIP motif discovery tool resulted in the identification of the known IRF4 binding motifs (AANNGAAA) described in previous studies (Brass et al., 1996; Pernis, 2002) (Figure 29A,B). In addition to this, we discovered IRF4 binding sites consistent with previous published studies, such as *Sub1*, *Tyr*, and *CCNC,* but IRF4 has been shown to regulate various biological process from pigmentation to general gene transcriptional regulation in myeloid cells (Praetorius et al., 2013; Shaffer et al., 2009).

5.3.1.1 MITF and IRF4 regulate pigmentation, autophagy and immunity related genes

Cooperative binding of IRF4, MITF and TFAP2A has been reported to regulate the expression of *TYR*, an enzyme that catalyses the production of pigment melanin (Praetorius et al., 2013). Peak annotation analysis assigned a total of 3964 IRF4 peaks to 3143 genes based on 20 kb -/+ distance from the transcription start site. Genome-wide analysis of overlaps in binding sites of IRF4 and MITF was carried out and identified 452 overlapping sites (Figure 30A) and 652 co-bound genes (Figure 30C).
Interestingly, we found that genes bound by both MITF and IRF4 were commonly enriched for pigmentation, autophagy processes and interferon signalling pathways (Figure 30E,F). Our analysis identified co-binding to 26 out of 97 pigmentation genes (P<3.9-07), including *TYR, HSP5, C10ORF11, MC1R, AP1G1*, *VPS33A*, and *ZEB2* (Figure 30D). For instance, *MC1R* is essential for UV-induced melanomagenesis and, similar to *IRF4,* allelic variants at MC1R are associated with poor tanning ability, skin cancer, and hair colour (Abdel-Malek et al., 1999; Suzuki et al., 1999). Our data provide evidence for the pigmentation phenotype observed in association with IRF4 and its role in modulating pigmentation processes.

Surprisingly, we observed that MITF and IRF4 also shared binding to autophagy related genes, including *GBA*, *MTOR* and *GNS.* The link between IRF4 and mTOR has been described in IL4 activated macrophages (M2) (Satoh et al., 2010), where IRF4 plays a role as a key transcription factor that allows mTOR to reprogram metabolic processes during M2 activation. Moreover, IRF4 has been shown to regulate expression of glycolytic genes (Man et al., 2013). IRF4 expression was induced by mTOR in M2 cells (Huang et al., 2016). Moreover, IRF4 deficient B cells showed weaker mTOR activation and reduced glucose uptake which, in turn, inhibit the autophagy response (Adams et al., 2016). This suggests a strong link between IRF4 and mTOR in regulating metabolic processes in immune cells. This link could be further expanded in melanoma cells, since glycolysis has been implicated as

an essential source of energy in advanced stage melanoma (Ho et al., 2012).

IRF4 and MITF were also bound to the regulatory regions of *STX16*, *CLTC, PICALM1* and *RAB27A*, all of which are involved in membrane reorganization and fusion. It is biologically relevant that IRF4 participates in regulating these sets of genes. In immune cells there is a continuous flow of endocytosis and exocytosis which requires the constant breakdown of membrane bound organelles. Notably, it has been shown that IRF4 directly regulates genes involved in membrane biogenesis in myeloma cells and that depletion of IRF4 resulted in cell death in these cells (Shaffer et al., 2009).

Importantly, we observed cooperative binding of MITF and IRF4 to interferon signalling genes including *STAT2, STAT3, STAT6, CCL3, ADAR1, IFI6, TRIM8, TRIM2, IRF9, ISG20, IFI35* and *CAMK2D.* Interestingly, *ADAR1* is an RNA-editing enzyme and *Adar* deficient mice show aberrant interferon induction and die at embryonic day E12.5 (Mannion et al., 2014). Notably, re-expression of *ADAR1* supressed melanoma growth and metastasis *in vivo* (Mannion et al., 2014; Shoshan et al., 2015). Furthermore, expression of chemokines and interferon inducible genes plays an essential role in eliciting immune response. This is important because harnessing the immunogenicity of melanoma cells could make them susceptible for elimination by immune cells. For instance, expression of the *CCL3* cytokine was sufficient to for the recruitment of $CD8^+$ effector T cells in cancer tissue (Harlin et al., 2009).

It is well known that during tumour progression PD-1/PD-L1 perform a vital role in escaping immune surveillance. It has been shown that PD-1 is expressed on the surface of various immune cells, including T cells, B cells and tumour infiltrating lymphocytes. Whereas PD-L1 is expressed on antigen presenting cells (APCs) and tumours, engagement of PD-L1 with PD-1 leads to T cell dysfunction and exhaustion. Therefore, overexpression of PD-L1 by tumour cells leads to the cells avoiding cytotoxic T cell-mediated killing (Sun et al., 2015). Immune checkpoint inhibitors such as anti PD1/PD-L1 antibodies have been developed as an effective treatment for melanoma (Tsai et al., 2014). Importantly, PD-1/PD-L1 expression can be regulated by Interferon regulatory factor and indeed we see an IRF4 peak in the promoter of PD-L1. In addition, IRF4 has been shown to promote the expression of PD-1 (Man et al., 2017).

In order to identify genes that are uniquely bound by either IRF4 and MITF, differential binding analysis was performed and resulted in the identification of 8167 distinct sites with at least two-fold difference and FDR<0.05 (Figure 31B). Interestingly, IRF4 (but not MITF) showed preferential binding to genes associated with haematopoietic processes, histone modification and RNA metabolic processes (*PSMB4, KDM6B, DMAP1, CELF2*), whereas MITF (and not IRF4) uniquely bound to sites associated with genes involved in

forebrain development and axogenesis (*PLXNA4, NR4A2, SLITG, CHRNB2*) (Figure 31C).

For example, IRF4 was found to bind the promoter of CELF2. This gene has been shown to regulate alternative splicing events during T cell signalling (Mallory et al., 2015). Furthermore, *DMAP1*, *KDM5A* and *KDM6B* were among the genes involved in histone modification pathways that *IRF4* bound to. Depletion of *DMAP1* has been associated with derepression of genes specific for germ line in melanoma (Cannuyer et al., 2015; Loriot et al., 2006) and mice carrying a hypomorphic allele of *DMAP1* induced hypo-methylation in the genome and developed aggressive T cell lymphoma with increased genomic instability (Gaudet et al., 2003).

Our observation indicates that IRF4 is a dynamic player in melanomagenesis. It binds to genes involved in various pathways including pigmentation, autophagy and interferon signalling. Importantly, IRF4 together with MITF, might modulate genes involved in immune surveillance in the tumour microenvironment.

Our results indicate that MITF positively regulates IRF4 expression. We found that the expression of MITF and IRF4 is positively correlated across 472 melanoma tumour samples in the TCGA data (Figure 27E). In addition, both IRF4 and MITF are highly expressed in melanoma tumours (Figure 27A). Therefore, changes in MITF activity or expression, such as during melanoma progression, is likely to affect IRF4 expression as well. In turn, this will most likely change the gene expression program correlated with both factors. This was reflected in our Pearson correlation analysis of transcripts that were correlated with both IRF4 and MITF in melanoma tumours in the TCGA data. It revealed that MITF and IRF4 are positively or inversely correlated in expression with the same subset of genes, hinting that they are important components of a gene regulatory network in melanoma tumours (Figure 27D).

Furthermore, distinct and overlapping binding targets of IRF4 and MITF in melanoma cells revealed co-binding to genes involved in processes such as pigmentation, immune regulation and membrane organization. This preliminary data will allow us to select IRF4 and MITF target genes for future studies in order to identify their functional role in melanoma development. In the future, we could perform RNA-seq with overexpression or silencing of IRF4 and combine with binding data to find target genes that are due to direct IRF4 loss.

5.3.2 TFEB binding sites mainly associate with lysosomal genes

TFEB is closely related to MITF and both proteins belong to the same MiT

transcription factor family (Steingrimsson et al., 2004). Notably, TFEB binds to the CLEAR element (TCACGTGA) in the promoters of lysosomal genes and orchestrates lysosome biogenesis and autophagy in order to promote cellular clearance pathways (Palmieri et al., 2011). We also observed that MITF binds to the promoter of TFEB and positively regulate its expression (Ballesteros et al., manuscript in preparation). Importantly, MITF and TFEB can heterodimerize and bind to the same E-box motif CACGTG through their bHLH domain (Steingrimsson et al., 2004). This suggests that there is a major overlap in their target selection which mediates cellular functions related to autophagy and pigmentation. Autophagy has a dual role in cancer development, one is to protect cells from mlaignancy by preventing accumulation of damaged organelles and proteins but the same mechanism is highly exploited in established tumours to overcome stressful condition (White, 2015). Therefore, both MITF and TFEB possibly play a dynamic role in regulating these processes in the course of melanoma progression. Furthermore, the melanosome is a lysosome related organelle. Therefore, TFEB might participate in the biogenesis and function of melanosome, thus affecting the pigmentation processes. To investigate overlap between MITF and TFEB genome wide binding sites, we carried out ChIP-seq against *eGFP* tagged TFEB as ChIP grade antibodies against TFEB are not available.

ChIP-seq analysis and peak calling identified 4307 consensus binding sites shared between the two biological replicate ChIP-seq experiments (Figure 32C). In addition, motif analysis identified an E-box motif with flanking T/A for both individual replicate experiments (Figure 32A,B). Annotation analysis of the peaks to genes based on a 20 kb +/- distance from transcription start sites assigned 3446 genes to TFEB binding peaks in this data set.

A total of 1207 binding peaks affecting 1266 genes overlapped between MITF and TFEB (Figure 33A) (Figure 33C). Together, MITF and TFEB co-bound to 64 of 139 autophagy genes, including *LAMP1, GNS, MAP1LC3B* and *ATP6V1C1*. It is worth mentioning that MITF was bound to more autophagy genes (82/139) than TFEB (65/139) (Figure 33D). This indicates that MITF is no less important for the autophagy process than TFEB. Consistently, gene ontology analysis on the overlapping genes revealed that MITF and TFEB bound sites were enriched for genes involved in autophagy and pigmentation (Figure 33F).

Initially, TFEB was shown to be an essential regulator of placental vascularization (Steingrimsson et al., 1998), where *Tfeb* mutant placenta failed to develop vasculature and branch normally due to loss of expression of VEGF, an important modulator for vasculogenesis. Interestingly, we found

MITF and TFEB ChIPseq peaks at 40 kb upstream and 8kb downstream of the *VEGFA* promoter. Additionally, in MITF knock out cells and MITF^{low} tumours we observed induced expression of *VEGFA,* indicating that MITF represses *VEGFA*. However, we speculate that TFEB activates *VEGFA* expression in the placenta since loss of TFEB leads to loss of *VEGFA* expression in that tissue. Together, this indicates that MITF and TFEB can bind to the same gene but one can activate whereas the other can repress it, suggesting an inverse gene regulatory network between two closely related transcription factors.

In fact, analysing transcripts coexpressed with MITF and TFEB in melanoma tumours showed that transcripts that positively correlate with TFEB were negatively correlated with MITF and vice versa. This indicates that MITF and TFEB inversely affect their gene expression network (Figure 27C). From our RNA-seq data of MITF-KO cells, we observed that a significant number of genes increased in expression upon loss of MITF yet do not have MITF binding sites in or near their promoters. This suggests indirect regulation by other factors. TFEB would be a good candidate due to its expression in melanoma and its ability to bind the same DNA binding motif as MITF. Moreover, there are many genes strongly bound by MITF where MITF depletion has no effects on gene expression. This suggests again that TFEB and MITF may positively activate the same subset of genes and thus compenstate for the loss of each other, but also inversely regulate some genes.

Furthermore, the target selection of TFEB and MITF as a heterodimers will be interesting in terms of their inverse gene regulatory network. This is especially interesting in the process of autophagy response where TFEB is transcloated into the nucleus under stress conditions, whereas MITF is predominantly in the nucleus in melanocytes. Perhaps the increased availabilty of TFEB in the nucleus might alter target selection of MITF as they have the ability to form heterodimer. At the same time, we cannot exclude the possible cytoplasmic function of these two factors. We know TFEB is predominantly in the cytoplasm under normal condition, and there are portions of MITF also present in the cytoplasm. Therefore, transcriptional independent function of these two factors might play a role in melanoma development.

It will be important to validate our observation with expression analysis after TFEB knockdown, which will allow us to dissect direct and indirect target genes sensitive to TFEB levels. In addition, it will enable us to identify the

nature of this inverse correlation of MITF and TFEB to better study their co-operative effects in gene regulatory networks in melanoma cells.

While we observed extensive overlap in binding sites between MITF and TFEB there are still major non-overlaps in their binding sites. Differential binding analysis led to the identification of 6493 statistically significant bound sites that differed between the two factors (Figure 34B). Gene ontology analysis on genes associated with differentially bound sites revealed that MITF preferentially bound to genes relevant to neuronal development and axogenesis, whereas TFEB showed enrichment for genes involved in DNA metabolic process (Figure 34C).

Interestingly, among the most differentially bound sites, we found an MITF peak containing 99 (A/CANNTG/T) motifs in intron 2 of the *ISPD* gene. This gene is essential for maintaining extracellular matrix structure through glycosylation of α-dystroglycan (DAG1), a transmembrane protein which acts as a scaffold that links the ECM to the intracellular compartment of cells, thus promoting cell migration. In order to do this DAG1 has to be glycosylated by *ISPD*. Mutations in this gene lead to a defect in eye and brain development and is the main cause of congenital muscular dystrophies (Cirak et al., 2013; Clements et al., 2017). This suggests that MITF target selection is preferentially oriented to neuronal related genes as it has been already shown to play a pivotal role during early development of melanocyte differentiation.

Collectively, our data revealed co-activity or co-binding of MITF and TFEB to autophagy and pigmentation related genes. Therefore, the overlapping function of MITF and TFEB could be to activate expression of genes responsible for melanoma differentiation and cellular stress response. In addition to this, we found that they belong to inversely correlated gene expression networks in melanoma. Possibly, unique targets of TFEB might negatively regulate the expression of genes which forms distinct network with MITF. All together, this information will allow us to select important targets that are co-bound by them to perform functional studies to depict functional effect of binding events. Unique and overlapping targets of MITF and TFEB will allow us to dissect possible unique interaction network with other transcription factors in melanoma. By mapping the unique interactome of MITF and TFEB, we might understand broader biological significance of their target selection.

To summarize the second part of this thesis we proposed a model which describes genome wide overlaping and unique sites of MITF, IRF4 and TFEB (Figure 36). With our analysis, we reported MITF and TFEB shared binding to significant number of lysosomal and pigmentation genes. We identified novel

binding sites shared between MITF and IRF4 are enriched for pigmentation, immune, and autophagy related genes. Unique binding sites were also identified to dissect the possible independent transcriptional function of each factor. We found unique MITF binding peaks were pereferentially present in genes responsible for nervous system development, whereas TFEB showed exclusive binding to DNA metabolic processes. The IRF4 exclusive peaks were enriched for genes related to hematopoietic cell differentiation. In summary, identification of list of MITF, IRF4 and TFEB genome wide binding targets will allow us to study functional effect of such binding events and their contribution in melanoma biology. Furthermore, the transcriptional redundancy and uniqe function of these transcription factor will allow us to pinpoint cellular pathways goverened by each transcription factors. Furthermore, it will allow us to investigate interdependency between each of them, and how that might affect their target selection duing the course of melanoma progression. This work will therefore open many possible avenues of investigations into the role of IRF4, MITF and TFEB, and their target genes in melanoma. This thesis describes the initial characterization of IRF4 and TFEB binding in melanoma cells. Further characterization and experimental work is needed to fully decipher the role of these transcription factors in melanoma.

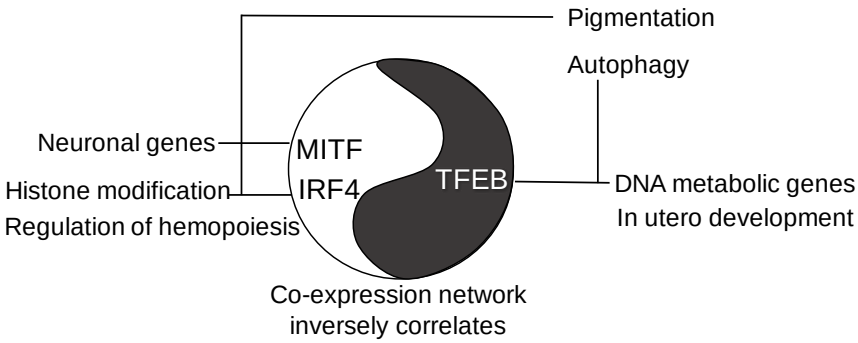

Figure 36. A model depicting relationship between MITF, IRF4 and TFEB and their target genes selection

References

Abdel-Malek, Z., Suzuki, I., Tada, A., Im, S., & Akcali, C. (1999). The melanocortin-1 receptor and human pigmentation. *Ann N Y Acad Sci, 885*, 117-133.

Adams, C. L., & Nelson, W. J. (1998). Cytomechanics of cadherin-mediated cell-cell adhesion. *Curr Opin Cell Biol, 10*(5), 572-577.

Adams, W. C., Chen, Y. H., Kratchmarov, R., Yen, B., Nish, S. A., Lin, W. W., Rothman, N. J., Luchsinger, L. L., Klein, U., Busslinger, M., Rathmell, J. C., Snoeck, H. W., & Reiner, S. L. (2016). Anabolism-Associated Mitochondrial Stasis Driving Lymphocyte Differentiation over Self-Renewal. *Cell Rep, 17*(12), 3142-3152. doi:10.1016/j.celrep.2016.11.065

Aksan, I., & Goding, C. R. (1998). Targeting the microphthalmia basic helix-loop-helix-leucine zipper transcription factor to a subset of E-box elements in vitro and in vivo. *Mol Cell Biol, 18*(12), 6930-6938.

Albino, A. P., Davis, B. M., & Nanus, D. M. (1991). Induction of Growth-Factor Rna Expression in Human-Malignant Melanoma - Markers of Transformation. *Cancer Research, 51*(18), 4815-4820.

Alexaki, V. I., Javelaud, D., Van Kempen, L. C., Mohammad, K. S., Dennler, S., Luciani, F., Hoek, K. S., Juarez, P., Goydos, J. S., Fournier, P. J., Sibon, C., Bertolotto, C., Verrecchia, F., Saule, S., Delmas, V., Ballotti, R., Larue, L., Saiag, P., Guise, T. A., & Mauviel, A. (2010). GLI2-mediated melanoma invasion and metastasis. *J Natl Cancer Inst, 102*(15), 1148-1159. doi:10.1093/jnci/djq257

Alizadeh, A. A., Eisen, M. B., Davis, R. E., Ma, C., Lossos, I. S., Rosenwald, A., Boldrick, J. C., Sabet, H., Tran, T., Yu, X., Powell, J. I., Yang, L., Marti, G. E., Moore, T., Hudson, J., Jr., Lu, L., Lewis, D. B., Tibshirani, R., Sherlock, G., Chan, W. C., Greiner, T. C., Weisenburger, D. D., Armitage, J. O., Warnke, R., Levy, R., Wilson, W., Grever, M. R., Byrd, J. C., Botstein, D., Brown, P. O., & Staudt, L. M. (2000). Distinct types of diffuse large B-cell lymphoma identified by gene expression profiling. *Nature, 403*(6769), 503-511. doi:10.1038/35000501

Alonso, S. R., Tracey, L., Ortiz, P., Perez-Gomez, B., Palacios, J., Pollan, M., Linares, J., Serrano, S., Saez-Castillo, A. I., Sanchez, L., Pajares, R., Sanchez-Aguilera, A., Artiga, M. J., Piris, M. A., & Rodriguez-Peralto, J. L. (2007). A high-throughput study in melanoma identifies epithelial-mesenchymal transition as a major determinant of metastasis. *Cancer Res, 67*(7), 3450-3460. doi:10.1158/0008-5472.CAN-06-3481

Amae, S., Fuse, N., Yasumoto, K., Sato, S., Yajima, I., Yamamoto, H., Udono, T., Durlu, Y. K., Tamai, M., Takahashi, K., & Shibahara, S. (1998). Identification of a novel isoform of microphthalmia-associated transcription factor that is enriched in retinal pigment epithelium. *Biochem Biophys Res Commun, 247*(3), 710-715.

Amiel, J., Watkin, P. M., Tassabehji, M., Read, A. P., & Winter, R. M. (1998). Mutation of the MITF gene in albinism-deafness syndrome (Tietz syndrome). *Clin Dysmorphol, 7*(1), 17-20.

Amin, M. B., Amin, M. B., Tamboli, P., Javidan, J., Stricker, H., Venturina, M. D., Deshpande, A., & Menon, M. (2002). Prognostic impact of histologic Subtyping of adult renal epithelial neoplasms - An experience of 405 cases. *American Journal of Surgical Pathology, 26*(3), 281-291. doi:Doi 10.1097/00000478-200203000-00001

Aponte, J. L., Chiano, M. N., Yerges-Armstrong, L. M., Hinds, D. A., Tian, C., Gupta, A., Guo, C., Fraser, D. J., Freudenberg, J. M., Rajpal, D. K., Ehm, M. G., & Waterworth, D. M. (2018). Assessment of rosacea symptom severity by genome-wide association study and expression analysis highlights immuno-inflammatory and skin pigmentation genes. *Hum Mol Genet*. doi:10.1093/hmg/ddy184

Arozarena, I., Bischof, H., Gilby, D., Belloni, B., Dummer, R., & Wellbrock, C. (2011). In melanoma, beta-catenin is a suppressor of invasion. *Oncogene, 30*(45), 4531-4543. doi:10.1038/onc.2011.162

Barrett, J. H., Iles, M. M., Harland, M., Taylor, J. C., Aitken, J. F., Andresen, P. A., Akslen, L. A., Armstrong, B. K., Avril, M. F., Azizi, E., Bakker, B., Bergman, W., Bianchi-Scarra, G., Bressac-de Paillerets, B., Calista, D., Cannon-Albright, L. A., Corda, E., Cust, A. E., Debniak, T., Duffy, D., Dunning, A. M., Easton, D. F., Friedman, E., Galan, P., Ghiorzo, P., Giles, G. G., Hansson, J., Hocevar, M., Hoiom, V., Hopper, J. L., Ingvar, C., Janssen, B., Jenkins, M. A., Jonsson, G., Kefford, R. F., Landi, G., Landi, M. T., Lang, J., Lubinski, J., Mackie, R., Malvehy, J., Martin, N. G., Molven, A., Montgomery, G. W., van Nieuwpoort, F. A., Novakovic, S., Olsson, H., Pastorino, L., Puig, S., Puig-Butille, J. A., Randerson-Moor, J., Snowden, H., Tuominen, R., Van Belle, P., van der Stoep, N., Whiteman, D. C., Zelenika, D., Han, J., Fang, S., Lee, J. E., Wei, Q., Lathrop, G. M., Gillanders, E. M., Brown, K. M., Goldstein, A. M., Kanetsky, P. A., Mann, G. J., Macgregor, S., Elder, D. E., Amos, C. I., Hayward, N. K., Gruis, N. A., Demenais, F., Bishop, J. A., Bishop, D. T., & Geno, M. E. L. C. (2011). Genome-wide association study identifies three new melanoma susceptibility loci. *Nat Genet, 43*(11), 1108-1113. doi:10.1038/ng.959

Batlle, E., Sancho, E., Franci, C., Dominguez, D., Monfar, M., Baulida, J., & Garcia De Herreros, A. (2000). The transcription factor snail is a repressor of E-cadherin gene expression in epithelial tumour cells. *Nat Cell Biol, 2*(2), 84-89. doi:10.1038/35000034

Behrens, J. (1993). The role of cell adhesion molecules in cancer invasion and metastasis. *Breast Cancer Res Treat, 24*(3), 175-184.

Bennett, D. C. (2003). Human melanocyte senescence and melanoma susceptibility genes. *Oncogene, 22*(20), 3063-3069. doi:10.1038/sj.onc.1206446

Bentley, N. J., Eisen, T., & Goding, C. R. (1994). Melanocyte-specific expression of the human tyrosinase promoter: activation by the microphthalmia gene product and role of the initiator. *Mol Cell Biol, 14*(12), 7996-8006.

Bertolotto, C., Busca, R., Abbe, P., Bille, K., Aberdam, E., Ortonne, J. P., & Ballotti, R. (1998). Different cis-acting elements are involved in the regulation of TRP1 and TRP2 promoter activities by cyclic AMP: pivotal role of M boxes (GTCATGTGCT) and of microphthalmia. *Mol Cell Biol, 18*(2), 694-702.

Bertolotto, C., Lesueur, F., Giuliano, S., Strub, T., de Lichy, M., Bille, K., Dessen, P., d'Hayer, B., Mohamdi, H., Remenieras, A., Maubec, E., de la Fouchardiere, A., Molinie, V., Vabres, P., Dalle, S., Poulalhon, N., Martin-Denavit, T., Thomas, L., Andry-Benzaquen, P., Dupin, N., Boitier, F., Rossi, A., Perrot, J. L., Labeille, B., Robert, C., Escudier, B., Caron, O., Brugieres, L., Saule, S., Gardie, B., Gad, S., Richard, S., Couturier, J., Teh, B. T., Ghiorzo, P., Pastorino, L., Puig, S., Badenas, C., Olsson, H., Ingvar, C., Rouleau, E., Lidereau, R., Bahadoran, P., Vielh, P., Corda, E., Blanche, H., Zelenika, D., Galan, P., French Familial Melanoma Study, G., Aubin, F., Bachollet, B., Becuwe, C., Berthet, P., Bignon, Y. J., Bonadona, V., Bonafe, J. L., Bonnet-Dupeyron, M. N., Cambazard, F., Chevrant-Breton, J., Coupier, I., Dalac, S., Demange, L., d'Incan, M., Dugast, C., Faivre, L., Vincent-Fetita, L., Gauthier-Villars, M., Gilbert, B., Grange, F., Grob, J. J., Humbert, P., Janin, N., Joly, P., Kerob, D., Lasset, C., Leroux, D., Levang, J., Limacher, J. M., Livideanu, C., Longy, M., Lortholary, A., Stoppa-Lyonnet, D., Mansard, S., Mansuy, L., Marrou, K., Mateus, C., Maugard, C., Meyer, N., Nogues, C., Souteyrand, P., Venat-Bouvet, L., Zattara, H., Chaudru, V., Lenoir, G. M., Lathrop, M., Davidson, I., Avril, M. F., Demenais, F., Ballotti, R., & Bressac-de Paillerets, B. (2011). A SUMOylation-defective MITF germline mutation predisposes to melanoma and renal carcinoma. *Nature, 480*(7375), 94-98. doi:10.1038/nature10539

Blazer, L. L., Lima-Fernandes, E., Gibson, E., Eram, M. S., Loppnau, P., Arrowsmith, C. H., Schapira, M., & Vedadi, M. (2016). PR Domain-containing Protein 7 (PRDM7) Is a Histone 3 Lysine 4 Trimethyltransferase. *J Biol Chem, 291*(26), 13509-13519. doi:10.1074/jbc.M116.721472

Bliss, J. M., Ford, D., Swerdlow, A. J., Armstrong, B. K., Cristofolini, M., Elwood, J. M., Green, A., Holly, E. A., Mack, T., MacKie, R. M., & et al. (1995). Risk of cutaneous melanoma associated with pigmentation characteristics and freckling: systematic overview of 10 case-control studies. The International Melanoma Analysis Group (IMAGE). *Int J Cancer, 62*(4), 367-376.

Boiko, A. D., Razorenova, O. V., van de Rijn, M., Swetter, S. M., Johnson, D. L., Ly, D. P., Butler, P. D., Yang, G. P., Joshua, B., Kaplan, M. J., Longaker, M. T., & Weissman, I. L. (2010). Human melanoma-initiating cells express neural crest nerve growth factor receptor CD271. *Nature, 466*(7302), 133-137. doi:10.1038/nature09161

Bollag, G., Clapp, D. W., Shih, S., Adler, F., Zhang, Y. Y., Thompson, P., Lange, B. J., Freedman, M. H., McCormick, F., Jacks, T., & Shannon, K. (1996). Loss of NF1 results in activation of the Ras signaling pathway and leads to aberrant growth in haematopoietic cells. *Nat Genet, 12*(2), 144-148. doi:10.1038/ng0296-144

Bollig, N., Brustle, A., Kellner, K., Ackermann, W., Abass, E., Raifer, H., Camara, B., Brendel, C., Giel, G., Bothur, E., Huber, M., Paul, C., Elli, A., Kroczek, R. A., Nurieva, R., Dong, C., Jacob, R., Mak, T. W., & Lohoff, M. (2012). Transcription factor IRF4 determines germinal center formation through follicular T-helper cell differentiation. *Proc Natl Acad Sci U S A, 109*(22), 8664-8669. doi:10.1073/pnas.1205834109

Bondurand, N., Pingault, V., Goerich, D. E., Lemort, N., Sock, E., Le Caignec, C., Wegner, M., & Goossens, M. (2000). Interaction among SOX10, PAX3 and MITF, three genes altered in Waardenburg syndrome. *Hum Mol Genet, 9*(13), 1907-1917.

Bonet, C., Luciani, F., Ottavi, J. F., Leclerc, J., Jouenne, F. M., Boncompagni, M., Bille, K., Hofman, V., Bossis, G., de Donatis, G. M., Strub, T., Cheli, Y., Ohanna, M., Luciano, F., Marchetti, S., Rocchi, S., Birling, M. C., Avril, M. F., Poulalhon, N., Luc, T., & Bertolotto, C. (2017). Deciphering the Role of Oncogenic MITFE318K in Senescence Delay and Melanoma Progression. *Jnci-Journal of the National Cancer Institute, 109*(8). doi:ARTN djw34010.1093/jnci/djw340

Brabletz, T., Jung, A., Reu, S., Porzner, M., Hlubek, F., Kunz-Schughart, L. A., Knuechel, R., & Kirchner, T. (2001). Variable beta-catenin expression in colorectal cancers indicates tumor progression driven by the tumor environment. *Proc Natl Acad Sci U S A, 98*(18), 10356-10361. doi:10.1073/pnas.171610498

Brakebusch, C., & Fassler, R. (2003). The integrin-actin connection, an eternal love affair. *EMBO J, 22*(10), 2324-2333. doi:10.1093/emboj/cdg245

Brandt, D. T., Marion, S., Griffiths, G., Watanabe, T., Kaibuchi, K., & Grosse, R. (2007). Dia1 and IQGAP1 interact in cell migration and phagocytic cup formation. *J Cell Biol, 178*(2), 193-200. doi:10.1083/jcb.200612071

Brass, A. L., Kehrli, E., Eisenbeis, C. F., Storb, U., & Singh, H. (1996). Pip, a lymphoid-restricted IRF, contains a regulatory domain that is important for autoinhibition and ternary complex formation with the Ets factor PU.1. *Genes Dev, 10*(18), 2335-2347.

Brass, A. L., Zhu, A. Q., & Singh, H. (1999). Assembly requirements of PU.1-Pip (IRF-4) activator complexes: inhibiting function in vivo using fused dimers. *EMBO J, 18*(4), 977-991. doi:10.1093/emboj/18.4.977

Bray, N. L., Pimentel, H., Melsted, P., & Pachter, L. (2016). Near-optimal probabilistic RNA-seq quantification. *Nat Biotechnol, 34*(5), 525-527. doi:10.1038/nbt.3519

Brown, M. C., Curtis, M. S., & Turner, C. E. (1998). Paxillin LD motifs may define a new family of protein recognition domains. *Nat Struct Biol, 5*(8), 677-678. doi:10.1038/1370

Budd, P. S., & Jackson, I. J. (1995). Structure of the Mouse Tyrosinase-Related Protein-2 Dopachrome Tautomerase (Tyrp2/Dct) Gene and Sequence of 2 Novel Slaty Alleles. *Genomics, 29*(1), 35-43. doi:DOI 10.1006/geno.1995.1212

Bulliard, J. L., Cox, B., & Elwood, J. M. (1994). Latitude Gradients in Melanoma Incidence and Mortality in the Non-Maori Population of New-Zealand. *Cancer Causes & Control, 5*(3), 234-240. doi:Doi 10.1007/Bf01830242

Calalb, M. B., Polte, T. R., & Hanks, S. K. (1995). Tyrosine phosphorylation of focal adhesion kinase at sites in the catalytic domain regulates kinase activity: a role for Src family kinases. *Mol Cell Biol, 15*(2), 954-963.

Cance, W. G., Harris, J. E., Iacocca, M. V., Roche, E., Yang, X., Chang, J., Simkins, S., & Xu, L. (2000). Immunohistochemical analyses of focal adhesion kinase expression in benign and malignant human breast and colon tissues: correlation with preinvasive and invasive phenotypes. *Clin Cancer Res, 6*(6), 2417-2423.

Cancer Genome Atlas, N. (2015). Genomic Classification of Cutaneous Melanoma. *Cell, 161*(7), 1681-1696. doi:10.1016/j.cell.2015.05.044

Cannuyer, J., Van Tongelen, A., Loriot, A., & De Smet, C. (2015). A gene expression signature identifying transient DNMT1 depletion as a causal factor of cancer-germline gene activation in melanoma. *Clin Epigenetics, 7*, 114. doi:10.1186/s13148-015-0147-4

Caramel, J., Papadogeorgakis, E., Hill, L., Browne, G. J., Richard, G., Wierinckx, A., Saldanha, G., Osborne, J., Hutchinson, P., Tse, G., Lachuer, J., Puisieux, A., Pringle, J. H., Ansieau, S., & Tulchinsky, E. (2013). A switch in the expression of embryonic EMT-inducers drives the development of malignant melanoma. *Cancer Cell, 24*(4), 466-480. doi:10.1016/j.ccr.2013.08.018

Carlsson, S. R., Roth, J., Piller, F., & Fukuda, M. (1988). Isolation and Characterization of Human Lysosomal Membrane-Glycoproteins, H-Lamp-1 and H-Lamp-2 - Major Sialoglycoproteins Carrying Polylactosaminoglycan. *Journal of Biological Chemistry, 263*(35), 18911-18919.

Carr, C. S., & Sharp, P. A. (1990). A helix-loop-helix protein related to the immunoglobulin E box-binding proteins. *Mol Cell Biol, 10*(8), 4384-4388.

Carrano, A. C., Eytan, E., Hershko, A., & Pagano, M. (1999). SKP2 is required for ubiquitin-mediated degradation of the CDK inhibitor p27. *Nature Cell Biology, 1*(4), 193-199. doi:Doi 10.1038/12013

Carreira, S., Goodall, J., Aksan, I., La Rocca, S. A., Galibert, M. D., Denat, L., Larue, L., & Goding, C. R. (2005). Mitf cooperates with Rb1 and activates p21Cip1 expression to regulate cell cycle progression. *Nature, 433*(7027), 764-769. doi:10.1038/nature03269

Carreira, S., Goodall, J., Denat, L., Rodriguez, M., Nuciforo, P., Hoek, K. S., Testori, A., Larue, L., & Goding, C. R. (2006). Mitf regulation of Dia1 controls melanoma proliferation and invasiveness. *Genes Dev, 20*(24), 3426-3439. doi:10.1101/gad.406406

Ceol, C. J., Houvras, Y., Jane-Valbuena, J., Bilodeau, S., Orlando, D. A., Battisti, V., Fritsch, L., Lin, W. M., Hollmann, T. J., Ferre, F., Bourque, C., Burke, C. J., Turner, L., Uong, A., Johnson, L. A., Beroukhim, R., Mermel, C. H., Loda, M., Ait-Si-Ali, S., Garraway, L. A., Young, R. A., & Zon, L. I. (2011). The histone methyltransferase SETDB1 is recurrently amplified in melanoma and accelerates its onset. *Nature, 471*(7339), 513-517. doi:10.1038/nature09806

Chahal, H. S., Lin, Y., Ransohoff, K. J., Hinds, D. A., Wu, W., Dai, H. J., Qureshi, A. A., Li, W. Q., Kraft, P., Tang, J. Y., Han, J., & Sarin, K. Y. (2016). Genome-wide association study identifies novel susceptibility loci for cutaneous squamous cell carcinoma. *Nat Commun, 7*, 12048. doi:10.1038/ncomms12048

Chang, A. E., Karnell, L. H., & Menck, H. R. (1998). The National Cancer Data Base report on cutaneous and noncutaneous melanoma: a summary of 84,836 cases from the past decade. The American College of Surgeons Commission on Cancer and the American Cancer Society. *Cancer, 83*(8), 1664-1678.

Chang, C. C., Lorek, J., Sabath, D. E., Li, Y., Chitambar, C. R., Logan, B., Kampalath, B., & Cleveland, R. P. (2002). Expression of MUM1/IRF4 correlates with clinical outcome in patients with B-cell chronic lymphocytic leukemia. *Blood, 100*(13), 4671-4675. doi:10.1182/blood-2002-01-0104

Chang, Y. M., Newton-Bishop, J. A., Bishop, D. T., Armstrong, B. K., Bataille, V., Bergman, W., Berwick, M., Bracci, P. M., Elwood, J. M., Ernstoff, M. S., Green, A. C., Gruis, N. A., Holly, E. A., Ingvar, C., Kanetsky, P. A., Karagas, M. R., Le Marchand, L., Mackie, R. M., Olsson, H., Osterlind, A., Rebbeck, T. R., Reich, K., Sasieni, P., Siskind, V., Swerdlow, A. J., Titus-Ernstoff, L., Zens, M. S., Ziegler, A., & Barrett, J. H. (2009). A pooled analysis of melanocytic nevus phenotype and the risk of cutaneous melanoma at different latitudes. *Int J Cancer, 124*(2), 420-428. doi:10.1002/ijc.23869

Cheli, Y., Giuliano, S., Botton, T., Rocchi, S., Hofman, V., Hofman, P., Bahadoran, P., Bertolotto, C., & Ballotti, R. (2011). Mitf is the key molecular switch between mouse or human melanoma initiating cells and their differentiated progeny. *Oncogene, 30*(20), 2307-2318. doi:10.1038/onc.2010.598

Cheli, Y., Giuliano, S., Fenouille, N., Allegra, M., Hofman, V., Hofman, P., Bahadoran, P., Lacour, J. P., Tartare-Deckert, S., Bertolotto, C., & Ballotti, R. (2012). Hypoxia and MITF control metastatic behaviour in mouse and human melanoma cells. *Oncogene, 31*(19), 2461-2470. doi:10.1038/onc.2011.425

Chin, L. (2003). The genetics of malignant melanoma: Lessons from mouse and man. *Nature Reviews Cancer, 3*(8), 559-570. doi:10.1038/nrc1145

Chin, L., Pomerantz, J., Polsky, D., Jacobson, M., Cohen, C., Cordon-Cardo, C., Horner, J. W., 2nd, & DePinho, R. A. (1997). Cooperative effects of INK4a and ras in melanoma susceptibility in vivo. *Genes Dev, 11*(21), 2822-2834.

Cirak, S., Foley, A. R., Herrmann, R., Willer, T., Yau, S., Stevens, E., Torelli, S., Brodd, L., Kamynina, A., Vondracek, P., Roper, H., Longman, C., Korinthenberg, R., Marrosu, G., Nurnberg, P., Consortium, U. K., Michele, D. E., Plagnol, V., Hurles, M., Moore, S. A., Sewry, C. A., Campbell, K. P., Voit, T., & Muntoni, F. (2013). ISPD gene mutations are a common cause of congenital and limb-girdle muscular dystrophies. *Brain, 136*(Pt 1), 269-281. doi:10.1093/brain/aws312

Clements, R., Turk, R., Campbell, K. P., & Wright, K. M. (2017). Dystroglycan Maintains Inner Limiting Membrane Integrity to Coordinate Retinal Development. *J Neurosci, 37*(35), 8559-8574. doi:10.1523/JNEUROSCI.0946-17.2017

Colaprico, A., Silva, T. C., Olsen, C., Garofano, L., Cava, C., Garolini, D., Sabedot, T. S., Malta, T. M., Pagnotta, S. M., Castiglioni, I., Ceccarelli, M., Bontempi, G., & Noushmehr, H. (2016). TCGAbiolinks: an R/Bioconductor package for integrative analysis of TCGA data. *Nucleic Acids Res, 44*(8), e71. doi:10.1093/nar/gkv1507

Cory, G. O., & Ridley, A. J. (2002). Cell motility: braking WAVEs. *Nature, 418*(6899), 732-733. doi:10.1038/418732a

Coxon, F. P., & Taylor, A. (2008). Vesicular trafficking in osteoclasts. *Seminars in Cell & Developmental Biology, 19*(5), 424-433. doi:10.1016/j.semcdb.2008.08.004

Cretney, E., Xin, A., Shi, W., Minnich, M., Masson, F., Miasari, M., Belz, G. T., Smyth, G. K., Busslinger, M., Nutt, S. L., & Kallies, A. (2011). The transcription factors Blimp-1 and IRF4 jointly control the differentiation and function of effector regulatory T cells. *Nat Immunol, 12*(4), 304-311. doi:10.1038/ni.2006

Cui, R. T., Widlund, H. R., Feige, E., Lin, J. Y., Wilensky, D. L., Igras, V. E., D'Orazio, J., Fung, C. Y., Schanbacher, C. F., Granter, S. R., & Fisher, D. E. (2007). Central role of p53 in the suntan response and pathologic hyperpigmentation. *Cell, 128*(5), 853-864. doi:10.1016/j.cell.2006.12.045

Davies, H., Bignell, G. R., Cox, C., Stephens, P., Edkins, S., Clegg, S., Teague, J., Woffendin, H., Garnett, M. J., Bottomley, W., Davis, N., Dicks, E., Ewing, R., Floyd, Y., Gray, K., Hall, S., Hawes, R., Hughes, J., Kosmidou, V., Menzies, A., Mould, C., Parker, A., Stevens, C., Watt, S., Hooper, S., Wilson, R., Jayatilake, H., Gusterson, B. A., Cooper, C., Shipley, J., Hargrave, D., Pritchard-Jones, K., Maitland, N., Chenevix-Trench, G., Riggins, G. J., Bigner, D. D., Palmieri, G., Cossu, A., Flanagan, A., Nicholson, A., Ho, J. W., Leung, S. Y., Yuen, S. T., Weber, B. L., Seigler, H. F., Darrow, T. L., Paterson, H., Marais, R., Marshall, C. J., Wooster, R., Stratton, M. R., & Futreal, P. A. (2002). Mutations of the BRAF gene in human cancer. *Nature, 417*(6892), 949-954. doi:10.1038/nature00766

Davis, I. J., Hsi, B. L., Arroyo, J. D., Vargas, S. O., Yeh, Y. A., Motyckova, G., Valencia, P., Perez-Atayde, A. R., Argani, P., Ladanyi, M., Fletcher, J. A., & Fisher, D. E. (2003). Cloning of an Alpha-TFEB fusion in renal tumors harboring the t(6;11)(p21;q13) chromosome translocation. *Proc Natl Acad Sci U S A, 100*(10), 6051-6056. doi:10.1073/pnas.0931430100

Davis, R. E., Brown, K. D., Siebenlist, U., & Staudt, L. M. (2001). Constitutive nuclear factor kappaB activity is required for survival of activated B cell-like diffuse large B cell lymphoma cells. *J Exp Med, 194*(12), 1861-1874.

Deakin, N. O., & Turner, C. E. (2008). Paxillin comes of age. *J Cell Sci, 121*(Pt 15), 2435-2444. doi:10.1242/jcs.018044

Debacq-Chainiaux, F., Erusalimsky, J. D., Campisi, J., & Toussaint, O. (2009). Protocols to detect senescence-associated beta-galactosidase (SA-betagal) activity, a biomarker of senescent cells in culture and in vivo. *Nat Protoc, 4*(12), 1798-1806. doi:10.1038/nprot.2009.191

Denecker, G., Vandamme, N., Akay, O., Koludrovic, D., Taminau, J., Lemeire, K., Gheldof, A., De Craene, B., Van Gele, M., Brochez, L., Udupi, G. M., Rafferty, M., Balint, B., Gallagher, W. M., Ghanem, G., Huylebroeck, D., Haigh, J., van den Oord, J., Larue, L., Davidson, I., Marine, J. C., & Berx, G. (2014). Identification of a ZEB2-MITF-ZEB1 transcriptional network that controls melanogenesis and melanoma progression. *Cell Death Differ, 21*(8), 1250-1261. doi:10.1038/cdd.2014.44

Dennler, S., Andre, J., Alexaki, I., Li, A., Magnaldo, T., ten Dijke, P., Wang, X. J., Verrecchia, F., & Mauviel, A. (2007). Induction of sonic hedgehog mediators by transforming growth factor-beta: Smad3-dependent activation of Gli2 and Gli1 expression in vitro and in vivo. *Cancer Research, 67*(14), 6981-6986. doi:10.1158/0008-5472.Can-07-0491

Deretic, V., Saitoh, T., & Akira, S. (2013). Autophagy in infection, inflammation and immunity. *Nat Rev Immunol, 13*(10), 722-737. doi:10.1038/nri3532

Derynck, R., & Zhang, Y. E. (2003). Smad-dependent and Smad-independent pathways in TGF-beta family signalling. *Nature, 425*(6958), 577-584. doi:10.1038/nature02006

Devreotes, P., & Horwitz, A. R. (2015). Signaling networks that regulate cell migration. *Cold Spring Harb Perspect Biol, 7*(8), a005959. doi:10.1101/cshperspect.a005959

Di Bernardo, M. C., Crowther-Swanepoel, D., Broderick, P., Webb, E., Sellick, G., Wild, R., Sullivan, K., Vijayakrishnan, J., Wang, Y., Pittman, A. M., Sunter, N. J., Hall, A. G., Dyer, M. J., Matutes, E., Dearden, C., Mainou-Fowler, T., Jackson, G. H., Summerfield, G., Harris, R. J., Pettitt, A. R., Hillmen, P., Allsup, D. J., Bailey, J. R., Pratt, G., Pepper, C., Fegan, C., Allan, J. M., Catovsky, D., & Houlston, R. S. (2008). A genome-wide association study identifies six susceptibility loci for chronic lymphocytic leukemia. *Nat Genet, 40*(10), 1204-1210. doi:10.1038/ng.219

Dillon, S. C., Zhang, X., Trievel, R. C., & Cheng, X. (2005). The SET-domain protein superfamily: protein lysine methyltransferases. *Genome Biol, 6*(8), 227. doi:10.1186/gb-2005-6-8-227

Dissanayake, S. K., Olkhanud, P. B., O'Connell, M. P., Carter, A., French, A. D., Camilli, T. C., Emeche, C. D., Hewitt, K. J., Rosenthal, D. T., Leotlela, P. D., Wade, M. S., Yang, S. W., Brant, L., Nickoloff, B. J., Messina, J. L., Biragyn, A., Hoek, K. S., Taub, D. D., Longo, D. L., Sondak, V. K., Hewitt, S. M., & Weeraratna, A. T. (2008). Wnt5A regulates expression of tumor-associated antigens in melanoma via changes in signal transducers and activators of transcription 3 phosphorylation. *Cancer Res, 68*(24), 10205-10214. doi:10.1158/0008-5472.CAN-08-2149

Do, T. N., Ucisik-Akkaya, E., Davis, C. F., Morrison, B. A., & Dorak, M. T. (2010). An intronic polymorphism of IRF4 gene influences gene transcription in vitro and shows a risk association with childhood acute lymphoblastic leukemia in males. *Biochim Biophys Acta, 1802*(2), 292-300. doi:10.1016/j.bbadis.2009.10.015

Dorsky, R. I., Moon, R. T., & Raible, D. W. (1998). Control of neural crest cell fate by the Wnt signalling pathway. *Nature, 396*(6709), 370-373. doi:10.1038/24620

Downward, J. (2003). Targeting ras signalling pathways in cancer therapy. *Nature Reviews Cancer, 3*(1), 11-22. doi:10.1038/nrc969

Du, J., Miller, A. J., Widlund, H. R., Horstmann, M. A., Ramaswamy, S., & Fisher, D. E. (2003). MLANA/MART1 and SILV/PMEL17/GP100 are transcriptionally regulated by MITF in melanocytes and melanoma. *Am J Pathol, 163*(1), 333-343. doi:10.1016/S0002-9440(10)63657-7

Du, J., Widlund, H. R., Horstmann, M. A., Ramaswamy, S., Ross, K., Huber, W. E., Nishimura, E. K., Golub, T. R., & Fisher, D. E. (2004). Critical role of CDK2 for melanoma growth linked to its melanocyte-specific transcriptional regulation by MITF. *Cancer Cell, 6*(6), 565-576. doi:10.1016/j.ccr.2004.10.014

Ducy, P., Schinke, T., & Karsenty, G. (2000). The osteoblast: A sophisticated fibroblast under central surveillance. *Science, 289*(5484), 1501-1504. doi:DOI 10.1126/science.289.5484.1501

Duffey, D. C., Chen, Z., Dong, G., Ondrey, F. G., Wolf, J. S., Brown, K., Siebenlist, U., & Van Waes, C. (1999). Expression of a dominant-negative mutant inhibitor-kappa B alpha of nuclear factor-kappa B in human head and neck squamous cell carcinoma inhibits survival, proinflammatory cytokine expression, and tumor growth in vivo. *Cancer Research, 59*(14), 3468-3474.

Duffy, D. L., Iles, M. M., Glass, D., Zhu, G., Barrett, J. H., Hoiom, V., Zhao, Z. Z., Sturm, R. A., Soranzo, N., Hammond, C., Kvaskoff, M., Whiteman, D. C., Mangino, M., Hansson, J., Newton-Bishop, J. A., Bataille, V., Hayward, N. K., Martin, N. G., Bishop, D. T., Spector, T. D., Montgomery, G. W., & GenoMEL. (2010). IRF4 Variants Have Age-Specific Effects on Nevus Count and Predispose to Melanoma. *American Journal of Human Genetics, 87*(1), 6-16. doi:10.1016/j.ajhg.2010.05.017

Eastham, A. M., Spencer, H., Soncin, F., Ritson, S., Merry, C. L. R., Stern, P. L., & Ward, C. M. (2007). Epithelial-mesenchymal transition events during human embryonic stem cell differentiation. *Cancer Research, 67*(23), 11254-11262. doi:10.1158/0008-5472.Can-07-2253

Eisenbeis, C. F., Singh, H., & Storb, U. (1995). Pip, a novel IRF family member, is a lymphoid-specific, PU.1-dependent transcriptional activator. *Genes Dev, 9*(11), 1377-1387.

Ekholm, S. V., & Reed, S. I. (2000). Regulation of G(1) cyclin dependent kinases in the mammalian cell cycle. *Current Opinion in Cell Biology, 12*(6), 676-684. doi:Doi 10.1016/S0955-0674(00)00151-4

Eriksson, N., Macpherson, J. M., Tung, J. Y., Hon, L. S., Naughton, B., Saxonov, S., Avey, L., Wojcicki, A., Pe'er, I., & Mountain, J. (2010). Web-based, participant-driven studies yield novel genetic associations for common traits. *PLoS Genet, 6*(6), e1000993. doi:10.1371/journal.pgen.1000993

Etienne-Manneville, S., & Hall, A. (2002). Rho GTPases in cell biology. *Nature, 420*(6916), 629-635. doi:10.1038/nature01148

Fallahi-Sichani, M., Becker, V., Izar, B., Baker, G. J., Lin, J. R., Boswell, S. A., Shah, P., Rotem, A., Garraway, L. A., & Sorger, P. K. (2017). Adaptive resistance of melanoma cells to RAF inhibition via reversible induction of a slowly dividing de-differentiated state. *Molecular Systems Biology, 13*(1). doi:ARTN 905 10.15252/msb.20166796

Farnham, P. J. (2009). Insights from genomic profiling of transcription factors. *Nat Rev Genet, 10*(9), 605-616. doi:10.1038/nrg2636

Feige, E., Yokoyama, S., Levy, C., Khaled, M., Igras, V., Lin, R. J., Lee, S., Widlund, H. R., Granter, S. R., Kung, A. L., & Fisher, D. E. (2011). Hypoxia-induced transcriptional repression of the melanoma-associated oncogene MITF. *Proc Natl Acad Sci U S A, 108*(43), E924-933. doi:10.1073/pnas.1106351108

Feldman, A. L., Law, M., Remstein, E. D., Macon, W. R., Erickson, L. A., Grogg, K. L., Kurtin, P. J., & Dogan, A. (2009). Recurrent translocations involving the IRF4 oncogene locus in peripheral T-cell lymphomas. *Leukemia, 23*(3), 574-580. doi:10.1038/leu.2008.320

Ferlay, J., Shin, H. R., Bray, F., Forman, D., Mathers, C., & Parkin, D. M. (2010). Estimates of worldwide burden of cancer in 2008: GLOBOCAN 2008. *Int J Cancer, 127*(12), 2893-2917. doi:10.1002/ijc.25516

Fernandez-Borja, M., Janssen, L., Verwoerd, D., Hordijk, P., & Neefjes, J. (2005). RhoB regulates endosome transport by promoting actin assembly on endosomal membranes through Dia1. *J Cell Sci, 118*(Pt 12), 2661-2670. doi:10.1242/jcs.02384

Ferron, M., Settembre, C., Shimazu, J., Lacombe, J., Kato, S., Rawlings, D. J., Ballabio, A., & Karsenty, G. (2013). A RANKL-PKC beta-TFEB signaling cascade is necessary for lysosomal biogenesis in osteoclasts. *Genes & Development, 27*(8), 955-969. doi:10.1101/gad.213827.113

Finck, B. N., & Kelly, D. P. (2006). PGC-1 coactivators: inducible regulators of energy metabolism in health and disease. *J Clin Invest, 116*(3), 615-622. doi:10.1172/JCI27794

Fitzpatrick, T. B., & Breathnach, A. S. (1963). [the Epidermal Melanin Unit System]. *Dermatol Wochenschr, 147*, 481-489.

Fock, V., Gudmundsson, S. R., Gunnlaugsson, H. O., Stefansson, J. A., Ionasz, V., Schepsky, A., Viarigi, J., Reynisson, I. E., Pogenberg, V., Wilmanns, M., Ogmundsdottir, M. H., & Steingrimsson, E. (2018). Subcellular localization and stability of MITF are modulated by the bHLH-Zip domain. *Pigment Cell Melanoma Res*. doi:10.1111/pcmr.12721

Fogh, J., Fogh, J. M., & Orfeo, T. (1977). One hundred and twenty-seven cultured human tumor cell lines producing tumors in nude mice. *J Natl Cancer Inst, 59*(1), 221-226.

Forbes, S. A., Bhamra, G., Bamford, S., Dawson, E., Kok, C., Clements, J., Menzies, A., Teague, J. W., Futreal, P. A., & Stratton, M. R. (2008). The Catalogue of Somatic Mutations in Cancer (COSMIC). *Curr Protoc Hum Genet, Chapter 10*, Unit 10 11. doi:10.1002/0471142905.hg1011s57

Fuhs, S. R., & Insel, P. A. (2011). Caveolin-3 Undergoes SUMOylation by the SUMO E3 Ligase PIASy SUMOYLATION AFFECTS G-PROTEIN-COUPLED RECEPTOR DESENSITIZATION. *Journal of Biological Chemistry, 286*(17), 14830-14841. doi:10.1074/jbc.M110.214270

Fumasoni, I., Meani, N., Rambaldi, D., Scafetta, G., Alcalay, M., & Ciccarelli, F. D. (2007). Family expansion and gene rearrangements contributed to the functional specialization of PRDM genes in vertebrates. *BMC Evol Biol, 7*, 187. doi:10.1186/1471-2148-7-187

Fuse, N., Yasumoto, K., Takeda, K., Amae, S., Yoshizawa, M., Udono, T., Takahashi, K., Tamai, M., Tomita, Y., Tachibana, M., & Shibahara, S. (1999). Molecular cloning of cDNA encoding a novel microphthalmia-associated transcription factor isoform with a distinct amino-terminus. *J Biochem, 126*(6), 1043-1051.

Galibert, M. D., Yavuzer, U., Dexter, T. J., & Goding, C. R. (1999). Pax3 and regulation of the melanocyte-specific tyrosinase-related protein-1 promoter. *J Biol Chem, 274*(38), 26894-26900.

Gao, J. J., Aksoy, B. A., Dogrusoz, U., Dresdner, G., Gross, B., Sumer, S. O., Sun, Y. C., Jacobsen, A., Sinha, R., Larsson, E., Cerami, E., Sander, C., & Schultz, N. (2013). Integrative Analysis of Complex Cancer Genomics and Clinical Profiles Using the cBioPortal. *Science Signaling, 6*(269). doi:ARTN pl1 DOI 10.1126/scisignal.2004088

Garraway, L. A., Widlund, H. R., Rubin, M. A., Getz, G., Berger, A. J., Ramaswamy, S., Beroukhim, R., Milner, D. A., Granter, S. R., Du, J., Lee, C., Wagner, S. N., Li, C., Golub, T. R., Rimm, D. L., Meyerson, M. L., Fisher, D. E., & Sellers, W. R. (2005). Integrative genomic analyses identify MITF as a lineage survival oncogene amplified in malignant melanoma. *Nature, 436*(7047), 117-122. doi:10.1038/nature03664

Gaudet, F., Hodgson, J. G., Eden, A., Jackson-Grusby, L., Dausman, J., Gray, J. W., Leonhardt, H., & Jaenisch, R. (2003). Induction of tumors in mice by genomic hypomethylation. *Science, 300*(5618), 489-492. doi:10.1126/science.1083558

Geiger, B., Bershadsky, A., Pankov, R., & Yamada, K. M. (2001). Transmembrane crosstalk between the extracellular matrix--cytoskeleton crosstalk. *Nat Rev Mol Cell Biol, 2*(11), 793-805. doi:10.1038/35099066

George, A., Zand, D. J., Hufnagel, R. B., Sharma, R., Sergeev, Y. V., Legare, J. M., Rice, G. M., Scott Schwoerer, J. A., Rius, M., Tetri, L., Gamm, D. M., Bharti, K., & Brooks, B. P. (2016). Biallelic Mutations in MITF Cause Coloboma, Osteopetrosis, Microphthalmia, Macrocephaly, Albinism, and Deafness. *Am J Hum Genet, 99*(6), 1388-1394. doi:10.1016/j.ajhg.2016.11.004

Giancotti, F. G., & Ruoslahti, E. (1999). Integrin signaling. *Science, 285*(5430), 1028-1032.

Gibbs, D. C., Ward, S. V., Orlow, I., Cadby, G., Kanetsky, P. A., Luo, L., Busam, K. J., Kricker, A., Armstrong, B. K., Cust, A. E., Anton-Culver, H., Gallagher, R. P., Zanetti, R., Rosso, S., Sacchetto, L., Ollila, D. W., Begg, C. B., Berwick, M., Thomas, N. E., & Group, G. E. M. S. (2017). Functional melanoma-risk variant IRF4 rs12203592 associated with Breslow thickness: a pooled international study of primary melanomas. *Br J Dermatol, 177*(5), e180-e182. doi:10.1111/bjd.15784

Girault, J. A., Labesse, G., Mornon, J. P., & Callebaut, I. (1999). The N-termini of FAK and JAKs contain divergent band 4.1 domains. *Trends Biochem Sci, 24*(2), 54-57.

Giuliano, S., Cheli, Y., Ohanna, M., Bonet, C., Beuret, L., Bille, K., Loubat, A., Hofman, V., Hofman, P., Ponzio, G., Bahadoran, P., Ballotti, R., & Bertolotto, C. (2010). Microphthalmia-associated transcription factor controls the DNA damage response and a lineage-specific senescence program in melanomas. *Cancer Res, 70*(9), 3813-3822. doi:10.1158/0008-5472.CAN-09-2913

Goding, C. R. (2011). Commentary. A picture of Mitf in melanoma immortality. *Oncogene, 30*(20), 2304-2306. doi:10.1038/onc.2010.641

Goley, E. D., & Welch, M. D. (2006). The ARP2/3 complex: an actin nucleator comes of age. *Nat Rev Mol Cell Biol, 7*(10), 713-726. doi:10.1038/nrm2026

Gonzalez, D. M., & Medici, D. (2014). Signaling mechanisms of the epithelial-mesenchymal transition. *Sci Signal, 7*(344), re8. doi:10.1126/scisignal.2005189

Goodall, J., Carreira, S., Denat, L., Kobi, D., Davidson, I., Nuciforo, P., Sturm, R. A., Larue, L., & Goding, C. R. (2008). Brn-2 represses microphthalmia-associated transcription factor expression and marks a distinct subpopulation of microphthalmia-associated transcription factor-negative melanoma cells. *Cancer Res, 68*(19), 7788-7794. doi:10.1158/0008-5472.CAN-08-1053

Goodall, J., Wellbrock, C., Dexter, T. J., Roberts, K., Marais, R., & Goding, C. R. (2004). The Brn-2 transcription factor links activated BRAF to melanoma proliferation. *Mol Cell Biol, 24*(7), 2923-2931.

Goulding, M. D., Chalepakis, G., Deutsch, U., Erselius, J. R., & Gruss, P. (1991). Pax-3, a novel murine DNA binding protein expressed during early neurogenesis. *EMBO J, 10*(5), 1135-1147.

Goulimari, P., Kitzing, T. M., Knieling, H., Brandt, D. T., Offermanns, S., & Grosse, R. (2005). Galpha12/13 is essential for directed cell migration and localized Rho-Dia1 function. *J Biol Chem, 280*(51), 42242-42251. doi:10.1074/jbc.M508690200

Grill, C., Bergsteinsdottir, K., Ogmundsdottir, M. H., Pogenberg, V., Schepsky, A., Wilmanns, M., Pingault, V., & Steingrimsson, E. (2013). MITF mutations associated with pigment deficiency syndromes and melanoma have different effects on protein function. *Human Molecular Genetics, 22*(21), 4357-4367. doi:10.1093/hmg/ddt285

Grossman, A., Mittrucker, H. W., Nicholl, J., Suzuki, A., Chung, S., Antonio, L., Suggs, S., Sutherland, G. R., Siderovski, D. P., & Mak, T. W. (1996). Cloning of human lymphocyte-specific interferon regulatory factor (hLSIRF/hIRF4) and mapping of the gene to 6p23-p25. *Genomics, 37*(2), 229-233. doi:10.1006/geno.1996.0547

Guan, J. L., Trevithick, J. E., & Hynes, R. O. (1991). Fibronectin/integrin interaction induces tyrosine phosphorylation of a 120-kDa protein. *Cell Regul, 2*(11), 951-964. doi:10.1091/mbc.2.11.951

Gudjohnsen, S. A. H., Atacho, D. A. M., Gesbert, F., Raposo, G., Hurbain, I., Larue, L., Steingrimsson, E., & Petersen, P. H. (2015). Meningeal Melanocytes in the Mouse: Distribution and Dependence on Mitf. *Frontiers in Neuroanatomy, 9*. doi:ARTN 149 10.3389/fnana.2015.00149

Gumbiner, B. M. (1996). Cell adhesion: the molecular basis of tissue architecture and morphogenesis. *Cell, 84*(3), 345-357.

Gupta, P. B., Kuperwasser, C., Brunet, J. P., Ramaswamy, S., Kuo, W. L., Gray, J. W., Naber, S. P., & Weinberg, R. A. (2005). The melanocyte differentiation program predisposes to metastasis after neoplastic transformation. *Nat Genet, 37*(10), 1047-1054. doi:10.1038/ng1634

Halaban, R., Krauthammer, M., Pelizzola, M., Cheng, E., Kovacs, D., Sznol, M., Ariyan, S., Narayan, D., Bacchiocchi, A., Molinaro, A., Kluger, Y., Deng, M., Tran, N., Zhang, W., Picardo, M., & Enghild, J. J. (2009). Integrative analysis of epigenetic modulation in melanoma cell response to decitabine: clinical implications. *PLoS One, 4*(2), e4563. doi:10.1371/journal.pone.0004563

Han, J., Kraft, P., Nan, H., Guo, Q., Chen, C., Qureshi, A., Hankinson, S. E., Hu, F. B., Duffy, D. L., Zhao, Z. Z., Martin, N. G., Montgomery, G. W., Hayward, N. K., Thomas, G., Hoover, R. N., Chanock, S., & Hunter, D. J. (2008). A genome-wide association study identifies novel alleles associated with hair color and skin pigmentation. *PLoS Genet, 4*(5), e1000074. doi:10.1371/journal.pgen.1000074

Han, J., Qureshi, A. A., Nan, H., Zhang, J., Song, Y., Guo, Q., & Hunter, D. J. (2011). A germline variant in the interferon regulatory factor 4 gene as a novel skin cancer risk locus. *Cancer Res, 71*(5), 1533-1539. doi:10.1158/0008-5472.CAN-10-1818

Hanahan, D., & Weinberg, R. A. (2011). Hallmarks of cancer: the next generation. *Cell, 144*(5), 646-674. doi:10.1016/j.cell.2011.02.013

Hanks, S. K., Calalb, M. B., Harper, M. C., & Patel, S. K. (1992). Focal adhesion protein-tyrosine kinase phosphorylated in response to cell attachment to fibronectin. *Proc Natl Acad Sci U S A, 89*(18), 8487-8491.

Harbst, K., Lauss, M., Cirenajwis, H., Winter, C., Howlin, J., Torngren, T., Kvist, A., Nodin, B., Olsson, E., Hakkinen, J., Jirstrom, K., Staaf, J., Lundgren, L., Olsson, H., Ingvar, C., Gruvberger-Saal, S. K., Saal, L. H., & Jonsson, G. (2014). Molecular and genetic diversity in the metastatic process of melanoma. *J Pathol, 233*(1), 39-50. doi:10.1002/path.4318

Harlin, H., Meng, Y., Peterson, A. C., Zha, Y., Tretiakova, M., Slingluff, C., McKee, M., & Gajewski, T. F. (2009). Chemokine expression in melanoma metastases associated with CD8+ T-cell recruitment. *Cancer Res, 69*(7), 3077-3085. doi:10.1158/0008-5472.CAN-08-2281

Hauck, C. R., Hsia, D. A., Puente, X. S., Cheresh, D. A., & Schlaepfer, D. D. (2002). FRNK blocks v-Src-stimulated invasion and experimental metastases without effects on cell motility or growth. *EMBO J, 21*(23), 6289-6302.

Hawkins, R. D., Bashiardes, S., Helms, C. A., Hu, L., Saccone, N. L., Warchol, M. E., & Lovett, M. (2003). Gene expression differences in quiescent versus regenerating hair cells of avian sensory epithelia: implications for human hearing and balance disorders. *Human Molecular Genetics, 12*(11), 1261-1272. doi:10.1093/hmg/ddg150

Hay, E. D. (1995). An overview of epithelio-mesenchymal transformation. *Acta Anat (Basel), 154*(1), 8-20.

Heasman, S. J., & Ridley, A. J. (2008). Mammalian Rho GTPases: new insights into their functions from in vivo studies. *Nat Rev Mol Cell Biol, 9*(9), 690-701. doi:10.1038/nrm2476

Heintel, D., Zojer, N., Schreder, M., Strasser-Weippl, K., Kainz, B., Vesely, M., Gisslinger, H., Drach, J., Gaiger, A., Jager, U., & Ludwig, H. (2008). Expression of MUM1/IRF4 mRNA as a prognostic marker in patients with multiple myeloma. *Leukemia, 22*(2), 441-445. doi:10.1038/sj.leu.2404895

Hemesath, T. J., Price, E. R., Takemoto, C., Badalian, T., & Fisher, D. E. (1998). MAP kinase links the transcription factor Microphthalmia to c-Kit signalling in melanocytes. *Nature, 391*(6664), 298-301. doi:10.1038/34681

Hemesath, T. J., Steingrimsson, E., McGill, G., Hansen, M. J., Vaught, J., Hodgkinson, C. A., Arnheiter, H., Copeland, N. G., Jenkins, N. A., & Fisher, D. E. (1994). microphthalmia, a critical factor in melanocyte development, defines a discrete transcription factor family. *Genes Dev, 8*(22), 2770-2780.

Hershey, C. L., & Fisher, D. E. (2005). Genomic analysis of the Microphthalmia locus and identification of the MITF-J/Mitf-J isoform. *Gene, 347*(1), 73-82. doi:10.1016/j.gene.2004.12.002

Hertwig, P. (1942). Neue Mutaionen und Kopplungsgruppen bei der Hausmaus. . *Z.Indukt.Abstammungs- u. Vererbungsl, Vererbungsl., 80*, 220-246.

Hezel, A. F., Kimmelman, A. C., Stanger, B. Z., Bardeesy, N., & Depinho, R. A. (2006). Genetics and biology of pancreatic ductal adenocarcinoma. *Genes Dev, 20*(10), 1218-1249. doi:10.1101/gad.1415606

Hildebrand, J. D., Schaller, M. D., & Parsons, J. T. (1993). Identification of sequences required for the efficient localization of the focal adhesion kinase, pp125FAK, to cellular focal adhesions. *J Cell Biol, 123*(4), 993-1005.

Ho, J., de Moura, M. B., Lin, Y., Vincent, G., Thorne, S., Duncan, L. M., Hui-Min, L., Kirkwood, J. M., Becker, D., Van Houten, B., & Moschos, S. J. (2012). Importance of glycolysis and oxidative phosphorylation in advanced melanoma. *Mol Cancer, 11*, 76. doi:10.1186/1476-4598-11-76

Hodgkinson, C. A., Moore, K. J., Nakayama, A., Steingrimsson, E., Copeland, N. G., Jenkins, N. A., & Arnheiter, H. (1993). Mutations at the mouse microphthalmia locus are associated with defects in a gene encoding a novel basic-helix-loop-helix-zipper protein. *Cell, 74*(2), 395-404.

Hoek, K. S., Eichhoff, O. M., Schlegel, N. C., Dobbeling, U., Kobert, N., Schaerer, L., Hemmi, S., & Dummer, R. (2008). In vivo switching of human melanoma cells between proliferative and invasive states. *Cancer Res, 68*(3), 650-656. doi:10.1158/0008-5472.CAN-07-2491

Hoek, K. S., & Goding, C. R. (2010). Cancer stem cells versus phenotype-switching in melanoma. *Pigment Cell Melanoma Res, 23*(6), 746-759. doi:10.1111/j.1755-148X.2010.00757.x

Hoek, K. S., Schlegel, N. C., Brafford, P., Sucker, A., Ugurel, S., Kumar, R., Weber, B. L., Nathanson, K. L., Phillips, D. J., Herlyn, M., Schadendorf, D., & Dummer, R. (2006). Metastatic potential of melanomas defined by specific gene expression profiles with no BRAF signature. *Pigment Cell Res, 19*(4), 290-302. doi:10.1111/j.1600-0749.2006.00322.x

Hoek, K. S., Schlegel, N. C., Eichhoff, O. M., Widmer, D. S., Praetorius, C., Einarsson, S. O., Valgeirsdottir, S., Bergsteinsdottir, K., Schepsky, A., Dummer, R., & Steingrimsson, E. (2008). Novel MITF targets identified using a two-step DNA microarray strategy. *Pigment Cell Melanoma Res, 21*(6), 665-676. doi:10.1111/j.1755-148X.2008.00505.x

Honey, K., & Rudensky, A. Y. (2003). Lysosomal cysteine proteases regulate antigen presentation. *Nature Reviews Immunology, 3*(6), 472-482. doi:10.1038/nri1110

Hsia, D. A., Mitra, S. K., Hauck, C. R., Streblow, D. N., Nelson, J. A., Ilic, D., Huang, S., Li, E., Nemerow, G. R., Leng, J., Spencer, K. S., Cheresh, D. A., & Schlaepfer, D. D. (2003). Differential regulation of cell motility and invasion by FAK. *J Cell Biol, 160*(5), 753-767. doi:10.1083/jcb.200212114

Hsu, S. C., Galceran, J., & Grosschedl, R. (1998). Modulation of transcriptional regulation by LEF-1 in response to Wnt-1 signaling and association with beta-catenin. *Mol Cell Biol, 18*(8), 4807-4818.

Huang, S., Shao, G., & Liu, L. M. (1998). The PR domain of the Rb-binding zinc finger protein RIZ1 is a protein binding interface and is related to the SET domain functioning in chromatin-mediated gene expression. *Journal of Biological Chemistry, 273*(26), 15933-15939. doi:DOI 10.1074/jbc.273.26.15933

Huang, S. C., Smith, A. M., Everts, B., Colonna, M., Pearce, E. L., Schilling, J. D., & Pearce, E. J. (2016). Metabolic Reprogramming Mediated by the mTORC2-IRF4 Signaling Axis Is Essential for Macrophage Alternative Activation. *Immunity, 45*(4), 817-830. doi:10.1016/j.immuni.2016.09.016

Hughes, M. J., Lingrel, J. B., Krakowsky, J. M., & Anderson, K. P. (1993). A helix-loop-helix transcription factor-like gene is located at the mi locus. *J Biol Chem, 268*(28), 20687-20690.

Huynh, K. K., Eskelinen, E. L., Scott, C. C., Malevanets, A., Saftig, P., & Grinstein, S. (2007). LAMP proteins are required for fusion of lysosomes with phagosomes. *EMBO J, 26*(2), 313-324. doi:10.1038/sj.emboj.7601511

Hynes, R. O., & Naba, A. (2012). Overview of the matrisome--an inventory of extracellular matrix constituents and functions. *Cold Spring Harb Perspect Biol, 4*(1), a004903. doi:10.1101/cshperspect.a004903

Ichii-Nakato, N., Takata, M., Takayanagi, S., Takashima, S., Lin, J., Murata, H., Fujimoto, A., Hatta, N., & Saida, T. (2006). High frequency of BRAFV600E mutation in acquired nevi and small congenital nevi, but low frequency of mutation in medium-sized congenital nevi. *J Invest Dermatol, 126*(9), 2111-2118. doi:10.1038/sj.jid.5700366

Iida, S., Rao, P. H., Butler, M., Corradini, P., Boccadoro, M., Klein, B., Chaganti, R. S., & Dalla-Favera, R. (1997). Deregulation of MUM1/IRF4 by chromosomal translocation in multiple myeloma. *Nat Genet, 17*(2), 226-230. doi:10.1038/ng1097-226

Ilic, D., Furuta, Y., Kanazawa, S., Takeda, N., Sobue, K., Nakatsuji, N., Nomura, S., Fujimoto, J., Okada, M., & Yamamoto, T. (1995). Reduced cell motility and enhanced focal adhesion contact formation in cells from FAK-deficient mice. *Nature, 377*(6549), 539-544. doi:10.1038/377539a0

Inamura, K., Fujiwara, M., Togashi, Y., Nomura, K., Mukai, H., Fujii, Y., Yamamoto, S., Yonese, J., Fukui, I., & Ishikawa, Y. (2012). Diverse Fusion Patterns and Heterogeneous Clinicopathologic Features of Renal Cell Carcinoma With t(6;11) Trans location. *American Journal of Surgical Pathology, 36*(1), 35-42. doi:DOI 10.1097/PAS.0b013e3182293ec3

Ito, A., Jippo, T., Wakayama, T., Morii, E., Koma, Y., Onda, H., Nojima, H., Iseki, S., & Kitamura, Y. (2003). SgIGSF: a new mast-cell adhesion molecule used for attachment to fibroblasts and transcriptionally regulated by MITF. *Blood, 101*(7), 2601-2608. doi:10.1182/blood-2002-07-2265

Izzard, C. S., & Lochner, L. R. (1976). Cell-to-substrate contacts in living fibroblasts: an interference reflexion study with an evaluation of the technique. *J Cell Sci, 21*(1), 129-159.

Javelaud, D., Alexaki, V. I., Pierrat, M. J., Hoek, K. S., Dennler, S., Van Kempen, L., Bertolotto, C., Ballotti, R., Saule, S., Delmas, V., & Mauviel, A. (2011). GLI2 and M-MITF transcription factors control exclusive gene expression programs and inversely regulate invasion in human melanoma cells. *Pigment Cell Melanoma Res, 24*(5), 932-943. doi:10.1111/j.1755-148X.2011.00893.x

Jenuwein, T. (2001). Re-SET-ting heterochromatin by histone methyltransferases. *Trends in Cell Biology, 11*(6), 266-273. doi:Doi 10.1016/S0962-8924(01)02001-3

Ji, Z. Y., Chen, Y. E., Kumar, R., Taylor, M., Njauw, C. N. J., Miao, B. C., Frederick, D. T., Wargo, J. A., Flaherty, K. T., Jonsson, G., & Tsao, H. (2015). MITF Modulates Therapeutic Resistance through EGFR Signaling. *Journal of Investigative Dermatology, 135*(7), 1863-1872. doi:10.1038/jid.2015.105

Ji, Z. Y., Flaherty, K. T., & Tsao, H. (2012). Targeting the RAS pathway in melanoma. *Trends in Molecular Medicine, 18*(1), 27-35. doi:10.1016/j.molmed.2011.08.001

Johannessen, C. M., Johnson, L. A., Piccioni, F., Townes, A., Frederick, D. T., Donahue, M. K., Narayan, R., Flaherty, K. T., Wargo, J. A., Root, D. E., & Garraway, L. A. (2013). A melanocyte lineage program confers resistance to MAP kinase pathway inhibition. *Nature, 504*(7478), 138-+. doi:10.1038/nature12688

Kalluri, R., & Weinberg, R. A. (2009). The basics of epithelial-mesenchymal transition. *J Clin Invest, 119*(6), 1420-1428. doi:10.1172/JCI39104

Karasarides, M., Chiloeches, A., Hayward, R., Niculescu-Duvaz, D., Scanlon, I., Friedlos, F., Ogilvie, L., Hedley, D., Martin, J., Marshall, C. J., Springer, C. J., & Marais, R. (2004). B-RAF is a therapeutic target in melanoma. *Oncogene, 23*(37), 6292-6298. doi:10.1038/sj.onc.1207785

Katoh, H., Hiramoto, K., & Negishi, M. (2006). Activation of Rac1 by RhoG regulates cell migration. *Journal of Cell Science, 119*(1), 56-65. doi:10.1242/jcs.02720

Khaled, M., Larribere, L., Bille, K., Aberdam, E., Ortonne, J. P., Ballotti, R., & Bertolotto, C. (2002). Glycogen synthase kinase 3beta is activated by cAMP and plays an active role in the regulation of melanogenesis. *J Biol Chem, 277*(37), 33690-33697. doi:10.1074/jbc.M202939200

Kim, D. S., Park, S. H., & Park, K. C. (2004). Transforming growth factor-beta1 decreases melanin synthesis via delayed extracellular signal-regulated kinase activation. *Int J Biochem Cell Biol, 36*(8), 1482-1491. doi:10.1016/j.biocel.2003.10.023

Kim, J. E., Leung, E., Baguley, B. C., & Finlay, G. J. (2013). Heterogeneity of expression of epithelial-mesenchymal transition markers in melanocytes and melanoma cell lines. *Front Genet, 4*, 97. doi:10.3389/fgene.2013.00097

Klein, U., Casola, S., Cattoretti, G., Shen, Q., Lia, M., Mo, T., Ludwig, T., Rajewsky, K., & Dalla-Favera, R. (2006). Transcription factor IRF4 controls plasma cell differentiation and class-switch recombination. *Nat Immunol, 7*(7), 773-782. doi:10.1038/ni1357

Koh, J., Enders, G. H., Dynlacht, B. D., & Harlow, E. (1995). Tumor-Derived P16 Alleles Encoding Proteins Defective in Cell-Cycle Inhibition. *Nature, 375*(6531), 506-510. doi:DOI 10.1038/375506a0

Kohler, B. A., Ward, E., McCarthy, B. J., Schymura, M. J., Ries, L. A. G., Eheman, C., Jemal, A., Anderson, R. N., Ajani, U. A., & Edwards, B. K. (2011). Annual Report to the Nation on the Status of Cancer, 1975-2007, Featuring Tumors of the Brain and Other Nervous System. *Journal of the National Cancer Institute, 103*(9), 714-736. doi:10.1093/jnci/djr077

Kornberg, R. D., & Lorch, Y. (1999). Twenty-five years of the nucleosome, fundamental particle of the eukaryote chromosome. *Cell, 98*(3), 285-294.

Kouzarides, T. (2007). Chromatin modifications and their function. *Cell, 128*(4), 693-705. doi:10.1016/j.cell.2007.02.005

Krasagakis, K., Garbe, C., Schrier, P. I., & Orfanos, C. E. (1994). Paracrine and Autocrine Regulation of Human Melanocyte and Melanoma Cell-Growth by Transforming Growth-Factor-Beta in-Vitro. *Anticancer Research, 14*(6b), 2565-2571.

Kuiper, R. P., Schepens, M., Thijssen, J., van Asseldonk, M., van den Berg, E., Bridge, J., Schuuring, E., Schoenmakers, E. F., & van Kessel, A. G. (2003). Upregulation of the transcription factor TFEB in t(6;11)(p21;q13)-positive renal cell carcinomas due to promoter substitution. *Hum Mol Genet, 12*(14), 1661-1669.

Kunz, M., Hartmann, A., Flory, E., Toksoy, A., Koczan, D., Thiesen, H. J., Mukaida, N., Neumann, M., Rapp, U. R., Brocker, E. B., & Gillitzer, R. (1999). Anoxia-induced up-regulation of interleukin-8 in human malignant melanoma - A potential mechanism for high tumor aggressiveness. *American Journal of Pathology, 155*(3), 753-763. doi:Doi 10.1016/S0002-9440(10)65174-7

Lamouille, S., Xu, J., & Derynck, R. (2014). Molecular mechanisms of epithelial-mesenchymal transition. *Nat Rev Mol Cell Biol, 15*(3), 178-196. doi:10.1038/nrm3758

Lang, D., Lu, M. M., Huang, L., Engleka, K. A., Zhang, M., Chu, E. Y., Lipner, S., Skoultchi, A., Millar, S. E., & Epstein, J. A. (2005). Pax3 functions at a nodal point in melanocyte stem cell differentiation. *Nature, 433*(7028), 884-887. doi:10.1038/nature03292

Langmead, B., Trapnell, C., Pop, M., & Salzberg, S. L. (2009). Ultrafast and memory-efficient alignment of short DNA sequences to the human genome. *Genome Biol, 10*(3), R25. doi:10.1186/gb-2009-10-3-r25

Laurette, P., Strub, T., Koludrovic, D., Keime, C., Le Gras, S., Seberg, H., Van Otterloo, E., Imrichova, H., Siddaway, R., Aerts, S., Cornell, R. A., Mengus, G., & Davidson, I. (2015). Transcription factor MITF and remodeller BRG1 define chromatin organisation at regulatory elements in melanoma cells. *Elife, 4*. doi:10.7554/eLife.06857

Le Douarin, N., & Kalcheim, C. (1999). The Migration of Neural Crest Cells. *Developmental and Cell Biology Series*, 23-59. doi:doi:10.1017/CBO9780511897948.005

Leroy, B., Girard, L., Hollestelle, A., Minna, J. D., Gazdar, A. F., & Soussi, T. (2014). Analysis of TP53 mutation status in human cancer cell lines: a reassessment. *Hum Mutat, 35*(6), 756-765. doi:10.1002/humu.22556

Levy, C., Sonnenblick, A., & Razin, E. (2003). Role played by microphthalmia transcription factor phosphorylation and its Zip domain in its transcriptional inhibition by PIAS3. *Mol Cell Biol, 23*(24), 9073-9080.

Li, B., Carey, M., & Workman, J. L. (2007). The role of chromatin during transcription. *Cell, 128*(4), 707-719. doi:10.1016/j.cell.2007.01.015

Li, H., Handsaker, B., Wysoker, A., Fennell, T., Ruan, J., Homer, N., Marth, G., Abecasis, G., Durbin, R., & Proc, G. P. D. (2009). The Sequence Alignment/Map format and SAMtools. *Bioinformatics, 25*(16), 2078-2079. doi:10.1093/bioinformatics/btp352

Li, Q., Murphy, M., Ross, J., Sheehan, C., & Carlson, J. A. (2004). Skp2 and p27(kip1) expression in melanocytic nevi and melanoma: an inverse relationship. *Journal of Cutaneous Pathology, 31*(10), 633-642. doi:DOI 10.1111/j.0303-6987.2004.00243.x

Lim, Y., Lim, S. T., Tomar, A., Gardel, M., Bernard-Trifilo, J. A., Chen, X. L., Uryu, S. A., Canete-Soler, R., Zhai, J., Lin, H., Schlaepfer, W. W., Nalbant, P., Bokoch, G., Ilic, D., Waterman-Storer, C., & Schlaepfer, D. D. (2008). PyK2 and FAK connections to p190Rho guanine nucleotide exchange factor regulate RhoA activity, focal adhesion formation, and cell motility. *J Cell Biol, 180*(1), 187-203. doi:10.1083/jcb.200708194

Lin, C. H., Wong, S. H., Kurzer, J. H., Schneidawind, C., Wei, M. C., Duque-Afonso, J., Jeong, J., Feng, X., & Cleary, M. L. (2018). SETDB2 Links E2A-PBX1 to Cell-Cycle Dysregulation in Acute Leukemia through CDKN2C Repression. *Cell Rep, 23*(4), 1166-1177. doi:10.1016/j.celrep.2018.03.124

Lin, L., Gerth, A. J., & Peng, S. L. (2004). Active inhibition of plasma cell development in resting B cells by microphthalmia-associated transcription factor. *J Exp Med, 200*(1), 115-122. doi:10.1084/jem.20040612

Lin, M. L., Zhan, Y. F., Villadangos, J. A., & Lew, A. M. (2008). The cell biology of cross-presentation and the role of dendritic cell subsets. *Immunology and Cell Biology, 86*(4), 353-362. doi:10.1038/icb.2008.3

Lister, J. A., Capper, A., Zeng, Z., Mathers, M. E., Richardson, J., Paranthaman, K., Jackson, I. J., & Elizabeth Patton, E. (2014). A conditional zebrafish MITF mutation reveals MITF levels are critical for melanoma promotion vs. regression in vivo. *J Invest Dermatol, 134*(1), 133-140. doi:10.1038/jid.2013.293

Liu, F., Visser, M., Duffy, D. L., Hysi, P. G., Jacobs, L. C., Lao, O., Zhong, K., Walsh, S., Chaitanya, L., Wollstein, A., Zhu, G., Montgomery, G. W., Henders, A. K., Mangino, M., Glass, D., Bataille, V., Sturm, R. A., Rivadeneira, F., Hofman, A., van, I. W. F., Uitterlinden, A. G., Palstra, R. J., Spector, T. D., Martin, N. G., Nijsten, T. E., & Kayser, M. (2015). Genetics of skin color variation in Europeans: genome-wide association studies with functional follow-up. *Hum Genet, 134*(8), 823-835. doi:10.1007/s00439-015-1559-0

Liu, S., Calderwood, D. A., & Ginsberg, M. H. (2000). Integrin cytoplasmic domain-binding proteins. *J Cell Sci, 113 (Pt 20)*, 3563-3571.

Liu, Y., Ye, F., Li, Q., Tamiya, S., Darling, D. S., Kaplan, H. J., & Dean, D. C. (2009). Zeb1 represses Mitf and regulates pigment synthesis, cell proliferation, and epithelial morphology. *Invest Ophthalmol Vis Sci, 50*(11), 5080-5088. doi:10.1167/iovs.08-2911

Loercher, A. E., Tank, E. M., Delston, R. B., & Harbour, J. W. (2005). MITF links differentiation with cell cycle arrest in melanocytes by transcriptional activation of INK4A. *J Cell Biol, 168*(1), 35-40. doi:10.1083/jcb.200410115

Loriot, A., De Plaen, E., Boon, T., & De Smet, C. (2006). Transient down-regulation of DNMT1 methyltransferase leads to activation and stable hypomethylation of MAGE-A1 in melanoma cells. *J Biol Chem, 281*(15), 10118-10126. doi:10.1074/jbc.M510469200

Lowy, D. R., & Willumsen, B. M. (1993). Function and Regulation of Ras. *Annual Review of Biochemistry, 62*, 851-891. doi:DOI 10.1146/annurev.bi.62.070193.004223

Lu, J., Hamze, Z., Bonnavion, R., Herath, N., Pouponnot, C., Assade, F., Fontaniere, S., Bertolino, P., Cordier-Bussat, M., & Zhang, C. X. (2012). Reexpression of oncoprotein MafB in proliferative beta-cells and Men1 insulinomas in mouse. *Oncogene, 31*(31), 3647-3654. doi:10.1038/onc.2011.538

Lu, P., Weaver, V. M., & Werb, Z. (2012). The extracellular matrix: a dynamic niche in cancer progression. *J Cell Biol, 196*(4), 395-406. doi:10.1083/jcb.201102147

Ludwig, J., Kerscher, S., Brandt, U., Pfeiffer, K., Getlawi, F., Apps, D. K., & Schagger, H. (1998). Identification and characterization of a novel 9.2-kDa membrane sector-associated protein of vacuolar proton-ATPase from chromaffin granules. *Journal of Biological Chemistry, 273*(18), 10939-10947. doi:DOI 10.1074/jbc.273.18.10939

Ma, X. M., & Blenis, J. (2009). Molecular mechanisms of mTOR-mediated translational control. *Nat Rev Mol Cell Biol, 10*(5), 307-318. doi:10.1038/nrm2672

Machanick, P., & Bailey, T. L. (2011). MEME-ChIP: motif analysis of large DNA datasets. *Bioinformatics, 27*(12), 1696-1697. doi:10.1093/bioinformatics/btr189

MacLennan, I. C. (1994). Germinal centers. *Annu Rev Immunol, 12*, 117-139. doi:10.1146/annurev.iy.12.040194.001001

Magnusdottir, E., Dietmann, S., Murakami, K., Gunesdogan, U., Tang, F., Bao, S., Diamanti, E., Lao, K., Gottgens, B., & Azim Surani, M. (2013). A tripartite transcription factor network regulates primordial germ cell specification in mice. *Nat Cell Biol, 15*(8), 905-915. doi:10.1038/ncb2798

Mallory, M. J., Allon, S. J., Qiu, J., Gazzara, M. R., Tapescu, I., Martinez, N. M., Fu, X. D., & Lynch, K. W. (2015). Induced transcription and stability of CELF2 mRNA drives widespread alternative splicing during T-cell signaling. *Proc Natl Acad Sci U S A, 112*(17), E2139-2148. doi:10.1073/pnas.1423695112

Man, K., Gabriel, S. S., Liao, Y., Gloury, R., Preston, S., Henstridge, D. C., Pellegrini, M., Zehn, D., Berberich-Siebelt, F., Febbraio, M. A., Shi, W., & Kallies, A. (2017). Transcription Factor IRF4 Promotes CD8(+) T Cell Exhaustion and Limits the Development of Memory-like T Cells during Chronic Infection. *Immunity, 47*(6), 1129-1141 e1125. doi:10.1016/j.immuni.2017.11.021

Man, K., Miasari, M., Shi, W., Xin, A., Henstridge, D. C., Preston, S., Pellegrini, M., Belz, G. T., Smyth, G. K., Febbraio, M. A., Nutt, S. L., & Kallies, A. (2013). The transcription factor IRF4 is essential for TCR affinity-mediated metabolic programming and clonal expansion of T cells. *Nat Immunol, 14*(11), 1155-1165. doi:10.1038/ni.2710

Mannion, N. M., Greenwood, S. M., Young, R., Cox, S., Brindle, J., Read, D., Nellaker, C., Vesely, C., Ponting, C. P., McLaughlin, P. J., Jantsch, M. F., Dorin, J., Adams, I. R., Scadden, A. D., Ohman, M., Keegan, L. P., & O'Connell, M. A. (2014). The RNA-editing enzyme ADAR1 controls innate immune responses to RNA. *Cell Rep, 9*(4), 1482-1494. doi:10.1016/j.celrep.2014.10.041

Martina, J. A., Chen, Y., Gucek, M., & Puertollano, R. (2012). MTORC1 functions as a transcriptional regulator of autophagy by preventing nuclear transport of TFEB. *Autophagy, 8*(6), 903-914. doi:10.4161/auto.19653

Massague, J. (2008). TGFbeta in Cancer. *Cell, 134*(2), 215-230. doi:10.1016/j.cell.2008.07.001

Matsui, T., Leung, D., Miyashita, H., Maksakova, I. A., Miyachi, H., Kimura, H., Tachibana, M., Lorincz, M. C., & Shinkai, Y. (2010). Proviral silencing in embryonic stem cells requires the histone methyltransferase ESET. *Nature, 464*(7290), 927-U149. doi:10.1038/nature08858

Matsuyama, T., Grossman, A., Mittrucker, H. W., Siderovski, D. P., Kiefer, F., Kawakami, T., Richardson, C. D., Taniguchi, T., Yoshinaga, S. K., & Mak, T. W. (1995). Molecular cloning of LSIRF, a lymphoid-specific member of the interferon regulatory factor family that binds the interferon-stimulated response element (ISRE). *Nucleic Acids Res, 23*(12), 2127-2136.

McGill, G. G., Haq, R., Nishimura, E. K., & Fisher, D. E. (2006). c-Met expression is regulated by Mitf in the melanocyte lineage. *J Biol Chem, 281*(15), 10365-10373. doi:10.1074/jbc.M513094200

McGill, G. G., Horstmann, M., Widlund, H. R., Du, J., Motyckova, G., Nishimura, E. K., Lin, Y. L., Ramaswamy, S., Avery, W., Ding, H. F., Jordan, S. A., Jackson, I. J., Korsmeyer, S. J., Golub, T. R., & Fisher, D. E. (2002). Bcl2 regulation by the melanocyte master regulator Mitf modulates lineage survival and melanoma cell viability. *Cell, 109*(6), 707-718.

McNeal, A. S., Liu, K., Nakhate, V., Natale, C. A., Duperret, E. K., Capell, B. C., Dentchev, T., Berger, S. L., Herlyn, M., Seykora, J. T., & Ridky, T. W. (2015). CDKN2B Loss Promotes Progression from Benign Melanocytic Nevus to Melanoma. *Cancer Discov, 5*(10), 1072-1085. doi:10.1158/2159-8290.CD-15-0196

Medina, D. L., Di Paola, S., Peluso, I., Armani, A., De Stefani, D., Venditti, R., Montefusco, S., Scotto-Rosato, A., Prezioso, C., Forrester, A., Settembre, C., Wang, W. Y., Gao, Q., Xu, H. X., Sandri, M., Rizzuto, R., De Matteis, M. A., & Ballabio, A. (2015). Lysosomal calcium signalling regulates autophagy through calcineurin and TFEB. *Nature Cell Biology, 17*(3), 288-+. doi:10.1038/ncb3114

Medina, D. L., Fraldi, A., Bouche, V., Annunziata, F., Mansueto, G., Spampanato, C., Puri, C., Pignata, A., Martina, J. A., Sardiello, M., Palmieri, M., Polishchuk, R., Puertollano, R., & Ballabio, A. (2011). Transcriptional activation of lysosomal exocytosis promotes cellular clearance. *Dev Cell, 21*(3), 421-430. doi:10.1016/j.devcel.2011.07.016

Milatovich, A., Travis, A., Grosschedl, R., & Francke, U. (1991). Gene for lymphoid enhancer-binding factor 1 (LEF1) mapped to human chromosome 4 (q23-q25) and mouse chromosome 3 near Egf. *Genomics, 11*(4), 1040-1048.

Miller, A. J., Levy, C., Davis, I. J., Razin, E., & Fisher, D. E. (2005). Sumoylation of MITF and its related family members TFE3 and TFEB. *Journal of Biological Chemistry, 280*(1), 146-155. doi:10.1074/jbc.M411757200

Miller, A. J., & Mihm, M. C., Jr. (2006). Melanoma. *N Engl J Med, 355*(1), 51-65. doi:10.1056/NEJMra052166

Mittrucker, H. W., Matsuyama, T., Grossman, A., Kundig, T. M., Potter, J., Shahinian, A., Wakeham, A., Patterson, B., Ohashi, P. S., & Mak, T. W. (1997). Requirement for the transcription factor LSIRF/IRF4 for mature B and T lymphocyte function. *Science, 275*(5299), 540-543.

Miyamoto, S., Teramoto, H., Coso, O. A., Gutkind, J. S., Burbelo, P. D., Akiyama, S. K., & Yamada, K. M. (1995). Integrin function: molecular hierarchies of cytoskeletal and signaling molecules. *J Cell Biol, 131*(3), 791-805.

Mollaaghababa, R., & Pavan, W. J. (2003). The importance of having your SOX on: role of SOX10 in the development of neural crest-derived melanocytes and glia. *Oncogene, 22*(20), 3024-3034. doi:10.1038/sj.onc.1206442

Morii, E., Tsujimura, T., Jippo, T., Hashimoto, K., Takebayashi, K., Tsujino, K., Nomura, S., Yamamoto, M., & Kitamura, Y. (1996). Regulation of mouse mast cell protease 6 gene expression by transcription factor encoded by the mi locus. *Blood, 88*(7), 2488-2494.

Muller, J., Krijgsman, O., Tsoi, J., Robert, L., Hugo, W., Song, C., Kong, X., Possik, P. A., Cornelissen-Steijger, P. D., Geukes Foppen, M. H., Kemper, K., Goding, C. R., McDermott, U., Blank, C., Haanen, J., Graeber, T. G., Ribas, A., Lo, R. S., & Peeper, D. S. (2014). Low MITF/AXL ratio predicts early resistance to multiple targeted drugs in melanoma. *Nat Commun, 5*, 5712. doi:10.1038/ncomms6712

Murakami, H., & Arnheiter, H. (2005). Sumoylation modulates transcriptional activity of MITF in a promoter-specific manner. *Pigment Cell Res, 18*(4), 265-277. doi:10.1111/j.1600-0749.2005.00234.x

Murakami, Y. (2002). Functional cloning of a tumor suppressor gene,TSLC1, in human non-small cell lung cancer. *Oncogene, 21*(45), 6936-6948. doi:DOI 10.1038/sj.onc.1205825

Murakami, Y. (2005). Involvement of a cell adhesion molecule, TSLC1/IGSF4, in human oncogenesis. *Cancer Sci, 96*(9), 543-552. doi:10.1111/j.1349-7006.2005.00089.x

Nabar, N. R., & Kehrl, J. H. (2017). The Transcription Factor EB Links Cellular Stress to the Immune Response. *Yale J Biol Med, 90*(2), 301-315.

Nakayama, A., Nguyen, M. T. T., Chen, C. C., Opdecamp, K., Hodgkinson, C. A., & Amheiter, H. (1998). Mutations in microphthalmia, the mouse homolog of the human deafness gene MITF, affect neuroepithelial and neural crest-derived melanocytes differently. *Mechanisms of Development, 70*(1-2), 155-166. doi:Doi 10.1016/S0925-4773(97)00188-3

Napolitano, G., & Ballabio, A. (2016). TFEB at a glance. *Journal of Cell Science, 129*(13), 2475-2481. doi:10.1242/jcs.146365

Natkunam, Y., Warnke, R. A., Montgomery, K., Falini, B., & van De Rijn, M. (2001). Analysis of MUM1/IRF4 protein expression using tissue microarrays and immunohistochemistry. *Mod Pathol, 14*(7), 686-694. doi:10.1038/modpathol.3880373

Navarini, A. A., Recher, M., Lang, K. S., Georgiev, P., Meury, S., Bergthaler, A., Flatz, L., Bille, J., Landmann, R., Odermatt, B., Hengartner, H., & Zinkernagel, R. M. (2006). Increased susceptibility to bacterial superinfection as a consequence of innate antiviral responses. *Proc Natl Acad Sci U S A, 103*(42), 15535-15539. doi:10.1073/pnas.0607325103

Nezami, A. G., Poy, F., & Eck, M. J. (2006). Structure of the autoinhibitory switch in formin mDia1. *Structure, 14*(2), 257-263. doi:10.1016/j.str.2005.12.003

Ngeow, K. C., Friedrichsen, H. J., Li, L. X., Zeng, Z. L., Andrews, S., Volpon, L., Brunsdon, H., Berridge, G., Picaud, S., Fischer, R., Lisle, R., Knapp, S., Filippakopoulos, P., Knowles, H., Steingrimsson, E., Borden, K. L. B., Patton, E. E., & Goding, C. R. (2018). BRAF/MAPK and GSK3 signaling converges to control MITF nuclear export. *Proceedings of the National Academy of Sciences of the United States of America, 115*(37), E8668-E8677. doi:10.1073/pnas.1810498115

Nishikawaji, T., Akiyama, Y., Shimada, S., Kojima, K., Kawano, T., Eishi, Y., Yuasa, Y., & Tanaka, S. (2016). Oncogenic roles of the SETDB2 histone methyltransferase in gastric cancer. *Oncotarget, 7*(41), 67251-67265. doi:10.18632/oncotarget.11625

Nishimura, E. K., Granter, S. R., & Fisher, D. E. (2005). Mechanisms of hair graying: Incomplete melanocyte stem cell maintenance in the niche. *Science, 307*(5710), 720-724. doi:10.1126/science.1099593

Nishimura, E. K., Jordan, S. A., Oshima, H., Yoshida, H., Osawa, M., Moriyama, M., Jackson, I. J., Barrandon, Y., Miyachi, Y., & Nishikawa, S. (2002). Dominant role of the niche in melanocyte stem-cell fate determination. *Nature, 416*(6883), 854-860. doi:DOI 10.1038/416854a

Nishimura, E. K., Suzuki, M., Igras, V., Du, J. Y., Lonning, S., Miyachi, Y., Roes, J., Beermann, F., & Fisher, D. E. (2010). Key Roles for Transforming Growth Factor beta in Melanocyte Stem Cell Maintenance. *Cell Stem Cell, 6*(2), 130-140. doi:10.1016/j.stem.2009.12.010

Nobes, C., & Hall, A. (1994). Regulation and function of the Rho subfamily of small GTPases. *Curr Opin Genet Dev, 4*(1), 77-81.

Nobes, C. D., & Hall, A. (1995). Rho, rac, and cdc42 GTPases regulate the assembly of multimolecular focal complexes associated with actin stress fibers, lamellipodia, and filopodia. *Cell, 81*(1), 53-62.

Nourse, J., Mellentin, J. D., Galili, N., Wilkinson, J., Stanbridge, E., Smith, S. D., & Cleary, M. L. (1990). Chromosomal translocation t(1;19) results in synthesis of a homeobox fusion mRNA that codes for a potential chimeric transcription factor. *Cell, 60*(4), 535-545.

Nurse, P. (1975). Genetic control of cell size at cell division in yeast. *Nature, 256*(5518), 547-551.

Oboki, K., Morii, E., Kataoka, T. R., Jippo, T., & Kitamura, Y. (2002). Isoforms of mi transcription factor preferentially expressed in cultured mast cells of mice. *Biochem Biophys Res Commun, 290*(4), 1250-1254. doi:10.1006/bbrc.2002.6332

Oeckinghaus, A., & Ghosh, S. (2009). The NF-kappa B Family of Transcription Factors and Its Regulation. *Cold Spring Harbor Perspectives in Biology, 1*(4). doi:ARTN a000034 10.1101/cshperspect.a000034

Ogata, M., Hino, S. I., Saito, A., Morikawa, K., Kondo, S., Kanemoto, S., Murakami, T., Taniguchi, M., Tanii, I., Yoshinaga, K., Shiosaka, S., Hammarback, J. A., Urano, F., & Imaizumi, K. (2006). Autophagy is activated for cell survival after endoplasmic reticulum stress. *Molecular and Cellular Biology, 26*(24), 9220-9231. doi:10.1128/Mcb.01453-06

Opdecamp, K., Nakayama, A., Nguyen, M. T. T., Hodgkinson, C. A., Pavan, W. J., & Arnheiter, H. (1997). Melanocyte development in vivo and in neural crest cell cultures: Crucial dependence on the Mitf basic-helix-loop-helix-zipper transcription. *Development, 124*(12), 2377-2386.

Palmieri, M., Impey, S., Kang, H., di Ronza, A., Pelz, C., Sardiello, M., & Ballabio, A. (2011). Characterization of the CLEAR network reveals an integrated control of cellular clearance pathways. *Hum Mol Genet, 20*(19), 3852-3866. doi:10.1093/hmg/ddr306

Palomero, T., Lim, W. K., Odom, D. T., Sulis, M. L., Real, P. J., Margolin, A., Barnes, K. C., O'Neil, J., Neuberg, D., Weng, A. P., Aster, J. C., Sigaux, F., Soulier, J., Look, A. T., Young, R. A., Califano, A., & Ferrando, A. A. (2006). NOTCH1 directly regulates c-MYC and activates a feed-forward-loop transcriptional network promoting leukemic cell growth. *Proc Natl Acad Sci U S A, 103*(48), 18261-18266. doi:10.1073/pnas.0606108103

Panetti, T. S. (2002). Tyrosine phosphorylation of paxillin, FAK, and p130CAS: effects on cell spreading and migration. *Front Biosci, 7*, d143-150.

Papp, T., Pemsel, H., Zimmermann, R., Bastrop, R., Weiss, D. G., & Schiffmann, D. (1999). Mutational analysis of the N-ras, p53, p16INK4a, CDK4, and MC1R genes in human congenital melanocytic naevi. *J Med Genet, 36*(8), 610-614.

Park, P. J. (2009). ChIP-seq: advantages and challenges of a maturing technology. *Nat Rev Genet, 10*(10), 669-680. doi:10.1038/nrg2641

Pastore, N., Brady, O. A., Diab, H. I., Martina, J. A., Sun, L., Huynh, T., Lim, J. A., Zare, H., Raben, N., Ballabio, A., & Puertollano, R. (2016). TFEB and TFE3 cooperate in the regulation of the innate immune response in activated macrophages. *Autophagy, 12*(8), 1240-1258. doi:10.1080/15548627.2016.1179405

Peinado, H., Olmeda, D., & Cano, A. (2007). Snail, Zeb and bHLH factors in tumour progression: an alliance against the epithelial phenotype? *Nat Rev Cancer, 7*(6), 415-428. doi:10.1038/nrc2131

Pennello, G., Devesa, S., & Gail, M. (2000). Association of surface ultraviolet B radiation levels with melanoma and nonmelanoma skin cancer in United States blacks. *Cancer Epidemiology Biomarkers & Prevention, 9*(3), 291-297.

Perera, R. M., Stoykova, S., Nicolay, B. N., Ross, K. N., Fitamant, J., Boukhali, M., Lengrand, J., Deshpande, V., Selig, M. K., Ferrone, C. R., Settleman, J., Stephanopoulos, G., Dyson, N. J., Zoncu, R., Ramaswamy, S., Haas, W., & Bardeesy, N. (2015). Transcriptional control of autophagy-lysosome function drives pancreatic cancer metabolism. *Nature, 524*(7565), 361-365. doi:10.1038/nature14587

Perez-Moreno, M., Jamora, C., & Fuchs, E. (2003). Sticky business: orchestrating cellular signals at adherens junctions. *Cell, 112*(4), 535-548.

Pernis, A. B. (2002). The role of IRF-4 in B and T cell activation and differentiation. *J Interferon Cytokine Res, 22*(1), 111-120. doi:10.1089/107999002753452728

Perrot, C. Y., Javelaud, D., & Mauviel, A. (2013). Overlapping activities of TGF-beta and Hedgehog signaling in cancer: therapeutic targets for cancer treatment. *Pharmacol Ther, 137*(2), 183-199. doi:10.1016/j.pharmthera.2012.10.002

Petit, V., Boyer, B., Lentz, D., Turner, C. E., Thiery, J. P., & Valles, A. M. (2000). Phosphorylation of tyrosine residues 31 and 118 on paxillin regulates cell migration through an association with CRK in NBT-II cells. *J Cell Biol, 148*(5), 957-970.

Pfaffl, M. W. (2001). A new mathematical model for relative quantification in real-time RT-PCR. *Nucleic Acids Res, 29*(9), e45.

Pierrat, M. J., Marsaud, V., Mauviel, A., & Javelaud, D. (2012). Expression of microphthalmia-associated transcription factor (MITF), which is critical for melanoma progression, is inhibited by both transcription factor GLI2 and transforming growth factor-beta. *J Biol Chem, 287*(22), 17996-18004. doi:10.1074/jbc.M112.358341

Pietenpol, J. A., Holt, J. T., Stein, R. W., & Moses, H. L. (1990). Transforming growth factor beta 1 suppression of c-myc gene transcription: role in inhibition of keratinocyte proliferation. *Proc Natl Acad Sci U S A, 87*(10), 3758-3762.

Pimentel, H., Bray, N. L., Puente, S., Melsted, P., & Pachter, L. (2017). Differential analysis of RNA-seq incorporating quantification uncertainty. *Nat Methods, 14*(7), 687-690. doi:10.1038/nmeth.4324

Ploper, D., Taelman, V. F., Robert, L., Perez, B. S., Titz, B., Chen, H. W., Graeber, T. G., von Euw, E., Ribas, A., & De Robertis, E. M. (2015). MITF drives endolysosomal biogenesis and potentiates Wnt signaling in melanoma cells. *Proc Natl Acad Sci U S A, 112*(5), E420-429. doi:10.1073/pnas.1424576112

Pogenberg, V., Ogmundsdottir, M. H., Bergsteinsdottir, K., Schepsky, A., Phung, B., Deineko, V., Milewski, M., Steingrimsson, E., & Wilmanns, M. (2012). Restricted leucine zipper dimerization and specificity of DNA recognition of the melanocyte master regulator MITF. *Genes Dev, 26*(23), 2647-2658. doi:10.1101/gad.198192.112

Pollock, P. M., Harper, U. L., Hansen, K. S., Yudt, L. M., Stark, M., Robbins, C. M., Moses, T. Y., Hostetter, G., Wagner, U., Kakareka, J., Salem, G., Pohida, T., Heenan, P., Duray, P., Kallioniemi, O., Hayward, N. K., Trent, J. M., & Meltzer, P. S. (2003). High frequency of BRAF mutations in nevi. *Nat Genet, 33*(1), 19-20. doi:10.1038/ng1054

Postigo, A. A., & Dean, D. C. (2000). Differential expression and function of members of the zfh-1 family of zinc finger/homeodomain repressors. *Proc Natl Acad Sci U S A, 97*(12), 6391-6396.

Potrony, M., Rebollo-Morell, A., Gimenez-Xavier, P., Zimmer, L., Puig-Butille, J. A., Tell-Marti, G., Sucker, A., Badenas, C., Carrera, C., Malvehy, J., Schadendorf, D., & Puig, S. (2017). IRF4 rs12203592 functional variant and melanoma survival. *Int J Cancer, 140*(8), 1845-1849. doi:10.1002/ijc.30605

Potterf, S. B., Furumura, M., Dunn, K. J., Arnheiter, H., & Pavan, W. J. (2000). Transcription factor hierarchy in Waardenburg syndrome: regulation of MITF expression by SOX10 and PAX3. *Hum Genet, 107*(1), 1-6.

Praetorius, C., Grill, C., Stacey, S. N., Metcalf, A. M., Gorkin, D. U., Robinson, K. C., Van Otterloo, E., Kim, R. S., Bergsteinsdottir, K., Ogmundsdottir, M. H., Magnusdottir, E., Mishra, P. J., Davis, S. R., Guo, T., Zaidi, M. R., Helgason, A. S., Sigurdsson, M. I., Meltzer, P. S., Merlino, G., Petit, V., Larue, L., Loftus, S. K., Adams, D. R., Sobhiafshar, U., Emre, N. C., Pavan, W. J., Cornell, R., Smith, A. G., McCallion, A. S., Fisher, D. E., Stefansson, K., Sturm, R. A., & Steingrimsson, E. (2013). A polymorphism in IRF4 affects human pigmentation through a tyrosinase-dependent MITF/TFAP2A pathway. *Cell, 155*(5), 1022-1033. doi:10.1016/j.cell.2013.10.022

Price, E. R., Ding, H. F., Badalian, T., Bhattacharya, S., Takemoto, C., Yao, T. P., Hemesath, T. J., & Fisher, D. E. (1998). Lineage-specific signaling in melanocytes. C-kit stimulation recruits p300/CBP to microphthalmia. *J Biol Chem, 273*(29), 17983-17986.

Rambow, F., Rogiers, A., Marin-Bejar, O., Aibar, S., Femel, J., Dewaele, M., Karras, P., Brown, D., Chang, Y. H., Debiec-Rychter, M., Adriaens, C., Radaelli, E., Wolter, P., Bechter, O., Dummer, R., Levesque, M., Piris, A., Frederick, D. T., Boland, G., Flaherty, K. T., van den Oord, J., Voet, T., Aerts, S., Lund, A. W., & Marine, J. C. (2018). Toward Minimal Residual Disease-Directed Therapy in Melanoma. *Cell, 174*(4), 843-855 e819. doi:10.1016/j.cell.2018.06.025

Rees, J. L. (2000). The melanocortin 1 receptor (MC1R): More than just red hair. *Pigment Cell Research, 13*(3), 135-140. doi:DOI 10.1034/j.1600-0749.2000.130303.x

Rees, J. L. (2003). Genetics of hair and skin color. *Annual Review of Genetics, 37*, 67-90. doi:10.1146/annurev.genet.37.110801.143233

Ren, X. D., Kiosses, W. B., Sieg, D. J., Otey, C. A., Schlaepfer, D. D., & Schwartz, M. A. (2000). Focal adhesion kinase suppresses Rho activity to promote focal adhesion turnover. *J Cell Sci, 113 (Pt 20)*, 3673-3678.

Rezza, A., Wang, Z. C., Sennett, R., Qiao, W. L., Wang, D. M., Heitman, N., Mok, K. W., Clavel, C., Yi, R., Zandstra, P., Ma'ayan, A., & Rendl, M. (2016). Signaling Networks among Stem Cell Precursors, Transit-Amplifying Progenitors, and their Niche in Developing Hair Follicles. *Cell Reports, 14*(12), 3001-3018. doi:10.1016/j.celrep.2016.02.078

Ridley, A. J., & Hall, A. (1992). Distinct patterns of actin organization regulated by the small GTP-binding proteins Rac and Rho. *Cold Spring Harb Symp Quant Biol, 57*, 661-671.

Ridley, A. J., Schwartz, M. A., Burridge, K., Firtel, R. A., Ginsberg, M. H., Borisy, G., Parsons, J. T., & Horwitz, A. R. (2003). Cell migration: integrating signals from front to back. *Science, 302*(5651), 1704-1709. doi:10.1126/science.1092053

Roczniak-Ferguson, A., Petit, C. S., Froehlich, F., Qian, S., Ky, J., Angarola, B., Walther, T. C., & Ferguson, S. M. (2012). The transcription factor TFEB links mTORC1 signaling to transcriptional control of lysosome homeostasis. *Sci Signal, 5*(228), ra42. doi:10.1126/scisignal.2002790

Rodeck, U., Bossler, A., Graeven, U., Fox, F. E., Nowell, P. C., Knabbe, C., & Kari, C. (1994). Transforming growth factor beta production and responsiveness in normal human melanocytes and melanoma cells. *Cancer Res, 54*(2), 575-581.

Rodeck, U., Melber, K., Kath, R., Menssen, H. D., Varello, M., Atkinson, B., & Herlyn, M. (1991). Constitutive Expression of Multiple Growth-Factor Genes by Melanoma-Cells but Not Normal Melanocytes. *Journal of Investigative Dermatology, 97*(1), 20-26. doi:DOI 10.1111/1523-1747.ep12477822

Rottner, K., Hall, A., & Small, J. V. (1999). Interplay between Rac and Rho in the control of substrate contact dynamics. *Curr Biol, 9*(12), 640-648.

Ruas, M., & Peters, G. (1998). The p16(INK4a)/CDKN2A tumor suppressor and its relatives. *Biochimica Et Biophysica Acta-Reviews on Cancer, 1378*(2), F115-F177. doi:Doi 10.1016/S0304-419x(98)00017-1

Rui, L., Schmitz, R., Ceribelli, M., & Staudt, L. M. (2011). Malignant pirates of the immune system. *Nat Immunol, 12*(10), 933-940. doi:10.1038/ni.2094

Russell, P., & Nurse, P. (1986). cdc25+ functions as an inducer in the mitotic control of fission yeast. *Cell, 45*(1), 145-153.

Saito, H., Yasumoto, K., Takeda, K., Takahashi, K., Fukuzaki, A., Orikasa, S., & Shibahara, S. (2002). Melanocyte-specific microphthalmia-associated transcription factor isoform activates its own gene promoter through physical interaction with lymphoid-enhancing factor 1. *J Biol Chem, 277*(32), 28787-28794. doi:10.1074/jbc.M203719200

Saito, M., Goto, A., Abe, N., Saito, K., Maeda, D., Ohtake, T., Murakami, Y., & Takenoshita, S. (2018). Decreased expression of CADM1 and CADM4 are associated with advanced stage breast cancer. *Oncol Lett, 15*(2), 2401-2406. doi:10.3892/ol.2017.7536

Salaverria, I., Philipp, C., Oschlies, I., Kohler, C. W., Kreuz, M., Szczepanowski, M., Burkhardt, B., Trautmann, H., Gesk, S., Andrusiewicz, M., Berger, H., Fey, M., Harder, L., Hasenclever, D., Hummel, M., Loeffler, M., Mahn, F., Martin-Guerrero, I., Pellissery, S., Pott, C., Pfreundschuh, M., Reiter, A., Richter, J., Rosolowski, M., Schwaenen, C., Stein, H., Trumper, L., Wessendorf, S., Spang, R., Kuppers, R., Klapper, W., Siebert, R., Molecular Mechanisms in Malignant Lymphomas Network Project of the Deutsche, K., German High-Grade Lymphoma Study, G., & Berlin-Frankfurt-Munster, N. H. L. t. g. (2011). Translocations activating IRF4 identify a subtype of germinal center-derived B-cell lymphoma affecting predominantly children and young adults. *Blood, 118*(1), 139-147. doi:10.1182/blood-2011-01-330795

Salti, G. I., Manougian, T., Farolan, M., Shilkaitis, A., Majumdar, D., & Das Gupta, T. K. (2000). Micropthalmia transcription factor: a new prognostic marker in intermediate-thickness cutaneous malignant melanoma. *Cancer Res, 60*(18), 5012-5016.

Samie, M., & Cresswell, P. (2015). The transcription factor TFEB acts as a molecular switch that regulates exogenous antigen-presentation pathways. *Nature Immunology, 16*(7), 729-+. doi:10.1038/ni.3196

Sancak, Y., Bar-Peled, L., Zoncu, R., Markhard, A. L., Nada, S., & Sabatini, D. M. (2010). Ragulator-Rag complex targets mTORC1 to the lysosomal surface and is necessary for its activation by amino acids. *Cell, 141*(2), 290-303. doi:10.1016/j.cell.2010.02.024

Sanchez-Tillo, E., Lazaro, A., Torrent, R., Cuatrecasas, M., Vaquero, E. C., Castells, A., Engel, P., & Postigo, A. (2010). ZEB1 represses E-cadherin and induces an EMT by recruiting the SWI/SNF chromatin-remodeling protein BRG1. *Oncogene, 29*(24), 3490-3500. doi:10.1038/onc.2010.102

Santini, R., Pietrobono, S., Pandolfi, S., Montagnani, V., D'Amico, M., Penachioni, J. Y., Vinci, M. C., Borgognoni, L., & Stecca, B. (2014). SOX2 regulates self-renewal and tumorigenicity of human melanoma-initiating cells. *Oncogene, 33*(38), 4697-4708. doi:10.1038/onc.2014.71

Sardiello, M., Palmieri, M., di Ronza, A., Medina, D. L., Valenza, M., Gennarino, V. A., Di Malta, C., Donaudy, F., Embrione, V., Polishchuk, R. S., Banfi, S., Parenti, G., Cattaneo, E., & Ballabio, A. (2009). A gene network regulating lysosomal biogenesis and function. *Science, 325*(5939), 473-477. doi:10.1126/science.1174447

Sastry, S. K., & Burridge, K. (2000). Focal adhesions: a nexus for intracellular signaling and cytoskeletal dynamics. *Exp Cell Res, 261*(1), 25-36. doi:10.1006/excr.2000.5043

Satoh, T., Takeuchi, O., Vandenbon, A., Yasuda, K., Tanaka, Y., Kumagai, Y., Miyake, T., Matsushita, K., Okazaki, T., Saitoh, T., Honma, K., Matsuyama, T., Yui, K., Tsujimura, T., Standley, D. M., Nakanishi, K., Nakai, K., & Akira, S. (2010). The Jmjd3-Irf4 axis regulates M2 macrophage polarization and host responses against helminth infection. *Nat Immunol, 11*(10), 936-944. doi:10.1038/ni.1920

Schaller, M. D., Otey, C. A., Hildebrand, J. D., & Parsons, J. T. (1995). Focal adhesion kinase and paxillin bind to peptides mimicking beta integrin cytoplasmic domains. *J Cell Biol, 130*(5), 1181-1187.

Schlaepfer, D. D., Hauck, C. R., & Sieg, D. J. (1999). Signaling through focal adhesion kinase. *Prog Biophys Mol Biol, 71*(3-4), 435-478.

Schlaepfer, D. D., Mitra, S. K., & Ilic, D. (2004). Control of motile and invasive cell phenotypes by focal adhesion kinase. *Biochim Biophys Acta, 1692*(2-3), 77-102. doi:10.1016/j.bbamcr.2004.04.008

Schliehe, C., Flynn, E. K., Vilagos, B., Richson, U., Swaminanthan, S., Bosnjak, B., Bauer, L., Kandasamy, R. K., Griesshammer, I. M., Kosack, L., Schmitz, F., Litvak, V., Sissons, J., Lercher, A., Bhattacharya, A., Khamina, K., Trivett, A. L., Tessarollo, L., Mesteri, I., Hladik, A., Merkler, D., Kubicek, S., Knapp, S., Epstein, M. M., Symer, D. E., Aderem, A., & Bergthaler, A. (2015). The methyltransferase Setdb2 mediates virus-induced susceptibility to bacterial superinfection. *Nat Immunol, 16*(1), 67-74. doi:10.1038/ni.3046

Selzer, E., Wacheck, V., Lucas, T., Heere-Ress, E., Wu, M., Weilbaecher, K. N., Schlegel, W., Valent, P., Wrba, F., Pehamberger, H., Fisher, D., & Jansen, B. (2002). The melanocyte-specific isoform of the microphthalmia transcription factor affects the phenotype of human melanoma. *Cancer Res, 62*(7), 2098-2103.

Sengupta, S., Peterson, T. R., & Sabatini, D. M. (2010). Regulation of the mTOR complex 1 pathway by nutrients, growth factors, and stress. *Mol Cell, 40*(2), 310-322. doi:10.1016/j.molcel.2010.09.026

Sennett, R., Wang, Z. C., Rezza, A., Grisanti, L., Roitershtein, N., Sicchio, C., Mok, K. W., Heitman, N. J., Clavel, C., Ma'ayan, A., & Rendl, M. (2015). An Integrated Transcriptome Atlas of Embryonic Hair Follicle Progenitors, Their Niche, and the Developing Skin. *Developmental Cell, 34*(5), 577-591. doi:10.1016/j.devcel.2015.06.023

Sensi, M., Catani, M., Castellano, G., Nicolini, G., Alciato, F., Tragni, G., De Santis, G., Bersani, I., Avanzi, G., Tomassetti, A., Canevari, S., & Anichini, A. (2011). Human cutaneous melanomas lacking MITF and melanocyte differentiation antigens express a functional Axl receptor kinase. *J Invest Dermatol, 131*(12), 2448-2457. doi:10.1038/jid.2011.218

Serbedzija, G. N., Bronner-Fraser, M., & Fraser, S. E. (1994). Developmental potential of trunk neural crest cells in the mouse. *Development, 120*(7), 1709-1718.

Sestakova, B., Ondrusova, L., & Vachtenheim, J. (2010). Cell cycle inhibitor p21/WAF1/CIP1 as a cofactor of MITF expression in melanoma cells. *Pigment Cell & Melanoma Research, 23*(2), 238-251. doi:10.1111/j.1755-148X.2010.00670.x

Settembre, C., De Cegli, R., Mansueto, G., Saha, P. K., Vetrini, F., Visvikis, O., Huynh, T., Carissimo, A., Palmer, D., Klisch, T. J., Wollenberg, A. C., Di Bernardo, D., Chan, L., Irazoqui, J. E., & Ballabio, A. (2013). TFEB controls cellular lipid metabolism through a starvation-induced autoregulatory loop. *Nature Cell Biology, 15*(6), 647-+. doi:10.1038/ncb2718

Settembre, C., Di Malta, C., Polito, V. A., Garcia Arencibia, M., Vetrini, F., Erdin, S., Erdin, S. U., Huynh, T., Medina, D., Colella, P., Sardiello, M., Rubinsztein, D. C., & Ballabio, A. (2011). TFEB links autophagy to lysosomal biogenesis. *Science, 332*(6036), 1429-1433. doi:10.1126/science.1204592

Settembre, C., Zoncu, R., Medina, D. L., Vetrini, F., Erdin, S., Erdin, S., Huynh, T., Ferron, M., Karsenty, G., Vellard, M. C., Facchinetti, V., Sabatini, D. M., & Ballabio, A. (2012). A lysosome-to-nucleus signalling mechanism senses and regulates the lysosome via mTOR and TFEB. *EMBO J, 31*(5), 1095-1108. doi:10.1038/emboj.2012.32

Shaffer, A. L., Emre, N. C., Romesser, P. B., & Staudt, L. M. (2009). IRF4: Immunity. Malignancy! Therapy? *Clin Cancer Res, 15*(9), 2954-2961. doi:10.1158/1078-0432.CCR-08-1845

Shakhova, O., Zingg, D., Schaefer, S. M., Hari, L., Civenni, G., Blunschi, J., Claudinot, S., Okoniewski, M., Beermann, F., Mihic-Probst, D., Moch, H., Wegner, M., Dummer, R., Barrandon, Y., Cinelli, P., & Sommer, L. (2012). Sox10 promotes the formation and maintenance of giant congenital naevi and melanoma. *Nat Cell Biol, 14*(8), 882-890. doi:10.1038/ncb2535

Sharpless, N. E., & DePinho, R. A. (1999). The INK4A/ARF locus and its two gene products. *Current Opinion in Genetics & Development, 9*(1), 22-30. doi:Doi 10.1016/S0959-437x(99)80004-5

Shields, J. M., Pruitt, K., McFall, A., Shaub, A., & Der, C. J. (2000). Understanding Ras: 'it ain't over 'til it's over'. *Trends in Cell Biology, 10*(4), 147-154.

Shigemura, T., Shiohara, M., Tanaka, M., Takeuchi, K., & Koike, K. (2010). Effect of the Mutant Microphthalmia-Associated Transcription Factor Found in Tietz Syndrome on the In Vitro Development of Mast Cells. *Journal of Pediatric Hematology Oncology, 32*(6), 442-447. doi:10.1097/MPH.0b013e3181d9da5d

Shipley, G. D., Pittelkow, M. R., Wille, J. J., Jr., Scott, R. E., & Moses, H. L. (1986). Reversible inhibition of normal human prokeratinocyte proliferation by type beta transforming growth factor-growth inhibitor in serum-free medium. *Cancer Res, 46*(4 Pt 2), 2068-2071.

Shirley, S. H., Greene, V. R., Duncan, L. M., Torres Cabala, C. A., Grimm, E. A., & Kusewitt, D. F. (2012). Slug expression during melanoma progression. *Am J Pathol, 180*(6), 2479-2489. doi:10.1016/j.ajpath.2012.02.014

Shoshan, E., Mobley, A. K., Braeuer, R. R., Kamiya, T., Huang, L., Vasquez, M. E., Salameh, A., Lee, H. J., Kim, S. J., Ivan, C., Velazquez-Torres, G., Nip, K. M., Zhu, K., Brooks, D., Jones, S. J., Birol, I., Mosqueda, M., Wen, Y. Y., Eterovic, A. K., Sood, A. K., Hwu, P., Gershenwald, J. E., Robertson, A. G., Calin, G. A., Markel, G., Fidler, I. J., & Bar-Eli, M. (2015). Reduced adenosine-to-inosine miR-455-5p editing promotes melanoma growth and metastasis. *Nat Cell Biol, 17*(3), 311-321. doi:10.1038/ncb3110

Shou, Y., Martelli, M. L., Gabrea, A., Qi, Y., Brents, L. A., Roschke, A., Dewald, G., Kirsch, I. R., Bergsagel, P. L., & Kuehl, W. M. (2000). Diverse karyotypic abnormalities of the c-myc locus associated with c-myc dysregulation and tumor progression in multiple myeloma. *Proc Natl Acad Sci U S A, 97*(1), 228-233.

Slack, B. E. (1998). Tyrosine phosphorylation of paxillin and focal adhesion kinase by activation of muscarinic m3 receptors is dependent on integrin engagement by the extracellular matrix. *Proc Natl Acad Sci U S A, 95*(13), 7281-7286.

Smirnova, E., Shurland, D. L., Ryazantsev, S. N., & van der Bliek, A. M. (1998). A human dynamin-related protein controls the distribution of mitochondria. *J Cell Biol, 143*(2), 351-358.

Smith, S. D., Kelley, P. M., Kenyon, J. B., & Hoover, D. (2000). Tietz syndrome (hypopigmentation/deafness) caused by mutation of MITF. *Journal of Medical Genetics, 37*(6), 446-448. doi:DOI 10.1136/jmg.37.6.446

Southard-Smith, E. M., Kos, L., & Pavan, W. J. (1998). Sox10 mutation disrupts neural crest development in Dom Hirschsprung mouse model. *Nat Genet, 18*(1), 60-64. doi:10.1038/ng0198-60

Staudt, V., Bothur, E., Klein, M., Lingnau, K., Reuter, S., Grebe, N., Gerlitzki, B., Hoffmann, M., Ulges, A., Taube, C., Dehzad, N., Becker, M., Stassen, M., Steinborn, A., Lohoff, M., Schild, H., Schmitt, E., & Bopp, T. (2010). Interferon-regulatory factor 4 is essential for the developmental program of T helper 9 cells. *Immunity, 33*(2), 192-202. doi:10.1016/j.immuni.2010.07.014

Steingrimsson, E., Copeland, N. G., & Jenkins, N. A. (2004). Melanocytes and the microphthalmia transcription factor network. *Annu Rev Genet, 38*, 365-411. doi:10.1146/annurev.genet.38.072902.092717

Steingrimsson, E., Moore, K. J., Lamoreux, M. L., Ferre-D'Amare, A. R., Burley, S. K., Zimring, D. C., Skow, L. C., Hodgkinson, C. A., Arnheiter, H., Copeland, N. G., & et al. (1994). Molecular basis of mouse microphthalmia (mi) mutations helps explain their developmental and phenotypic consequences. *Nat Genet, 8*(3), 256-263. doi:10.1038/ng1194-256

Steingrimsson, E., Tessarollo, L., Pathak, B., Hou, L., Arnheiter, H., Copeland, N. G., & Jenkins, N. A. (2002). Mitf and Tfe3, two members of the Mitf-Tfe family of bHLH-Zip transcription factors, have important but functionally redundant roles in osteoclast development. *Proceedings of the National Academy of Sciences of the United States of America, 99*(7), 4477-4482. doi:10.1073/pnas.072071099

Steingrimsson, E., Tessarollo, L., Reid, S. W., Jenkins, N. A., & Copeland, N. G. (1998). The bHLH-Zip transcription factor Tfeb is essential for placental vascularization. *Development, 125*(23), 4607-4616.

Stott, F. J., Bates, S., James, M. C., McConnell, B. B., Starborg, M., Brookes, S., Palmero, I., Ryan, K., Hara, E., Vousden, K. H., & Peters, G. (1998). The alternative product from the human CDKN2A locus, p14(ARF), participates in a regulatory feedback loop with p53 and MDM2. *Embo Journal, 17*(17), 5001-5014. doi:DOI 10.1093/emboj/17.17.5001

Strub, T., Giuliano, S., Ye, T., Bonet, C., Keime, C., Kobi, D., Le Gras, S., Cormont, M., Ballotti, R., Bertolotto, C., & Davidson, I. (2011). Essential role of microphthalmia transcription factor for DNA replication, mitosis and genomic stability in melanoma. *Oncogene, 30*(20), 2319-2332. doi:10.1038/onc.2010.612

Sturm, R. A., Fox, C., McClenahan, P., Jagirdar, K., Ibarrola-Villava, M., Banan, P., Abbott, N. C., Ribas, G., Gabrielli, B., Duffy, D. L., & Peter Soyer, H. (2014). Phenotypic characterization of nevus and tumor patterns in MITF E318K mutation carrier melanoma patients. *J Invest Dermatol, 134*(1), 141-149. doi:10.1038/jid.2013.272

Su, Y. P., Wei, W., Robert, L., Xue, M., Tsoi, J., Garcia-Diaz, A., Moreno, B. H., Kim, J., Ng, R. H., Lee, J. W., Koya, R. C., Comin-Anduix, B., Graeber, T. G., Ribas, A., & Heath, J. R. (2017). Single-cell analysis resolves the cell state transition and signaling dynamics associated with melanoma drug-induced resistance. *Proceedings of the National Academy of Sciences of the United States of America, 114*(52), 13679-13684. doi:10.1073/pnas.1712064115

Subramanian, A., Tamayo, P., Mootha, V. K., Mukherjee, S., Ebert, B. L., Gillette, M. A., Paulovich, A., Pomeroy, S. L., Golub, T. R., Lander, E. S., & Mesirov, J. P. (2005). Gene set enrichment analysis: a knowledge-based approach for interpreting genome-wide expression profiles. *Proc Natl Acad Sci U S A, 102*(43), 15545-15550. doi:10.1073/pnas.0506580102

Sulem, P., Gudbjartsson, D. F., Stacey, S. N., Helgason, A., Rafnar, T., Magnusson, K. P., Manolescu, A., Karason, A., Palsson, A., Thorleifsson, G., Jakobsdottir, M., Steinberg, S., Palsson, S., Jonasson, F., Sigurgeirsson, B., Thorisdottir, K., Ragnarsson, R., Benediktsdottir, K. R., Aben, K. K., Kiemeney, L. A., Olafsson, J. H., Gulcher, J., Kong, A., Thorsteinsdottir, U., & Stefansson, K. (2007). Genetic determinants of hair, eye and skin pigmentation in Europeans. *Nat Genet, 39*(12), 1443-1452. doi:10.1038/ng.2007.13

Sun, Z., Fourcade, J., Pagliano, O., Chauvin, J. M., Sander, C., Kirkwood, J. M., & Zarour, H. M. (2015). IL10 and PD-1 Cooperate to Limit the Activity of Tumor-Specific CD8+ T Cells. *Cancer Res, 75*(8), 1635-1644. doi:10.1158/0008-5472.CAN-14-3016

Suzuki, I., Im, S., Tada, A., Scott, C., Akcali, C., Davis, M. B., Barsh, G., Hearing, V., & Abdel-Malek, Z. (1999). Participation of the melanocortin-1 receptor in the UV control of pigmentation. *J Investig Dermatol Symp Proc, 4*(1), 29-34.

Sviderskaya, E. V., Hill, S. P., Evans-Whipp, T. J., Chin, L., Orlow, S. J., Easty, D. J., Cheong, S. C., Beach, D., DePinho, R. A., & Bennett, D. C. (2002). p16(Ink4a) in melanocyte senescence and differentiation. *Jnci-Journal of the National Cancer Institute, 94*(6), 446-454.

Tachibana, M. (1999). Sound needs sound melanocytes to be heard. *Pigment Cell Res, 12*(6), 344-354.

Takeda, K., Takemoto, C., Kobayashi, I., Watanabe, A., Nobukuni, Y., Fisher, D. E., & Tachibana, M. (2000). Ser298 of MITF, a mutation site in Waardenburg syndrome type 2, is a phosphorylation site with functional significance. *Hum Mol Genet, 9*(1), 125-132.

Takeda, K., Yasumoto, K., Kawaguchi, N., Udono, T., Watanabe, K., Saito, H., Takahashi, K., Noda, M., & Shibahara, S. (2002). Mitf-D, a newly identified isoform, expressed in the retinal pigment epithelium and monocyte-lineage cells affected by Mitf mutations. *Biochim Biophys Acta, 1574*(1), 15-23.

Takeda, K., Yasumoto, K., Takada, R., Takada, S., Watanabe, K., Udono, T., Saito, H., Takahashi, K., & Shibahara, S. (2000). Induction of melanocyte-specific microphthalmia-associated transcription factor by Wnt-3a. *J Biol Chem, 275*(19), 14013-14016.

Takeichi, M. (1991). Cadherin cell adhesion receptors as a morphogenetic regulator. *Science, 251*(5000), 1451-1455.

Takemoto, C. M., Yoon, Y. J., & Fisher, D. E. (2002). The identification and functional characterization of a novel mast cell isoform of the microphthalmia-associated transcription factor. *J Biol Chem, 277*(33), 30244-30252. doi:10.1074/jbc.M201441200

Taniguchi, T., Ogasawara, K., Takaoka, A., & Tanaka, N. (2001). IRF family of transcription factors as regulators of host defense. *Annual Review of Immunology, 19*, 623-655. doi:DOI 10.1146/annurev.immunol.19.1.623

Tassabehji, M., Newton, V. E., Liu, X. Z., Brady, A., Donnai, D., Krajewska-Walasek, M., Murday, V., Norman, A., Obersztyn, E., Reardon, W., & et al. (1995). The mutational spectrum in Waardenburg syndrome. *Hum Mol Genet, 4*(11), 2131-2137.

Tassabehji, M., Newton, V. E., & Read, A. P. (1994). Waardenburg syndrome type 2 caused by mutations in the human microphthalmia (MITF) gene. *Nat Genet, 8*(3), 251-255. doi:10.1038/ng1194-251

Teitelbaum, S. L. (2000). Bone resorption by osteoclasts. *Science, 289*(5484), 1504-1508.

Terragni, J., Nayak, G., Banerjee, S., Medrano, J. L., Graham, J. R., Brennan, J. F., Sepulveda, S., & Cooper, G. M. (2011). The E-box binding factors Max/Mnt, MITF, and USF1 act coordinately with FoxO to regulate expression of proapoptotic and cell cycle control genes by phosphatidylinositol 3-kinase/Akt/glycogen synthase kinase 3 signaling. *J Biol Chem, 286*(42), 36215-36227. doi:10.1074/jbc.M111.246116

Theveneau, E., & Mayor, R. (2012). Neural crest delamination and migration: from epithelium-to-mesenchyme transition to collective cell migration. *Dev Biol, 366*(1), 34-54. doi:10.1016/j.ydbio.2011.12.041

Thiery, J. P. (2002). Epithelial-mesenchymal transitions in tumour progression. *Nat Rev Cancer, 2*(6), 442-454. doi:10.1038/nrc822

Thomson, J. A., Murphy, K., Baker, E., Sutherland, G. R., Parsons, P. G., Sturm, R. A., & Thomson, F. (1995). The brn-2 gene regulates the melanocytic phenotype and tumorigenic potential of human melanoma cells. *Oncogene, 11*(4), 691-700.

Thurber, A. E., Douglas, G., Sturm, E. C., Zabierowski, S. E., Smit, D. J., Ramakrishnan, S. N., Hacker, E., Leonard, J. H., Herlyn, M., & Sturm, R. A. (2011). Inverse expression states of the BRN2 and MITF transcription factors in melanoma spheres and tumour xenografts regulate the NOTCH pathway. *Oncogene, 30*(27), 3036-3048. doi:10.1038/onc.2011.33

Tietz, W. (1963). A syndrome of deaf-mutism associated with albinism showing dominant autosomal inheritance. *Am J Hum Genet, 15*, 259-264.

Tirosh, I., Izar, B., Prakadan, S. M., Wadsworth, M. H., 2nd, Treacy, D., Trombetta, J. J., Rotem, A., Rodman, C., Lian, C., Murphy, G., Fallahi-Sichani, M., Dutton-Regester, K., Lin, J. R., Cohen, O., Shah, P., Lu, D., Genshaft, A. S., Hughes, T. K., Ziegler, C. G., Kazer, S. W., Gaillard, A., Kolb, K. E., Villani, A. C., Johannessen, C. M., Andreev, A. Y., Van Allen, E. M., Bertagnolli, M., Sorger, P. K., Sullivan, R. J., Flaherty, K. T., Frederick, D. T., Jane-Valbuena, J., Yoon, C. H., Rozenblatt-Rosen, O., Shalek, A. K., Regev, A., & Garraway, L. A. (2016). Dissecting the multicellular ecosystem of metastatic melanoma by single-cell RNA-seq. *Science, 352*(6282), 189-196. doi:10.1126/science.aad0501

Titz, B., Lomova, A., Le, A., Hugo, W., Kong, X. J., ten Hoeve, J., Friedman, M., Shi, H. B., Moriceau, G., Song, C. Y., Hong, A. Y., Atefi, M., Li, R., Komisopoulou, E., Ribas, A., Lo, R. S., & Graeber, T. G. (2016). JUN dependency in distinct early and late BRAF inhibition adaptation states of melanoma. *Cell Discovery, 2*. doi:UNSP 16028 10.1038/celldisc.2016.28

Toutant, M., Costa, A., Studler, J. M., Kadare, G., Carnaud, M., & Girault, J. A. (2002). Alternative splicing controls the mechanisms of FAK autophosphorylation. *Mol Cell Biol, 22*(22), 7731-7743.

Tredan, O., Galmarini, C. M., Patel, K., & Tannock, I. F. (2007). Drug resistance and the solid tumor microenvironment. *Journal of the National Cancer Institute, 99*(19), 1441-1454. doi:10.1093/jnci/djm135

Tsai, K. K., Zarzoso, I., & Daud, A. I. (2014). PD-1 and PD-L1 antibodies for melanoma. *Human Vaccines & Immunotherapeutics, 10*(11), 3111-3116. doi:10.4161/21645515.2014.983409

Tsao, H., Chin, L., Garraway, L. A., & Fisher, D. E. (2012). Melanoma: from mutations to medicine. *Genes & Development, 26*(11), 1131-1155. doi:10.1101/gad.191999.112

Tsuboi, K., Iida, S., Inagaki, H., Kato, M., Hayami, Y., Hanamura, I., Miura, K., Harada, S., Kikuchi, M., Komatsu, H., Banno, S., Wakita, A., Nakamura, S., Eimoto, T., & Ueda, R. (2000). MUM1/IRF4 expression as a frequent event in mature lymphoid malignancies. *Leukemia, 14*(3), 449-456.

Turner, C. E., Glenney, J. R., Jr., & Burridge, K. (1990). Paxillin: a new vinculin-binding protein present in focal adhesions. *J Cell Biol, 111*(3), 1059-1068.

Udono, T., Yasumoto, K., Takeda, K., Amae, S., Watanabe, K., Saito, H., Fuse, N., Tachibana, M., Takahashi, K., Tamai, M., & Shibahara, S. (2000). Structural organization of the human microphthalmia-associated transcription factor gene containing four alternative promoters. *Biochim Biophys Acta, 1491*(1-3), 205-219.

Ueda, Y., & Richmond, A. (2006). NF-kappa B activation in melanoma. *Pigment Cell Research, 19*(2), 112-124. doi:10.1111/j.1600-0749.206.00304.x

Ullrich, N., Loffek, S., Horn, S., Ennen, M., Sanchez-del-Campo, L., Zhao, F., Breitenbuecher, F., Davidson, I., Singer, B. B., Schadendorf, D., Goding, C. R., & Helfrich, I. (2015). MITF is a critical regulator of the carcinoembryonic antigen-related cell adhesion molecule 1 (CEACAM1) in malignant melanoma. *Pigment Cell & Melanoma Research, 28*(6), 736-740. doi:10.1111/pcmr.12414

Uranishi, M., Iida, S., Sanda, T., Ishida, T., Tajima, E., Ito, M., Komatsu, H., Inagaki, H., & Ueda, R. (2005). Multiple myeloma oncogene 1 (MUM1)/interferon regulatory factor 4 (IRF4) upregulates monokine induced by interferon-gamma (MIG) gene expression in B-cell malignancy. *Leukemia, 19*(8), 1471-1478. doi:10.1038/sj.leu.2403833

Vachtenheim, J., Ondrusova, L., & Borovansky, J. (2010). SWI/SNF chromatin remodeling complex is critical for the expression of microphthalmia-associated transcription factor in melanoma cells. *Biochem Biophys Res Commun, 392*(3), 454-459. doi:10.1016/j.bbrc.2010.01.048

VanBrocklin, M. W., Robinson, J. P., Lastwika, K. J., Khoury, J. D., & Holmen, S. L. (2010). Targeted delivery of NRASQ61R and Cre-recombinase to post-natal melanocytes induces melanoma in Ink4a/Arflox/lox mice. *Pigment Cell Melanoma Res, 23*(4), 531-541. doi:10.1111/j.1755-148X.2010.00717.x

Vandamme, N., & Berx, G. (2014). Melanoma cells revive an embryonic transcriptional network to dictate phenotypic heterogeneity. *Front Oncol, 4*, 352. doi:10.3389/fonc.2014.00352

Vandewalle, C., Van Roy, F., & Berx, G. (2009). The role of the ZEB family of transcription factors in development and disease. *Cell Mol Life Sci, 66*(5), 773-787. doi:10.1007/s00018-008-8465-8

Vanhille, B., Vanek, M., Richener, H., Green, J. R., & Bilbe, G. (1993). Cloning and Tissue Distribution of Subunit-C, Subunit-D, and Subunit-E of the Human Vacuolar H+-Atpase. *Biochemical and Biophysical Research Communications, 197*(1), 15-21. doi:DOI 10.1006/bbrc.1993.2434

Visvikis, O., Ihuegbu, N., Labed, S. A., Luhachack, L. G., Alves, A. F., Wollenberg, A. C., Stuart, L. M., Stormo, G. D., & Irazoqui, J. E. (2014). Innate host defense requires TFEB-mediated transcription of cytoprotective and antimicrobial genes. *Immunity, 40*(6), 896-909. doi:10.1016/j.immuni.2014.05.002

Vlckova, K., Vachtenheim, J., Reda, J., Horak, P., & Ondrusova, L. (2018). Inducibly decreased MITF levels do not affect proliferation and phenotype switching but reduce differentiation of melanoma cells. *J Cell Mol Med, 22*(4), 2240-2251. doi:10.1111/jcmm.13506

Wan, P. T., Garnett, M. J., Roe, S. M., Lee, S., Niculescu-Duvaz, D., Good, V. M., Jones, C. M., Marshall, C. J., Springer, C. J., Barford, D., Marais, R., & Cancer Genome, P. (2004). Mechanism of activation of the RAF-ERK signaling pathway by oncogenic mutations of B-RAF. *Cell, 116*(6), 855-867.

Webb, D. J., Donais, K., Whitmore, L. A., Thomas, S. M., Turner, C. E., Parsons, J. T., & Horwitz, A. F. (2004). FAK-Src signalling through paxillin, ERK and MLCK regulates adhesion disassembly. *Nat Cell Biol, 6*(2), 154-161. doi:10.1038/ncb1094

Weeraratna, A. T., Jiang, Y., Hostetter, G., Rosenblatt, K., Duray, P., Bittner, M., & Trent, J. M. (2002). Wnt5a signaling directly affects cell motility and invasion of metastatic melanoma. *Cancer Cell, 1*(3), 279-288.

Weilbaecher, K. N., Motyckova, G., Huber, W. E., Takemoto, C. M., Hemesath, T. J., Xu, Y., Hershey, C. L., Dowland, N. R., Wells, A. G., & Fisher, D. E. (2001). Linkage of M-CSF signaling to Mitf, TFE3, and the osteoclast defect in Mitf(mi/mi) mice. *Mol Cell, 8*(4), 749-758.

Weinberg, R. A. (2007). Dynamics of cancer: Incidence, inheritance, and evolution. *Nature, 449*(7165), 978-+. doi:10.1038/449978a

Welch, M. D., & Mullins, R. D. (2002). Cellular control of actin nucleation. *Annu Rev Cell Dev Biol, 18*, 247-288. doi:10.1146/annurev.cellbio.18.040202.112133

Wellbrock, C., & Marais, R. (2005). Elevated expression of MITF counteracts B-RAF-stimulated melanocyte and melanoma cell proliferation. *J Cell Biol, 170*(5), 703-708. doi:10.1083/jcb.200505059

Wellbrock, C., Ogilvie, L., Hedley, D., Karasarides, M., Martin, J., Niculescu-Duvaz, D., Springer, C. J., & Marais, R. (2004). V599EB-RAF is an oncogene in melanocytes. *Cancer Res, 64*(7), 2338-2342.

Wellbrock, C., Rana, S., Paterson, H., Pickersgill, H., Brummelkamp, T., & Marais, R. (2008a). Oncogenic BRAF Regulates Melanoma Proliferation through the Lineage Specific Factor MITF. *PLoS One, 3*(7). doi:ARTN e2734 10.1371/journal.pone.0002734

Wellbrock, C., Rana, S., Paterson, H., Pickersgill, H., Brummelkamp, T., & Marais, R. (2008b). Oncogenic BRAF regulates melanoma proliferation through the lineage specific factor MITF. *PLoS One, 3*(7), e2734. doi:10.1371/journal.pone.0002734

White, E. (2015). The role for autophagy in cancer. *Journal of Clinical Investigation, 125*(1), 42-46. doi:10.1172/Jci73941

Widmer, D. S., Cheng, P. F., Eichhoff, O. M., Belloni, B. C., Zipser, M. C., Schlegel, N. C., Javelaud, D., Mauviel, A., Dummer, R., & Hoek, K. S. (2012). Systematic classification of melanoma cells by phenotype-specific gene expression mapping. *Pigment Cell Melanoma Res, 25*(3), 343-353. doi:10.1111/j.1755-148X.2012.00986.x

Widmer, D. S., Hoek, K. S., Cheng, P. F., Eichhoff, O. M., Biedermann, T., Raaijmakers, M. I. G., Hemmi, S., Dummer, R., & Levesque, M. P. (2013). Hypoxia contributes to melanoma heterogeneity by triggering HIF1alpha-dependent phenotype switching. *J Invest Dermatol, 133*(10), 2436-2443. doi:10.1038/jid.2013.115

Wu, M., Hemesath, T. J., Takemoto, C. M., Horstmann, M. A., Wells, A. G., Price, E. R., Fisher, D. Z., & Fisher, D. E. (2000). c-Kit triggers dual phosphorylations, which couple activation and degradation of the essential melanocyte factor Mi. *Genes Dev, 14*(3), 301-312.

Xu, W., Gong, L., Haddad, M. M., Bischof, O., Campisi, J., Yeh, E. T., & Medrano, E. E. (2000). Regulation of microphthalmia-associated transcription factor MITF protein levels by association with the ubiquitin-conjugating enzyme hUBC9. *Exp Cell Res, 255*(2), 135-143. doi:10.1006/excr.2000.4803

Yagi, T., & Takeichi, M. (2000). Cadherin superfamily genes: functions, genomic organization, and neurologic diversity. *Genes Dev, 14*(10), 1169-1180.

Yajima, I., & Larue, L. (2008). The location of heart melanocytes is specified and the level of pigmentation in the heart may correlate with coat color. *Pigment Cell & Melanoma Research, 21*(4), 471-476. doi:10.1111/j.1755-148X.2008.00483.x

Yamagata, T., Nishida, J., Tanaka, S., Sakai, R., Mitani, K., Yoshida, M., Taniguchi, T., Yazaki, Y., & Hirai, H. (1996). A novel interferon regulatory factor family transcription factor, ICSAT/Pip/LSIRF, that negatively regulates the activity of interferon-regulated genes. *Mol Cell Biol, 16*(4), 1283-1294.

Yang, S., Wang, X., Contino, G., Liesa, M., Sahin, E., Ying, H., Bause, A., Li, Y., Stommel, J. M., Dell'antonio, G., Mautner, J., Tonon, G., Haigis, M., Shirihai, O. S., Doglioni, C., Bardeesy, N., & Kimmelman, A. C. (2011). Pancreatic cancers require autophagy for tumor growth. *Genes Dev, 25*(7), 717-729. doi:10.1101/gad.2016111

Yasumoto, K., Yokoyama, K., Shibata, K., Tomita, Y., & Shibahara, S. (1994). Microphthalmia-associated transcription factor as a regulator for melanocyte-specific transcription of the human tyrosinase gene. *Mol Cell Biol, 14*(12), 8058-8070.

Yasumoto, K., Yokoyama, K., Takahashi, K., Tomita, Y., & Shibahara, S. (1997). Functional analysis of microphthalmia-associated transcription factor in pigment cell-specific transcription of the human tyrosinase family genes. *J Biol Chem, 272*(1), 503-509.

Yokoyama, S., Woods, S. L., Boyle, G. M., Aoude, L. G., MacGregor, S., Zismann, V., Gartside, M., Cust, A. E., Haq, R., Harland, M., Taylor, J. C., Duffy, D. L., Holohan, K., Dutton-Regester, K., Palmer, J. M., Bonazzi, V., Stark, M. S., Symmons, J., Law, M. H., Schmidt, C., Lanagan, C., O'Connor, L., Holland, E. A., Schmid, H., Maskiell, J. A., Jetann, J., Ferguson, M., Jenkins, M. A., Kefford, R. F., Giles, G. G., Armstrong, B. K., Aitken, J. F., Hopper, J. L., Whiteman, D. C., Pharoah, P. D., Easton, D. F., Dunning, A. M., Newton-Bishop, J. A., Montgomery, G. W., Martin, N. G., Mann, G. J., Bishop, D. T., Tsao, H., Trent, J. M., Fisher, D. E., Hayward, N. K., & Brown, K. M. (2011). A novel recurrent mutation in MITF predisposes to familial and sporadic melanoma. *Nature, 480*(7375), 99-103. doi:10.1038/nature10630

Yonemura, S., Itoh, M., Nagafuchi, A., & Tsukita, S. (1995). Cell-to-cell adherens junction formation and actin filament organization: similarities and differences between non-polarized fibroblasts and polarized epithelial cells. *J Cell Sci, 108 (Pt 1)*, 127-142.

Young, N. P., Kamireddy, A., Van Nostrand, J. L., Eichner, L. J., Shokhirev, M. N., Dayn, Y., & Shaw, R. J. (2016). AMPK governs lineage specification through Tfeb-dependent regulation of lysosomes. *Genes Dev, 30*(5), 535-552. doi:10.1101/gad.274142.115

Yu, G., Wang, L. G., Han, Y., & He, Q. Y. (2012). clusterProfiler: an R package for comparing biological themes among gene clusters. *OMICS, 16*(5), 284-287. doi:10.1089/omi.2011.0118

Zamir, E., Katz, B. Z., Aota, S., Yamada, K. M., Geiger, B., & Kam, Z. (1999). Molecular diversity of cell-matrix adhesions. *J Cell Sci, 112 (Pt 11)*, 1655-1669.

Zavadil, J., & Bottinger, E. P. (2005). TGF-beta and epithelial-to-mesenchymal transitions. *Oncogene, 24*(37), 5764-5774. doi:10.1038/sj.onc.1208927

Zhang, M., Song, F., Liang, L., Nan, H., Zhang, J., Liu, H., Wang, L. E., Wei, Q., Lee, J. E., Amos, C. I., Kraft, P., Qureshi, A. A., & Han, J. (2013). Genome-wide association studies identify several new loci associated with pigmentation traits and skin cancer risk in European Americans. *Hum Mol Genet, 22*(14), 2948-2959. doi:10.1093/hmg/ddt142

Zhang, Y., Liu, T., Meyer, C. A., Eeckhoute, J., Johnson, D. S., Bernstein, B. E., Nusbaum, C., Myers, R. M., Brown, M., Li, W., & Liu, X. S. (2008). Model-based analysis of ChIP-Seq (MACS). *Genome Biol, 9*(9), R137. doi:10.1186/gb-2008-9-9-r137

Zhang, Y. P., Xiong, Y., & Yarbrough, W. G. (1998). ARF promotes MDM2 degradation and stabilizes p53: ARF-INK4a locus deletion impairs both the Rb and p53 tumor suppression pathways. *Cell, 92*(6), 725-734. doi:Doi 10.1016/S0092-8674(00)81401-4

Appendix 1

R scripts contain instruction to use DiffBind package to extract common peaks for replicates of ChIP-seq experiments. Followed by annotating peaks to genes then performing GO term analysis with ChIPseeker and Cluster profiler. Last part of the script consists of walkthrough for generating tagheatmap of peaks over MITF binding regions.

```
#First part is to generate commmon peaksets for each replicate of TFEB, IRF4 and
MITF
#load Diffbind package
library(DiffBind)
#Creat a tab limited file containing peaks name, associated path and bam file
path, and import it
samples<-read.table(file="./all.csv",sep=",",head=T,stringsAsFactors = F)
#creat a dba object
compare<-dba(sampleSheet=samples)
# generate a consensus peakset for every set of samples that have identical
  metadata values except the Replicate number.
All_consensus<- dba.peakset(compare, consensus=-DBA_REPLICATE)
#extreacting tfeb overlap
tfeboverlap=dba(All_consensus, mask=All_consensus$masks$TFEB,minOverlap = 2)
#retrieve the consensus peaksets in bed file
tfebconsensuspeaks <- dba.peakset(tfeboverlap,bRetrieve=TRUE)
write.table(tfebconsensuspeaks,"TFEBreplicatecommonpeak.txt",sep="\t")
#extreacting IRF4 overlap
irf4overlap=dba(All_consensus, mask=All_consensus$masks$IRF4,minOverlap = 2)
irf4consensuspeaks <- dba.peakset(irf4overlap,bRetrieve=TRUE)
write.table(irf4consensuspeaks,"IRF4replicatecommonpeak.txt",sep="\t")
#extreacting MITF overlap
MITFoverlap=dba(All_consensus, mask=All_consensus$masks$MITF,minOverlap = 2)
MITFconsensuspeaks <- dba.peakset(MITFoverlap,bRetrieve=TRUE)
write.table(MITFconsensuspeaks,"MITFreplicatecommonpeak.txt",sep="\t")

#Annotating the peaksets and loading required packges
library(ReactomePA)
library(GenomicRanges)
library(Biostrings)
library(GenomicFeatures)
library(BSgenome)
library(ChIPseeker)
library(ChIPpeakAnno)
library(TxDb.Hsapiens.UCSC.hg19.knownGene)
txdb <- TxDb.Hsapiens.UCSC.hg19.knownGene
require(clusterProfiler)
```

```
#read in the common peaks for MITF
MITFChIP<-readPeakFile("./Peaks_x_ChIPseeker/MITF-com-Peaks.txt")
#Annotate the peaks to genomic region
MITFChIPanno1<-annotatePeak(MITFChIP, TxDb = txdb, annoDb = "org.Hs.eg.db")
MITFChIPanno2<-as.data.frame(MITFChIPanno1)
#subset the genes based on distance from TSS 20kb +/-
MITFChIPannosub<-subset(MITFChIPanno2, MITFChIPanno2$distanceToTSS < 20000 &
MITFChIPanno2$distanceToTSS > -20000)
write.table(MITFChIPannosub,file="MITFChIPAnno20kbTSS.txt",sep = "\t",dec="'")
#Annotation of IRF4 peaks
IRF4ChIP<-readPeakFile("./Peaks_x_ChIPseeker/IRF4-com-Peaks.txt")
IRF4ChIPanno<-annotatePeak(IRF4ChIP, TxDb = txdb, annoDb = "org.Hs.eg.db")
IRF4ChIPanno1<-as.data.frame(IRF4ChIPanno)
IRF4ChIPannosub<-subset(IRF4ChIPanno1, IRF4ChIPanno1$distanceToTSS < 20000 &
IRF4ChIPanno1$distanceToTSS > -20000)
write.table(IRF4ChIPannosub,file="IRF4ChIPanno20kbTSS.txt",sep = "\t",dec="'")
#Annotation of TFEB peaks
TFEBCHIP<-readPeakFile("./Peaks_x_ChIPseeker/TFEB-com-Peaks.txt")
TFEBCHIPanno<-annotatePeak(TFEBCHIP, TxDb = txdb, annoDb = "org.Hs.eg.db")
TFEBCHIPanno1<-as.data.frame(TFEBCHIPanno)
TFEBCHIPannosub<-subset(TFEBCHIPanno1, TFEBCHIPanno1$distanceToTSS < 20000 &
TFEBCHIPanno1$distanceToTSS > -20000)
write.table(TFEBCHIPannosub,file="TFEBCHIPanno20kbTSS.txt",sep = "\t",dec="'")
#to make compared pathway
peakAnnoListMITFTFEB<-setNames(list(MITFChIPannosub,TFEBCHIPannosub),c("MITF","TFEB
"))

genes = lapply(peakAnnoListMITFIRF4, function(i) as.data.frame(i)$geneId)
names(genes) = sub("_", "\n", names(genes))
#pathway analysis for commonly bound genes
compKEGG <- compareCluster(geneCluster   = genes,
                           fun           = "enrichKEGG",
                           pvalueCutoff  = 0.05,
                           pAdjustMethod = "BH")
dotplot(compKEGG, showCategory = 10, title = "KEGG Pathway Enrichment Analysis")
compGOBP <- compareCluster(geneCluster   = genes,

fun="enrichGO",ont="BP",pvalueCutoff=0.005,OrgDb='org.Hs.eg.db')
#plotting the gene
dotplot(compGOBP, showCategory = 10,font.size=18)

 #Matrices of peaks over MITF binding sites
 MITFChIPsummit<-readPeakFile("./Peaks_x_ChIPseeker/MITFChIPseqLauret09_summits.bed"
 )
 MITFChIPanno3<-annotatePeak(MITFChIPsummit, TxDb = txdb, annoDb = "org.Hs.eg.db")
 MITFwindow <- as.data.frame(MITFChIPanno3)
 MITFwindow2 <- MITFwindow
 MITFwindow2$start <- (MITFwindow$start - 10000)
 MITFwindow2$end <- (MITFwindow$end + 10000)
 MITFwindow3 <- makeGRangesFromDataFrame(MITFwindow2)
 mitfonmitf <- getTagMatrix(MITFGRanges, windows=MITFwindow3)
 TFEBCHIPGranges<-unique(as.GRanges(TFEBCHIPanno))

 #generating TFEB peaks matrix over MITF peaks
 mitfontfeb<-getTagMatrix(TFEBCHIPGranges, windows=MITFwindow3)
 mitftfebtagMatrixList <- setNames(list(mitfonmitf, mitfontfeb), c("MITF", "TFEB"))
 tagHeatmap(mitftfebtagMatrixList, xlim=c(-10000,10000), color =c("red","black"))
 IRF4CHIPGranges<-unique(as.GRanges(IRF4ChIPanno))
 #generating IRF4 peaks matrix over MITF peaks
 IRF4tagMatrix <- getTagMatrix(IRF4CHIPGranges, windows=MITFwindow3)
 mitfirf4tagMatrixList <- setNames(list(mitfonmitf,IRF4tagMatrix), c("MITF",
 "IRF4"))
 tagHeatmap(mitfirf4tagMatrixList, xlim=c(-10000,10000), color =c("red","blue"))
```

Appendix 2

R script contains instruction for performing differential binding analysis for transcription factor binding using DiffBind package. Then retrieving differential bound sites.

```
#Read in tab limited file containing peak path for TFEB and MITF
MitfTfeb<-read.table(file="./tfeb-mitf.txt",sep=",",head=T,stringsAsFactors = F)
#creat dba object
MitfTfeb<-dba(sampleSheet=MitfTfeb)
#generate consensus peaks from replicates
consensusREP<- dba.peakset(MitfTfeb, consensus=-DBA_REPLICATE)
consensusREP<- dba(consensusREP,mask = consensusREP$masks$Consensus, minOverlap =
2)
#generate Venn plot from overlapping TFEB and MITF peaks
dba.plotVenn(consensusREP,consensusREP$masks$Consensus)
#retrieve consensus peaksets of MITF and TFEB
consensusMITFTFEB <- dba.peakset(consensusREP,bRetrieve=TRUE)
write.table(consensusMITFTFEB,"MITF-TFEB-COMMONPEAKS.txt",sep="\t")
#differential binding analysis for MITF-TFEB overlapping peaks
MitfTfeb<-dba.count(MitfTfeb,summits=0)
dba.plotPCA(MitfTfeb,DBA_FACTOR,label=DBA_FACTOR)
MitfTfeb<-dba.contrast(MitfTfeb,categories = DBA_FACTOR,minMembers = 2)
MitfTfeb<-dba.analyze(MitfTfeb)
dba.plotMA(MitfTfeb,fold=5)
#retrieving significantly bound sites with 5 fold difference
sigSitesTFEB <- dba.plotVolcano(MitfTfeb, fold=5)
sigSitesTFEB<-as.data.frame(sigSitesTFEB)
write.table(sigSitesTFEB, row.names=F, sep="\t",
file="sigSiteTFEB5Fold.txt",dec=",")
#another way of retrieving overlapping and unique peaks
olap<-dba.overlap(consensus,consensus$masks$Consensus)
UniqueTFEB<-olap$onlyA
UniqueMITF<-olap$onlyB
overlap<-olap$inAll
write.table(UniqueTFEB, row.names=F, sep="\t", file="TFEBonly.txt")
write.table(UniqueMITF, row.names=F, sep="\t", file="MITFonly.txt")
write.table(overlap, row.names=F, sep="\t", file="mitftfeboverlap.txt")

#differential binding analysis for MITF and IRF4
IRF4MITF<-read.table(file="./MITF-IRF4",sep=",",head=T,stringsAsFactors = F)
IRF4MITF<-dba(sampleSheet=IRF4MITF)
consensusREP1<- dba.peakset(IRF4MITF, consensus=-DBA_REPLICATE)
consensusREP1<- dba(consensusREP1,mask = consensusREP1$masks$Consensus, minOverlap
= 1)
consensusMITFIRF4 <- dba.peakset(consensusREP1,bRetrieve=TRUE)
write.table(consensusMITFIRF4,"MITF-IRF4-COMMONPEAKS.txt",sep="\t")
countmitfirf4<-dba.count(IRF4MITF,summits = 0)
countmitfirf4con<-dba.contrast(countmitfirf4,categories = DBA_FACTOR,minMembers =
2)
countmitfirf4ana<-dba.analyze(countmitfirf4con)
countmitfirf4ana.DB <- dba.report(countmitfirf4ana)
dba.plotPCA(countmitfirf4ana,DBA_FACTOR,label=DBA_REPLICATE)
dba.plotVenn(countmitfirf4ana,countmitfirf4ana$masks$Consensus)
consensusIRF4MITF<-dba.peakset(IRF4MITF,consensus = DBA_FACTOR,minOverlap = 2)
olapmitfirf4<-dba.overlap(consensusIRF4MITF,consensusIRF4MITF$masks$Consensus)
UniqueIRF4<-olapmitfirf4$onlyA
UniqueMITF<-olapmitfirf4$onlyB
write.table(UniqueIRF4, row.names=F, sep="\t", file="IRF4only.txt")
write.table(UniqueMITF, row.names=F, sep="\t", file="MITFonlyinIRF4.txt")
dba.plotMA(countmitfirf4ana,fold=5)
sigSitesIRF4 <- dba.plotVolcano(countmitfirf4ana, fold=2)
sigSitesIRF4<-as.data.frame(sigSitesIRF4)
write.table(sigSitesIRF4, row.names=F, sep="\t", file="sigSiteIRF4.txt",dec=",")
```

Appendix 3

R script containing differential expression analysis using Sleuth, GO and KEGG analysis, and ranking the DEGs for GSEA analysis.

```
#Load sleuth
library("sleuth")
#specify the directory where kallisto output located
base_dir <- "/Users/ramiledilshat/Library/Mobile
Documents/com~apple~CloudDocs/kallistooutput"
#fetch the name of each folder containing kallisto output for each sample
sample_id<- dir(file.path(base_dir,"kallisto"))
#attach sample name to each associated file path
kal_dirs <- sapply(sample_id, function(id) file.path(base_dir, "kallisto",id))
#print out to check if sample id corresponds to correct folder
kal_dirs
#load biomart package
library("biomaRt")
#fetch gene names
mart <- biomaRt::useMart(biomart = "ENSEMBL_MART_ENSEMBL",
                         dataset = "hsapiens_gene_ensembl",
                         host = 'www.ensembl.org')
t2g <- biomaRt::getBM(attributes = c("ensembl_transcript_id",
"ensembl_gene_id","external_gene_name"), mart = mart)
t2g <- dplyr::rename(t2g, target_id = ensembl_transcript_id,ens_gene =
ensembl_gene_id, ext_gene = external_gene_name)
#load the file in dataframe format containing information of each sample name and
sample type
s2c<-read.table(file="/Users/ramiledilshat/Library/Mobile
Documents/com~apple~CloudDocs/kallistooutput/info.txt",header=T,stringsAsFactors =
F)
#merge the information data frame with sample path and sample names
s2c <- dplyr::mutate(s2c, path = kal_dirs)
#print out everything is correct
s2c
#Build a sleuth project
so <- sleuth_prep(s2c, target_mapping = t2g)
#Fit to LRT model to assess differential expression due to MITF knock out
so <- sleuth_fit(so, ~condition, 'full')
so <- sleuth_fit(so, ~1, 'reduced')
so <- sleuth_lrt(so, 'reduced', 'full')
#perform wald test also to get differentially expressed genes
so_wald <- sleuth_wt(so,"conditionMITF_KO")
#to obtain the result from wald test
so_results_wt<-sleuth_results(so_wald,"conditionMITF_KO")
#get transcript id with qvalue <0.05
so_results_wt_sig<-so_results_wt$target_id[which(so_results_wt$qval<0.05)]
#To obtain the result from lrt test
lrt_results <- sleuth_results(so, 'reduced:full', test_type = 'lrt')
#get transcript id with qvalue <0.05
lrt_results_sig<-lrt_results$target_id[which(lrt_results$qval < 0.05)]
# subset shared id between two tests
shared_ids <- so_results_wt_sig[so_results_wt_sig %in% lrt_results_sig]
#results merged from shared lrt and wald tests
shared_results_deg <- so_results_wt[so_results_wt$target_id %in% shared_ids,]
#write the results of differentially expressed genes
write.table(shared_results_deg,file="./PAPER/DEGS",dec =",",sep="\t")
#Generate rank file for GSEA analysis
#The metric score to use is the sign of the fold change multiplied by the inverse
```

```
of the p-value
#final result table of differentially expressed genes assigned to x
x<-shared_results
attach(x)
#take the sign of fold change
x$bsign=sign(b)
#take the negative log10 of pvalue
x$logp=-log10(pval)
#gnerate metrix score with new column used for ranking and pathway analysis
x$metric= x$logp/x$bsign
#makes new table with only gene names and metric score
y<-x[,c("external_gene_name","metric")]
#remove duplicated gene names
y<-y[!duplicated(y),]
#write the rank file in tab limited format
write.table(y,file="expression0.05.rnk",quote=F,sep="\t",row.names=F)
#Gene ontology and KEGG pathway analysis
#load cluster profiler, package used for the analysis
library(clusterProfiler)
#Cluster profiler needs ENTREZ gene id for the analysis. New dataframe with
genenames and entrez gene id
gene.df<-bitr(shared_results_deg$ext_gene,fromType = "SYMBOL",
              toType = c("ENSEMBL","ENTREZID"), OrgDb = org.Hs.eg.db)
#rename the column name of date frame
colnames(gene.df)<-c("ext_gene","ENSEMBL","ENTREZID")
#merge data frame with table containing differentially expressed genes
gene.df<-merge(gene.df,shared_results_deg,by="ext_gene")
#make new data frame consists of only entrez gene id and foldchange
genelist<-data.frame(genes=gene.df$ENTREZID,fc=gene.df$b)
#remove duplicated gene names
genelist<-genelist[!duplicated(genelist$genes), ]
#remove NAs
genelist<-genelist[!(is.na(genelist$genes)), ]
geneList=genelist[,2]
names(geneList)<-as.character(genelist[,1])
#sort gene list based on logfold change
geneList = sort(geneList, decreasing = TRUE)
#new data frame with sorted genelist with fold change
mydf <- data.frame(Entrez=names(geneList), FC=geneList)
#spcify repressed and induced genes in the dataframe
mydf <- mydf[abs(mydf$FC) > 0.7,]
mydf$group <- "upregulated"
mydf$group[mydf$FC < 0]<-"dowregulated"
mydf$othergroup <- "A"
mydf$othergroup[mydf$FC < 0] <- "B"
#run cluster profiler for GO cellular component
GO <- compareCluster(Entrez~group, data=mydf,
fun="enrichGO",ont="CC",pvalueCutoff=0.1,OrgDb='org.Hs.eg.db')
#run cluster profiler for KEGG pathway
KEGG <- compareCluster(Entrez~group, data=mydf, fun="enrichKEGG",organism =
"hsa",minGSSize = 5,keyType="kegg",qvalueCutoff = 0.2,pAdjustMethod="fdr")
```

Appendix 4

R script below consist of instructions about how to run TCGA-biolink

```
#load TCGAbiolink package
library(TCGAbiolinks)
#Query platform illumina Hiseq with a RNA-seq results from melanoma samples
query.exp.hg38 <- GDCquery(project = "TCGA-SKCM",
                           data.category = "Gene expression",
                           data.type = "Gene expression quantification",
                           experimental.strategy = "RNA-Seq",
                           platform = "Illumina HiSeq",
                           file.type = "results",
                           legacy=T)
# Download all samples  with platform IlluminaHiSeq_RNASeqV2
GDCdownload(query.exp.hg38)
# Prepare expression matrix with geneID in the rows and samples (barcode) in the
  columns
# rsem.genes.results as values and save results in rda
BRCARnaseqSE <- GDCprepare(query.exp.hg38,save=TRUE,save.filename = "tcgaskcm.rda",
                           remove.files.prepared = TRUE)
skcmmatrix <- assay(BRCARnaseqSE,"raw_count")
# normalization of genes
dataNorm <- TCGAanalyze_Normalization(tabDF =skcmmatrix, geneInfo =  geneInfo)
# quantile filter of genes
dataFilt <- TCGAanalyze_Filtering(tabDF = dataNorm,
                                  method = "quantile",
                                  qnt.cut =  0.25)

# To extract rna-seq expression value of mitf low and mitf high samples
#First extract MITF expression from all melanoma samples
MITF<-subset(dataFilt,rownames(dataFilt)=="MITF")
#write MITF expression including barcodes in tab limited format
write.table(MITF,file="mitfexpression.txt",sep="\t")
#then creat a text file from highest 40 and lowest 40 samples with MITF
expression, and read in the table
mitflow<-read.table(file="Allmitflowsamples.txt")
mitflow$V1<-as.character(mitflow$V1)
mitfhigh<-read.table(file="AllMITFhigh.txt")
mitfhigh$V1<-as.character(mitfhigh$V1)
#Filter the transcriptome profile of mitf high and low samples from the data matrix
mitfhigh1 =dataFilt[,mitfhigh$V1]
mitflow1 =dataFilt[,mitflow$V1]
#Diff.expr.analysis (DEA) using MITF high and low samples
degMITFlowHigh <- TCGAanalyze_DEA(mat1 =dataFilt[,mitfhigh$V1],
                                  mat2 = dataFilt[,mitflow$V1],
                                  Cond1type = "HIGH",
                                  Cond2type = "LOW",
                                  fdr.cut = 0.01 ,
                                  logFC.cut = 1,
                                  method = "glmLRT")
#DEGs table with expression values in mitf high and mitf low melanoma tumour
samples
degMITFlowHighFiltLevel <- TCGAanalyze_LevelTab(degMITFlowHigh,"HIGH","LOW",

dataFilt[,mitfhigh$V1],dataFilt[,mitflow$V1])
#write the final DEGs table in xlsx file
write.xlsx(degMITFlowHighFiltLevel,file="DEGMITFlowMITFhighTCGA-SKCM.xls")
```

Appendix 5

A

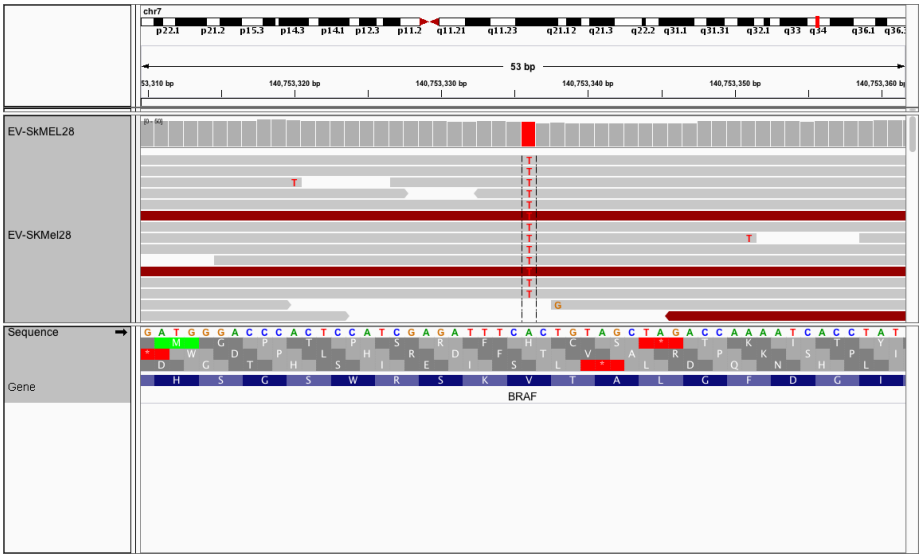

B

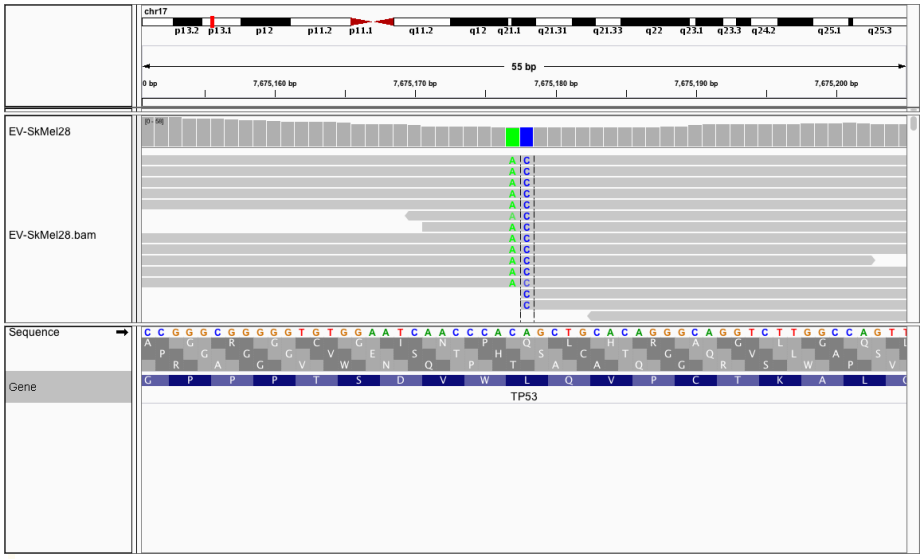

A,B. IGV track of alignment file (bam) of EV-SkMel28 cells lines confirming respectively the (BRAFV600E) mutation (c.1799T>A) and p53 mutation c.del434 435insTG.

Appendix 6

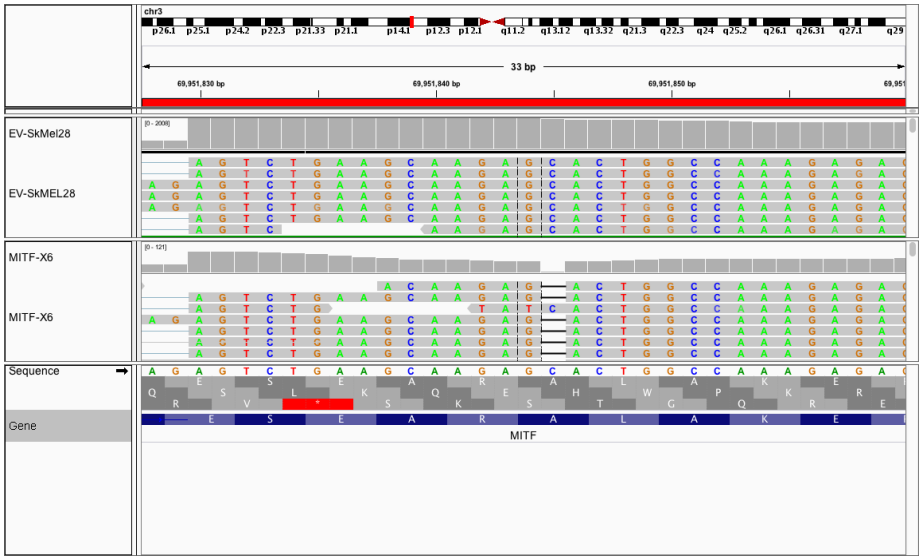

IGV track of alignment file (bam) of EV-SkMel28 and MITF-X6 cells lines confirming the acquired mutation, a 1 bp deletion at position A198 and an addition mutation of amino acid substituition A197I- R198-I.